Impact of the platelet collagen receptor GPVI on inflammation and extracellular matrix remodelling in abdominal aortic aneurysm formation and progression

Inaugural-Dissertation

zur Erlangung des Doktorgrades
der Mathematisch-Naturwissenschaftlichen Fakultät
der Heinrich-Heine-Universität Düsseldorf

vorgelegt von

Tobias Feige
aus Duisburg

Düsseldorf, März 2026

Aus der Arbeitsgruppe Experimentelle Vaskuläre Medizin
der Klinik für Gefäß- und Endovaskularchirurgie
des Universitätsklinikums der Heinrich-Heine-Universität Düsseldorf

Gedruckt mit der Genehmigung der
Mathematisch-Naturwissenschaftlichen Fakultät der
Heinrich-Heine-Universität Düsseldorf

Berichterstatter:
1. Prof. Dr. Margitta Elvers
2. Prof. Dr. Patricia Hidalgo

Tag der mündlichen Prüfung: 10.11.2026

1 Table of content

1 Table of content I

Abstract V

Zusammenfassung VII

List of tables IX

List of figures X

List of abbreviation XII

1 Introduction 1

1.1 Platelets 1

1.1.1 Platelet physiology 2

1.1.2 Platelet-signalling in the primary haemostasis 3

1.1.3 Platelet-signalling in the secondary haemostasis 7

1.1.4 The main platelet collagen receptor GPVI 8

1.2 The abdominal aortic aneurysm 13

1.2.1 Epidemiology and prevalence of abdominal aortic aneurysms 15

1.2.2 Pathophysiological mechanisms of AAA formation and progression 16

1.2.3 Preclinical and clinical implication of platelet function for AAA formation and progression. 21

1.3 Aim of the study 24

1.3.1 Crosstalk of platelets with macrophages and fibroblasts aggravates inflammation, aortic wall stiffening, and osteopontin release in abdominal aortic aneurysm 24

1.3.2 GPVI-mediated platelet activation and procoagulant activity aggravate inflammation and aortic wall remodelling in abdominal aortic aneurysm 25

1.3.3 Revacept (GPVI-FC) treatment attenuates experimental induced abdominal aortic aneurysm formation in mice 25

2 Material and methods 27

2.1 Material 27

2.1.1 Experimental animals 27

2.1.2 General devices ... 28

2.1.3 General material ... 29

2.1.4 Chemicals ... 30

2.1.5 Buffers and solutions ... 31

2.1.6 Antibodies ... 32

2.1.7 Software ... 33

2.2 Methods ... 34

2.2.1 The external porcine pancreatic elastase model ... 34

2.2.2 *In vivo* Revacept application ... 34

2.2.3 Ultrasound imaging ... 35

2.2.4 Murine blood collection and blood cell count determination ... 35

2.2.5 Flow cytometry ... 36

2.2.6 Immunofluorescence staining of murine aortic tissue ... 37

2.2.7 *Ex vivo* thrombus formation ... 38

2.2.8 Statistics ... 39

3 Results ... 40

3.1 Crosstalk of platelets with macrophages and fibroblasts aggravates inflammation, aortic wall stiffening, and osteopontin release in abdominal aortic aneurysm ... 40

3.2 GPVI-mediated platelet activation and procoagulant activity aggravate inflammation and aortic wall remodelling in abdominal aortic aneurysm ... 76

3.3 Revacept (GPVI-FC) treatment attenuates experimental induced abdominal aortic aneurysm formation in mice ... 132

3.3.1 Humanised GPVI mice revealed an unaltered aortic diameter under naive conditions ... 133

3.3.2 Revacept treatment attenuates aortic diameter progression in ePPE induced AAA formation ... 135

3.3.3 Revacept does not affect platelet degranulation and integrin $\alpha_{IIb}\beta_3$ activation in experimental AAA formation ... 139

3.3.4 Reduced procoagulant activity of platelets derived from Revacept treated ePPE mice ... 142

4 Discussion ... 148

4.1 Crosstalk of platelets with macrophages and fibroblasts aggravates inflammation, aortic wall stiffening, and osteopontin release in abdominal aortic aneurysm 148

4.1.1 Persistent platelet hyperreactivity as a novel pathological hallmark in patients diagnosed with AAA 149

4.1.2 Platelet depletion attenuates vascular inflammation and aortic wall remodelling in experimental induced AAA formation 151

4.1.3 GPVI-mediated platelet activation amplifies the OPN-dependent vascular inflammatory response in the AAA pathology 153

4.2 GPVI-mediated platelet activation and procoagulant activity aggravate inflammation and aortic wall remodelling in abdominal aortic aneurysm 155

4.2.1 Genetic deletion of platelet GPVI impairs inflammation by affecting neutrophil infiltration and NET formation in early AAA 156

4.2.2 Platelet GPVI significantly contributes to progressive aortic wall remodelling in experimental induced AAA formation 158

4.2.3 GPVI-mediated platelet activation reinforces VSMC loss in experimental induced AAA formation 163

4.2.4 GPVI as potential translational target for the development of novel pharmacological therapies in AAA formation and progression. 165

4.2.5 GPVI as potential biomarker for AAA prediction and risk stratification 168

4.3 Revacept (GPVI-FC) treatment attenuates experimental induced AAA formation in mice 169

4.4 Conclusion and outlook 173

5 References 175

6 Appendix 195

6.1 Supplemental figures 195

6.1.1 GPVI-mediated platelet activation and procoagulant activity aggravate inflammation and aortic wall remodelling in abdominal aortic aneurysm 195

6.1.2 Revacept (GPVI-FC) treatment attenuates experimental induced abdominal aortic aneurysm formation in mice 196

6.2 List of publications 202

6.3 International conferences 205

6.4 Reuse of own publications 206

6.5 Publishing licences of self-created figures 207

6.6 Curriculum vitae 209

6.7 Affidavit 210

6.8 Eidesstattliche Erklärung 210

7 Danksagung 211

Abstract

An abdominal aortic aneurysm (AAA) is a life-threatening, atherosclerosis-related cardiovascular disease, associated with a high mortality rate following aortic rupture. Pathologically, an AAA is defined by a progressive and irreversible dilation of the abdominal aortic vessel wall, and clinically diagnosed by a 1.5-fold increase in the infrarenal aortic diameter. In 2019, the global prevalence of AAA among individuals aged 30–79 years was estimated at approximately 0.92%, translating into a total of 35.12 million cases worldwide. From a pathophysiological perspective, an AAA is predominantly characterised by three major hallmarks, including the adverse remodelling of the aortic wall, a chronic vascular inflammation, and the formation of a platelet-rich intraluminal thrombus (ILT). The AAA prevalence strongly correlates with age, whereas male sex, smoking, obesity, hypertension, hypercholesterolemia, coexisting cardiovascular diseases (CVDs), or a positive family history represent additional independent risk factors. Despite extensive preclinical and clinical investigations, no pharmacological therapy –effectively targeting aneurysm growth– has been implemented into the clinical routine to date. Once the aneurysm progression surpasses a pre-defined threshold, surgical repair remains the only effective therapeutic strategy to protect patients for fatal aortic rupture.

Besides their pivotal role in haemostasis, dysregulated platelet function has been shown to be implicated as a major driver of different pathological processes in the context of various CVDs. In recent years, multiple preclinical studies have demonstrated protective effects of antiplatelet therapies on AAA formation and progression. Nevertheless, the precise mechanisms by which platelets reinforce aneurysm growth remain poorly understood. Accordingly, this study investigated platelet-driven mechanisms and identified platelets as key mediators of the AAA pathogenesis by reinforcing both vascular inflammation and adverse aortic wall remodelling within the aneurysmal segment. Furthermore, clinical profiling of platelets derived from AAA patients identified a persistent hyperreactive platelet phenotype under both resting conditions and upon activation of the main collagen receptor glycoprotein (GP)VI. By considering its central role in platelet activation, GPVI has emerged as a potent therapeutic target for the development of novel antithrombotic therapies, as GPVI-signalling has been shown to be implicated in the pathogenesis of various CVDs. Accordingly, this work investigated the contribution of GPVI-mediated platelet activation for the formation and progression of AAA, with the objective of evaluating the therapeutic potential of GPVI targeting in order to effectively restrict aneurysm growth. In this context, genetic deletion of GPVI in mice offered protection against experimental induced AAA formation, as evidenced by a markedly attenuated aortic diameter progression in two distinct *in vivo* mouse models. Mechanistically, GPVI-deficiency resulted in a pronounced

reduction in the vascular inflammatory response, characterised by reduced neutrophil recruitment into the aneurysmal tissue, paralleled by decreased release of both neutrophil-derived elastase and neutrophil extracellular trap (NET) formation. In addition to that, significantly reduced levels of circulating matrix metalloproteinases (MMPs) were detected in the absence of GPVI, culminating in a preserved aortic wall integrity. These experimental findings were further confirmed in a first translational approach in mice, as pharmacological inhibition of GPVI –using a GPVI-blocking antibody– effectively restricted aneurysm growth *in vivo*. Despite intensified evaluation of potential pharmacological approaches over the recent years, a successful clinical translation is still lacking. Thus, this work additionally investigated the therapeutic potential of the soluble dimeric GPVI-Fc fusion protein Revacept *in vivo.* Within this translational framework, prophylactic administration of Revacept markedly attenuated aortic diameter progression, paralleled by a substantially reduced aneurysm growth rate. Collectively, these initial findings highlight the potential of Revacept as a novel pharmacological approach to effectively restrict AAA progression.

Zusammenfassung

Ein abdominelles Aortenaneurysma (AAA) ist eine lebensbedrohliche, mit Atherosklerose assoziierte Herz-Kreislauf-Erkrankung, die mit einer hohen Mortalitätsrate nach Aortenruptur verbunden ist. Pathologisch wird ein AAA durch eine progressive und irreversible Erweiterung der Gefäßwand der abdominalen Aorta definiert und klinisch durch eine 1,5-fache Zunahme des infrarenalen Aortendurchmessers diagnostiziert. Im Jahr 2019 wurde die weltweite AAA Prävalenz bei Personen im Alter von 30–79 Jahren auf etwa 0,92 % geschätzt, was insgesamt einer Zahl von 35,12 Millionen Fällen weltweit entspricht. Aus pathophysiologischer Sicht ist ein AAA vor allem durch drei Hauptmerkmale gekennzeichnet: eine progressive Umstrukturierung der Aortenwand, eine chronische vaskuläre Entzündung, sowie die Bildung eines thrombozytenreichen intraluminalen Thrombus (ILT). Neben dem Alter, mit dem die Prävalenz eines AAA stark korreliert, stellen das männliche Geschlecht, Rauchen, Adipositas, Hypertonie, Hypercholesterinämie, bestehende kardiovaskuläre Erkrankungen oder eine positive Familienanamnese zusätzliche unabhängige Risikofaktoren dar. Trotz intensiver präklinischer und klinischer Studien ist es bis zum jetzigen Zeitpunkt nicht gelungen eine pharmakologische Therapie, die das Aneurysmawachstum wirksam hemmt, in die klinische Routine zu implementieren. Sobald das Aneurysmawachstum einen klinisch vordefinierten Grenzwert überschreitet, stellt die chirurgische Intervention die einzige wirksame therapeutische Strategie zum Schutz der Patienten vor einer fatalen Aortenruptur dar.

Neben der zentralen Rolle von Thrombozyten in der Hämostase konnte gezeigt werden, dass eine dysregulierte Thrombozytenfunktion wesentlich zu verschiedenen pathologischen Prozessen im Kontext diverser kardiovaskulärer Erkrankungen beiträgt. In den letzten Jahren konnten verschiedene präklinische Studien protektive Effekte von antithrombozytären Therapien auf die AAA-Entstehung nachweisen. Dennoch sind die genauen Mechanismen, durch die Thrombozyten das Aneurysmawachstum fördern, bislang nur unzureichend aufgeklärt. Dementsprechend untersuchte die hier vorliegende Arbeit Thrombozyten vermittelte Mechanismen und identifizierte dabei Thrombozyten als zentrale Mediatoren der AAA-Pathogenese, indem sie sowohl die vaskuläre Entzündung, als auch die progressive Umstrukturierung der Aortenwand innerhalb des aneurysmatischen Segments verstärken. Klinische Analysen von Thrombozyten aus AAA-Patienten zeigten zudem ein persistentes hyperreaktives Thrombozytenaktivierungsprofil, sowohl ohne zusätzliche Stimulation durch Agonisten als auch nach Aktivierung des Kollagenrezeptors Glykoprotein (GP)VI. Angesichts seiner zentralen Rolle in der Thrombozytenaktivierung hat GPVI als therapeutisches Ziel für die Entwicklung neuartiger antithrombotischer Therapien an Bedeutung gewonnen, da

nachgewiesen werden konnte, dass der GPVI-Signalweg an der Pathogenese verschiedener kardiovaskulärer Erkrankungen beteiligt ist. Aufbauend darauf wurde in der vorliegenden Arbeit der Beitrag der GPVI-vermittelten Thrombozytenaktivierung zur Entstehung und Progression des AAA untersucht, mit dem Ziel, das therapeutische Potenzial einer GPVI-spezifischen Intervention zur wirksamen Limitierung des Aneurysmawachstums zu evaluieren. In diesem Zusammenhang konnte gezeigt werden, dass die genetische Deletion des murinen GPVI Schutz vor der experimentell induzierten AAA-Bildung bot, was sich in einer deutlich abgeschwächten Progression des Aortendurchmessers in zwei unterschiedlichen *in vivo* Maus-Modellen widerspiegelte. Mechanistisch führte eine GPVI-Defizienz zu einer ausgeprägten Reduktion der vaskulären Entzündungsreaktion, gekennzeichnet durch eine verminderte Neutrophilen-Rekrutierung in das aneurysmatische Gewebe. Diese wurde zudem t von einer reduzierten Freisetzung von Neutrophiler-Elastase, sowie der verminderten Bildung sogenannter *neutrophil extracellular traps* (NETs) begleitet. Darüber hinaus wurden in Abwesenheit von GPVI eine deutlich reduzierte Konzentration an zirkulierenden Matrix-Metalloproteinasen (MMPs) nachgewiesen, was zu einer Erhaltung der Aortenwandintegrität führte. Diese experimentellen Befunde wurden in einem ersten translationalen Ansatz weiter bestätigt. Die pharmakologische Inhibierung der GPVI-vermittelten Thrombozytenaktivierung mittels eines GPVI-blockierenden Antikörpers führte zu einer effektiven Beschränkung des Aneurysmawachstums. Trotz der intensivierten Evaluierung potenzieller pharmakologischer Kandidaten zur Behandlung des AAA in den letzten Jahren bleibt eine erfolgreiche klinische Umsetzung bislang aus. Daher wurde in der vorliegenden Arbeit zusätzlich das therapeutische Potenzial des löslichen dimeren GPVI-Fc-Fusionsproteins Revacept analysiert. Innerhalb dieses translationalen Ansatzes führte die prophylaktische Applikation von Revacept zu einer deutlichen Verminderung Zunahme des Aortendurchmessers, einhergehend mit einer signifikant reduzierten Aneurysmawachstumsrate. Zusammengefasst unterstreichen diese ersten Ergebnisse das Potenzial von Revacept als neuartige pharmakologische Strategie zur wirksamen Begrenzung der AAA-Progression.

List of tables

Table 1. Platelet granule content. Content of platelet-derived α-granules, dense granules and lysosomes. 6
Table 2. Risk factors for AAA formation. 14
Table 3. Effects of antiplatelet therapies on experimental induced AAA formation in mice and rats. 22
Table 4. General devices 28
Table 5. General material 29
Table 6. Chemicals 30
Table 7. Buffers and solutions 31
Table 8. Dyes 32
Table 9. Antibodies for flow cytometry 32
Table 10. Antibodies for immunofluorescence staining 33
Table 11. Software 33

List of figures

Figure 1. Platelet-related physiological and pathophysiological processes 1
Figure 2. The role of platelets in primary haemostasis..... 4
Figure 3. Intracellular platelet signalling pathways..... 5
Figure 4. Structure of the main collagen receptor GPVI 9
Figure 5. GPVI-mediated intracellular signalling pathways 11
Figure 6. Categorisation of abdominal aortic aneurysms 13
Figure 7. Pathophysiological mechanisms of AAA formation and progression 18
Figure 8. Morphological structure of a three-layered ILT 20
Figure 9. *In vivo* Revacept application in ePPE operated mice..... 35
Figure 10. The flow chamber system for the analysis of *ex vivo* thrombus formation 38
Figure 12. Humanised GPVI mice revealed an unaltered aortic diameter under naive conditions.....134
Figure 13. Revacept treatment attenuates aortic diameter progression in ePPE induced AAA progression.....136
Figure 14. Revacept treatment leads to reduced aneurysm growth rate in ePPE induced AAA progression.....137
Figure 15. Platelet, RBC and WBC counts of Revacept treated mice are unaltered at day 28 post ePPE surgery 138
Figure 16. Treatment with Revacept leads to unaltered platelet activation in ePPE operated mice 140
Figure 17. Platelet glycoprotein exposition in Revacept treated mice at day 28 post ePPE surgery 141
Figure 18. Reduced procoagulant activity of platelets derived from Revacept treated ePPE mice 143
Figure 19. Platelets from Revacept treated ePPE mice revealed a reduced FasL surface exposition at day 28 post surgery 144
Figure 20. The formation of circulating platelet-leukocyte aggregates is unaffected by Revacept treatment at day 28 after ePPE induced AAA formation 145
Figure 21. CD40L surface externalisation and VWF-binding to platelets were unaltered in Revacept treated ePPE operated mice at day 28 147
Figure 22. Mechanistical contribution of platelet function to the AAA pathogenesis 148
Figure 23. Impact of platelet GPVI on inflammation and aortic wall remodelling in AAA formation and progression 155

Figure S1. Reduced number of FasL positive platelets in GPVI-deficient mice during early PPE-induced AAA formation 195

Figure S2. Platelet, RBC and WBC counts of naive humanised *(h)Gp6*$^{+/+}$ mice 196

Figure S3. Platelet activation profile of naive *hGp6*$^{+/+}$ mice 197

Figure S4. Platelets from naive *hGp6*$^{+/+}$ mice revealed an enhanced procoagulant activity 198

Figure S5. Platelet glycoprotein exposition of naive *hGp6*$^{+/+}$ mice 199

Figure S6. CD40L exposition, VWF binding and platelet-leukocyte aggregate formation in naive *hGp6*$^{+/+}$ mice 200

Figure S7. Naive *hGp6*$^{+/+}$ mice revealed an unaltered *ex vivo* thrombus formation under high arterial shear rates 201

List of abbreviation

°C	Grad Celsius
AAA	Abdominal aortic aneurysm
ACD	Acid citrate dextrose
ACS	Acute coronary syndromes
ADAM10	A disintegrin and metalloprotease 10
ADP	Adenosindiphosphate
AngII	Angiotensin II
APC	Allophycocyanin
ApoE	Apolipoprotein E
ASA	Acetylsalicylic acid
ATP	Adenosintriphosphate
BAPN	β-aminopropionitrile
BSA	Bovine serum albumin
Btk	Bruton tyrosine kinase
$C_6H_8O_7$	Citric acid
Ca^{2+}	Calcium
$CaCl_2$	Calcium chloride
Ccl2	C-C motif chemokine ligand 2
CD	Cluster of differentiation
citH3	Citrullinated histone 3
Col1a1	Collagen type I
Col3a1	Collagen type III
COX	Cyclooxygenases
CRP	Collagen-related peptide
ctrl.	Control
CVDs	Cardiovascular diseases
Cy5	Cyanine 5
DAG	Diacylglycerol
DALYs	Disability-adjusted life-years
dH_2O	Distilled water
DiOC6	3,3'-Dihexyloxacarbocyanine Iodide
EACTS	European Association for Cardio-Thoracic Surgery
ECM	Extracellular matrix

EDTA	Ethylenediaminetetraacetate
Eln	Elastin
eNOS	Endothelial nitric oxide synthase
ePPE	External porcine pancreatic elastase infusion
EtOH	Ethanol
EVAR	Endovascular aneurysm repair
FasL	Fas ligand
FcRγ	Fc receptor γ-chain,
FELASA	Federation of European Laboratory Animal Science Association
FITC	Fluorescein-isothiocyanate
FSC	Forward scatter
g	Gram
Gads	Grb2-related adaptor downstream of Shc
GP	Glycoprotein
GPO sequence	Glycine-proline-hydroxyproline sequence
h	Hour
HCT	Haematocrit
HEPES	2-[4-(2-hydroxyethyl)piperazin-1-yl] ethanesulfonic acid
HGB	Haemoglobin
hGPVI	Humanised GPVI
i.p.	Intraperitoneal
ICAM-1	Intracellular adhesion molecule-1
Ig	Immunoglobulin
IL	Interleukin
ILT	Intraluminal thrombus
IP_3	Inositol-1,4,5-trisphosphate
ITAM	Immunoreceptor tyrosine-based activation motif
KCl	Potassium chloride
$KMnO_4$	Potassium permanganate
L	Litre
LAT	Linker of activated T cells
MCP-1	Macrophage chemoattractant protein-1
$MgCl_2$	Magnesium chloride
Min	Minute
MMP	Matrix metalloproteinase

MPO	Myeloperoxidase
MPV	Mean platelet volume
Na_2HPO_4	Sodium phosphate, dibasic
Na_3VO_4	Sodium orthovanadate
NaCl	Sodium chloride
NaH_2PO_4	Sodium dihydrogen phosphate
$NaHCO_3$	Sodium hydrogen carbonate
NaN_3	Sodium azide
NETs	Neutrophil extracellular traps
NO	Nitric oxide
OAR	Open aortic repair
OPN	Osteopontin
PADI4	Protein arginine deiminase 4
PAR	Protease-activated receptor
PBS	Phosphate-buffered saline
PCT	Plateletcrit
PDW	Platelet distribution width
PE	Phycoerythrin
PFA	Paraformaldehyde
PGE_1	Prostaglandin E1
PGI_2	Prostacyclin2
PI3K	Phosphoinositide-3 kinase
PIP_2	Phosphatidylinositol-4,5 bisphosphate
PKC	Protein kinase C
PLC	Phospholipase C
Plt	Platelet
PPE	Porcine pancreatic elastase infusion
PS	Phosphatidylserine
RBC	Red blood cell
RDW	Red blood cell distribution width
RGD sequence	Arginine-glycine-aspartic acid sequence
ROS	Reactive oxygen species
s.c.	Subcutaneous
SEM	Standard error of the mean
sGPVI	Soluble GPVI

SLP76	Src homology 2 domain–containing leukocyte phosphoprotein of 76 kDa
SPF	Specific pathogen-free
Spp1	Secreted phosphoprotein 1
STS	Society of Thoracic Surgeons
TAT complex	Thrombin-antithrombin complex
TIMP	Tissue inhibitor of metalloproteinase
Tnf-a	Tumour necrosis factor-alpha
TP	T prostanoid receptor
TRAP (CD40L)	Tumour necrosis factor-related activation protein
TRIPLE	Thrombotic Reactivity Indicator using Platelet GPVI, CD36 Expression, and Age
TSP	Thrombospondin
TxA_2	Thromboxane A_2
U46	U46619 (thromboxane A2 analogue)
VCAM-1	Vascular adhesion molecule-1
VSMC	Vascular smooth muscle cell
VWF	Von Willebrand factor
WBC	White blood cell
WT	Wild-type

1 Introduction

1.1 Platelets

Platelets represent the key mediators of haemostasis by preventing excessive blood loss at the site of vascular injury. Within the process of haemostasis subsequent platelet activation, aggregation and the release of secondary mediators, such as cytokines, chemokines and growth factors, are essential steps in mediating the formation of a haemostatic plug, in order to arrest blood loss [1, 2]. Thus, platelets are crucial for sufficiently sustaining vascular integrity. Besides their fundamental role in haemostasis, it has become apparent during the last decades that platelets are capable of modulating further physiological processes, including angiogenesis, tissue regeneration, wound healing, as well as the inflammatory response by e.g. promoting innate and adaptive immune cell interactions (**Figure 1A**) [2, 3].

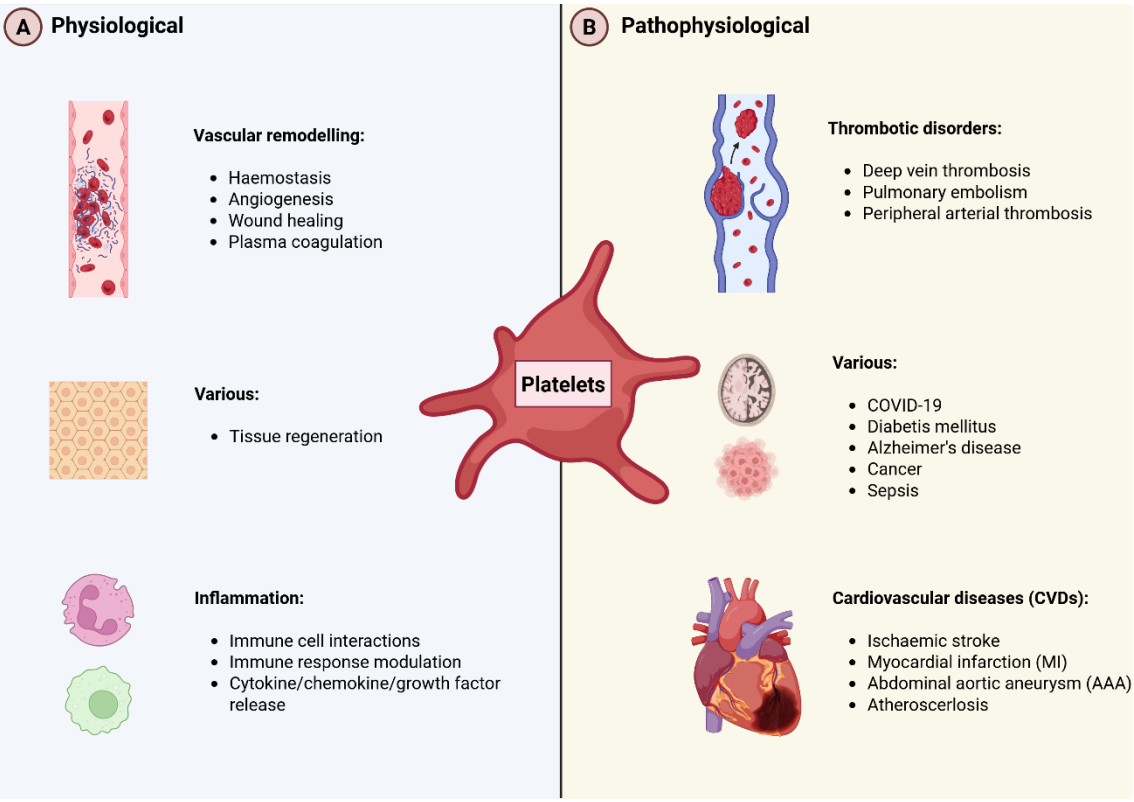


Figure 1. Platelet-related physiological and pathophysiological processes. (**A**) Platelets represent the key mediators of haemostasis by preventing excessive blood loss at the site of vascular injury. Beyond their role in haemostasis, platelets contribute to various physiological processes, including angiogenesis, tissue regeneration wound healing, as well as inflammation. (**B**) However, dysregulated platelet function is linked to the development of pathophysiological conditions, including thrombotic disorders, Alzheimer's disease, cancer and different cardiovascular diseases (e.g. ischaemic stroke, MI, atherosclerosis, or AAA). AAA = Abdominal aortic aneurysm; MI = Myocardial infarction. Modified from [4] (created with BioRender.com).

However, it has been reported that altered platelet function is linked to the development of pathophysiological conditions, including thrombotic disorders, tumour growth, fibrosis, chronic inflammation, COVID-19, or the Alzheimer's disease [3, 5]. Beyond this, dysregulated platelet function and activity are related to the onset and progression of different cardiovascular diseases (CVDs), such as stroke, atherosclerosis, myocardial infarction, or the formation of abdominal aortic aneurysms (AAA) (**Figure 1B**). Due to their pivotal role in both physiological and pathological processes, targeting platelet function has emerged as a promising approach to develop novel therapeutic interventions [6, 7].

1.1.1 Platelet physiology

Besides red blood cells (RBCs) and leukocytes, the discoid shaped platelets represent the third type of blood cell within the circulation [8]. Thereby, platelets are the smallest cellular components within the blood, with an average diameter of 1–3 µm in humans, respectively 0.5 µm in mice. Human platelet counts typically range from 150–400 x 10^3 platelets per µL, whereas murine blood contains around 1,100 × 10^3 platelets per µL. Regardless of their numerical abundance, platelets —similar to leukocytes— account for only a minor fraction of the human total blood cell volume relative to the other circulating haematopoietic cells [9-11]. Despite lacking a nucleus, platelets contain residual mRNA that sustains a limited capacity for de novo protein synthesis, thereby enabling a restricted dynamic regulation of their functional responses during haemostasis and inflammation. Platelets are produced within the process of thrombopoiesis, a highly regulated mechanism mediated by the cytoplasmic fragmentation of megakaryocytes in the bone marrow. Once circulating within the bloodstream, human platelets exhibit an average lifespan of 7–10 days, while murine platelets persist for 3–4 days. After becoming senescent or activated, platelets are cleared from the circulation via phagocytosis by macrophages in the liver or spleen [8, 10, 12].

As mentioned previously, platelets contribute to a range of physiological processes, including angiogenesis, tissue regeneration, and wound healing. However, their evolutionarily conserved and primary function is haemostasis. At the site of a vascular injury, the subendothelial extracellular matrix (ECM) is exposed towards the bloodstream, triggering platelet adhesion, activation, and aggregation, which culminates in the formation of a haemostatic plug. Haemostasis proceeds in two interdependent stages: the primary haemostasis, mainly driven by platelet activation as well as aggregation, and the secondary haemostasis, in which the newly formed platelet plug is stabilised via fibrin-mediated crosslinking [2, 3, 13]. In order to identify platelet-related disorders including thrombocytopenia or thrombocytosis, the platelet function

can be analysed based on common haematological indices such as platelet count, mean platelet volume (MPV), platelet distribution width (PDW), and plateletcrit (PCT). In this context, MPV and PDW provide complementary measures of platelet size and size variability, whereas the PCT quantifies the relative fractional contribution of platelets to the total circulating blood volume [14-16].

1.1.2 Platelet-signalling in the primary haemostasis

The process of haemostasis can be subdivided into two successive stages, the primary and secondary haemostasis, which are both characterised by distinct cellular and molecular mechanisms. At the site of a vascular injury, the initiation of the primary haemostasis results in the formation of an unstable haemostatic plug, thus preserving vascular integrity in order to arrest excessive blood loss. Under physiological conditions, platelets circulate within the bloodstream in a resting state, which is maintained by the continuous release of endothelial-derived inhibitors, such as nitric oxide (NO) and prostacyclin (PGI_2). This in turn prevents the adhesion of platelets from the circulation to the intact endothelium (**Figure 2**) [17-19].

Within the injured vasculature, the subendothelial ECM, consisting of various adhesive macromolecules, including collagen, laminin, thrombospondin (TSP) and vitronectin, becomes exposed to the bloodstream [20-22]. This exposure facilitates the immobilisation of plasma-derived von Willebrand factor (VWF) on the fibrillar collagen type I and III of the ECM, thus promoting the interaction of the collagen-bound VWF with the platelet glycoprotein (GP)Ib-IX-V receptor complex [21, 23]. Thereby, the GPIb-V-IX complex consists of the four subunits GPIbα (130 kDa; 25,000 copies), GPIbβ (25 kDa; 25,000 copies), GPV (88 kDa; 12,500 copies) and GPIX (22 kDa; 25,000 copies), with GPIbα mediating the interaction with the collagen-bound VWF through high-affinity binding of its A1 domain. However, VWF binding to the GPIb-IX-V complex induces weak platelet activation and facilitates an initial and unstable interaction of platelets to the damaged vessel wall [24-26]. This transient adhesion —so-called tethering— subsequently allows binding of the main collagen receptor GPVI (60–65 kDa; 4,000–6,000 copies) to its ligand (**Section 1.1.4**) [27]. Collagen-mediated GPVI activation results in the induction of different intracellular signalling pathways, thus promoting integrin activation, α- and dense granule release, cytoskeletal reorganisation, as well as the activation and recruitment of additional platelets from the circulation to the site of vascular injury (**Figure 2**) [22, 28, 29]**.** However, stable platelet adhesion to the exposed subendothelial ECM and subsequent platelet aggregation are highly dependent on the integrin $\alpha_{IIb}\beta_3$ (GPIIb/IIIa)-signalling. This heterodimeric transmembrane receptor is composed of an α (142 kDa)- and β-subunit (95 kDa) and represents

the most abundant platelet surface glycoprotein, with an estimated number of 80,000 copies per platelet [30-32].

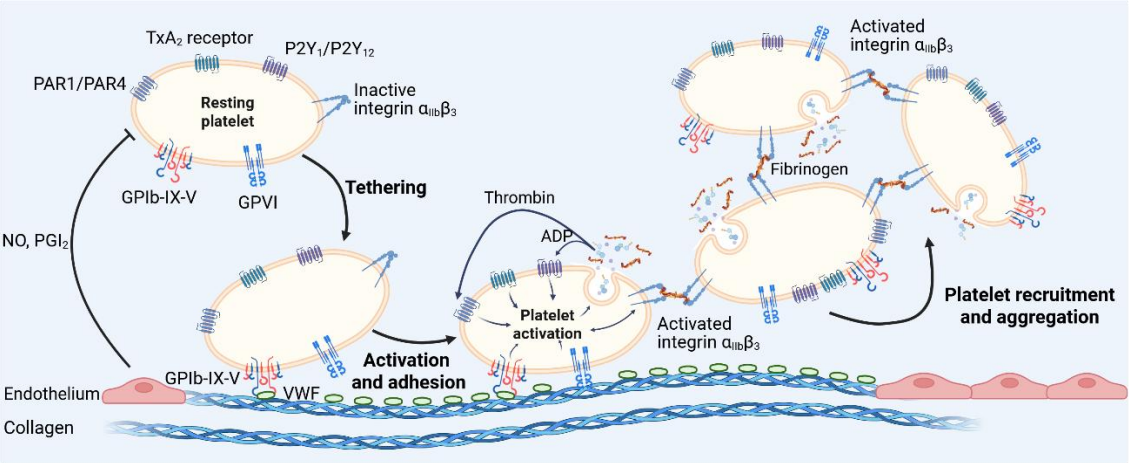


Figure 2. The role of platelets in primary haemostasis. Under physiological conditions, platelets are circulating within the bloodstream in a resting state, maintained by the release of endothelial-derived inhibitors, such as NO and PGI_2. Upon a vascular injury, the interaction of the platelet GPIb-IX-V complex with collagen-bound VWF results in a transient and unstable adhesion (tethering). Subsequent binding of the collagen receptor GPVI to its ligand triggers platelet activation through the induction of intracellular signalling cascades. This activation promotes α- and dense granule degranulation, leading to the local release of secondary mediators. These mediators, in turn, amplify platelet recruitment from the circulation, thereby driving platelet aggregation and thrombus formation. ADP = adenosine diphosphate; GP = Glycoprotein; NO = Nitric oxide; PAR = Protease-activated receptor; PGI_2 = Prostacyclin; TxA_2 = Thromboxane A_2; VWF = Von Willebrand factor. Modified from [22] (created with BioRender.com).

In addition to that, the integrin $\alpha_{IIb}\beta_3$ is also stored within the α-granules. Under resting conditions, the integrin $\alpha_{IIb}\beta_3$ is present on the platelet surface in an inactive conformation, which is characterised by a low affinity for its ligands, fibrinogen, fibronectin, fibrin, vitronectin, TSP, and VWF [22, 33, 34]. Ligand-binding is thereby mediated by the arginine-glycine-aspartic acid (RGD) sequence of the respective ligand, whereas fibrinogen exhibits the highest binding affinity. Besides the integrin $\alpha_{IIb}\beta_3$, platelets express various other integrins on their surface, which are composed of distinct subunit combinations [1, 35, 36]. These include the integrin $\alpha_2\beta_1$, which functions as a collagen receptor, the integrin $\alpha_5\beta_1$ as a fibronectin receptor, integrin $\alpha_6\beta_1$ as a laminin receptor, and integrin $\alpha_v\beta_3$ which binds vitronectin (**Figure 3**) [22, 37]. However, engagement of the platelet collagen receptor GPVI with subendothelial collagen initiates intracellular signalling cascades, which in turn promote integrin $\alpha_{IIb}\beta_3$ activation. This process involves a conformational conversion of the integrin $\alpha_{IIb}\beta_3$ from an inactive to an active state, thus enabling high-affinity binding of its ligands, such as fibrinogen, fibronectin, fibrin, TSP, and collagen-bound VWF [22]. The GPVI-mediated conversion of the integrin $\alpha_{IIb}\beta_3$ from a low-

affinity to a high-affinity state is classically referred to as inside-out signalling. In addition to that, GPVI-mediated platelet activation further promotes the translocation of integrin $\alpha_{IIb}\beta_3$ from the α-granules to the platelet surface [18, 37, 38].

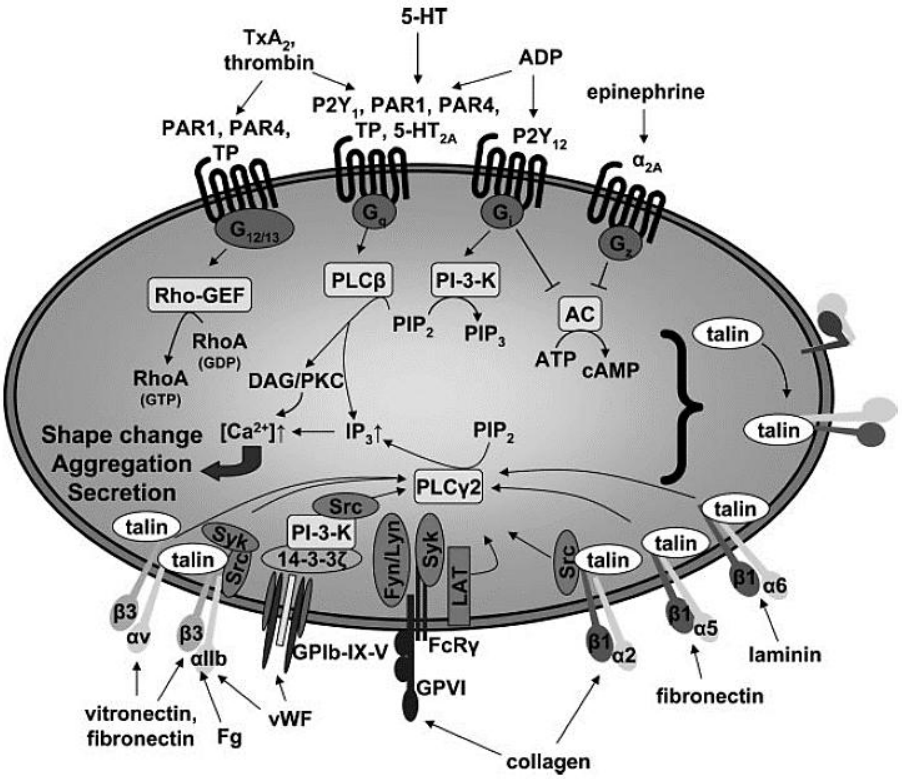


Figure 3. Intracellular platelet signalling pathways. Platelet activation is mediated by various ligand-receptor interactions, promoting the initiation of different intracellular downstream signalling pathways. Engagement of the platelet collagen receptor GPVI initiates an ITAM-dependent signalling cascade leading to PLCγ2-mediated platelet activation. PLC activation in turn promotes the formation of IP_3 and DAG, leading to intracellular calcium mobilisation. These processes induce the conformational change of the integrin $\alpha_{IIb}\beta_3$ from a low to a high affinity state (inside-out signalling), thus enabling binding of fibrinogen or VWF. Ligand binding to the active integrin $\alpha_{IIb}\beta_3$ (outside-in signalling) amplifies PLCγ2-meditated platelet activation, thus contributing calcium mobilisation, platelet shape change, and aggregation. VWF binding to the GPIb-IX-V complex additional contributes to PLCγ2-meditated platelet activation. In addition, thrombin-induced PAR1 and PAR4-mediated signalling, ADP binding to $P2Y_1$ or $P2Y_{12}$, as well as TxA_2-mediated TP receptor signalling further amplifies calcium mobilisation, platelet shape change, platelet activation and aggregation. ADP = Adenosine diphosphate; ATP = Adenosine triphosphate; Fg = fibrinogen; GDP = Guanosine diphosphate; GP = Glycoprotein; GTP = Guanosine triphosphate; IP_3 = inositol-1,4,5-trisphosphate; DAG = Diacylglycerol; PAR = Protease-activated receptor; PI-3-K = Phosphoinositide-3 kinase; AC = Adenylyl cyclase; PIP2 = Phosphatidylinositol-4,5 bisphosphate; PIP3 = Phosphatidylinositol-3,4,5 trisphosphate; PKC = protein kinase C; PLC = Phospholipase C; Rho-GEF = Rho-specific guanine nucleotide exchange factor; TP = T prostanoid receptor; TxA_2 = Thromboxane A2. Taken from [22].

Upon ligand binding, the activated integrin $\alpha_{IIb}\beta_3$ undergoes further conformational rearrangements, including transphosphorylation of its cytoplasmic domains, which initiate intracellular signalling cascades and is paralleled by the clustering of the integrin $\alpha_{IIb}\beta_3$ at the platelet surface. This outside-in signalling is pivotal for different processes by promoting and amplifying platelet spreading, cytoskeletal reorganisation, and fibrin-dependent stabilisation of the newly formed haemostatic plug via fibrinogen bridging [22, 33].

Table 1. Platelet granule content. Content of platelet-derived α-granules, dense granules and lysosomes. ADP = adenosine diphosphate; ATP = adenosine triphosphate; CCL = Chemokine (C-C motif) ligand; CXCL = Chemokine (C-X-C motif) ligand; EGF = Epidermal growth factor; GP = Glycoprotein; GTP = Guanosine triphosphate; HGF = Hepatocyte growth factor; IGF = Insulin-like growth factor; TGF = Transforming growth factor; TSP = Thrombospondin; UTP = Uridine triphosphate; VWF = Von Willebrand factor. Modified from [34].

Granule	Type	Content
α-granule	Adhesion proteins:	Fibrinogen, fibronectin, vitronectin, VWF, TSP
	Membrane proteins:	Integrin $\alpha_{IIb}\beta_3$, GPIb-IX-V complex, P-selectin
	Chemokines:	CXCL1, CXCL4, CXCL5, CXCL8, CLL2, CLL3, CLL5
	Growth factors:	EGF, HGF, IGF, TGFβ
	Coagulants:	Factor V, IX, XIII
	Anticoagulants:	Antithrombin
	Angiogenic factors:	Vascular endothelium growth factor, fibroblast growth factor, platelet-derived growth factor, angiostatin, endostatin
Dense granule	Cations:	Ca^{2+}, Mg^{2+}, K^{+}
	Phosphates:	Polyphosphate, pyrophosphate
	Bioactive molecules:	Serotonin, histamine, epinephrine
	Nucleotides:	ADP, ATP, UTP, GTP
Lysosome	Degrading enzymes:	Elastase, collagenase, cathepsins

Besides integrin $\alpha_{IIb}\beta_3$ activation, GPVI-mediated platelet stimulation induces the exocytosis of the intracellular α- and dense granules. Fusion of these granules with the plasma membrane leads to the release of various secondary mediators, including adenosine diphosphate (ADP), adenosine triphosphate (ATP), and fibrinogen (**Table 1**) [22].

In addition to that, upon platelet activation, intracellular *de novo* synthesis and the subsequent release of thromboxane A_2 (TxA_2) is promoted. Thereby, TxA_2 generation is mediated by conversion of arachidonic acid by the cyclooxygenases1/2 (COX1/2) resulting in the formation of prostaglandin H_2 (PGH_2). In turn, PGH_2 acts as a substrate for the thromboxane synthase and is subsequently converted into TxA_2. The release of these platelet-derived secondary mediators,

such as ADP or TxA_2, is capable of reinforcing platelet activation in an autocrine and paracrine manner (**Figure 3**) [39-41]. Binding of TxA_2 to the G protein–coupled receptors, the T prostanoid receptor (TP) α and β, initiates intracellular signalling cascades that primarily involve G protein-mediated phospholipase C activation, resulting in inositol-1,4,5-trisphosphate (IP_3)-dependent calcium mobilisation [42-44]. This TxA_2-driven intracellular calcium mobilisation in turn facilitates integrin $\alpha_{IIb}\beta_3$ activation, thus promoting cytoskeletal reorganisation leading to platelet shape change [40]. Besides TxA_2-induced signalling, ADP represents another crucial platelet-derived second-wave mediator that amplifies platelet activation and recruitment. In this context, ADP-mediated platelet activation is promoted by binding to the platelet-specific G protein-coupled receptors $P2Y_1$ and $P2Y_{12}$ [45-48]. The activation of $P2Y_1$ via ADP stimulation leads to downstream activation of phospholipase C (PLC) β and the subsequent hydrolysation of phosphatidylinositol-4,5 bisphosphate (PIP_2) to IP_3 and diacylglycerol (DAG), resulting in intracellular calcium mobilisation and integrin $\alpha_{IIb}\beta_3$ activation. In addition, ADP-mediated $P2Y_{12}$ activation facilitates adenylyl cyclase inhibition, followed by phosphoinositide-3 kinase (PI3K) activation. Thereby, $P2Y_1$ and $P2Y_{12}$-induced downstream signalling promotes intracellular calcium mobilisation and cytoskeletal rearrangement, thus reinforcing platelet recruitment and subsequent aggregation (**Figure 3**) [46, 49, 50]. Beyond the release of different secondary mediators, α-granule secretion upon platelet activation leads to the release of various adhesion proteins, including fibrinogen, fibronectin, VWF, and TSP, that facilitate the recruitment of additional platelets from the circulation to the site of vascular injury. In addition to that, platelet degranulation promotes the translocation of additional integrin $\alpha_{IIb}\beta_3$ and the integrin β_3 subunit from α-granules to the platelet surface, thereby amplifying the adhesive capacity of activated platelets (**Table 1**) [33, 34]. Beyond recruitment, platelet aggregation represents another crucial step in the formation of a haemostatic plug, in order to prevent excessive haemorrhage. In this process, platelet aggregation is reinforced by binding of fibrinogen to activated integrin $\alpha_{IIb}\beta_3$ on the platelet surface, mediating the formation of fibrinogen bridges, resulting in platelet crosslinking. Due to the recruitment of additional platelets from the circulation to the site of vascular injury, an unstable cellular thrombus is formed, which is subsequently stabilised within the process of secondary haemostasis by the incorporation and crosslinking of fibrin [18, 23, 37].

1.1.3 Platelet-signalling in the secondary haemostasis

Plasma coagulation factors play a pivotal role within the process of secondary haemostasis. Thereby, initiation of the coagulation cascade facilitates the factor Xa-mediated cleavage of prothrombin into thrombin [51, 52]. The serine protease thrombin acts as a strong platelet

agonist, promoting platelet activation and recruitment by binding to the G protein-coupled protease-activated receptors 1 and 4 (PAR1 and PAR4) in human platelets, while thrombin-induced platelet activation in murine platelets is mediated by PAR3 and PAR4 (**Figure 3**). Besides its role in platelet activation, thrombin mediates the cleavage of fibrinogen to fibrin, which in turn is subsequently incorporated into the growing thrombus [40, 53, 54]. The subsequent crosslinking of fibrin results in the formation of a stabilising fibrin network, which is paralleled by the recruitment of RBCs and other blood cells to further stabilise the newly formed thrombus [55]. In addition to that, exposure of phosphatidylserine (PS) on the platelet surface upon activation is a crucial process to ensure the formation of stable three-dimensional thrombi to prevent excessive blood loss due to a vascular injury [56, 57]. PS exposure on the platelet membrane provides a procoagulant surface, leading to the formation of the prothrombinase complex, which in turn facilitates the cleavage of prothrombin into thrombin. In this context, platelets directly contribute to the local thrombin generation, which in turn promotes activation and subsequent recruitment of additional platelets from the circulation into the growing thrombus. Thus, PS-mediated thrombin generation plays a critical role in secondary haemostasis by amplifying thrombus formation and stabilisation at the site of vascular injury [23, 58].

1.1.4 The main platelet collagen receptor GPVI

1.1.4.1 Structure of GPVI

GPVI represents the main collagen receptor on platelets and plays a crucial role in platelet activation, in order to prevent excessive haemorrhage after vascular injury. Thereby, GPVI activation results in the induction of different intracellular signalling pathways, mediating integrin activation, α- and dense granule release, cytoskeletal reorganisation, procoagulant activity, as well as the activation and recruitment of additional platelets from the circulation [28, 29]. GPVI is a type I transmembrane protein of the immunoglobulin superfamily, with a molecular weight of 60–65 kDa [27].

Genetically, the gene for GPVI expression (*GP6*) is encoded on chromosome 19q13.4 within the human genome and consists of 8 exons (**Figure 4**) [59, 60]. GPVI is thereby exclusively expressed in megakaryocytes and platelets, with an average number of 3,000–4,000 copies per platelet in humans, respectively 4,500–5,500 in mice [61, 62]. On the platelet surface, GPVI is primary expressed in a monomeric form. However, due to diffusion processes and upon platelet activation, GPVI is capable to dimerise on the platelet surface [63, 64]. Structurally, the GPVI receptor is composed of two extracellular collagen-binding immunoglobulin (Ig) C2-like domains

(D1 and D2) located above a mucin-like stalk, a transmembrane region exhibiting a positively charged arginine, and a short cytoplasmic tail of 51 amino acids with a proline-rich binding motif for the SH3 domain of Src kinases Fyn and Lyn, as well as a calmodulin binding site [65-68]. In addition, the transmembrane domain is noncovalently linked via the positively charged arginine group to a homodimeric Fc receptor γ-chain (FcRγ), which exhibits an immunoreceptor, tyrosine-based activation motif (ITAM) [27, 69]. Upon GPVI activation, ITAM-dependent binding and activation of Syk facilitates the initiation of intracellular downstream signalling cascades (**Figure 4**) [60, 70, 71].

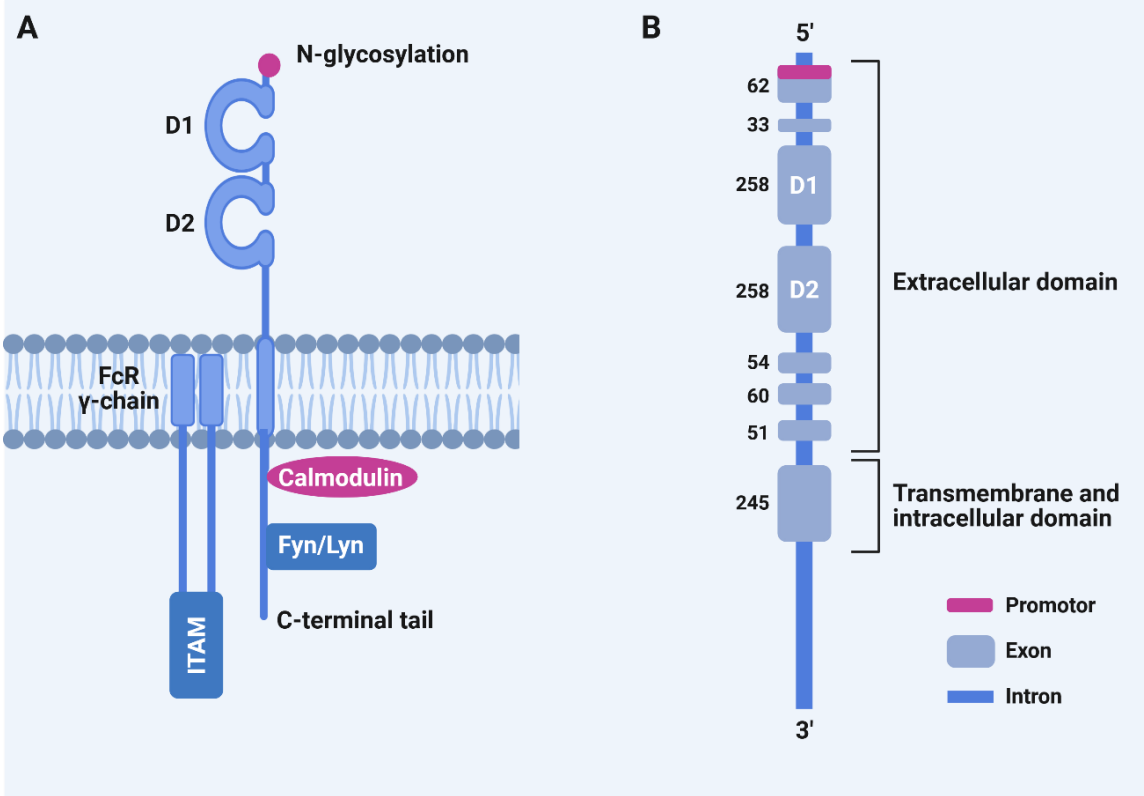


Figure 4. Structure of the main collagen receptor GPVI. (**A**) The main collagen receptor GPVI receptor is composed of two extracellular collagen-binding immunoglobulin (Ig) C2-like domains D1 and D2, a mucin-like stalk, a transmembrane region, and a cytoplasmatic tail of 51 amino acids with binding sites for the SH3 domain of Src kinases Fyn and Lyn, as well as for calmodulin. The transmembrane domain is noncovalently linked to a FcRγ-chain, which exhibits an ITAM sequence. (**B**) Genetically, the human *GP6* gene consists of 8 exons. Thereby, exon 1—7 encode for the extracellular domain, while exon 8 encodes for the transmembrane domain and the cytoplasmatic tail. FcRγ = Fc receptor γ-chain; GP = Glycoprotein; ITAM = Immunoreceptor tyrosine-based activation motif. Modified from [72, 73] (created with BioRender.com).

1.1.4.2 GPVI-mediated intracellular signalling pathways

As mentioned before, collagen represents the main GPVI ligand. Thereby, collagen binding to GPVI is mediated via a repetitive glycine-proline-hydroxyproline (GPO) sequence within the structure of fibrous collagen, which exhibits a pronounced high-affinity for the D1 domain of the dimeric form of GPVI. In contrast, collagen binding to the monomeric GPVI isoform is notably absent [74-76]. This highlights the critical role of GPVI dimerisation, a process which is predominantly facilitated via the D2 domain, to ensure sufficient collagen binding and thereby enabling subsequent GPVI-dependent platelet activation and aggregation [64, 77]. However, throughout the last years, several other ligands for GPVI have been identified. Beside collagen, binding of laminin, fibronectin, vitronectin, adiponectin, but also amyloid β 40 to GPVI has been reported by different studies [78-82]. Moreover, it was recently shown that GPVI directly contributes to thrombus growth and stabilisation via the interaction with fibrinogen and fibrin [83]. Besides natural GPVI ligands, several synthetic GPVI-specific ligands have been developed during the last decades. In this context, the synthetic collagen-related peptides (CRP) are capable of mimicking collagen-mediated GPVI activation by binding to GPVI via repetitive GPO motifs within their helical structure [84-86].

However, ligand binding to GPVI promotes intracellular downstream signalling, which is initiated by Src-dependent phosphorylation of the conserved tyrosine residuals within the ITAM sequence of the homodimeric FcRγ-chain (**Figure 5**) [87, 88]. ITAM-tyrosine phosphorylation is thereby mediated by the Src family kinases Lyn and Fyn, which facilitate the recruitment of Syk via its SH2 domains and subsequent activation due to Src kinase-dependent phosphorylation, as well as autophosphorylation [70, 71]. Syk activation results in downstream activation of the membrane adaptor protein linker of activated T cells (LAT) via phosphorylation, which in turn facilitates the recruitment of PLCγ2, the Bruton's tyrosine kinase (Btk), Grb2-related adaptor downstream of Shc (Gads), the leukocyte phosphoprotein of 76 kDa (SLP76), and PI3K, resulting in the formation of a downstream signalling complex at the cell membrane (signalosome) [70, 89-91]. In turn, LAT-mediated PI3K activation, promotes the generation of the second messenger phosphatidylinositol-3,4,5 trisphosphate (PIP_3) [89, 92, 93]. In this context, PIP_3 formation facilitates subsequent Btk recruitment, which becomes active via autophosphorylation and additional phosphorylation by Lyn. Subsequently, Btk mediates PLCγ2 recruitment to the membrane and subsequent activation by phosphorylation [94, 95]. After activation, PLCγ2 promotes the hydrolysation of PIP_2 into IP_3 and DAG, resulting in protein kinase C (PKC) activation and subsequent intracellular calcium mobilisation. These downstream signalling events culminate in α- and dense granule secretion, as well as integrin $\alpha_{IIb}\beta_3$ activation, thus promoting platelet activation and aggregation (**Figure 5**) [34, 59, 96-98].

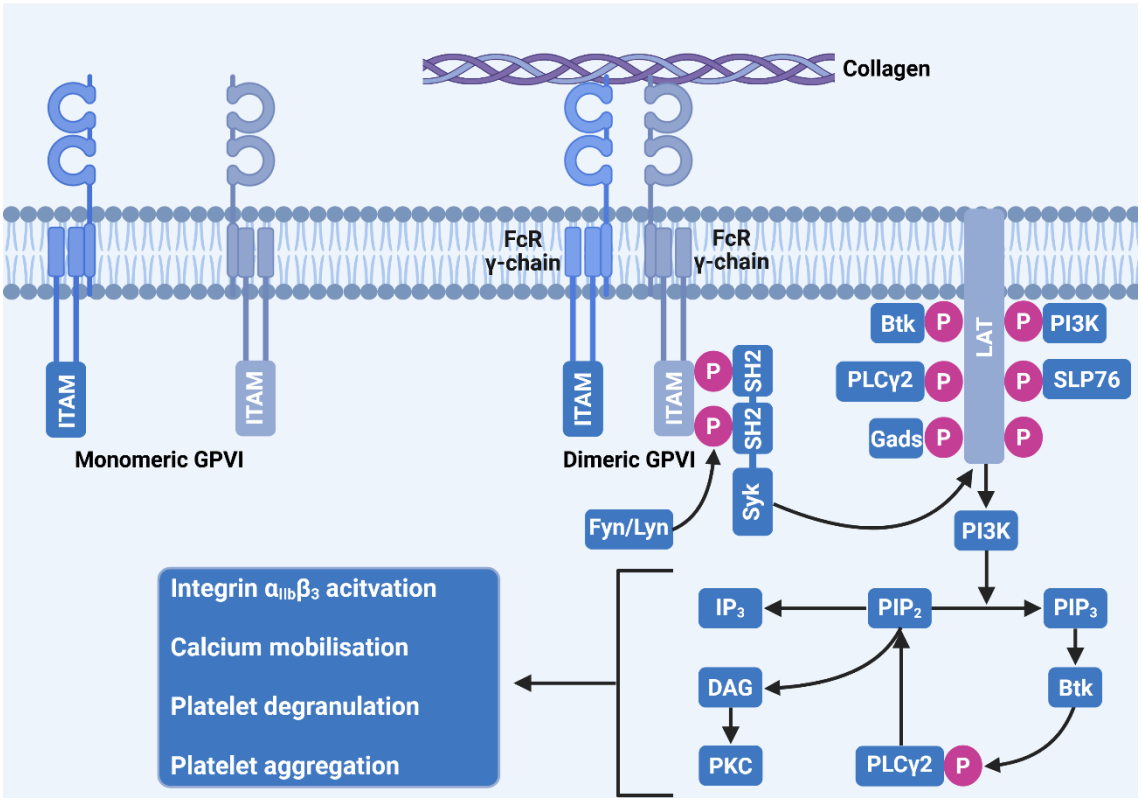


Figure 5. GPVI-mediated intracellular signalling pathways. Ligand binding to the dimeric form of GPVI promotes phosphorylation of the FcRγ ITAM sequence by the Src family kinases Fyn and Lyn. Thereby, ITAM phosphorylation facilitates recruitment and subsequent activation of Syk. Engagement of Syk initiates the formation of a downstream signalling complex composed of different kinases and adaptor proteins, including LAT, PLCγ2, Btk, Gads, SLP-76, and PI3K. Thereby, downstream activation of PLCγ2 promotes the formation of IP_3 and DAG, leading to PKC activation and subsequent intracellular calcium mobilisation. These downstream signalling events culminate in platelet degranulation, as well as integrin $\alpha_{IIb}\beta_3$ activation, thus promoting platelet activation and aggregation. Btk = Bruton tyrosine kinase; DAG = Diacylglycerol; FcRγ = Fc receptor γ; Gads = Grb2-related adaptor downstream of Shc; GP = Glycoprotein; IP_3 = Inositol-1,4,5-trisphosphate; ITAM = Immunoreceptor tyrosine-based activation motif; LAT = Linker of activated T cells; PI3K = Phosphoinositide-3 kinase; PIP_2 = Phosphatidylinositol-4,5 bisphosphate; PIP_3 = Phosphatidylinositol-3,4,5 trisphosphate; PKC = protein kinase C; PLC = Phospholipase C; SLP76 = Leukocyte phosphoprotein of 76-kDa. Modified from[3, 70] (created with BioRender.com).

1.1.4.3 Proteolytic GPVI shedding

Ligand binding, as well as pathophysiological shear stress, can initiate proteolytic cleavage of the GPVI receptor from the platelet surface [99-101]. This process, also referred to as receptor shedding, plays a pivotal role in regulating platelet responses upon activation, thus allowing platelets to adapt to different extrinsic conditions [101, 102]. Thereby, GPVI shedding from the platelet surface is mediated by the metalloproteinase A disintegrin and metalloprotease 10 (ADAM10), resulting in the loss of the ligand-binding site of the GPVI receptor by formation of a soluble ectodomain fragment (sGPVI) with an approximate size of 50–55 kDa [103-105].

Thus, ADAM10-mediated proteolytic cleavage of GPVI reduces the receptor surface abundance, resulting in an attenuated platelet reactivity. During the last decades, various studies reported significantly elevated plasma levels of sGPVI in patients with different thrombotic disorders, including myocardial infarction, ischaemic stroke, or the acute coronary syndrome [106-108]. Additionally, under other pathophysiological conditions such as rheumatoid arthritis, Alzheimer's disease, or sepsis, circulating sGPVI was found to be enhanced [100, 109, 110]. Therefore, sGPVI represents a potent marker for platelet activation under pathophysiological conditions, as well as for the prediction of bleeding complications. Thus, proteolytic GPVI shedding reflects a pivotal platelet-specific biomarker for the clinical risk stratification for thrombotic disorders [106, 111, 112].

1.1.4.4 Pharmacological targeting of platelet GPVI-signalling

Due to its pivotal role in platelet activation, targeting platelet GPVI function has emerged as a promising approach to develop novel therapeutic interventions for thrombotic disorders. Increased expression of GPVI has been observed in patients with acute coronary syndromes (ACS), reflecting an enhanced thrombotic risk and identifying GPVI as a potential biomarker for risk stratification [106, 113]. Therefore, pharmacological inhibition of GPVI-signalling is currently under the scope of investigation as a novel antithrombotic approach to reduce cardiovascular events [106, 114-116]. Thereby, experimental studies targeting GPVI activation either by using a pharmacological approach or via GPVI-deficient mice revealed an impact of GPVI-signalling on different diseases including arterial thrombosis, ischaemic stroke, myocardial infarction, and acute lung injury [79, 117, 118]. A recent study by Navarro *et al*. reported protection against arterial thrombosis and ischaemic stroke in mice after GPVI blockade with the novel humanised platelet GPVI Fab inhibitor EMA601 [117]. In addition, administration of the immunodepleting GPVI antibody JAQ1 led to attenuated stroke development in a murine cerebral artery occlusion model [119]. In this context, a randomised phase 1b/2a clinical trial (trial registration: NCT03803007) using the humanised platelet GPVI Fab fragment inhibitor Glenzocimab (ACT017) revealed beneficial effects in acute ischaemic stroke patients. In this study, Glenzocimab administration resulted in reduced intracerebral haemorrhage, as well as an overall improved mortality rate [114]. Another promising therapeutic approach is the use of GPVI fusion proteins. GPVI-Fc, is a fusion protein consisting of a Fc fragment fused to endogenous platelet GPVI. Mechanistically, GPVI-Fc prevents GPVI binding to its ligand by covering the exposed collagen after a vessel wall injury. Thus, GPVI-Fc impedes GPVI-mediated platelet activation and aggregation. Thereby, administration of GPVI-Fc in a mouse model of acute myocardial

infarction revealed a protective effect, indicated by a reduced infarct size and preserved left ventricular function [79]. Beyond this, a randomised phase II clinical trial with the GPVI-Fc fusion protein Revacept showed an improved outcome in patients with symptomatic carotid stenosis (trial registration: NCT01645306) [116, 120]. In 2023, Burkard *et al*. demonstrated that targeting GPVI either via JAQ1 treatment or by the use of GPVI deficient mice offered protection against neutrophil-mediated pulmonary inflammation in a model of LPS-induced acute lung injury [118]. These pre-clinical and clinical data reinforce the relevance of GPVI as a promising target for developing novel platelet-specific therapies to offer protection against different thrombotic and cardiovascular disorders.

1.2 The abdominal aortic aneurysm

An abdominal aortic aneurysm (AAA) represents a life-threatening atherosclerosis-related cardiovascular disorder, which is associated with a substantial mortality rate upon rupture [121-123]. Pathologically, an AAA is characterised by a progressive and irreversible dilation of all three layers (tunica intima, media, and adventitia) of the abdominal aortic vessel wall.

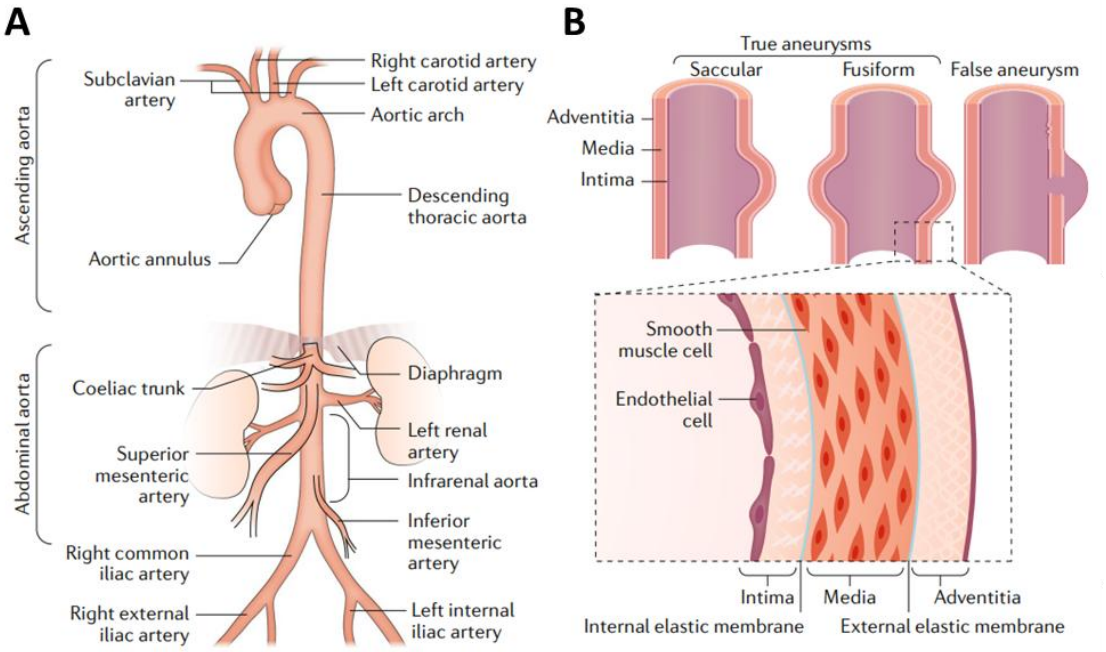


Figure 6. Categorisation of abdominal aortic aneurysms. (**A**) Schematic overview of the ascending and abdominal aorta. Around 80% of all diagnosed AAAs are located beneath the renal arteries (infrarenal), while aneurysm formation within the thoracic, juxtarenal, or suprarenal segment are rarely present. (**B**) AAAs can be categorised upon their morphological characteristics. Fusiform aneurysms, are defined by the circumferential dilation of the aortic wall, while in saccular aneurysms, the aortic wall integrity is only affected one-sided. AAA = Abdominal aortic aneurysm. Modified from [124].

Thereby, AAAs predominantly occur within the infrarenal region of the abdominal aorta, accounting for more than 80% of all diagnosed AAA cases [125, 126] (**Figure 6A**). In contrast, aneurysm formation located within the thoracic, juxtarenal, or suprarenal region of the aorta is rarely present [124, 127-129]. Clinically, an AAA is diagnosed when the infrarenal aortic diameter reveals a 1.5-fold enlargement, respectively exceeds a dilation of more than 30 mm, in comparison with a normal, undilated suprarenal segment of the aorta [126, 130, 131]. Based on these clinical thresholds, the AAA incidence can be further categorised into small-size (< 55 mm in aortic diameter) and large-size aneurysms (≥ 55 mm in aortic diameter), in order to stratify whether clinical intervention is necessary [121, 132, 133]. In addition to that, AAAs can be classified according to their morphological characteristics. Thus, AAAs can be divided into fusiform, characterised by the circumferential dilation of the aortic wall, and saccular aneurysms, where the aortic wall integrity is affected in a one-sided manner [134, 135] (**Figure 6B**).

However, a solid risk stratification with regard to AAA growth is crucial, as with the predominantly asymptomatic expansion of the aortic lumen, the risk for a fatal rupture increases exponentially, leading to mortality rates of up to 80–90% in affected AAA patients [136-138]. Thus, the AAA prevalence is mainly driven in an age-dependent manner, while other independent risk factors including male sex, smoking, obesity, hypertension, hypercholesterolaemia, coexisting cardiovascular diseases, as well as a positive family history further reinforce the risk for AAA development (**Table 2**) [127, 139-144].

Table 2. Risk factors for AAA formation. AAA = Abdominal aortic aneurysm. Modified from [139].

Risk factor	**Relative risk**
Male sex	5.93
Hypertension	1.66
Per 20 mmHg enhancement in systolic blood pressure	1.14
Per 20 mmHg enhancement in diastolic blood pressure	1.28
Current smoking	4.87
Former smoking	2.10
Positive family history for AAA	3.80
Cardiovascular and other disorders	
Coronary artery disease	2.29
Peripheral artery disease	2.50
Diabetes	0.58

Pathophysiologically, the AAA formation is predominantly characterised by three key hallmarks (**Section 1.2.2**). (I) The progressive remodelling of the aortic wall, including elastin fragmentation, as well as loss of vascular smooth muscle cells (VSMCs). (II) A chronic inflammation within the aneurysm segment, mediated by the recruitment of circulating inflammatory cells (e.g. neutrophils and macrophages) to the site of AAA formation [145-147]. (III) The formation of a platelet-rich so-called intraluminal thrombus (ILT), which exhibits a multi-layered structure and is present in approximately 75% of all patients diagnosed with AAA [148, 149]. These pathophysiological mechanisms accumulate into an adversely affected aortic wall integrity, thus facilitating the progressive dilation of the respective aortic segment. As mentioned before, risk stratification with regard to AAA growth plays a crucial role within the clinical practice, in order to prevent fatal rupture. Therefore, when the aortic diameter expansion exceeds pre-defined clinical thresholds the only effective treatment option in order to target AAA growth remains surgical intervention either via an endovascular aneurysm repair (EVAR) or open aortic repair (OAR). In this context, commonly aneurysms with an aortic diameter of ≥ 55 mm are considered for clinical intervention [150-153]. Despite considerable efforts during the last years to develop pharmacological approaches in order to attenuate aneurysm growth, no drug-based therapy has demonstrated clinical efficacy yet. Although, beneficial effects of promising pharmacological candidates have been reported in cohort studies with smaller sample sizes, confirmation by larger randomised controlled trials has not been successful to date. As several clinical trials failed to effectively reduce aneurysm progression, this underlines that translating preclinical findings into a non-invasive drug-based treatment remains challenging [154-156]. Therefore, investigating the underlying mechanisms that provoke AAA initiation and progression is crucial to identify promising novel targets. This in turn represents a critical step towards developing potential pharmacological approaches that sufficiently attenuate AAA growth.

1.2.1 Epidemiology and prevalence of abdominal aortic aneurysms

The global prevalence of AAA development among individuals with an age ranging from 30–79 years was assessed at approximately 0.92%, resulting in a total of 35.12 million patients diagnosed for AAA worldwide (2019). In addition to that, aortic aneurysms were the tenth leading cause of death among CVDs worldwide with a total number of 160,000 AAA-related deaths in 2019 [157, 158]. In this context, the global burden of AAA, reflected by the absolute disability-adjusted life-years (DALYs), increased from 18.84 per 100,000 population in 1990 to an estimated absolute DALY burden of 31.08 per 100,000 population in 2021. Despite this, the

concurrent relative decline in the age-standardised DALY rate (ASDR), when considering demographic changes, from 48.7 (1990) to 36.54 (2021) clearly highlights the beneficial effects of progress in diagnostic and therapeutic strategies for the treatment of CVDs [159]. Meanwhile, the AAA incidence was shown to be 4–5-fold higher in men compared to women, translating to an estimated prevalence of 1.46% in men, respectively 0.39% in women. This clearly marks a sexual dimorphism in the onset and progression of the AAA disease [158]. As mentioned beforehand, besides other independent risk factors, such as obesity or hypertension, the AAA prevalence is highly age-dependent. In this context, the incidence was shown to increase from 3.3%–7.6% in individuals with an age of more than 60 years up to more than 10% among individuals over 80 years of age [160, 161]. Besides ageing, smoking represents an additional prominent and independent risk factor, that drives AAA development. Thus, lifetime smoking substantially increases the AAA prevalence, conferring a 4-fold higher risk in relation to non-smokers, accompanied by an acceleration in aneurysmal growth of more than 10% [162-164]. However, the overall clinical outcome for the treatment of AAA progression has been markedly improved over the last decades, mainly driven by the expansion of AAA screening programs, improved clinical care, and the use of minimally invasive surgical repair strategies. Despite this progress, the universal application of these improvements in the clinical routine is still lacking, as inequities between sexes, races, and ethnic groups remain evident [165-167].

1.2.2 Pathophysiological mechanisms of AAA formation and progression

The aorta represents the largest artery of the vascular system and is crucial for the systemic distribution of oxygenated blood from the left ventricle in order to ensure perfusion of the surrounding organs [168]. Thereby, the aorta directly contributes to systemic blood pressure regulation by buffering the cardiac pulsatile output during systole, due to the compliant aortic wall structure, derived from both muscular and elastic wall components [169-171]. Reflecting its critical physiological and clinical role, the joint guidelines from the European Association for Cardio-Thoracic Surgery (EACTS) and the Society of Thoracic Surgeons (STS) have recently designated that the aorta should be considered an independent organ of the cardiovascular system. This recognition highlights the pathophysiological relevance of the aorta, thus fostering medical research into novel therapeutic approaches for aortic diseases [172].

Structurally, the aortic wall is composed of three distinct concentric layers: the tunica intima, tunica media, and tunica adventitia. Thereby, the tunica intima represents the luminal layer primarily consisting of a monolayer of endothelial cells, thus serving as an interface between the aortic wall and the circulating blood. By the release of endothelial-derived inhibitors, such as NO

and PGI_2, the endothelium prevents the activation of platelets from the circulation, thus acting as an antithrombotic surface [17, 173]. In contrast, the tunica media (middle layer) is primarily composed of VSMCs interspread with a meshwork of ECM proteins, consisting of elastin and collagen fibres. The outer layer of the aortic wall, the tunica adventitia, is predominantly composed of connective tissue, fibroblasts, and a dense network of microvessels, the *vasa vasorum*, which maintain sufficient oxygen and nutrient supply to the aortic wall [169, 173-176]. Thereby, these different vascular layers are capable via, either vasodilation or vasoconstriction, of rapidly adapting to hemodynamic fluctuations, as well as acute alterations in systemic blood pressure. However, with increasing age the abdominal aorta undergoes structural remodelling which is characterised by progressive wall thickening, luminal expansion, enhanced oxidative stress, and calcification of the aortic tissue, accompanied with profound alterations in collagen, elastin, and VSMC composition [168, 170, 177-179]. In this context, arterial stiffening, as well as structural wall remodelling represent major hallmarks of vascular aging and are considered as independent risk factors for various CVDs, including hypertension, myocardial infarction, stroke, and the formation of AAA [179, 180]. As mentioned beforehand, the pathophysiology of AAA formation and progression is predominantly characterised by three key features: (I) the progressive remodelling of the aortic wall, (II) a chronic inflammation within the aneurysm segment, mediated by the recruitment of circulating inflammatory cells, and (III) the formation of a platelet-rich ILT (**Figure 7**) [181-183].

(I) Progressive aortic wall remodelling. This process involves the degradation and reorganisation of the ECM, thus directly compromising aortic wall integrity due to VSMC loss and the proteolytic degradation of structural key components within the tunica media, predominantly of elastin and collagen fibres [125, 146, 147, 184]. In this context it was shown that this proteolytic degradation of the ECM is mainly driven by the enhanced activity of matrix metalloproteinases (MMPs) within the aortic tissue, which is due to dysregulation between MMPs and their endogenous inhibitors, the tissue inhibitors of metalloproteinases (TIMPs) [185-187]. In particular, TIMP1 and TIMP2 were found to be highly downregulated in aortic tissue of AAA patients with large sized aneurysms with a diameter expansion of more than 55 mm [186]. This is paralleled by a significant upregulation of MMP1, MMP2, MMP9, and MMP12 in aortic aneurysms, thus directly attenuating aortic wall integrity by proteolytic degradation of ECM components [185, 187-191]. Thereby, MMP1 is involved in the degradation of type I and III collagen, while MMP2, MMP9, and MMP12 are capable of cleaving both type IV collagen and elastin [125, 192]. Beyond this, the sustained proteolytic activity and oxidative stress compromise VSMC-matrix interactions, facilitating VSMC detachment and subsequent apoptosis [193-196]. These remodelling

processes culminate into the thinning and weakening of the tunica media, thus negatively affecting aortic vessel wall integrity and fostering aneurysm growth and rupture risk (**Figure 7**).

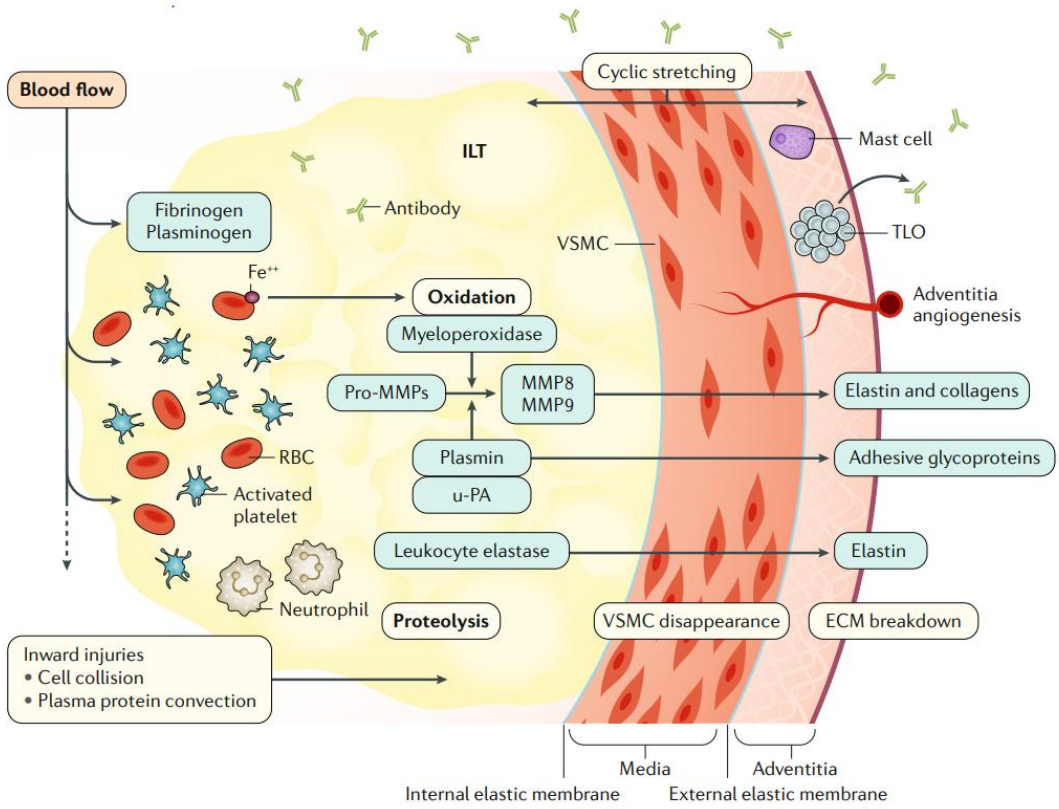


Figure 7. Pathophysiological mechanisms of AAA formation and progression. The AAA formation is predominantly characterised by three major pathophysiological hallmarks. (I) The progressive remodelling of the aortic wall, mediated by an enhanced MMP activity within the aortic tissue, due to dysregulation of TIMPs. The proteolytic ECM degradation accumulates in elastin and collagen fragmentation, as well as VSMC loss, resulting in a compromised aortic wall integrity. (II) A chronic inflammation within the aneurysm segment, mediated by the recruitment of circulating inflammatory cells (e.g. neutrophils and macrophages) to the site of AAA formation. Leukocyte infiltration promotes MMP activity and the formation of ROS, thus reinforcing the progressive aortic wall degradation. (III) The formation of a platelet-rich ILT. AAA = Abdominal aortic aneurysm; ECM = Extracellular matrix; ILT = Intraluminal thrombus; MMP = matrix metalloproteinase; ROS = Reactive oxygen species; TIMP = Tissue inhibitors of metalloproteinases; VSMC= Vascular smooth muscle cells. Modified from [124].

(II) Chronic inflammation within the aneurysm segment. As mentioned beforehand, the AAA pathology is tightly linked to chronic inflammation, characterised by the infiltration of immune cells into both the aortic wall and the ILT [197, 198]. Infiltrating immune cells actively drive aneurysm progression by the release of proinflammatory cytokines, chemokines, reactive oxygen species (ROS), as well as ECM degrading proteinases such as MMPs. Thus, promoting a persistent inflammatory milieu that in turn amplifies further immune cell recruitment to the growing aneurysm [199-203]. Thereby both, innate immune cells including macrophages,

neutrophils, natural killer cells, mast cells, and dendritic cells as well as adaptive immune cells such as T and B lymphocytes have been identified within the aneurysm tissue and are implicated in fostering aneurysm formation and expansion (**Figure 7**) [198, 204-211]. In this context, invading macrophages and neutrophils were shown to be the major sources for ROS, such as superoxide ($O_2^{\bullet -}$) or hydrogen peroxide (H_2O_2), resulting in enhanced oxidative stress within the aneurysm segment. ROS generation directly contributes to the progressive aortic wall remodelling by facilitating VSMC apoptosis and upregulation of MMPs [124, 212, 213]. In addition to that, endothelial dysfunction mediated by endothelial nitric oxide synthase (eNOS) uncoupling leads to a reduced NO bioavailability [214]. This in turn culminates into an enhanced expression of intracellular adhesion molecules, including the vascular adhesion molecule-1 (VCAM-1), intracellular adhesion molecule-1 (ICAM-1), and E-selectin. This is paralleled by the enhanced expression of chemokines such as the macrophage chemoattractant protein-1 (MCP-1), as well as interleukin 8 (IL8), thus reinforcing the recruitment of further immune cells from the circulation into the growing aneurysm [214-218]. Moreover, in the recent years, activation and subsequent infiltration of neutrophils into the aortic tissue has emerged as an additional major driver of the AAA pathology. Thereby, the release of neutrophil-derived elastase, MMP9, and ROS fosters the proteolytic degradation of the ECM, as well as VSMC loss (**Figure 7**) [219, 220]. Besides this, the excessive activation of neutrophils can further promote the formation of so-called neutrophil extracellular traps (NETs), meshworks mainly composed of chromatin, histones (e.g. citrullinated histone 3 (citH3)), neutrophil-derived elastase, MMP9, and myeloperoxidase (MPO) [221-223]. In regard to this, it was reported that AAA patients revealed an elevated content of NETs in both the aortic vessel wall and within the ILT, indicated by significantly enhanced citH3 plasma and tissue levels. This was paralleled by a high abundance of citH3 positive neutrophils in the aortic tissue of AAA patients [224]. Thereby, this AAA-related reinforcement of NET formation, directly provides a persistent proinflammatory environment, that in turn promotes the recruitment of further immune cells into the growing aneurysm.

(III) The formation of a platelet-rich ILT. The ILT represents a platelet- and RBC-rich dynamic neo-tissue, which is present in approximately 75% of patients diagnosed with AAA (**Figure 8A**). Thereby, the ILT provides a proteolytic and oxidative environment, thus driving the progressive aortic wall degradation, while being continuously renewed by the circulating blood [181, 182, 225]. Structurally, the ILT is characterised by a complex predominantly three-layered architecture (**Figure 8B**) [148]. The medial and abluminal layers of the ILT are largely acellular and characterised by progressive fibrinolytic activity, interspread with extracellular matrix components and a low number of VSMCs. In contrast, the luminal layer consists mainly of a dense fibrin network enriched with platelets, leukocytes, and RBCs [226-228].

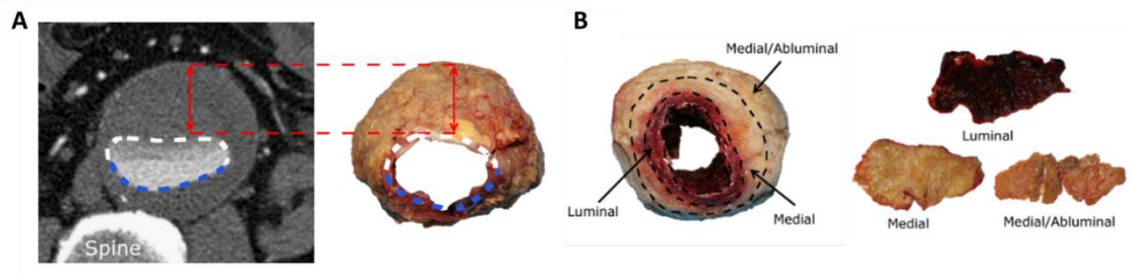


Figure 8. Morphological structure of a three-layered ILT. (**A**) Representative CT image of a multi-layered ILT. (**B**) The ILT structure is characterized by a complex predominantly three-layered architecture, which can be divided in a luminal, medial and abluminal layer. Thereby, the luminal layer consists out of a dense fibrin network enriched with platelets, leukocytes, and RBCs. The medial and abluminal layer are predominantly acellular, interspread with different ECM components and a low number of VSMCs. ECM = Extracellular matrix; ILT = Intraluminal thrombus; VSMC = Vascular smooth muscle cells. Modified from [148].

Thereby, the cellular components of the luminal layer are permanently renewed by the constant incorporation of blood cells from the circulation [181]. Due to the recruitment of inflammatory cells such as neutrophils, and macrophages, as well as RBCs and platelets a highly localised oxidative and proinflammatory environment characterised by the presence of cytokines, ROS, and ECM degrading proteases is evident within the ILT tissue. This persistent inflammation acts as a potent paracrine driver for the aneurysm progression by reinforcing proteolytic degradation of ECM components e.g. via MMP9 and loss of VSMCs, thus further compromising aortic wall integrity [228, 229]. Thereby, ECM degrading biomolecules are capable of diffusing from the luminal layer to the aortic vessel wall via a dense network of so-called canaliculi, which traverse the ILT tissue [227, 230]. Besides its well-established contribution to inflammation and aortic wall degradation, different studies reported a biomechanical protective role of the ILT in patients with AAA pathology.

In this context it was shown that the ILT size adversely correlates with both the peak wall stress and mean wall stress within the aneurysm segment. However, it has to be considered that the ILT size is highly linked to an increased aneurysm growth as well as elevated risk for aortic rupture. Therefore, the proinflammatory and proteolytic contribution of the ILT in AAA progression might prevail over its putative biomechanical protective effects by attenuating aortic wall stress [231, 232]. This highlights the ambivalent role of the ILT as a bioactive neo-tissue for aneurysm growth and aortic rupture in patients with AAA.

1.2.3 Preclinical and clinical implication of platelet function for AAA formation and progression.

Besides their fundamental role in haemostasis, it has become apparent that dysregulated platelet function and activity are prompt driver for the progression of various CVDs, including stroke, atherosclerosis, and myocardial infarction [6, 107, 233-235]. Different studies reported decreased platelet counts in patients diagnosed with AAA. Thereby, platelet counts were shown to adversely correlate with an increase in aneurysm size. Especially in AAA patients with large-size aneurysm, which are defined by an aortic diameter of >55 mm, platelet counts were found to be significantly reduced, compared to small-size aneurysms [236, 237]. In this context, reduced platelets counts can be linked to the incidence of a consumption coagulopathy, due to platelet hyperreactivity, indicated by enhanced plasma levels of soluble P-selectin in AAA patients [181, 238, 239]. In addition to that, excessive recruitment of platelets from the circulation into the ILT, may also contribute to reduced platelet counts observed in the AAA pathology [181, 240]. Nevertheless, the underlying mechanisms by which platelets may contribute to the formation and progression of aortic aneurysms are not fully clarified yet.

However, throughout the last years various preclinical studies have reported beneficial effects of antiplatelet therapies on aneurysm growth and rupture risk in different experimental animal models for AAA formation (**Table 3**) [241]. Treatment of mice with clopidogrel, a potent $P2Y_{12}$ inhibitor impairing ADP-mediated platelet activation and aggregation, resulted in significantly attenuated aortic diameter progression in the angiotensin II (AngII) mouse model for experimentally induced AAA formation. Mechanistically, reduced aneurysm growth was due to a reduction in elastin fragmentation and MMP activity, accompanied by a diminished migration of macrophages into the aneurysmal segment [242]. In contrast to this, clopidogrel application in mice already exhibiting an established AAA failed to effectively restrict aortic diameter progression [243]. However, the risk of rupture-induced death was shown to be significantly reduced in AAA mice treated with clopidogrel, compared to the placebo group. This finding was paralleled by a reduction in platelet and macrophage recruitment, as well as MMP activity within the aneurysmal segment (**Table 3**) [243]. Comparable findings regarding the effect of the commonly used COX1 inhibitor aspirin (acetylsalicylic acid (ASA)) have been reported. The application of ASA as an antiplatelet therapy in mice with an established AAA showed no beneficial effects on the subsequent aneurysm growth. As already demonstrated for clopidogrel, ASA treatment significantly lowered the risk of aortic rupture in the AngII mouse model, accompanied by attenuated macrophage infiltration and MMP activity within the aortic tissue [243]. However, a recent study by Liu *et al*. revealed that dual antiplatelet therapy with ASA and the $P2Y_{12}$ inhibitor ticagrelor effectively limited the aortic diameter expansion in mice with an

established AAA (AngII mouse model). This was linked to reduction in vascular inflammation and MMP content in the aneurysmal segment (**Table 3**).

Table 3. Effects of antiplatelet therapies on experimental induced AAA formation in mice and rats. AAA = Abdominal aortic aneurysm; ASA = Acetylsalicylic acid (Aspirin); COX1 = Cyclooxygenases-1; ILT = Intraluminal thrombus; MMP = Matrix metalloproteinase; ROS = Reactive oxygen species. Modified from [241].

Antiplatelet therapy	Outcome	Proposed mechanism
Clopidogrel ($P2Y_{12}$ inhibitor) [242]	↓ Aortic diameter progression ↓ Elastin fragmentation ↓ ROS generation ↓ Macrophage infiltration and MMPs. – Rupture risk	Inhibition of platelet activation reduces inflammation-mediated AAA formation
Clopidogrel ($P2Y_{12}$ inhibitor) or ASA (COX1 inhibitor) [243]	↓ Rupture-induced death ↓ Aortic thrombus formation ↓ Platelet accumulation ↓ Inflammatory cytokine production ↓ Macrophage accumulation ↓ MMP activity – Aortic diameter progression	Antiplatelet therapy reduces rupture risk but not aortic diameter progression in established AAA
Ticagrelor ($P2Y_{12}$ inhibitor) and ASA (COX1 inhibitor) (Dual therapy) [241]	↓ Aortic diameter progression ↓ AAA incidence ↓ Aortic wall inflammation ↓ MMP synthesis	Combined platelet inhibition reduces wall inflammation and elastin fragmentation
Abciximab (Integrin $\alpha_{IIb}\beta_3$ inhibitor) [181]	↓ Aortic diameter ↓ILT area	Prevention of ILT propagation and platelet-mediated release of procoagulant factors

Conversely, the application of single antiplatelet treatment with either ASA, or ticagrelor alone failed to effectively restrict aneurysm progression [241]. Beyond this, directly targeting platelet activation in a xenograft transplant model in rats by using abciximab, an integrin $\alpha_{IIb}\beta_3$ inhibitor, resulted in a restricted ILT formation and aneurysm expansion, paralleled by a reduction of platelet-mediated release of procoagulant factors [181].

These data highlight the relevance of platelet activation and function in the progression of the AAA pathology, as well as the potential of antiplatelet therapies to effectively attenuate aneurysm growth and rupture risk. Despite compelling preclinical evidence, the clinical translation of these findings has proven difficult, as the efficiency of antiplatelet therapies in the

context of the AAA pathology is still a subject of an ongoing debate [241, 244]. For instance, a randomised controlled trial using low-dose ASA revealed no beneficial effects on small-size aneurysms with an aortic diameter of < 40 mm [245]. Moreover, administration of low-dose ASA in another clinical trial failed to attenuate the risk of aortic rupture in patients with AAA and in contrast, was shown to be associated with an increased mortality post-rupture [156]. Conversely, other clinical studies demonstrated that treatment with low-dose ASA was capable of effectively restricting aortic diameter progression of small-size aneurysm with an initially aortic diameter of 35 mm, respectively 39 mm [246]. In line, pharmacological intervention with ASA in AAA patients with mid-size aneurysms of 40–49 mm provided evidence to be associated with an attenuated aortic diameter expansion [245]. However, these contradictory results highlight the relevance of further preclinical and clinical investigations of the underlying mechanisms of the AAA pathology, in order to identify novel therapeutic targets for the AAA pathology.

1.3 Aim of the study

The AAA pathology is characterised by an asymptomatic, progressive dilation of the abdominal aorta, which substantially increases the risk of fatal rupture over time. Once the aneurysmal diameter exceeds established clinical thresholds, surgical intervention remains the only treatment option, as no pharmacological therapy has been shown to effectively attenuate aneurysm growth to date. Although several promising candidates have been investigated in recent years, successful clinical translation has remained elusive, as multiple trials have failed to achieve the primary endpoint of limiting aneurysm expansion. Consequently, the evaluation of novel therapeutic targets in *in vivo* models of experimentally induced AAA continues to be of critical importance for advancing the development of effective pharmacological interventions against AAA progression. In recent years, accumulating evidence has revealed that dysregulated platelet function not only acts as a key driver of AAA progression but also represents a promising therapeutic target for pharmacological interventions aimed to effectively restrict aneurysm growth. However, the molecular and cellular mechanisms by which platelets modulate AAA formation remain not fully understood. Therefore, the aim of this study was to further investigate the underlying platelet-mediated effects on aneurysm growth by utilising different *in vivo* mouse models of experimental induced AAA formation, in order to identify novel platelet-specific targets.

1.3.1 Crosstalk of platelets with macrophages and fibroblasts aggravates inflammation, aortic wall stiffening, and osteopontin release in abdominal aortic aneurysm

The aim of this study was to investigate the overall impact of platelets on AAA formation and progression, especially on inflammation and ECM remodelling of the aortic tissue. Therefore, administration of a platelet-depleting antibody in experimental induced AAA formation using the porcine pancreatic elastase infusion (PPE) mouse model over a time course of 10 days was conducted. Subsequent analyses focused on aortic diameter progression and elastin integrity. In addition, transcriptional profiling of aortic tissue from platelet-depleted PPE mice was performed to assess proinflammatory cytokine (*Il1b, Il6, Il8, Il10, Il12, Ccl2,* and *Tnf-a*) and stiffness-related (*Mmp2, Mmp9, Col1a1, Col3a1, Eln,* and *Spp1*) gene expression. Beyond this, platelet function during AAA pathogenesis was characterised by analysing platelet degranulation, integrin $\alpha_{IIb}\beta_3$ activation, and procoagulant activity in two different established *in vivo* models –the AngII and PPE mouse models– of experimental induced AAA formation, as well as in AAA patients.

1.3.2 GPVI-mediated platelet activation and procoagulant activity aggravate inflammation and aortic wall remodelling in abdominal aortic aneurysm

Due to its pivotal role in platelet activation, targeting platelet GPVI has emerged as a promising approach for developing novel therapeutic interventions for thrombotic disorders. For instance, GPVI-signalling was reported to be associated with the onset and progression of different CVDs, such as myocardial infarction, and stroke. Therefore, the underlying effects of GPVI-mediated platelet activation on AAA formation and progression were investigated, in order to evaluate whether GPVI is a potential target to restrict aneurysm growth. GPVI-deficient mice were analysed in two different experimental models for AAA formation – the PPE and external (e)PPE mouse model – over a time course of 28 days with regard to aortic diameter progression. Moreover, the impact of GPVI-signalling on modulating the early inflammatory response (day 7) during AAA development was investigated by evaluating neutrophil and macrophage infiltration into aneurysmal tissue, the formation of NETs, levels of different circulating cytokines (IL1α, IL1β, IL6, IL10, IL17A, INF-γ, and GM-CSF), and the formation of platelet–leukocyte aggregates across different leukocyte subsets. In parallel, progressive ECM remodelling in GPVI-deficient PPE mice was assessed by quantifying aortic intima/media thickness, elastin degradation, and plasma concentrations of osteopontin (OPN), MMP2, and MMP9. As a first translational approach for a therapeutic intervention a GPVI-blocking antibody was administrated following experimental induced AAA formation, in order to evaluate whether directly targeting GPVI is capable of effectively restricting aneurysm growth in the ePPE mouse model.

1.3.3 Revacept (GPVI-FC) treatment attenuates experimental induced abdominal aortic aneurysm formation in mice

Although several promising candidates for a pharmacological intervention in the AAA pathology have been investigated in recent years, successful clinical translation remains elusive. Multiple clinical trials evaluating drug-based therapies have failed to meet the primary endpoint of effectively limiting AAA growth and progression. Consequently, *in vivo* studies using experimental animal models of AAA formation remain essential in order to identify novel therapeutic targets and advance the development of pharmacological strategies aimed at restricting aneurysm progression. Based on the mechanistical insides regarding the impact of GPVI-signalling on AAA formation and progression (**Section 1.3.2**), the initial translation approach from the previously mentioned study was extended by investigating whether Revacept is capable of effectively attenuating aneurysm growth. Mechanistically, Revacept (GPVI-Fc) binds to the exposed collagen, thus preventing GPVI binding to collagen and the

subsequent GPVI-mediated platelet activation, and aggregation. Given that Revacept treatment already demonstrated a beneficial effect in symptomatic carotid stenosis patients in a randomised phase II clinical trial, the effect of Revacept on AAA progression was investigated in a preclinical setting within this study. Therefore, Revacept was administrated over a time course of 28 days in the ePPE mouse model for experimental AAA induction to evaluate whether a prophylactic treatment with Revacept effectively addresses aneurysm growth *in vivo*. Thus, ePPE operated Revacept-treated mice were analysed with regard to overall survival, aortic diameter progression, and AAA incidence. Additionally, the effects of Revacept application on basal platelet function were assessed in these mice by analysing platelet degranulation, integrin $\alpha_{IIb}\beta_3$ activation, glycoprotein exposition, as well as procoagulant activity.

2 Material and methods

In the following section only the materials and methods are listed, which are not included within the publications shown in this dissertation.

Publications:

"GP VI–Mediated Platelet Activation and Procoagulant Activity Aggravate Inflammation and Aortic Wall Remodeling in Abdominal Aortic Aneurysm" (*ATVB*, 2024)

"Crosstalk of platelets with macrophages and fibroblasts aggravates inflammation, aortic wall stiffening, and osteopontin release in abdominal aortic aneurysm" (*CVR*, 2024)

2.1 Material

2.1.1 Experimental animals

Humanised *(h)Gp6*$^{+/+}$ (C57BL/6N-*Gp6*$^{tm1(hGP6)geno}$*/AdcorNEU*) mice were kindly provided by Prof. Dr. Götz Münch (AdvanceCOR GmbH, Martinsried, Germany). Mice were bred and kept in the animal facility (ZETT) of the Heinrich-Heine-University Duesseldorf. For the analysis of experimental indued AAA formation, utilising the ePPE mouse model, *hGp6*$^{+/+}$ with an age of 10–12 weeks were used. As female mice exhibit a reduced inducibility of experimental AAA formation due to cyclical hormonal fluctuations only male mice were operated [247]. For the analysis of basal platelet function of naive mice C57BL/6N (WT) and *hGp6*$^{+/+}$ mice with an age of 10–12 weeks were used. All mice were kept under standard laboratory specific pathogen-free (SPF) conditions in Macrolon cages type III with *ad libitum* access to food (standard laboratory diet) and water in an environmentally controlled room at 22 ± 1 °C with a 12 h day-night cycle, according to the guidelines of the Federation of European Laboratory Animal Science Association (FELASA). All animal experiments were conducted according to the Declaration of Helsinki and were approved by the Ethics Committee of the State Ministry of Agriculture, Nutrition and Forestry of the State of North Rhine-Westphalia, Germany (permit number: O84/23, 81-02.04.40.2023.VG040, and 81-02.04.2021.A429).

2.1.2 General devices

Table 4. General devices

Device	Model	Model and company
Automatic microtome	Microm HM355	Thermo Fisher Scientific
Bench scales	A Secura®	Mettler
	AE166	Mettler
	Practum®	Sartorius
Centrifuges	2-16	Sigma
	D-6020	Neolab
	5415-C	Eppendorf
	5804-R	Eppendorf
Flow chamber system		Maastricht Instruments
Flow cytometer	FACS Calibur	Becton Dickinson
	FACS Symphony	
Haematology analyser	KX-21N	Sysmex
	XP-300	
Incubator	BE300	Memmert
	Melag 206	neoLab
Laminarflow hood	BSB 3A	Gelaire
Magnetic stirrer	RET basic	IKA Labortechnik
Micropipettes	peQlab;	Eppendorf
	ErgoOne	
Microscope colour camera	Axiocam 503 color	Zeiss
Microscope lamp module	HXP 120C	Zeiss
Microscopes	Axio Observer D1 (inverse)	Zeiss
	Axioskop	
Microtiter plate reader	GloMax® Multi +	Promega
	Detectionsystem with	
	Instinct® Software	
Microwave	NN-E201WM	Panasonic
Multichannel pipette	Peqpette	Peqlab
Multi-dispenser pipette	Multipette® plus	Eppendorf
Paraffin Dispenser	43900	Medax
	47311	

Paraffin section flotation bath	MH8517	Electrothermal
pH-Meter	pH526	WTW
Pipettor	Pipetboy acu	Integra Biosciences
Roll mixer	RM5	CAT
Syringe pumpe	KDS-100-CE	kd Scientific
Thermo shaker	TS-100C	BioSan
Ultrasound imaging system	Vevo 3100® High-Resolution In Vivo Micro-Imaging System	VisualSonics

2.1.3 General material

Table 5. General material

Material	**Company**
Citrat tubes	BD Vacutainer; Becton Dickinson
Coverslides	24x60 mm; Engelbrecht 24x70 mm; O. Kindler
FACS-tubes	5 mL, PS, 75x12 mm; Sarstedt
Glass capillaries	Minicaps®, Na-heparin; Hirschmann
Safe-lock tubes (0.2; 0.5; 1.5; 2 mL)	Sarstedt
Slides	76x26 mm; Engelbrecht
Pipette tips (10-20; 200; 1000 µL)	TipOne
Syringes (1; 2; 5; 10; 20 mL)	Injekt®; Braun
Transfer pipettes (2; 5; 10; 25 mL)	Stripetten; Corning
Filter	Syringe filter 0.22 µm; TPP
Conical tube (15; 50 mL)	Polypropylen conical tube; Falcon®

2.1.4 Chemicals

Table 6. Chemicals

Chemicals	Company
0.9% NaCl solution	Fresenius Kabi
2-[4-(2-hydroxyethyl)piperazin-1-yl] ethanesulfonic acid (HEPES)	9105; Carl ROTH GmbH
Adenosine diphosphate (ADP)	A2754; Sigma-Aldrich
Bovine serum albumin (BSA)	A7906; Sigma-Aldrich
Buprenorphine	Sigma-Aldrich
Calcium chloride ($CaCl_2$)	C5080; Sigma-Aldrich
Citric acid ($C_6H_8O_7$)	6490; Sigma-Aldrich
Collagen (Horm®)	1130630; Takeda
Collagen related peptide (CRP)	XL1; University of Cambridge, UK
Ethanol 100% (EtOH)	Merck Millipore
Ethylenediaminetetraacetate (EDTA) solution (0.5 M)	03690; Sigma-Aldrich
Fluoromount-G®	0100-01, Southern Biotech
Glucose	HN06; Carl ROTH GmbH
Heparin-Sodium-25000	2047217; B Braun
Isoflurane	Piramal critical care
Magnesium chloride ($MgCl_2$)	KK36; Carl ROTH GmbH
PAR4 peptide	3494; Tocris Bioscience
Phosphate-buffered saline (PBS)	D8537; Sigma-Aldrich
Potassium chloride (KCl)	9023717; Merck Millipore
Potassium permanganate ($KMnO_4$)	8004; Carl ROTH GmbH
Revacept DP-03 (GPVI-Fc, 2.4 mg/mL)	AdvanceCOR GmbH
Sodium acid (NaN_3)	S2002; Sigma-Aldrich
Sodium chloride (NaCl)	3014; Sigma-Aldrich
Sodium dihydrogen phosphate (NaH_2PO_4)	6345; Merck Millipore
Sodium hydrogen carbonate ($NaHCO_3$)	6885; Carl ROTH GmbH
Sodium orthovanadate (Na_3VO_4)	S6508; Sigma-Aldrich
Sodium phosphate, dibasic (Na_2HPO_4)	4984; Carl ROTH GmbH
Trisodium citrate	3580; Carl ROTH GmbH
Trizma® hydrochlorid	T5941; Sigma-Aldrich

Trizma®-base	T6066; Sigma-Aldrich
Type I Porcine Pancreatic Elastase	E1250; Sigma-Aldrich
U46619 (U46)	Tocris Bioscience
β-aminopropionitrile (BAPN)	A3134-25G; Sigma-Aldrich

2.1.5 Buffers and solutions

Table 7. Buffers and solutions

Buffer/Solution	**Components**
Acid citrate dextrose (ACD) buffer (Blood collection)	12.5 g Na_3-citrate 6.82 g citric acid 10 g glucose 500 mL dH_2O pH 4.69
ADP solution (20 mM)	0.1 g ADP 11.7 mL PBS pH 7.4
Binding buffer (1x) (AnnexinV binding)	10 mM Hepes (pH 7.4) 140 mM NaCl 2.5 mM $CaCl_2$
$CaCl_2$ solution (100 mM)	1.47 g $CaCl_2$ 100 mL dH_2O
Heparin-solution (20 U/mL)	40 µL heparin sodium 25000 I.E 10 ml PBS
Murine Tyrode's buffer	134 mM NaCl 12 mM $NaHCO_3$ 2.9 mM KCl 0.34 mM Na_2HPO_4 20 mM HEPES 10 mM $MgCl_2$ 5 mM glucose 0.2 mM $CaCl_2$ pH 7.35

2.1.6 Antibodies

Table 8. Dyes

Dye	Dilution	Company
AnnexinV, Alexa Fluor™ 647	1:20	A23204; Invitrogen
Cy™5 Annexin V	1:10	559934; BD Bioscience
DiOC6(3) (3,3'-Dihexyloxacarbocyanine Iodide)	1:1200	D273; Invitrogen
Fibrinogen From Human Plasma, Alexa Fluor™ 546	1:100	F13192; Invitrogen

Table 9. Antibodies for flow cytometry

Antibody	Clone	Conjugate	Dilution	Company
Armenian hamster anti-mouse CD178 (FasL)	MFL3	PE	1:20	106605; BioLegend
Armenian hamster anti-mouse CD42d	1C2	APC	1:30	148505; BioLegend
Armenian hamster anti-mouse TRAP/CD40L	MR1	FITC	1:10	Ab24934; abcam
Mouse anti-human GPVI	HY101	PE	1:10	565241; BD Bioscience
Rabbit anti-mouse VWF	-	FITC	1:10	P150-1; Emfret Analytics
Rat anti-mouse CD11b	M1/70	APC	1:100	553312; BD Biosciences
Rat anti-mouse CD14	Sa14-2	APC	1:100	123311; BioLegend
Rat anti-mouse CD19	6D5	APC	1:100	115512; BioLegend
Rat anti-mouse CD3	17A2	APC	1:100	100235; BioLegend
Rat anti-mouse CD41/61 (active form)	JON/A	PE	1:100	D200; Emfret Analytics
Rat anti-mouse CD41/61 (total)	Leo.F2	PE	1:100	M025-2; Emfret Analytics
Rat anti-mouse CD42a	Xia.B4	FITC	1:30	M051-1; Emfret Analytics
Rat anti-mouse CD42b	Xia.G5	PE	1:10	M040-2; Emfret Analytics
Rat anti-mouse CD42c	Xia.C3	FITC	1:30	M050-1; Emfret Analytics
Rat anti-mouse CD45	30-F11	APC	1:100	559864; BD Biosciences
Rat anti-mouse CD49b	Sam.G4	FITC	1:100	M070-1; Emfret Analytics
Rat anti-mouse CD49e	Tap.A12	FITC	1:10	M080-1; Emfret Analytics
Rat anti-mouse CD61	Luc.H11	FITC	1:100	M031-1; Emfret Analytics
Rat anti-mouse CD62P	Wug.E9	FITC	1:100	D200; Emfret Analytics
Rat anti-mouse GPVI	JAQ1	FITC	1:10	M011-1; Emfret Analytics
Rat anti-mouse Ly6G	1A8	APC	1:100	127614; BioLegend
Rat anti-mouse TER-119	TER-119	FITC	1:20	11-5921-82; Invitrogen

Table 10. Antibodies for immunofluorescence staining

Antibody	Type	Dilution	Company
Rabbit anti-mouse FasL	Primary antibody	1:50	ab15285; Abcam
Rabbit IgG isotype control	Primary antibody	1:50	3900S; Cell Signaling
highly cross-adsorbed Alexa Fluor™ Plus 555 conjugated secondary antibody	secondary antibody	1:200	A32794; Invitrogen™

2.1.7 Software

Table 11. Software

Software	Company	Application
BD FACSDiva™ 9.0.2	BD Biosciences	Generation of flow cytometric data
BioRender	Biorender.com	Generation of graphical figures
ChatGPT (GPT-5.2)	OpenAI	Editing
Endnote X8	Clarivate	Citations
FlowJo Single Cell Analysis v10	FlowJo LLC	Gating of flow cytometric data
Graph Pad Prism 8.4.3	GraphPad Software; LLC	Graph generation and statistical analysis
Image J 1.53t	Wayne Rasband and contributors, National Institutes of Health, USA	Quantification of immunofluorescence images
Microsoft Office 365	Microsoft Corporation	Writing
VEVO Lab 5.5.0 Software	VisualSonics	Generation and analysis of ultrasound images
ZEN 3.5 (blue edition)	Zeiss	Generation and quantification of immunofluorescence images

2.2 Methods

2.2.1 The external porcine pancreatic elastase model

The ePPE model is an experimental *in vivo* mouse model to investigate the pathophysiological mechanisms of AAA initiation and progression in mice by the external application of porcine pancreatic elastase to the abdominal infrarenal aorta. The ePPE surgery was conducted with male humanised *(h)Gp6*$^{+/+}$ mice aged 10–12 weeks as described elsewhere [248]. In short, mice received a local subcutaneous (*s.c.*) injection of buprenorphine (0.1 mg/kg body weight) 30 min before PPE surgery. During surgery the mice were anesthetised with 2–3% of inhaled isoflurane. The anaesthesia was continuously monitored throughout surgery. In addition, all mice received an *s.c.* injection of buprenorphine (0.1 mg/kg body weight) every 6 h within the daylight phase and via the drinking water (0.3 µg/mL in H_2O) during the night phase for 3 consecutive days post ePPE surgery. As a first step, a laparotomy was performed and the infrarenal aorta was separated from the *vena cava*, in order to enable the external elastase application. Next, a shell of parafilm was placed around the infrarenal aorta, to prevent excessive damage to the surrounding blood vessels and tissue. Elastase application (25.5 U/mL) was performed for 5 min. Afterwards, the elastase was removed and the aortic segment was washed with 0.9% NaCl. Thereafter the parafilm was removed and the laparotomy was closed. In addition to elastase treatment all mice received 0.1% β-aminopropionitrile (BAPN) via drinking water over the whole observation period of 28 days, starting 3 days prior ePPE surgery. Thereby, BAPN treatment inhibits elastin and collagen cross-linking, in order to reflect the human AAA pathology as closely as possible. All ePPE surgeries were performed by Dr. rer. nat. Agnes Bosbach (Clinic for Vascular and Endovascular Surgery, Research Group for Experimental Vascular Medicine, University Hospital of the Heinrich-Heine-University, Duesseldorf, Germany).

2.2.2 *In vivo* Revacept application

Humanised *(h)Gp6*$^{+/+}$ mice underwent ePPE surgery as described previously (**Section 2.2.1**). All mice received Revacept DP-03 (10 mg/kg body weight, GPVI-Fc 2.4 mg/mL, ePPE Revacept) or a respective vehicle control (ePPE ctrl) over a time course of 28 days. Revacept application was conducted every 2–3 days, starting 12 h before surgery via intraperitoneal (*i.p.*) injections (**Figure 9**). Revacept and the respective vehicle control were kindly provided by Prof. Dr. Götz Münch (AdvanceCOR GmbH, Martinsried, Germany).

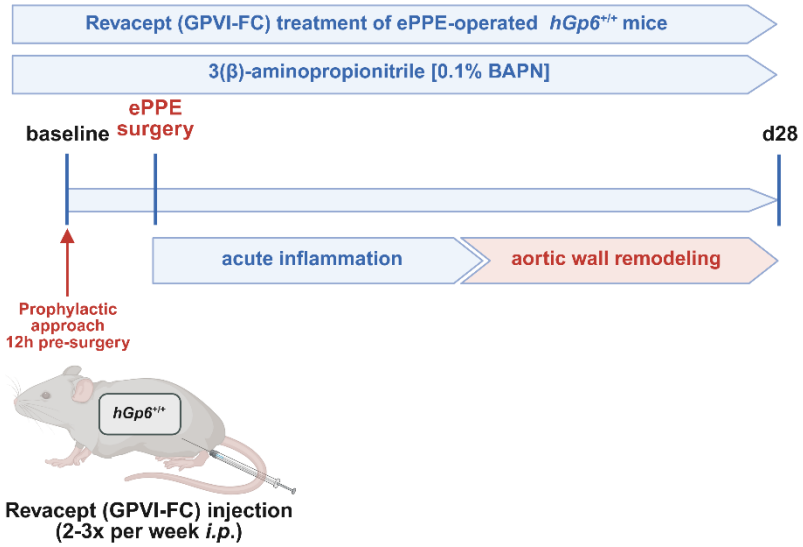


Figure 9. *In vivo* Revacept application in ePPE operated mice. Schematic overview of experimental procedure: humanised (*h*)*Gp6*$^{+/+}$ mice underwent ePPE surgery and received Revacept (10 mg/kg body weight, GPVI-FC, ePPE Revacept) or a respective vehicle control (ePPE ctrl) over a time course of 28 days. Mice were injected every 2–3 days, starting 12 h before surgery (created with BioRender.com). BAPN = β-aminopropionitrile; ctrl = control; ePPE = External porcine pancreatic elastase (application); *i.p.* = intraperitoneal (created with BioRender.com).

2.2.3 Ultrasound imaging

To visualise AAA initiation and progression in ePPE operated mice aneurysm formation was regularly monitored by ultrasound imaging over the whole observation period of 28 days. The maximal dilation of the abdominal aorta within the aneurysm segment was measured before surgery (baseline) and at day 3, 7, 14, 21 and 28 after surgery. For ultrasound imaging mice were anaesthetised with 2–3% isoflurane and placed on a heating plate at 37 °C. The anaesthesia was continuously maintained and monitored throughout the whole procedure. Ultrasound measurements were performed using a Vevo 3100® High-Resolution In Vivo Micro-Imaging System (VisualSonics). The inner aortic diameter progression was monitored using a standardised imaging algorithm with longitudinal B–mode images of the systolic phase.

2.2.4 Murine blood collection and blood cell count determination

For murine whole blood collection, mice were initially anaesthetised with 2–3% of isoflurane using an adjustable respirator. Sufficient anaesthesia was verified by testing the toe pain reflex. Blood withdrawal was subsequently conducted via retrobulbar puncture of the venous plexus using a microcapillary. Blood samples for flow cytometric analysis (**Section 2.2.5**) were collected

in 300 µL of heparin solution (20 U/mL). For *ex vivo* flow chamber experiments (**Section 2.2.6**) acid citrate dextrose (ACD)-anticoagulated blood with a dilution factor of 1:10 was used. For the determination of blood cell counts, murine whole blood was collected into ethylenediaminetetraacetate (EDTA) coated Microvettes® (#20.1341, Sarstedt) and analysed using a haematology analyser (Sysmex KX21N, Norderstedt).

2.2.5 Flow cytometry

For flow cytometric analysis, murine whole blood was collected in 300 µL of heparin solution (20 U/mL) as described previously (**Section 2.2.4**). Next, whole blood samples were washed three times by adding 500 µL murine Tyrode's buffer (137 mM NaCl, 2.8 mM KCl, 12 mM $NaHCO_3$, 0.4 mM NaH_2PO_4 and 5.5 mM glucose, pH 6.5) and subsequent centrifugation at 650 x *g* for 5 min. After the final centrifugation step, all whole blood samples were resuspended in murine Tyrode's buffer supplemented with 1 mM $CaCl_2$. Platelet activation of murine whole blood samples was conducted via two-colour flow cytometric analysis. For this purpose, specific antibodies for the degranulation marker P-selectin (CD62P, Wug.E9-FITC, 1:100, #D200, Emfret Analytics) and the active integrin $\alpha_{IIb}\beta_3$ (JON/A-PE, 1:100, #D200, Emfret Analytics) were used. In addition, platelets were activated with different agonists (adenosine diphosphate (ADP; #A2754, Sigma-Aldrich), collagen-related peptide (CRP; Richard Farndale, University of Cambridge, Cambridge, UK), the thromboxane A2 analogue U46619 (U46; #1932, Tocris) or PAR4 peptide (PAR4; #3494, Tocris)). Therefore, samples were incubated with the antibodies and the indicated agonists for 15 min at RT in the dark. Platelet glycoprotein exposure was analysed using specific antibodies against integrin α_5 (CD49e, Tap.A12-FITC, 1:100, # M080-1, Emfret Analytics), GPIX (CD42a, Xia.B4-FITC, 1:100, #M051-1, Emfret analytics), GPIbα (CD42b, Xia.G5-PE, 1:10, #M040-2, Emfret Analytics), GPIbβ (CD42c, Xia.C3-FITC, 1:30, #M050-1, Emfret analytics), GPV (CD42d, 1C2-APC, 1:30, #148505, BioLegend) or GPVI (JAQ1-FITC, 1:10, #M011-1, Emfret Analytics). To investigate glycoprotein upregulation on the platelet surface, as well as VWF-binding and CD40L exposition, washed whole blood samples were labelled for integrin α_2 (CD49b, Sam.G4-FITC, 1:100, #M070-1, Emfret Analytics), integrin $\alpha_{IIb}\beta_3$ (CD41/61, Leo.F2-PE, 1:100, #M025-2, Emfret Analytics), integrin β_3 (CD61, Luc.H11-FITC, 1:100, #M031-1, Emfret Analytics), VWF (VWF-FITC, 1:10, #P150-1, Emfret Analytics) and CD40L (TRAP/CD40L, MR1-FITC, 1:10, #Ab24934, Abcam), and incubated with the indicated agonists. Samples were incubated for 15 min at RT in the dark and the reaction was stopped by adding 300 µL of PBS. For the analysis of PS-exposure washed murine whole blood was resuspended in 1x binding buffer (10 µM HEPES, 140 µM NaCl, 2.5 mM $CaCl_2$, pH 7.4). Subsequently, murine whole blood was

labelled with Annexin V (Cy™ 5 Annexin V, 1:10, #559934, BD Biosciences), in order to detect exposed PS on the cell surface, and activated with the indicated agonists. All samples were incubated for 20 min at RT in the dark. After incubation the reaction was stopped by adding 300 µL 1x binding buffer to all samples. For platelet Fas ligand (FasL) exposure whole blood samples were labelled with specific antibodies against FasL (CD178, MFL3-PE, 1:20, #106605, BioLegend). The reaction was stopped by adding 300 µL of PBS. For the analysis of circulating platelet-leukocyte aggregate formation washed murine whole blood samples were stained for leukocytes (CD45, 30-F11-APC, 1:100, #559864, BD Biosciences), neutrophils (Ly6G, 1A8-APC, 1:100, #127614, BD Biosciences), T cells (CD3, 17A2-APC, 1:100, #100235, BioLegend), B cells (CD19, 6D5-APC, 1:100, #115512, BioLegend) macrophages or granulocytes (CD14, Sa14-2-APC, 1:100, #123311, BioLegend and CD11b, M1/70-APC, 1:100, #553312, BD Biosciences). Aggregate formation with the different leukocyte subtypes was determined as double positive events, whereas GPIbα (CD42b, Xia.G5-PE, 1:10, #M040-2, Emfret Analytics) was used as platelet marker. In order to determine the formation of circulating platelet-RBC aggregates, whole blood samples were stained for RBCs (TER-119-FITC, 1:20, #11-5921-82, Invitrogen) and platelets (CD42b, Xia.G5-PE, 1:10, #M040-2, Emfret Analytics). All samples were incubated for 15 min at RT in the dark. After incubation, the reaction was stopped by adding 200 µL of PBS. All samples were analysed using a BD FACSymphony™ A Cell Analyzer (BD Biosciences).

2.2.6 Immunofluorescence staining of murine aortic tissue

Aortic tissue from PPE operated GPVI-deficient and WT mice was harvested at day 7 post surgery. The paraffin-embedded tissue was sliced into 5 µM sections using an automatic microtome (Microm HM355, Thermo Fisher Scientific). For immunofluorescence staining the sections were deparaffinised and hydrated in a first step. In order to secure sufficient antigen unmasking, all sections were heated at 300 W for 10 min in citrate buffer (pH 6.0). After unmasking, all sections were blocked using DPBS supplemented with 0.3% Triton X-100 and 5% goat serum for 1 h at RT. For staining of the FasL content within the aortic tissue, all sections were incubated with the respective primary antibody (anti-FasL, #ab15285, Abcam, 1:50) at 4°C overnight. The respective IgG antibody was used as control (IgG Isotype Control, #3900S, Cell Signaling, 1:50). After incubation with the primary antibody all sections were subsequently incubated for 1 h at RT with a highly cross-adsorbed Alexa Fluor™ Plus 555 conjugated secondary antibody (#A32794, Invitrogen™, 1:200). Nuclei were stained via DAPI (4', 6-Diamidine-2'-phenylindole dihydrochloride, #10236276001, Roche, 1:3000). Image acquisition

was performed using an Axio Observer.D1 microscope (Zeiss). The FasL content was analysed as the percentage of total aortic tissue using Image J (version 1.53t).

2.2.7 *Ex vivo* thrombus formation

The day prior the experiment, cover slips (24 x 60 mm) were coated with 200 µg/mL collagen (Horm® collagen reagent, #1130630, Takeda Austria GmbH) in a humidity chamber at 4 °C overnight. The next day, all cover slips were blocked with 1% BSA (bovine serum albumin, in PBS) for 1 h at RT. For the *ex vivo* thrombus formation experiments ACD-anticoagulated murine whole blood was collected as described previously (**Section 2.2.4**) and pre-incubated with 8.5 µg/mL AF546 fibrinogen (1:100, #F13192, Invitrogen™) and 0.5 µg/mL 3,3'-Dihexyloxacarbocyanine Iodide (DiOC6, 1:1200, #D273, Sigma-Aldrich) and for 10 min at RT.

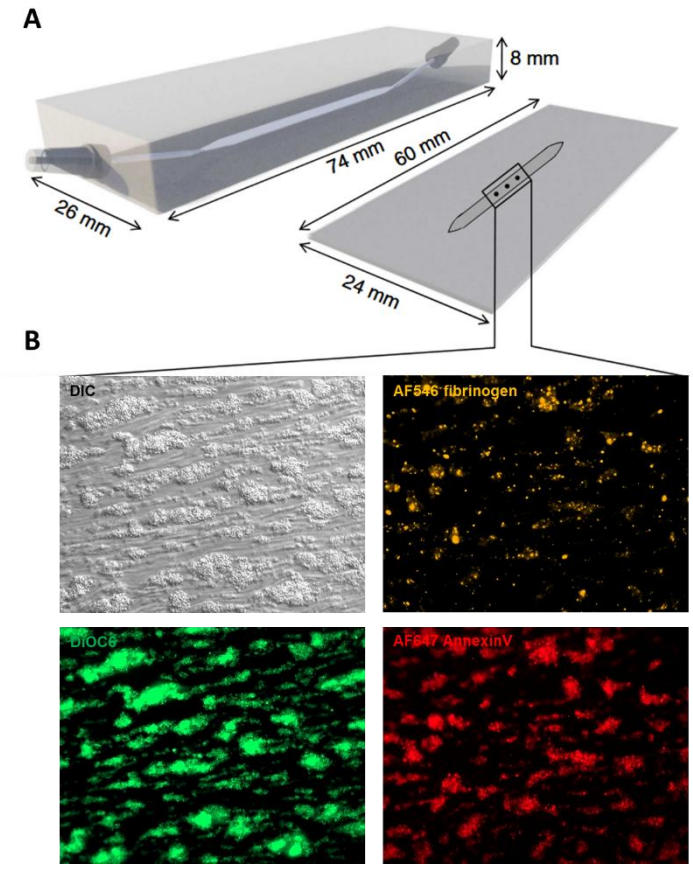


Figure 10. The flow chamber system for the analysis of *ex vivo* thrombus formation. (**A**) Schematic illustration of the flow chamber system for the analysis of *ex vivo* thrombus formation. (**B**) Exemplary images of surface coverage (DiOC6), fibrin/fibrinogen content (AF546 fibrinogen) and PS exposure (AF647 AnnexinV) of murine thrombi after flow at an arterial shear rate of 1,700 s^{-1} (12.75 mL/h). Modified from [249].

After incubation, the whole blood sample was drawn into a 1 mL syringe and subsequently perfused via a pulse-free pump over the collagen-coated cover slips for 3 min using the Maastricht flow chamber system (50 µm x 5 mm) with an arterial shear rate of 1,700 s^{-1} (12.75 mL/h) (**Figure 10A**). Afterwards, the flow chamber was perfused with PBS at a shear rate of 1,000 s^{-1} (7.53 mL/h). Next, the cover slips were removed from the flow chamber system and subsequently fixated with 4% paraformaldehyde (PFA) for 15 min at RT. After fixation, all cover slides were stained with AF647 AnnexinV (1:20, #A23204, Invitrogen™) diluted in 1x binding buffer and embedded with Fluoromount-G® (#0100-01, Southern Biotech). For analysis five representative images were taken using an Axio Observer.D1 microscope (Zeiss). *Ex vivo* thrombus formation, thrombus volume, fibrin/fibrinogen content and PS exposure (**Figure 10B**) of murine thrombi after flow were determined using Image J (version 1.53t).

2.2.8 Statistics

Data are presented as arithmetic means ± standard error of the mean (SEM). Statistical analysis was performed using GraphPad Prism 8 (version 8.4.3). The indicated sample size for each experiment reflects the number of independent biological replicates. Due to the use of inbred strains a normal distribution for the analysis of murine data was assumed. Statistical differences were determined using an unpaired student's t-test or an unpaired multiple t-test for the comparison of two groups. Additionally, a one-way ANOVA with Tukey's multiple comparison post-hoc test, or a two-way ANOVA with a Sidak's, respectively Tukey's multiple comparison post-hoc test was conducted, for the analysis of more than two groups. For evaluation of survival rates of ePPE operated mice a Log-rank (Mantel-Cox) model was applied. The AAA incidence was analysed using a Fisher's exact test. For the correlation of two variables a parametric Pearson correlation was used. Statistical adjustments for multiple comparisons were applied solely within the statistical analysis of the individual experiments (within-test corrections), without performing experiment-wide/across-test corrections. Significant differences are indicated by asterisks (* $p < 0.05$; ** $p < 0.01$; *** $p < 0.001$; **** $p < 0.0001$).

3 Results

3.1 Crosstalk of platelets with macrophages and fibroblasts aggravates inflammation, aortic wall stiffening, and osteopontin release in abdominal aortic aneurysm

Wagenhäuser MU*[1], Mulorz J*[1], Krott KJ*[1], Bosbach A*[1], **Feige T[1]**, Rhee YH[1], Chatterjee M[2], Petzold N[1], Böddeker C[1], Ibing W[1], Krüger I[1], Popovic AM[1], Roseman A[3], Spin JM[3,4], Tsao PS[3,4], Schelzig H[1], Elvers M[1]

* contributed equally

[1]Department of Vascular- and Endovascular Surgery, University Hospital Düsseldorf, Heinrich-Heine University, Düsseldorf, Germany

[2]Department of Pharmacology, Experimental Therapy and Toxicology, University Hospital Tübingen, Tübingen, Germany

[3]VA Palo Alto Health Care System, Palo Alto, CA, United States

[4]Stanford University, Department of Cardiovascular Medicine, Stanford, CA, United States

Published in: *Cardiovascular Research (CVR)* in 2024

Impact Factor: 13.3 (2024)

License number for republishing: 6192491110157.

Own contribution to publication: Cytokine gene expression of differentiated macrophages (**Figure 3E**). Analysis of AngII treated mice (*ApoE*$^{-/-}$ ctrl. Ang II vs *ApoE*$^{-/-}$ depl. AngII and *ApoE*$^{-/-}$ sham vs *ApoE*$^{-/-}$ AngII) including: flow cytometric analysis of platelet activation, PS-exposure and integrin β_3 externalisation; ultrasound measurements; histological staining and blood cell counts (**Figure 6 and S4**). Patient data: flow cytometric analysis of platelet activation, PS-exposure in AAA patients (**Figure 7A**). Investigation, data analysis, statistical analysis, figure visualisation.

ESC European Society of Cardiology
Cardiovascular Research (2024) **120**, 417–432
https://doi.org/10.1093/cvr/cvad168

Crosstalk of platelets with macrophages and fibroblasts aggravates inflammation, aortic wall stiffening, and osteopontin release in abdominal aortic aneurysm

Markus U. Wagenhäuser[1†], Joscha Mulorz[1†], Kim J. Krott[1†], Agnes Bosbach[1†], Tobias Feige[1], Yae H. Rhee[1], Madhumita Chatterjee [2], Niklas Petzold[1], Christopher Böddeker[1], Wiebke Ibing[1], Irena Krüger[1], Ana M. Popovic[1], Ann Roseman[3], Joshua M. Spin[3,4], Philip S. Tsao[3,4], Hubert Schelzig[1], and Margitta Elvers [1]*

[1]Department of Vascular and Endovascular Surgery, University Hospital Düsseldorf, Heinrich-Heine University, Moorenstrasse 5, 40225 Düsseldorf, Germany; [2]Department of Pharmacology, Experimental Therapy and Toxicology, University Hospital Tübingen, Wilhelmstrasse 5, 72074 Tübingen, Germany; [3]VA Palo Alto Health Care System, Palo Alto, 3801 Miranda Avenue, 94304 CA, USA; and [4]Department of Cardiovascular Medicine, Stanford University, 291 Campus Drive Stanford, 94305 CA, USA

Received 23 March 2023; revised 1 August 2023; accepted 23 September 2023; online publish-ahead-of-print 17 November 2023

Time for primary review: 43 days

See the editorial comment for this article 'Abdominal aortic aneurysms and platelets: infiltration, inflammation, and elastin disintegration', by B. Li *et al.*, https://doi.org/10.1093/cvr/cvae010.

Aims Abdominal aortic aneurysm (AAA) is a highly lethal disease with progressive dilatation of the abdominal aorta accompanied by degradation and remodelling of the vessel wall due to chronic inflammation. Platelets play an important role in cardiovascular diseases, but their role in AAA is poorly understood.

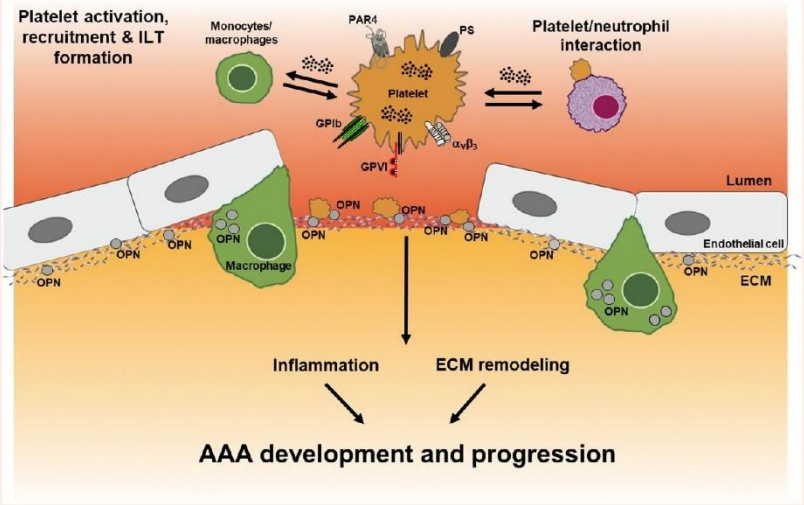
Methods and results The present study revealed that platelets play a crucial role in promoting AAA through modulation of inflammation and degradation of the extracellular matrix (ECM). They are responsible for the up-regulation of *SPP1* (*osteopontin, OPN*) gene expression in macrophages and aortic tissue, which triggers inflammation and remodelling and also platelet adhesion and migration into the abdominal aortic wall and the intraluminal thrombus (ILT). Further, enhanced platelet activation and pro-coagulant activity result in elevated gene expression of various cytokines, *Mmp9* and *Col1a1* in macrophages and *Il-6* and *Mmp9* in fibroblasts. Enhanced platelet activation and pro-coagulant activity were also detected in AAA patients. Further, we detected platelets and OPN in the vessel wall and in the ILT of patients who underwent open repair of AAA. Platelet depletion in experimental murine AAA reduced inflammation and ECM remodelling, with reduced elastin fragmentation and aortic diameter expansion. Of note, OPN co-localized with platelets, suggesting a potential role of OPN for the recruitment of platelets into the ILT and the aortic wall.

Conclusion In conclusion, our data strongly support the potential relevance of anti-platelet therapy to reduce AAA progression and rupture in AAA patients.

* Corresponding author. Tel: +0211 8108851, E-mail: margitta.elvers@med.uni-duesseldorf.de
† Contributed equally.
© The Author(s) 2023. Published by Oxford University Press on behalf of the European Society of Cardiology. All rights reserved. For permissions, please e-mail: journals.permissions@oup.com

Downloaded from https://academic.oup.com/cardiovascres/article/120/4/417/7425469 by guest on 04 July 2024

Graphical Abstract



Keywords Platelets • Abdominal aortic aneurysm • Inflammation • ECM remodelling • Osteopontin

1. Introduction

Abdominal aortic aneurysm (AAA) is a localized, progressive dilatation of the abdominal aorta caused by chronic inflammation resulting in adverse remodelling of the aortic wall. Well-established risk factors include age, hypertension, male gender, and smoking. In Western countries, the incidence of AAA is ~0.4–0.67% annually and reaches up to 5–10% in men over 65 years of age.[1] As AAA diameter increases, the risk of fatal rupture rises exponentially. Despite remarkable advances in understanding the underlying pathological mechanisms during the past years, endovascular and open repair remain the only AAA treatment options. Although potential candidates exist, such as metformin, non-invasive drug-based therapies are pending clinical implementation, since prospective randomized trials have either not demonstrated efficacy or are yet to be performed.[2–6]

Characteristic features of AAA pathophysiology are the recruitment of infiltrating inflammatory leucocytes, together with the activation of proteolytic enzymes leading to extracellular matrix (ECM) degradation, which weakens the aortic vessel wall.[7,8] In this context, the formation of an intraluminal thrombus (ILT) may be critical for the progress of the disease, since the ILT modulates both, biomechanical parameters and inflammatory processes in the AAA vessel wall.[9,10] The vast majority of AAAs is accompanied by an ILT, although its disease-specific role is still widely debated.[11,12] The key elements of inflammatory processes and the formation of an ILT suggest that platelets and their activation might play a significant role for AAA initiation and progression, particularly as evidence has accumulated for platelet-based acceleration of various cardiovascular diseases (CVDs).[13]

Various pre-clinical animal models exist, allowing mechanistic insights into various aspects of AAA disease.[14] Of these, the angiotensin-II (Ang-II) infusion model provides features of dissection and aneurysm formation and has demonstrated a beneficial effect in AAA rupture rates and reduced macrophage recruitment into the AAA wall in response to antiplatelet drugs.[15] Further, the platelet integrin $\alpha_{IIb}\beta_3$ inhibitor abciximab and/or a $P2Y_{12}$ receptor antagonist both blocked AAA growth in a rat xenograft aneurysm model.[16,17] To date, no study has explored the role of platelets in the pancreatic porcine elastase (PPE) infusion model. The PPE model reproduces many features of human AAA and was therefore used in this study.[14]

Small clinical trials have supported the hypothesis that platelet activation contributes to AAA development and progression, because antiplatelet medication with low-dose aspirin has been shown to be beneficial for patients with small AAAs, as indicated by decreased aneurysm size and less frequent need for surgical repair.[18] In patients with large AAAs, platelet activation is enhanced with increased levels of soluble CD40L, thrombin anti-thrombin complex complex formation, P-selectin exposure, and fibrinogen binding.[19]

In conclusion, both experimental and clinical data strongly suggest that in AAA, impaired endothelial function causes platelet activation, leading to ILT formation and promoting a persistent renewal of cellular activity at the luminal interface via aggregation, entrapment, and recruitment of activated platelets, establishing a chronic inflammatory response. Thus, platelet activation may play a pivotal role in AAA formation and progression. Despite these theoretical considerations and encouraging results in pre-clinical animal models and small clinical trials, there is a significant lack of understanding on how platelets contribute to AAA development and progression. More insights into the specific role of platelets in AAA disease and their activation mechanisms are urgently needed to allow the development of appropriate antiplatelet targets. Here, we present findings regarding platelet contribution to AAA disease opening the way for potential novel therapies.

2. Methods

2.1 Study approval

All animal experiments were conducted according to the Declaration of Helsinki. This study was conducted according to the German and US law

Downloaded from https://academic.oup.com/cardiovascres/article/120/4/417/7425469 by guest on 04 July 2024

for the welfare of animals. The protocol was reviewed and approved by the local government authority: Germany: Heinrich Heine University Animal Care Committee and State Agency for Nature, Environment and Consumer Protection of North Rhine-Westphalia LANUV, Recklinghausen, NRW, Germany Permit Numbers 81-02.04.2018.A409 and 81-02.05.40.21.041; USA: C57BL/6 wild-type male mice were purchased from the Jackson Laboratory. Animals were housed in a temperature-controlled and humidity-controlled room under a 12-h light/dark cycle (6:30 am/6:30 pm). All animal protocols were approved by the VA Institutional Animal Care and Use Committee and followed the National Institutes of Health and US Department of Agriculture Guidelines for Care and Use of Animals in Research.

Experiments with human tissues and blood were reviewed and approved by the Ethics Committee of the Heinrich Heine University, who approved the collection and analysis of the tissue samples. Subjects provided informed consent prior to their participation in the study (patients' consent): permitted ethical votes: ID: 2018-140-KFogU, 5731R (2018-222_1), and 2018-248-FmB. The study was conducted in accordance with the Declaration of Helsinki principles and the International Council for Harmonization Guidelines on Good Clinical Practice.

2.2 Human AAA samples

Fresh citrate anticoagulated blood was collected from healthy volunteers between 18 and 70 years of age into Vacutainer® sodium citrate tubes (BD, NJ, USA, BD Vacutainer®, #367714). Blood of older (>60 years) healthy volunteers was used as age-matched controls (AMCs) for the comparison with AAA patients (study number: 2018-140-KFogU). Human AAA blood was collected pre-surgery, and tissue samples were collected and obtained from our local Biobank at the Department of Vascular and Endovascular Surgery at University Hospital Düsseldorf (study number: 5731R and 2018-248-FmB).

2.3 Human platelet and plasma preparation

Platelet count and mean platelet volume (MPV) in blood from AMCs and AAA patients were analysed using a haematology analyser (Sysmex KX-21N, Norderstedt, Germany). For plasma and platelet preparation, blood was centrifuged at 231 *g* for 10 min. Afterwards, the upper phase, i.e. the platelet-rich plasma (PRP), was carefully transferred into Dulbecco's phosphate buffered saline (DPBS, pH 6.5) containing apyrase (2.5 U/mL) (Sigma-Aldrich, Aufkirchen, Germany , #A7646) and prostaglandin E1 (PGE_1, 1 µM) (Sigma-Aldrich, #P5515). The DPBS PRP mixture was centrifuged at 1000 *g* for 6 min without brakes. The formed pellet was re-suspended in Tyrode's buffer (137 mM NaCl, 2.8 mM KCl, 12 mM $NaHCO_3$, 0.4 mM NaH_2PO_4, and 5.5 mM glucose, pH 6.5). Tyrode's buffer is especially suitable to maintain the normal physiological function of isolated platelets. The cell count was determined using a haematology analyser (Sysmex KX-21N, Norderstedt, Germany) and adjusted for the following experiment. For plasma sample preparation, the citrate tube was centrifuged again at 1500 *g* for 10 min and at 4°C after PRP extraction. The generated platelet-free plasma was transferred into fresh collection tubes and stored at −70°C for later experiments.

2.4 Generation of platelet releasates

Isolated platelets (70×10^6) from healthy volunteers were activated with adenosine diphosphate (ADP) (10 µM, 10 min) and CRP (5 µg/mL, 5 min), and control samples were treated with Tyrode's buffer. The reaction was stopped by the addition of apyrase (2 µL, 0.25 U/mL) and centrifuged at 850 *g* for 10 min. Finally, the activated platelet supernatant was collected and stored at −20°C until use.

2.5 Experimental animals: the PPE mouse model

Ten-week-old standard C57BL/6J mice were purchased through Jackson or Janvier Laboratory. To induce experimental AAA, mice were anaesthetized with 2–3% isoflurane and received a locally subcutaneous (s.c.) injection of buprenorphine (0.1 mg/kg) (Temgesic, Eumedica) 30 min before surgery. After median laparotomy, the proximal and distal infrarenal aortas were temporarily ligated to create an aortotomy above the iliac bifurcation. A catheter was inserted into the distal end of the aortotomy and used to infuse the aorta with sterile isotonic saline (NaCl, 0.9%) containing Type I PPE (2.5 U/mL) (Sigma-Aldrich, #E1250) at 120 mm Hg for 5 min. The vessels in control mice were infused with sodium chloride only. After removal of the infusion catheter, the aortotomy was closed without constriction of the aortal lumen. Finally, the abdomen was closed. For pain relief, all animals received buprenorphine s.c. every 6 h during the daylight phase for 3 days and in the dark phase via drinking water (0.3 µg/mL). At the endpoints of the experiments (Days 3, 10, and 28), mice were euthanized under deep isoflurane anaesthesia followed by cervical dislocation. For the platelet depletion experiments, mice were injected with platelet depletion antibody (Emfret Analytics, polyclonal anti-GPIb alpha #R300) and a corresponding IgG antibody (Emfret Analytics, #C301) as controls after surgery (Days 0 and 5). Endpoints of the experiments were Days 3 and 10 post-(PPE)surgery.

2.6 Platelet preparation and total blood cell count in mice

Murine blood was collected and transferred into a heparin solution (20 U/mL). Platelet count and MPV were determined using a haematology analyser (Sysmex KX-21N, Norderstedt, Germany). For platelet preparation, the blood was centrifuged at 250 *g* at RT for 5 min. Then, the supernatant was centrifuged again at 50 *g* for 6 min. To collect PRP, the supernatant of the last step was centrifuged with apyrase (0.02 U/mL) and prostacyclin (PGI_2, 0.5 µM) at 650 *g* and RT for 5 min. Plasma samples were stored at −70°C for later experiments. The platelet pellet was re-suspended and washed twice in murine Tyrode's buffer (136 mM NaCl, 0.4 mM Na_2HPO_4, 2.7 mM KCl, 12 mM $NaHCO_3$, 0.1% glucose, 0.35% BSA, and pH 7.4) supplemented with PGI_2 (0.5 µM) and apyrase (0.02 U/mL) by centrifugation at 650 *g* at RT for 5 min. Finally, platelets were re-suspended in Tyrode's buffer and incubated at 37°C until use.

2.7 Transmission electron microscopy

Aortic tissue was harvested from PPE-operated mice. Briefly, the aorta was perfused with heparin (180 units/15 mL PBS) from the left ventricle (butterfly puncture) to right atrium (incision). Thereafter, perfusion was slowly carried out with 4% paraformaldehyde (in PBS pH 7.4). Afterwards, aortic tissue was fixed with a solution of 2% glutaraldehyde and 2% paraformaldehyde in cacodylate buffer (0.1 M, pH 7.2) at RT overnight. The next day, samples were washed twice in sodium cacodylate buffer (0.1 M) at RT for 10 min, post-fixed with 2% aqueous osmium tetroxide (OsO_4) at RT for 5 h, washed twice with milliQ water, and stained *en bloc* with 4% uranyl acetate overnight. After dehydration through a graded ethanol series and propylene oxide, the tissue was infiltrated and embedded in 100% eponate 12 resin (Ted Pella, Inc., Redding, CA, USA). Polymerization was performed at 60°C for 24 h. Ultrathin sections were cut using a Leica Ultracut microtome (Leica, Deerfield, IL, USA) and then post-stained with Reynolds lead citrate. The stained samples were examined in a FEI Tecnai G2 Spirit BioTWIN transmission electron microscope (Hillsboro, OR, USA) operated at 80 kV. Electron micrographs were taken with an AMT XR41 CCD camera from Advanced Microscopy Techniques, Corporation (Woburn, MA, USA).

2.8 Flow cytometry

For flow cytometry of human platelets, whole blood (fresh citrate anticoagulated blood) was used and diluted 1:10 in human Tyrode's buffer (137 mM NaCl, 2.8 mM KCl, 12 mM $NaHCO_3$, 0.4 mM NaH_2PO_4 and 5.5 mM glucose, and pH 6.5). Heparinized mouse blood was washed twice at 250 *g* for 5 min by discarding the supernatant and resuspending the blood pellet in murine Tyrode's buffer (136 mM NaCl, 0.4 mM Na_2HPO_4, 2.7 mM KCl, 12 mM $NaHCO_3$, 0.1% glucose, 0.35% BSA, and

Downloaded from https://academic.oup.com/cardiovascres/article/120/4/417/7425469 by guest on 04 July 2024

pH 7.4). Finally, the pellet was diluted in mouse Tyrode's buffer including $CaCl_2$ (2 mM). Blood samples were mixed with antibodies and stimulated with indicated agonists at RT for 15 min in the dark. The reaction was stopped by the addition of DPBS, and samples were analysed on a FACSCalibur flow cytometer (BD Biosciences).

Briefly, two-colour analysis of murine or human platelet activation was performed using fluorophore-labelled antibodies for P-selectin expression (Emfret Analytics, Wug.E9-FITC, #M130-1, and BD Biosciences, anti-human CD62P-PE, #348107) and the active form of $\alpha_{IIb}\beta_3$ integrin (Emfret Analytics, JON/A-PE, #M023-2, and BD Biosciences anti-human PAC-1-FITC, #340507). For analysis of α_5 glycoprotein surface expression and up-regulation as well as activation of integrin β_3 expression, blood samples were mixed with specific antibodies (Emfret Analytics, β_3 chain, GPIIIa, Luc.H11-FITC, #M031-1 or Integrin α_5/CD49e, Tap.A12-FITC, and anti-human CD61-PE, #555754, BD Biosciences) and incubated for 15 min at RT in the dark. For the analysis of CD45-platelet and Ly6G-platelet aggregates, specific antibodies were used (Emfret Analytics, GPIb/CD42b, Xia.G5-PE; BD Biosciences, anti-mouse CD45-APC, #559864, and BioLegend, anti-mouse Ly-6G-APC, #127614). For detection of phosphatidylserine (PS) exposure, Cy™5 Annexin V (BD Biosciences) was used—staining was performed while using binding buffer (10 mM Hepes, 140 mM NaCl, 2.5 mM $CaCl_2$, and pH 7.4) instead of DPBS. By treating platelets with soluble full-length OPN (0.01 µg/µL in H_2O; PeproTech, #120-35) and soluble cleaved OPN (0.01 µg/µL), the influence of osteopontin on platelet activation should be analysed. Additionally, circulating levels of chemokines and other inflammatory mediators including CXCL8 [interleukin (IL)-8], CCL2 [monocyte chemoattractant protein (MCP)-1], CCL5 (RANTES), CXCL8 (IL-8), IL-6, P-selectin, PSGL-1, IL-1β, IFN-γ, IFN-α2, IL–10, and IL-12p70 were determined in the plasma of AAA patients and AMCs by flow cytometric multiplex analysis (cytometric bead array-CBA) [Biolegend, San Diego, CA, USA, LEGENDplex™ Human Thrombosis Panel (10-plex) #740892 and LEGENDplex™ Human Inflammation Panel 1 (13-plex) #740809 #740895] according to the manufacturer's instructions using a BD FACSLyric™ flow cytometer.

2.9 Statistics

Data are shown as arithmetic means ± SEM, and statistical analysis was performed using GraphPad Prism Version 8.4.3. For each experiment, sample size reflects the number of independent biological replicates and is provided in the figure legend. Statistical testing for mice was performed based on the assumption of normality because of low numbers of replicates and the use of inbred animals. Equality is part of the determination of statistical significances using GraphPad Prism 8 software and its recommended tests, which we applied throughout this study. Where necessary, clinical data were evaluated to check the normality of the distribution using the Shapiro–Wilk test.

Thus, data between two comparative groups, an unpaired student's *t*-test with Welch's correction or multiple *t*-test, were used. For non-parametric data, a Mann–Whitney *U* test was used. Comparison of more than two groups was performed using a one-way or two-way ANOVA with Sidak's, Holm–Sidak's, or Tukey's multiple comparison correction. *P*-values of <0.05 were considered significant.

3. Results

3.1 Platelet depletion alleviates inflammation and experimental AAA progression

We induced experimental murine AAA utilizing the PPE model and performed platelet depletion by administrating an antiplatelet antibody (or control polyclonal immunoglobulins) at Days 0 and 5 following surgery (*Figure 1A* and *B*). We found that platelet depletion significantly attenuated the diameter progression of AAA over a 10-day time course by ultrasound tracking (*Figure 1C–E*; see Supplementary material online, *Figure S1A*). Further, our data demonstrated enhanced aortic pulse wave velocity (PWV) following the initiation of experimental AAA in the control group at Day 10 post-surgery suggesting significant structural stiffening effects in the aortic wall. Of note, such changes in aortic PWV were not found in the platelet-depleted group, suggesting aggravating effects of platelets with adverse stiffness promoting structural remodelling (*Figure 1F*). In the thoracic aorta, stable media lamellar units and lack of elastic degradation were found in both groups (see Supplementary material online, *Figure S1B–E*). In addition to the effects seen in the structural architecture of the AAA wall, our findings demonstrated that platelets and macrophages were recruited into the AAA wall at Day 3 post-surgery. Platelet depletion reduced the number of macrophages in the AAA wall, suggesting potential platelet-mediated modulating effects of the inflammatory process following murine AAA induction (*Figure 1G* and *H*; see Supplementary material online, *Figure S1F* and *G*). In line with this finding, inflammatory gene expression analysis of whole AAA tissue explants revealed down-regulation of major inflammatory genes in the platelet-depleted group vs. the control antibody treated group at Day 3 post-surgery (*Figure 1I*).

3.2 Platelet depletion reverses adverse remodelling of the ECM

We next analysed platelet-associated adverse remodelling effects on the ECM of the AAA wall. Exemplary experiments show fragmented, and at given locations completely disrupted, elastin membranes within the tunica media in the AAA wall of PPE mice as shown by transmission electron microscopy (TEM) (*Figure 2A* and *B*). Therefore, we analysed AAA wall fragmentation in more detail by haematoxylin/eosin and Verhoeff van Gieson staining. To examine the impact of platelets on elastin membrane integrity, histological evaluation of AAA explants was performed. Our results show that the intima media thickness of the AAA wall of platelet-depleted mice was thinner compared with control mice at 10 Days post-surgery (*Figure 2C*). Additionally, the aortic tissue displayed significantly less fragmentation of elastin membranes in AAA explants of platelet-depleted vs. control mice (*Figure 2D*).

These morphologic findings were supported by a partially altered structural gene expression profile in AAA of platelet-depleted mice. In detail, AAA whole tissue explants of platelet-depleted mice showed reduced expression levels of matrix metalloproteinase (*Mmp*) *9* and *collagen I*, while *collagen III*, *Mmp2*, and *elastin* (*Eln*) expression were unaltered (*Figure 2E*). MMP9 is considered to be a major elastolytic enzyme that reduces resilience and elasticity of conduit arteries and was down-regulated in whole AAA explants of platelet-depleted vs. control mice 10 days post-surgery (*Figure 2E*), consistent with the aforementioned reduced elastin fragmentation in the same group. Notably, we found that osteopontin (*Spp1*/OPN), a multifunctional and highly phosphorylated glycoprotein, was up-regulated at the gene expression level in aortic tissue of PPE-operated mice and in the plasma following murine experimental AAA induction. *Spp1* expression was down-regulated within the AAA wall of platelet-depleted mice compared with control mice, and OPN protein was reduced in the plasma (*Figure 2F* and *G*).

3.3 Platelets alter gene expression in macrophages

Since OPN was altered at the transcriptional and protein level upon platelet depletion, we elected to study the major source of OPN. We incubated macrophages (PMA-stimulated THP-1 cells; differentiated macrophages), human aortic smooth muscle cell (hASMCs), and human aortic fibroblasts (hAoFs) with the releasates of ADP (stimulating $P2Y_{12}$) or collagen related peptide (CRP, stimulating the collagen receptor GPVI) activated platelets. Our results demonstrated that macrophages are the major cell type with the highest *SPP1* expression when compared with resident cells of the AAA wall, such as hASMC and hAoF (*Figure 3A*). Although platelets themselves carry OPN (*Figure 3B*), differentiated macrophages remained the primary source for OPN protein and *SPP1* gene expression *in vitro* (*Figure 3C* and *D*; see Supplementary material online, *Figure S2A*). To verify whether platelets are capable of altering gene expression in macrophages, we exposed cultures of pro-inflammatory macrophages to releasates of

Downloaded from https://academic.oup.com/cardiovascres/article/120/4/417/7425469 by guest on 04 July 2024

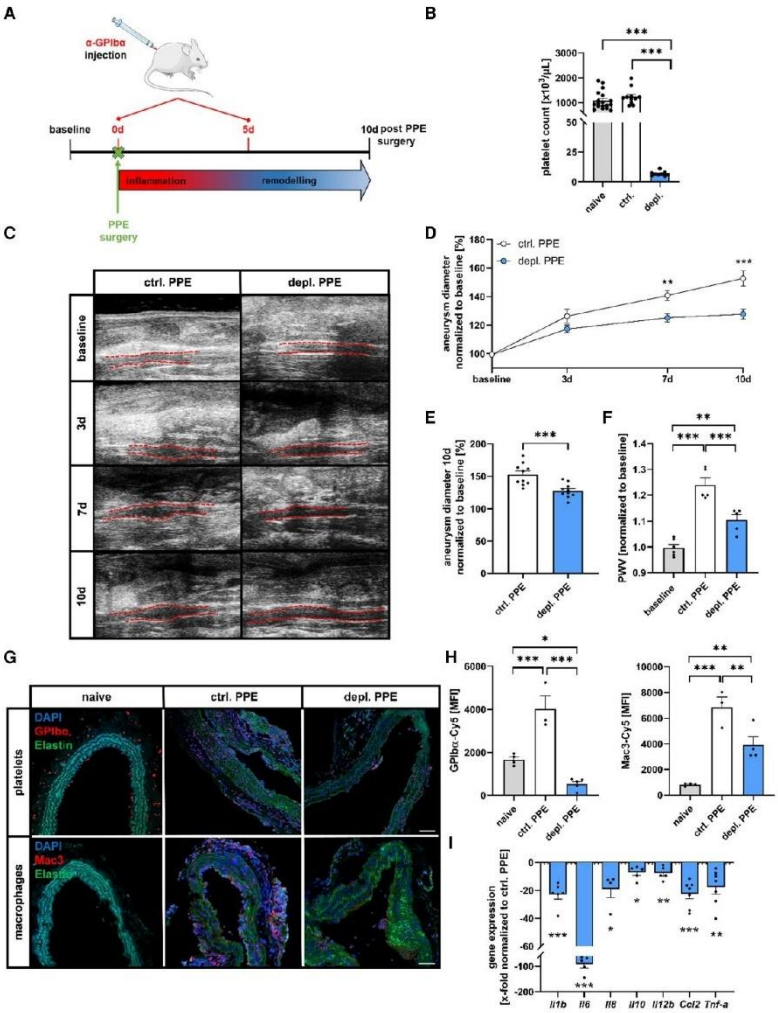


Figure 1 Platelet depletion reduces AAA progression and attenuates inflammatory response. (*A*) Schematic of experimental procedure: C57BL/6J mice received a platelet-depleting anti-GPIbα (depl.) or IgG control (ctrl.) antibody (at Days 0 and 5) after PPE surgery. Generated with BioRender. (*B*) Platelet counts of unoperated mice before and after platelet depletion ($n = 11$–18). (*C*) Ultrasound images at indicated time points (baseline, Days 3, 7, and 10) of depleted and control mice after PPE surgery to investigate aneurysm development. (*D*) Aneurysm diameter was determined by ultrasound measurements at the indicated time points ($n = 10$). Data were normalized to baseline. (*E*) Aortic diameter progression of depl. PPE and ctrl. PPE mice at Day 10 post-surgery, normalized to baseline ($n = 10$). (*F*) Calculated PWV 10 days after PPE surgery, normalized to baseline ($n = 5$–6). (*G*) Representative immunofluorescence (IF) images of platelets (CD42b/anti-GPIbα, upper panels), macrophages (anti-Mac3, red, lower panels), nuclei (DAPI), and elastin (autofluorescence) in aortic tissue sections of depl. PPE and ctrl. PPE at Day 3 post-surgery ($n = 3$–5). Scale bar: 50 µm. Aortic tissue of naive mice served as control ($n = 4$). (*H*) Quantification of platelet (GPIbα, left) and macrophage (Mac3, right) migration into the aortic tissue of depl. PPE and ctrl. PPE mice at Day 3 post-surgery ($n = 3$–5). Naive mice served as control ($n = 4$). (*I*) Inflammatory gene expression in aortic tissue of depl. PPE mice 3 days after surgery. Fold changes were normalized to ctrl. PPE mice ($n = 4$–7). Data are represented as mean ± SEM. Statistical significances were determined by one-way ANOVA with Holm–Sidak's multiple comparison (*B*, *F*, *H*), two-way ANOVA with Sidak's multiple comparison test (*D*), unpaired Student's *t*-test (*E*), or multiple *t*-test (*I*). $^{*}P < 0.05$, $^{**}P < 0.01$, $^{***}P < 0.001$. Ccl, CC chemokine ligand; DAPI, 4′,6-diamidino-2-phenylindole.

Downloaded from https://academic.oup.com/cardiovascres/article/120/4/417/7425469 by guest on 04 July 2024

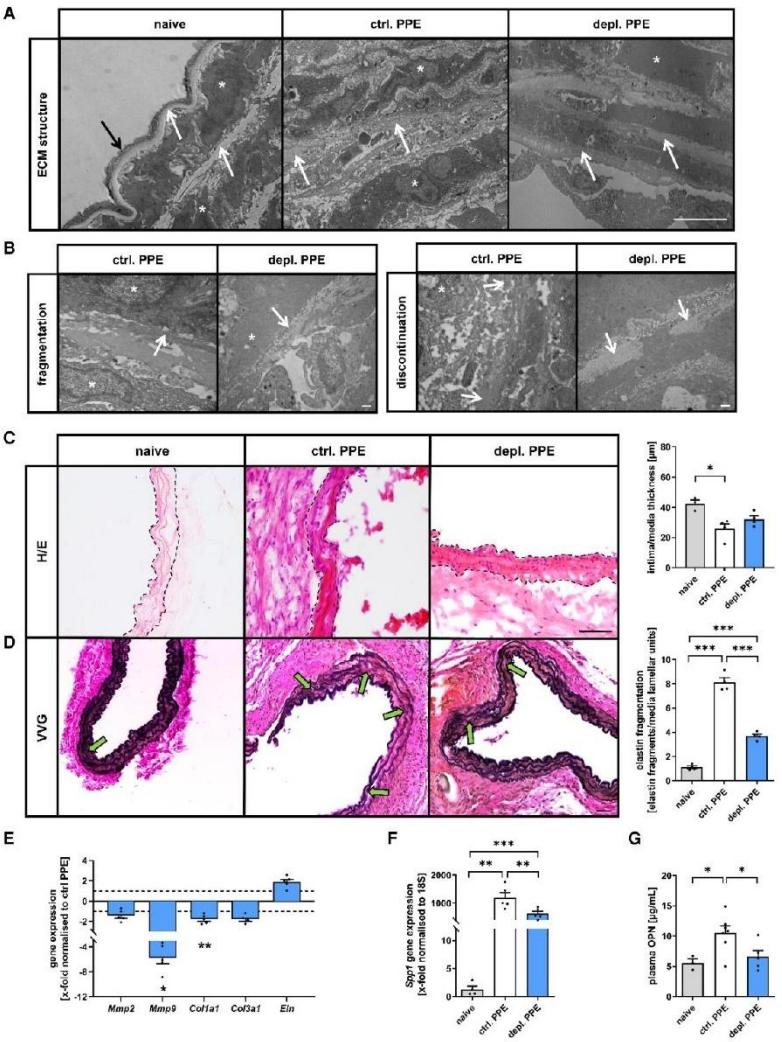


Figure 2 Platelet depletion alters ECM remodelling in PPE-operated mice 10 days after surgery. (*A–G*) C57BL/6J mice received a platelet depleting anti-GPIbα (depl.) or IgG control (ctrl.) antibody (at Days 0 and 5) after PPE surgery and were sacrificed at Day 10 for tissue preparation. (*A*) Exemplary TEM images of aortic tissue from depl. PPE and ctrl. PPE mice 10 days after surgery. Aortic tissue of naive mice served as control (2900× magnification, $n = 2$). Black arrow indicates elastin, white arrowheads indicate endothelial layer, and stars indicate vascular smooth muscle cells. Scale bars: 10 µm. (*B*) TEM images of fragmented and discontinuous aortic elastic tissue from depl. PPE and ctrl. PPE mice at Day 10 post-surgery (13,000× magnification, $n = 2$). Scale bars: 0.5 µm. (*C* and *D*) Representative images of aortic tissue from naive and PPE-operated mice using (*C*) haematoxylin-eosin (H/E) staining and (*D*) Verhoeff van Gieson (VVG) staining. Intima/media thickness was determined after H/E staining ($n = 3–4$), and elastin fragmentation (breakdowns) was counted after VVG staining ($n = 4$). Scale bars: (*C*) 50 µm and (*D*) 100 µm. (*E*) Stiffness-related gene expression in aortic tissue of naive and PPE-operated mice. Fold change was normalized to ctrl. PPE mice ($n = 4–5$). (*G*) *Spp1* (OPN) gene expression in aortic tissue of naive and PPE-operated mice. Fold change was normalized to 18S housekeeping gene ($n = 4–5$). (*H*) Osteopontin plasma concentration (µg/mL) in naive and PPE-operated mice ($n = 3–7$). Data are represented as mean ± SEM. Statistical significances were determined by one-way ANOVA with Holm–Sidak's multiple comparison test (*C*, *D*, *F*, and *G*) and multiple *t*-test (*E*). $^{*}P < 0.05$, $^{**}P < 0.01$, $^{***}P < 0.001$. Col, collagen; ctrl, control; depl., depletion; Eln, elastin; Mmp, matrix metalloproteinase; OPN, osteopontin; *Spp1*, secreted phosphoprotein 1.

Downloaded from https://academic.oup.com/cardiovascres/article/120/4/417/7425469 by guest on 04 July 2024

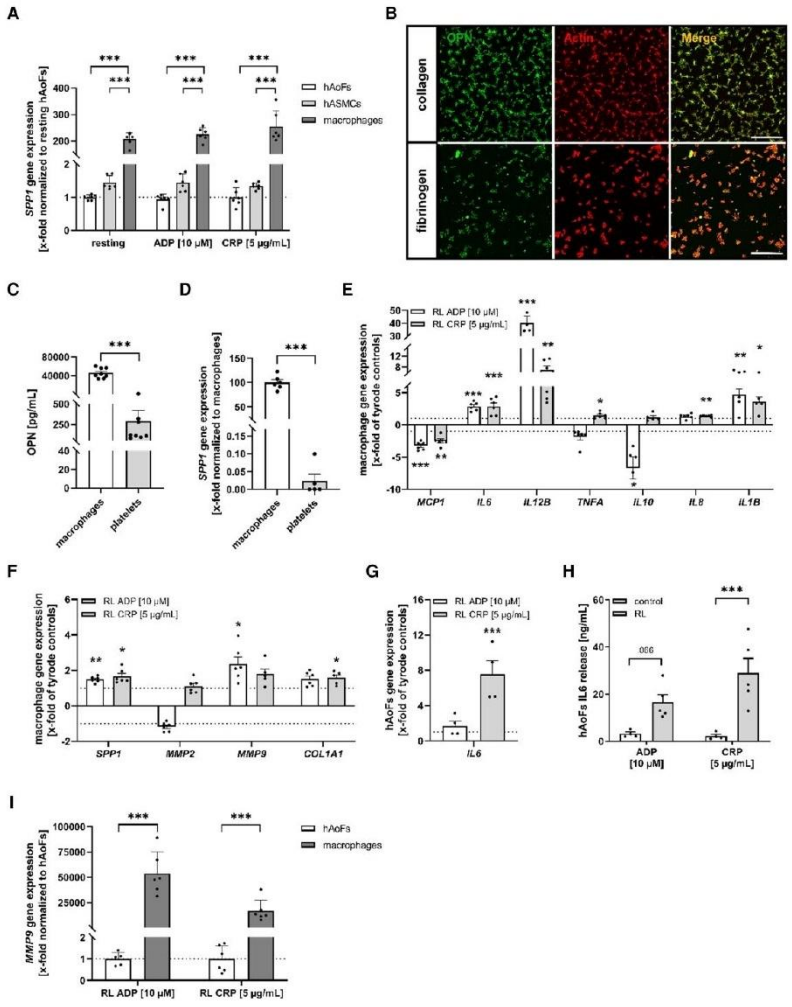


Figure 3 Platelet releasates affect inflammatory and stiffness-related gene expression of macrophages *in vitro*. (*A*) *SPP1* gene expression of hAoFs, hASMCs, and differentiated macrophages (derived from PMA-activated THP-1 cells) in cell culture experiments stimulated with releasates (RLs) of human platelets for 6 h ($n = 6$). Platelets were stimulated with indicated agonists. Fold changes of hASMCs and differentiated macrophages were normalized to hAoFs treated with resting platelet releasates. (*B*) Representative fluorescence images of OPN (anti-OPN) in adherent platelets (actin staining with rhodamine-phalloidin) on collagen (200 µg/mL) and fibrinogen (100 µg/mL) after 20 min ($n = 3$). Scale bar: 50 µm. (*C*) OPN release of differentiated macrophages and ADP (10 µM) stimulated platelets was determined by ELISA ($n = 8$). (*D*) *SPP1* gene expression in differentiated macrophages and resting platelets ($n = 5$–6). (*E* and *F*) Inflammatory and stiffness-related gene expression of differentiated macrophages, incubated with releasates of human platelets (RL) for 6 h. Platelets were stimulated with indicated agonists. Fold change was normalized to corresponding tyrode controls ($n = 4$–6). (*G*) *IL6* gene expression of hAoFs, incubated with releasates of human platelets (RL) for 24 h. Platelets were stimulated with indicated agonists. ($n = 4$). (*H*) IL6 release of hAoFs, incubated with releasates of human platelets (RL) for 24 h. Platelets were stimulated with indicated agonists ($n = 4$–5). (*I*) *MMP9* gene expression of hAoFs and macrophages in cell culture experiments stimulated with releasates (RL) of human platelets for 6 h ($n = 5$–6). Platelets were stimulated with indicated agonists. Fold changes were normalized to hAoFs gene expression. Data are represented as mean ± SEM. Statistical significances were determined by two-way ANOVA with Sidak's multiple comparison (*A*, H, *I*), unpaired Student's *t*-test (*C*, *D*, and *G*) or multiple *t*-test (E and *F*). $^*P < 0.05$, $^{**}P < 0.01$, $^{***}P < 0.001$. Col, collagen; RL, releasate; *SPP1*, secreted phosphoprotein 1.

Downloaded from https://academic.oup.com/cardiovascres/article/120/4/417/7425469 by guest on 04 July 2024

activated platelets (with ADP and CRP) *in vitro* (*Figure 3E* and *F*). The data revealed that platelet releasates alter inflammatory gene expression in macrophages. Activated platelet releasates caused marked up-regulation of key inflammatory genes, such as *IL-6*, *IL-12B*, and *IL-1B* but only moderate gene expression of tumour necrosis factor (TNF)-α or IL-8 (*Figure 3E*). We next studied the influence of releasates on stiffness-related gene expression in macrophages. Releasates from activated platelets enhanced the gene expression of *SPP1, MMP9, and collagen Ia1* in macrophages (*Figure 3F*), which supports our *in vivo* findings and suggests that a crosstalk between platelets and macrophages may be a central mechanism for AAA initiation and diameter progression. In addition, we could show for the first time that treatment of hAoFs with releasates of CRP-activated platelets induced IL-6 gene expression and IL-6 release from these cells (*Figure 3G* and *H*). These results strongly suggest a significant contribution of platelets in paracrine effects of fibroblasts that amplify monocyte recruitment and activation in the pathogenesis of AAA.[20] Next, we also analysed the platelet-induced MMP9 expression of hAoFs by incubating the cells with the supernatant of ADP- and CRP-activated platelets. As shown in *Figure 3I*, we detected MMP9 expression also in hAoFs when incubated with the supernatant of activated platelets. However, according to the current literature, MMP9 gene expression was low in AoFs compared with macrophages (*Figure 3I*).[21]

3.4 Platelets adhere to immobilized osteopontin via integrin $\alpha_V\beta_3$ under static and dynamic conditions

To determine the impact of OPN in platelet-mediated responses in inflammation and aortic wall remodelling in AAA, we analysed the expression of OPN in aortic explants. While only limited OPN expression was detected in the aortic wall of naive mice, we found elevated OPN protein expression in AAA explants 28 days post-surgery (*Figure 4A*). To analyse a potential role for aortic OPN in recruiting platelets to the vessel wall in AAA, we determined platelet adhesion to immobilized full-length and cleaved OPN under static conditions. Cleavage of OPN was achieved by thrombin treatment and verified by silver staining (see Supplementary material online, *Figure S2B*). Activation of human platelets with ADP and CRP resulted in enhanced platelet adhesion to full-length and cleaved OPN with similar amplitude (*Figure 4B*). Control experiments examined platelet adhesion to fibrinogen (positive control) and BSA (negative control) and revealed that platelet adhesion on OPN is highly up-regulated after platelet activation. Incubation of platelets with the $\alpha_V\beta_3$ inhibiting antibody MAB1976 revealed that platelets adhere to OPN—at least partially—through integrin $\alpha_V\beta_3$ because platelet adhesion to OPN was significantly reduced compared with controls (*Figure 4C*).

Under high arterial shear conditions, we next examined thrombus formation on a collagen matrix and compared the surface coverage of three-dimensional thrombi with platelet adhesion and aggregate formation on a mixed collagen-OPN matrix using a well-established *ex vivo* flow chamber system. As shown in *Figure 4D*, increased thrombus formation was observed on the collagen-OPN matrix compared with collagen alone, suggesting that OPN not only affects platelet adhesion but also thrombus formation under high arterial shear flow conditions found in the aorta (*Figure 4D*). Platelet adhesion to immobilized OPN induced the formation of filopodia and lamellipodia in platelets indicating that platelet adhesion to OPN affects cytoskeletal remodelling and increases the platelet surface area. Again, no major alterations in cytoskeletal remodelling were detected between platelets adhering to full-length and cleaved OPN. However, platelet activation by ADP or CRP strongly supported the formation of lamellipodia of platelets on the OPN matrix (*Figure 4E*; see Supplementary material online, *Figure S2C*). When we analysed platelet adhesion to collagen-full length OPN or collagen-cleaved OPN surfaces and compared them with collagen alone, we did not detect any significant changes under static conditions (see Supplementary material online, *Figure S2D*). Furthermore, platelet adhesion was unaltered when platelets were pre-treated with soluble full-length or cleaved OPN (see Supplementary material online, *Figure S2E*), suggesting that arterial shear conditions are crucial for amplified platelet adhesion and thrombus formation on a collagen-OPN matrix. To examine if soluble OPN is able to amplify platelet activation, we determined active integrin $\alpha_{IIb}\beta_3$ and P-selectin exposure by flow cytometry. However, our results revealed no impact of soluble OPN on platelet activation following treatment with standard agonists such as ADP and CRP (see Supplementary material online, *Figure S2F* and *G*).

3.5 Platelet activation and pro-coagulant activity are key elements for the progression of experimental AAA

Next, we examined if aberrant platelet activation is responsible for the observed platelet-mediated effects on inflammation and remodelling in AAA. To this end, we determined platelet integrin $\alpha_{IIb}\beta_3$ activation and P-selectin exposure as marker for degranulation using flow cytometry. As shown in *Figure 5A*, blood was drawn at various time points (Days 3, 10, and 28 post-surgery) (schematic overview, *Figure 5A*), and aneurysm formation was monitored over a time period of 28 days after PPE surgery and compared with sham-operated controls (*Figure 5B*; see Supplementary material online, *Figure S3A*). At an early time point (Day 3), slightly reduced P-selectin exposure and integrin activation but unaltered PS exposure were observed following platelet stimulation with PAR4 peptide that activated the thrombin receptor PAR4 (*Figure 5C*). At Day 10 post-PPE surgery, no differences were detected in the activation or pro-coagulant activity in platelets from PPE-operated mice compared with sham-operated controls (*Figure 5D*). However, at a later time point (Day 28), we detected significantly enhanced P-selectin exposure and integrin $\alpha_{IIb}\beta_3$ activation after stimulation of the collagen receptor GPVI using CRP. In addition, pro-coagulant activity of platelets isolated from PPE-operated mice was enhanced compared with sham-operated controls (*Figure 5E*).

Determination of Spearman's correlation coefficient between the diameter of the aneurysm and Annexin V binding to platelets at Days 3 and 28 after PPE surgery revealed a strong correlation between aortic diameter expansion and elevated pro-coagulant activity (*Figure 5F*) emphasizing a role for PS at the platelet surface in AAA pathology. It is worth mentioning that the number and size of platelets (see Supplementary material online, *Figure S3B and C*) and the exposure of integrins on the platelet surface under resting and stimulated conditions (see Supplementary material online, *Figure S3D and E*) were not altered at Days 3, 10, and 28 after induction of AAA when compared with sham-operated controls. Furthermore, elevated platelet–neutrophil conjugates were detected in PPE-operated mice at Day 3 post-surgery compared with sham-operated controls (*Figure 5G*), while no alterations were determined when we analysed leucocyte–platelet conjugates (see Supplementary material online, *Figure S3F*).

3.6 Platelet depletion reduces aortic diameter progression in experimental Ang-II–induced AAA formation

To confirm the importance of platelets in AAA formation and progression in another experimental mouse model of AAA, we depleted platelets in Ang-II–infused apolipoprotein E (ApoE) knock-out mice. We found that platelet depletion significantly attenuated the diameter progression of AAA over a 7-day time course by ultrasound tracking (*Figure 6A* and *B*; see Supplementary material online, *Figure S4C*). In line with platelet depletion in PPE mice (*Figure 2C* and *D*), we detected unaltered intima/media thickness but reduced elastin fragmentation in platelet-depleted Ang-II–infused ApoE mice (see Supplementary material online, *Figure S4A and B*). Next, we examined whether this is due to aberrant platelet activation as observed in PPE mice. First, we confirmed aneurysm formation and progression in Ang-II–infused ApoE mice compared with sham controls (*Figure 6C*; see Supplementary material online, *Figure S4D*). In Ang-II–infused ApoE knock-out mice, significantly reduced P-selectin exposure and integrin $\alpha_{IIb}\beta_3$ activation in response to different concentrations of CRP and PAR4 peptide were observed at an early time point (Day 3;

Downloaded from https://academic.oup.com/cardiovascres/article/120/4/417/7425469 by guest on 04 July 2024

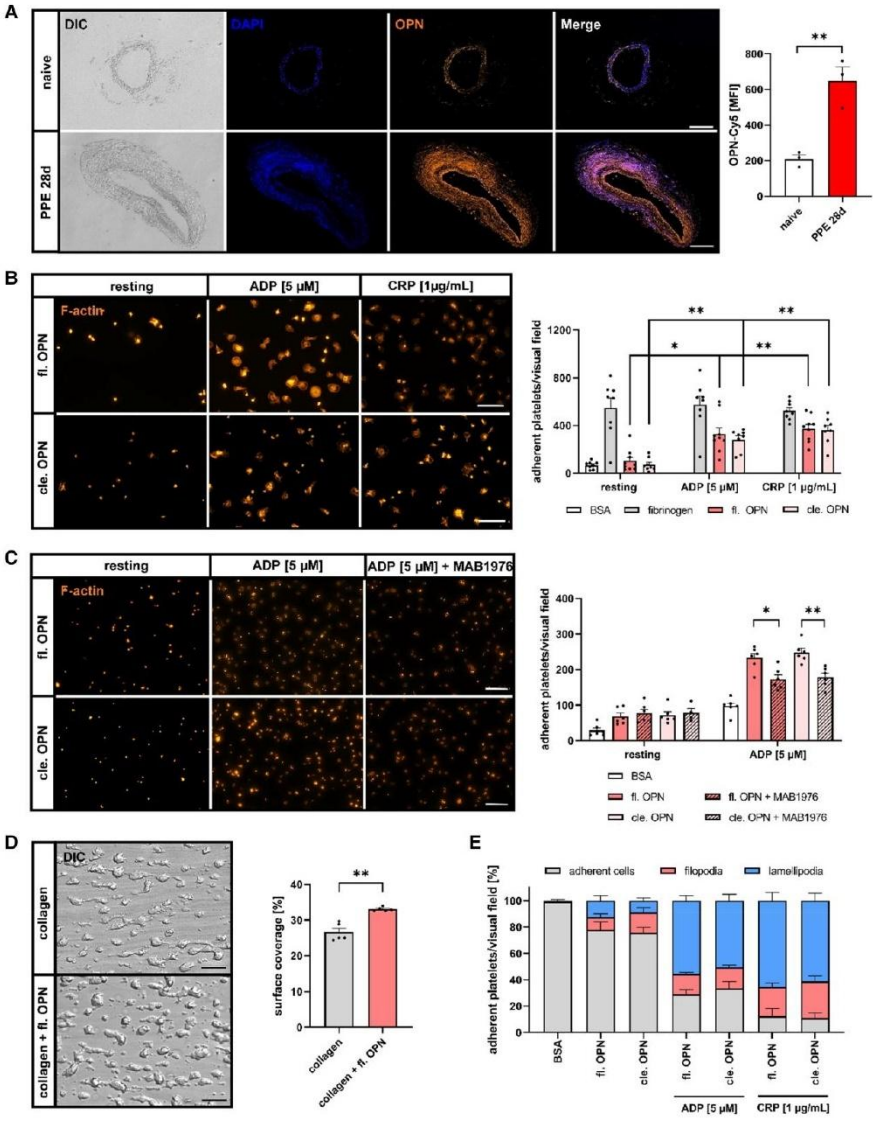


Figure 4 Platelets adhere to immobilized full-length osteopontin via integrin $\alpha_V\beta_3$ under static and dynamic conditions. (*A*) Representative immunofluorescence (IF) images and quantification of aortic tissue from naive and PPE-operated mice at Day 28 post-surgery, specifically stained for osteopontin (anti-OPN) and nuclei (DAPI) ($n = 3$). Scale bar: 50 µm. (*B*) Representative images and quantification of adherent human platelets stimulated with indicated agonists, on BSA (1%), fibrinogen (100 µg/mL), and cleaved or full-length osteopontin (5 µg/mL) after 30 min. Adherent platelets were visualized by rhodamine-phalloidin staining (F-actin) ($n = 5$). Scale bar: 20 µm. (*C*) Representative images and quantification of adherent resting and activated (ADP 10 µM) human platelets, on BSA (1%) and cleaved or full-length osteopontin (5 µg/mL) after treatment with or without MAB1976 ($\alpha_V\beta_3$ inhibiting antibody) for 30 min ($n = 5$). Scale bar: 50 µm. (*D*) Representative images and quantification of thrombus formation experiments with human whole blood on a

(continued)

Downloaded from https://academic.oup.com/cardiovascres/article/120/4/417/7425469 by guest on 04 July 2024

Figure 4 Continued
collagen matrix (200 µg/mL) and a collagen/full-length osteopontin matrix (collagen: 200 µg/mL, fl. OPN: 100 µg/mL) at an arterial shear rate of 1700s^{-1} ($n = 5$). Scale bar: 50 µm. (*E*) Number of filopodia-forming and lamellipodia-forming platelets spread on different matrices, indicated as percent of adherent cells per visual field ($n = 5$). Data are represented as mean ± SEM. Statistical significances were determined by two-way ANOVA with Tukey's multiple comparison (*B* and *C*) or unpaired Student's *t*-test (*D*). *$P < 0.05$, **$P < 0.01$. BSA, bovine serum albumin; cle., cleaved; DAPI, 4′, 6-diamidino-2-phenylindole; DIC, differential interference contrast; fl., full-length; OPN, osteopontin; PPE, porcine pancreatic elastase (infusion).

Figure 6D). Furthermore, agonist induced up-regulation of integrin $\alpha_{IIb}\beta_3$ at the platelet surface was reduced as well. In contrast to PPE-induced AAA formation, no major alterations of platelet activation were detected in Ang-II–infused ApoE knock-out mice at later time points (Days 10 and 28) (*Figure 6E* and *F*; see Supplementary material online, *Figure S4E*). Pro-coagulant activity of platelets from Ang-II–infused ApoE knock-out mice was unaltered at all-time points examined (*Figure 6E* and *F*). In control experiments, we confirmed unaltered platelet counts and size in ApoE knock-out mice (see Supplementary material online, *Figure S4F* and *G*).

3.7 Platelet activation, pro-coagulant activity, and OPN protein expression are important pathological features in patients with AAA

To study the relevance of platelet activation on inflammation in patients with AAA, we first determined integrin $\alpha_{IIb}\beta_3$ activation and *P*-selectin exposure of platelets from AAA patients. As shown in *Figure 7A*, we found elevated platelet activation in resting platelets, suggesting a pre-activated state of platelets in the blood circulation of AAA patients. Stimulation of the platelet collagen receptor GPVI reveals that the threshold where CRP is able to activate platelets is reduced in patients with AAA compared with age-matched healthy controls, as elevated platelet activation was detectable even with low-dose CRP (0.1 µg/mL). In addition, we detected elevated integrin $\alpha_{IIb}\beta_3$ activation after ADP stimulation of platelets (*Figure 7A*; see Supplementary material online, *Figure S5A*). Furthermore, reduced platelet counts, but unaltered platelet size (MPV), were detected in AAA patients compared with AMCs (see Supplementary material online, *Figure S5B*). Clinical characteristics of the AAA patient cohort are shown in Supplementary material online, *Table S1*.

Next, we analysed aortic tissue and the ILT of AAA patients who underwent open surgical repair. Analysis of the ILT of different patients revealed that platelets and OPN protein accumulate and—more importantly—co-localize in the ILT suggesting that OPN protein accumulation might also modulate platelet recruitment, platelet adhesion, and accumulation in the ILT (*Figure 7B*; see Supplementary material online, *Figure S6B* and *C*). In line with the results from experimental AAA, we identified platelets in the aortic wall of patient specimens, suggesting platelet migration into AAA tissue (*Figure 7C* and *D*; see Supplementary material online, *Figure S6A*). Furthermore, platelets co-localize to macrophages and fibroblasts in the vessel wall suggesting a crosstalk of these cells upon AAA progression in patients (*Figure 7C*). Next, we detected high OPN protein expression in the abdominal aortic wall of patient specimens, suggesting that OPN might be—at least in part—responsible for the recruitment of platelets to aortic tissue (*Figure 7D*; see Supplementary material online, *Figure S6A*). This is strengthened by the observed co-localization of platelets and OPN (*Figure 7D*).

Furthermore, we detected co-localization of macrophages and fibroblasts with OPN suggesting that these cells might be recruited to the aortic wall by OPN as well (*Figure 7D*). In addition to enhanced platelet activation and platelet recruitment to the aortic wall and the ILT, we detected elevated levels of inflammatory and anti-inflammatory cytokines such as IL-8, IL-10, IL-12, and IFN-α in the patient plasma (*Figure 7E*). In contrast, no alterations were detected in the plasma of AAA patients with regard to soluble *P*-selectin, PSGL-1, RANTES, IL-1β, IL-6, and INF-γ (see Supplementary material online, *Figure S5C* and *D*). Furthermore, plasma levels of MMP2 and MMP9 were unaltered in AAA patients (*Figure 7F*). However, we again detected elevated OPN plasma levels in these patients, suggesting an important role of OPN for inflammation and remodelling of the abdominal aortic wall (*Figure 7F*).

4. Discussion

In this study, we found that platelets play a crucial role in AAA, likely due to the modulation of inflammation and degradation of the ECM induced by the functional crosstalk with macrophages and fibroblasts. Platelet depletion in experimental AAA reduced inflammation and aortic remodelling, leading to significantly reduced aortic diameter expansion in these mice. In AAA patients and in experimental mice, platelet activation and pro-coagulant activity were enhanced and might be responsible for platelet-induced effects on AAA pathology. Furthermore, we detected platelets and OPN in the vessel wall and in the ILT of patients who underwent open repair of AAA. Of note, OPN co-localized with platelets, suggesting a potential role for OPN in the recruitment of platelets to the ILT and probably to the aortic wall.

AAA is a multi-factorial disease, which is characterized by chronic inflammation and degradation of the ECM in the abdominal aortic wall, often accompanied by the formation of an ILT. Increased platelet activation and aggregation is a characteristic feature of many CVDs, increasing the risk for thrombo-embolic events.[13,22–25] Here, we provide evidence for enhanced platelet activation at later time points in mice with experimental AAA (PPE-operated mice) and in patients with AAA. Both PPE-operated mice and AAA patients exhibit elevated platelet responses after stimulation of the major collagen receptor GPVI using CRP, especially with low concentrations of the agonist. This, together with elevated platelet activation in resting, non-stimulated circulating platelets suggest that the threshold to induce platelet responses is reduced in experimental mice and in patients with AAA. The chronic inflammatory state in AAA might be a decisive determinant in priming circulating platelets for subsequent pro-coagulant and pro-thrombotic activity.

Recently, enhanced platelet reactivity (only *P*-selectin, no integrin activation) has been detected following thrombin and thromboxane receptor activation using platelets from AAA patients and experimental mice.[26] In contrast to our study, the authors used human platelets from healthy participants at any age as controls (not age-matched, although platelets behave differently with increasing age) and murine platelets isolated from a mouse model with topical application of elastase to induce AAA. In addition, they analysed the thrombin/thromboxane receptor pathway in murine and human platelets but did not stimulate platelets with ADP or collagen/CRP to activate the major collagen receptor GPVI. Another study from Robless *et al.*[27] detected elevated spontaneous platelet aggregation in AAA patients and in patients with peripheral artery disease (PAD), suggesting enhanced platelet activation even in the absence of agonists. In contrast with our data, no differences were observed in PAC-1 binding or *P*-selectin exposure in resting platelets of patients with AAA or PAD. This is striking because the conformational change of integrin $\alpha_{IIb}\beta_3$ in its active form is a prerequisite for (spontaneous) platelet aggregation.[28] In another study, high glycocalicin levels were detected in patients with AAA, suggesting increased platelet destruction due to elevated platelet activation in these patients. Consequently, the authors detected decreased platelet counts. However, no alterations in platelet counts were observed in the here investigated AAA cohort compared with AMCs. Notably, while our study compares platelet counts between patients with AAA and age-matched

Downloaded from https://academic.oup.com/cardiovascres/article/120/4/417/7425469 by guest on 04 July 2024

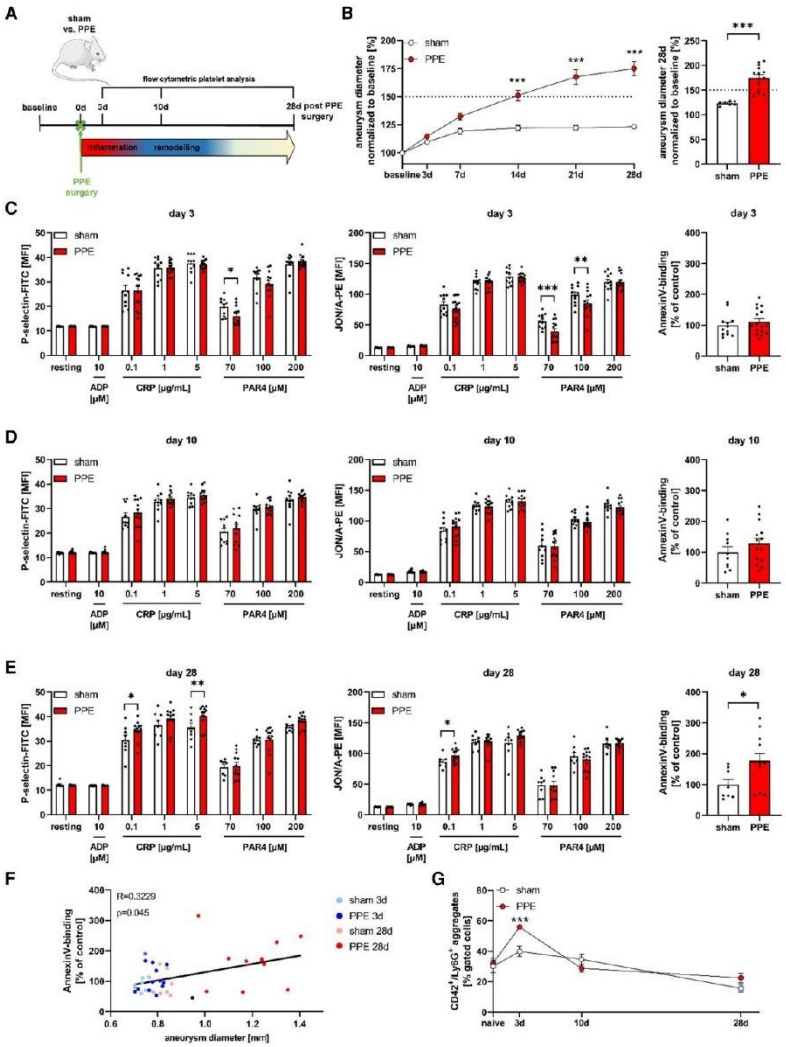


Figure 5 Platelet activation and pro-coagulant activity is crucial for the AAA progression in the murine PPE model. (*A*) Schematic of experimental procedure: C57BL/6J mice underwent sham or PPE surgery. Mice were sacrificed at indicated time points for flow cytometric analysis of platelets in whole blood at Days 3, 10, and 28. (*B*) Ultrasound measurements were performed prior surgery (baseline) and at Days 3, 7, 14, 21, and 28 to investigate aneurysm diameter ($n = 8–13$). Data were normalized to baseline (*C–E*) platelet degranulation (*P*-selectin-FITC), active integrin $\alpha_{IIb}\beta_3$ externalization (JON/A-PE), and AnnexinV-binding to platelets from sham or PPE-operated mice at Days 3 (*C*), 10 (*D*), and 28 (*E*) after PPE surgery and were determined by flow cytometry. Platelets were stimulated with indicated agonists ($n = 7–15$). Data are represented as MFI or percent-gated cells normalized to control. (*F*) Spearman's correlation between the diameter of the aneurysm and AnnexinV-binding at Days 3 and 28 after PPE surgery ($n = 8–15$). (*G*) Aggregate formation of platelets ($CD42^+$) and neutrophils ($Ly6G^+$) in whole blood of naive, sham, or PPE-operated mice at Days 3, 10, and 28 after surgery determined by flow cytometry ($n = 5–6$). Data are represented as mean ± SEM. Statistical significances were determined by two-way ANOVA with Sidak's multiple comparison test (*B* and *G*), unpaired Student's *t*-test, or multiple *t*-test (*C*, D and *E*). $^*P < 0.05$, $^{**}P < 0.01$, $^{***}P < 0.001$. MFI, mean fluorescence intensity; PAR4, protease-activated receptor 4 activating peptide.

Downloaded from https://academic.oup.com/cardiovascres/article/120/4/417/7425469 by guest on 04 July 2024

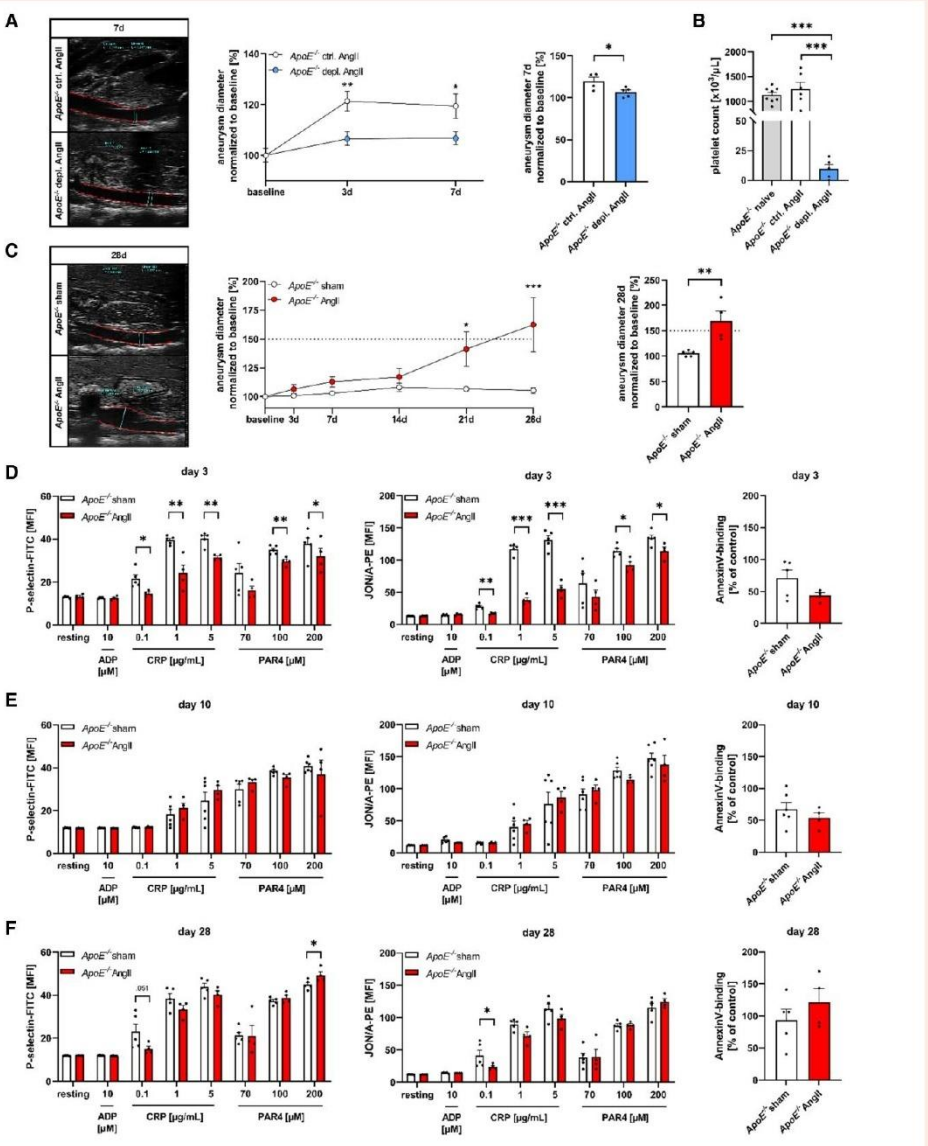


Figure 6 Platelet depletion reduces aortic diameter progression in experimental Ang-II–induced AAA formation. (*A*) *ApoE*$^{-/-}$ mice received a platelet depleting anti-GPIbα (depl.) or IgG control (ctrl.) antibody (at Days 0 and 5) after osmotic mini-pump implantation. Aortic diameter progression of depl. *ApoE*$^{-/-}$ and ctrl. *ApoE*$^{-/-}$ mice infused with Ang-II was measured via ultrasound over a time period of 7 days ($n = 4–5$). Data were normalized to baseline. (*B*) Platelet counts of naive, depl. and ctrl. *ApoE*$^{-/-}$ mice before and after platelet depletion ($n = 4–6$). (*C*) Aortic diameter progression in sham or Ang-II–infused *ApoE*$^{-/-}$ mice over a time period of 28 days was determined via ultrasound measurements ($n = 4–5$). Data were normalized to baseline. (*D–F*) Platelet degranulation (*P*-selectin-FITC), active integrin $\alpha_{IIb}\beta_3$ externalisation (JON/A-PE), and AnnexinV-binding to platelets in sham or Ang-II–infused *ApoE*$^{-/-}$ mice at 3 (*C*), 10 (*D*), (continued)

Downloaded from https://academic.oup.com/cardiovascres/article/120/4/417/7425469 by guest on 04 July 2024

Figure 6 Continued
and 28 days (*E*) after osmotic mini-pump implantation were analysed via flow cytometry. Platelets were stimulated with indicated agonists ($n = 4–5$). Data are represented as MFI or percent-gated cells normalized to control. Statistical significances were determined by two-way ANOVA with Sidak's multiple comparison test (*A* and *C*), unpaired Student's *t*-test (*A* and *C*), one-way ANOVA with Holm–Sidak's multiple comparison test (*B*), or multiple *t*-test (*D*, *E* and *F*). $^{*}P < 0.05$, $^{**}P < 0.01$, $^{***}P < 0.001$. ctrl, control; depl., depletion; MFI, mean fluorescence intensity; PAR4, protease-activated receptor 4 activating peptide.

healthy volunteers, Milne *et al.*[29] used carotid artery stenosis patients as controls. An increase in platelet activation was also observed after endovascular repair of AAA,[30] while our analysis of platelet activation in AAA patients occurred before any treatment.

In addition to enhanced platelet activation in mice and patients, we detected elevated PS exposure at the surface of platelets as a marker for pro-coagulant activity. Enhanced pro-coagulant activity might result from elevated platelet activation. However, it has been shown that inflammatory cytokines may enhance pro-coagulant activity of platelets.[31] Pro-coagulant activity of resting and activated platelets might be responsible for elevated thrombin plasma levels in AAA patients,[32,33] which is a common feature in this disease. Thus, it is not surprising that there is a correlation between elevated pro-coagulant activity of platelets (PS exposure) and aortic diameter expansion in PPE-operated mice (*Figure 5F*). However, the correlation is relatively weak, both in regards to the *R* and the *P*-values that might be due—at least in part—to the variable results from flow cytometric analysis.

So far, a small number of experimental studies have analysed the role of platelets in AAA. Touat *et al.*[17] have used a xenograft model of rats to induce aneurysms. They showed that platelet inhibition by abciximab (which blocks integrin $\alpha_{IIb}\beta_3$) limited aortic aneurysm expansion, suggesting that platelet stimulation, and in particular integrin $\alpha_{IIb}\beta_3$ activation, may be a promising target in the prevention of AAA progression. To date, platelet responses have been analysed mainly in the Ang-II infusion model. Liu *et al.*[34] showed that treatment of mice with clopidogrel, an antagonist of the ADP receptor $P2Y_{12}$, prevents Ang-II–induced AAA formation by protecting the elastic cell lamina in the mouse aorta. Further, the authors found reduced macrophage infiltration and MMP2 expression after clopidogrel treatment. In a more recent study, Owens *et al.*[15] found the reduced rupture of established AAAs and improved the survival of mice after clopidogrel treatment. However, all these studies have been done in Ang-II–infused mice, an experimental model that has been shown to primarily feature aortic dissection as a precursor to aortic aneurysm formation. In agreement with these results obtained from Ang-II–infused mice, we detected reduced inflammation and reduced elastin fragmentation in platelet-depleted PPE-operated mice, suggesting that platelet-mediated processes play a role in both aortic dissection and aortic aneurysm formation. However, since platelet activation in experimental PPE mice is comparable with platelet activation in AAA patients including elevated platelet pro-coagulant activity, we believe that the PPE mouse model is a more convenient model to analyse platelet-induced effects on AAA formation and progression.

In contrast to the studies mentioned above, a recent study of Liu *et al.*[35] provided evidence for a protective effect of platelets in the Ang-II–induced mouse model, in which platelet infusion significantly reduced aortic diameter elevation and inflammatory responses. However, differences in the experimental design and the fact that the Ang-II infusion model is a dissection model and does not reflect alterations in platelet activation as observed in PPE mice and in AAA patients might be responsible for differences in results.

The translation of experimental findings into clinical routine has been an issue for AAA in the past. Several trials for different drug classes have failed to confirm a clinical benefit.[36–38] These disease-specific translational difficulties could have several causal reasons, including limitations in experimental mouse models and the multi-factorial character of AAA disease. Researchers have not yet succeeded in identifying a decisive and causal factor for AAA development. In the eyes of the authors, there are multiple reasons why platelets could be a major contributor to AAA development. Platelets represent by far the largest cellular compartment of the blood in terms of quantity, and the presence of an ILT suggests continuous activation in the aneurysmatic abdominal segment. This together with the comparable results in platelet activation, pro-coagulant activity, and OPN expression and localization in PPE-operated mice and in patients with AAA presented herein suggests that the PPE model represents an appropriate model to mimic human AAA pathology.

Interestingly, one study of P-selectin knock-out mice has utilized the PPE mouse model.[39] Genetic deficiency of P-selectin was shown to be protective, as these mice showed attenuated aneurysm formation after infusion with PPE. However, the authors claim that P-selectin deficiency resulted in reduced inflammation and aortic wall remodelling according to abdominal aortic tissue samples from Day 14, which were stained with either haematoxylin/eosin, Masson's trichrome, or Verhoeff's van Gieson. Moreover, P-selectin is exposed not only at the platelet but also at the endothelial membrane. Thus, the presented effects on inflammation and remodelling cannot be attributed solely to platelets and would need to be verified using techniques other than histology.

OPN is a matricellular cytokine that binds to integrins and CD44 and is elevated in many pathological conditions including AAA.[40] It is synthesized by macrophages, vascular smooth muscles cells (VSMCs), and endothelial cells, and its gene expression is highly up-regulated in the aortic wall of AAA patients. Here, we show that platelets enhanced OPN gene expression in macrophages but not in VSMCs or aortic fibroblasts. Platelets contribute to elevated OPN plasma levels through the release of OPN from intracellular stores. OPN plays an important role in inflammatory processes in atherosclerosis, cancer, and several chronic inflammatory diseases.[41] OPN is also known for its role in repair and remodelling processes of the vasculature. The proliferation, migration, and accumulation of VSMCs and the expression of MMPs via the NF-κB signalling pathway are up-regulated by OPN, thereby accelerating the degradation of extracellular matrix in AAA.[42,43] We propose that platelets in-part exert their function in AAA through mediation by OPN and provide strong evidence for OPN to play a role in the recruitment of platelets to the aortic wall and the ILT, suggesting a vicious cycle of platelet-mediated up-regulation of OPN in the plasma and the aortic wall that allows migration of platelets into aortic tissue, amplifying their detrimental effects on the pathology of AAA. Thus, it is not surprising that OPN knock-out mice show attenuated aneurysm formation after Ang-II infusion.[44] In contrast, the analysis of OPN deficient mice in the PPE model showed no protection. However, the study was performed with a limited number of mice, suggesting that the results have to be confirmed by additional experiments.[45] However, OPN is not the only factor through which platelets can affect AAA, because they also amplify inflammation by up-regulating various cytokines in macrophages and fibroblasts (IL-6) and by inducing the up-regulation of proteins involved in ECM remodelling (MMP9, COL1A1), and can contribute to AAA pathology by elevated platelet activation and pro-coagulant activity. Moreover, platelets contain MMP9 and MMP2 that might be released upon platelet activation in AAA, directly contributing to ECM remodelling.[46]

From a clinical point of view, the question arises as to which AAA patient sub-cohort could benefit most from anti-platelet therapy. Major differences in the efficacy of antiplatelet therapy have been linked to the size of the aneurysm. While patients with small-size aneurysms often did not benefit from anti-platelet therapy or even show elevated risk of bleeding, beneficial effects have been provided for patients with large aneurysms.[18,38,47,48] This might be due to the fact that in patient cohorts including very small AAA, an ILT is seldom present.[18] Enlargement of an AAA is usually associated with the development of an ILT.[18] Based on our results, the ILT or its surface could play a prominent role in the recruitment of platelets. From this, ILT-based endpoints could also become more important

Downloaded from https://academic.oup.com/cardiovascres/article/120/4/417/7425469 by guest on 04 July 2024

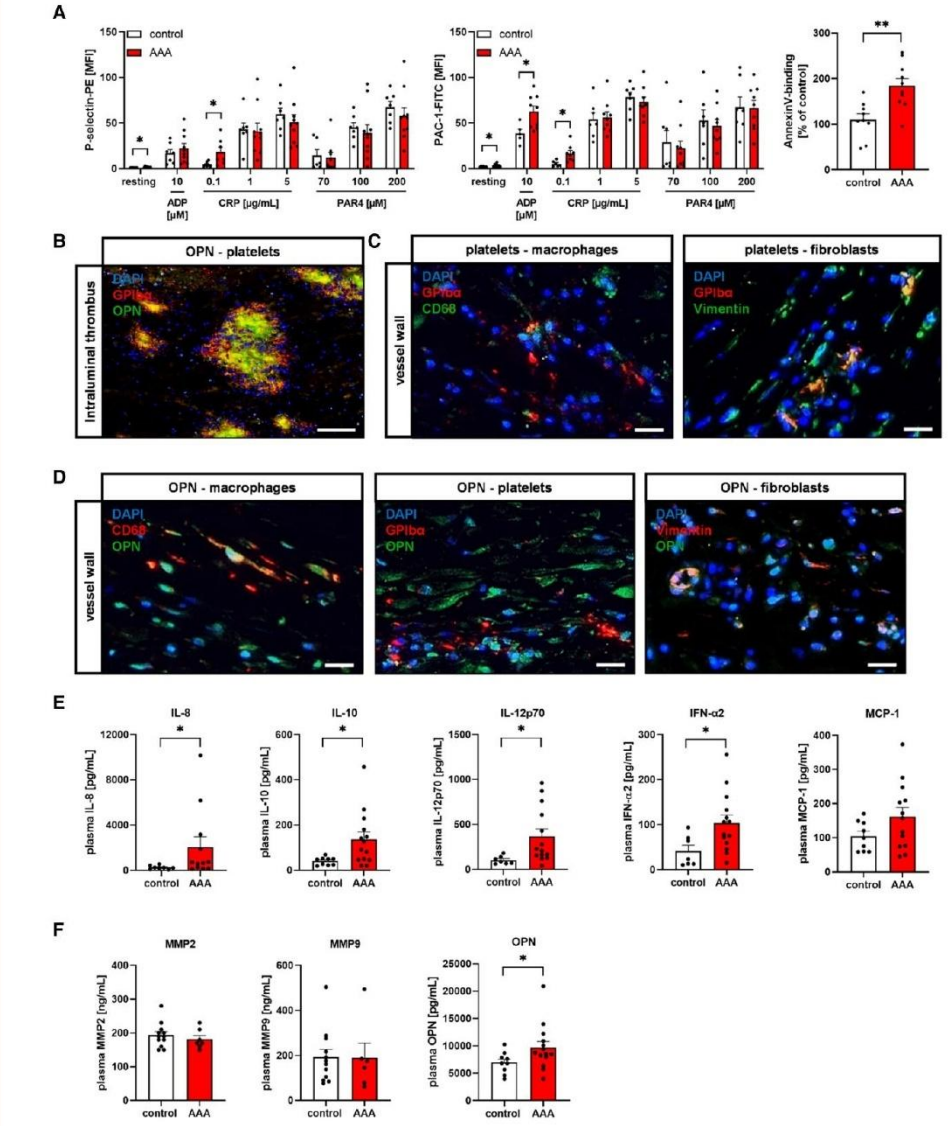


Figure 7 Platelet activation, pro-coagulant activity, and osteopontin are important in AAA pathology. (*A*) Platelet degranulation (P-selectin-PE), active integrin $\alpha_{IIb}\beta_3$ externalization (PAC-1-FITC), and AnnexinV-binding to platelets in whole blood of AAA patients and AMCs were determined by flow cytometry ($n = 5$–10). Data are represented as MFI or percent-gated cells normalized to control. (*B*) Representative immunofluorescence images of platelets (anti-CD42b/GPIbα, 2 µg/mL), osteopontin (anti-OPN, 20 µg/mL), and nuclei (DAPI) in the luminal layer of intraluminal thrombi ($n = 5$) of AAA patients. Scale bar: 100 µm. (*C*) Immunofluorescence staining of platelets (anti-CD42b/GPIbα, 2 µg/mL), nuclei (DAPI), macrophages (anti-CD68 AA 21-120, 10 µg/mL), and fibroblasts (anti-vimentin, 20 µg/mL) respectively in aortic vessel wall of AAA patients. Scale bar: 20 µm. (*D*) Double-staining of osteopontin (anti-OPN, 20 µg/mL) and nuclei (DAPI) with macrophages (anti-CD68, 10 µg/mL), platelets (anti-CD42b/GPIbα, 2 µg/mL), and fibroblasts (anti-vimentin, (continued)

Downloaded from https://academic.oup.com/cardiovascres/article/120/4/417/7425469 by guest on 04 July 2024

Figure 7 Continued
20 μg/mL) in aortic vessel wall. Scale bar: 20 μm. (*E*) Plasma concentration of circulating chemokines and inflammatory markers of AAA patients and AMCs were determined by flow cytometric multiplex analysis (cytometric bead array) ($n = 7–14$). (*F*) Plasma concentration of MMP2, MMP9, and OPN in AAA patients and AMCs using ELISA ($n = 7–14$). Data are represented as mean ± SEM. Statistical significances were determined by multiple *t*-test and unpaired Student's *t*-test (*A*) or unpaired *t*-test with Welch's correction (*E* and *F*). $*P < 0.05$, $**P < 0.01$. DAPI, 4′, 6-diamidino-2-phenylindole; IFN, interferon; OPN, osteopontin; PAR4, protease-activated receptor 4 activating peptide.

for considerations of patient management and anti-platelet therapy in the future. Of note, the clinical implementation of ILT surface measurement to conclude could be comparatively simple to implement but may require further prospective patient studies to evaluate critical endpoints. Considering our findings in summary, the question arises whether an alternative platelet aggregation inhibition, possibly based on GPVI receptor inhibition, might be beneficial. Although our results may advocate for such, further mechanistic insights and data from clinical trials are warranted to substantiate this thesis further.

In summary, own data as well as results from different groups highly support the potential for antithrombotic/antiplatelet strategies in patients to modulate the progression and rupture of AAA. It will be of great importance to identify druggable targets to limit platelet activation and procoagulant activity for this purpose.

Supplementary material

Supplementary material is available at *Cardiovascular Research* online.

Authors' contributions

M.U.W., H.S., and M.E. designed the study. M.U.W., J.M., K.J.K., T.F., A.B., Y.H.R., M.C., N.P., C.B, W.I., I.K., A.M.P., and J.M.S. performed experiments. M.U.W., K.J.K., M.C., and M.E. analysed and interpreted data. M.U.W., K.J.K., and M.E. wrote the manuscript with all the authors providing feedback. M.U.W., J.M., K.J.K., and A.B. contributed equally to this study.

Acknowledgements

We thank Martina Spelleken for excellent technical assistance, Sandra Szczutkowski and Christos Dimopoulos for histology and platelet adhesion experiments, and the centre for Advanced Imaging (CAi) for technical support.

Conflict of interest: None declared.

Funding

This work was supported by the Deutsche Forschungsgemeinschaft (DFG, German Research Foundation) Grant Nos. GZ: WA 3533/3-1 to M.U.W. and EL 651/6-1 and EL 651/8-1 to M.E. and by the Collaborative Research Centre TRR259 (Aortic Disease)—Grant Nos. 397484323, TP A07 to H.S. and M.E.

Data availability

The original contributions presented in the study are included in the article; further inquiries can be directed to the corresponding author.

References

1. Eckstein HH, Böckler D, Flessenkämper I, Schmitz-Rixen T, Debus S, Lang W. Ultrasonographic screening for the detection of abdominal aortic aneurysms. *Dtsch Arztebl Int* 2009;**106**:657.
2. Cameron SJ, Russell HM, Phillip Owens A. Antithrombotic therapy in abdominal aortic aneurysm: beneficial or detrimental? *Blood* 2018;**132**:2619–2628.
3. Golledge J, Morris DR, Pinchbeck J, Rowbotham S, Jenkins J, Bourke M, Bourke B, Norman PE, Jones R, Moxon JV. Editor's choice—metformin prescription is associated with a reduction in the combined incidence of surgical repair and rupture related mortality in patients with abdominal aortic aneurysm. *Eur J Vasc Endovasc Surg* 2019;**57**:94–101.
4. Karrowni W, Dughman S, Hajj GP, Miller FJ. Statin therapy reduces growth of abdominal aortic aneurysms. *J Investig Med* 2011;**59**:1239.
5. Kunath A, Unosson J, Friederich-Persson M, Bjarnegård N, Becirovic-Agic M, Björck M, Mani K, Wanhainen A, Wägsäter D. Inhibition of angiotensin-induced aortic aneurysm by metformin in apolipoprotein E-deficient mice. *JVS Vasc Sci* 2021;**2**:33–42.
6. Sutton SS, Magagnoli J, Cummings TH, Hardin JW. Association between metformin and abdominal aortic aneurysm in diabetic and non-diabetic US veterans. *J Investig Med* 2020;**68**:1015–1018.
7. Sakalihasan N, Limet R, Defawe OD. Abdominal aortic aneurysm. *Lancet* 2005;**365**:1577–1589.
8. Shimizu K, Mitchell RN, Libby P. Inflammation and cellular immune responses in abdominal aortic aneurysms. *Arterioscler Thromb Vasc Biol* 2006;**26**:987–994.
9. Kazi M, Thyberg J, Religa P, Roy J, Eriksson P, Hedin U, Swedenborg J. Influence of intraluminal thrombus on structural and cellular composition of abdominal aortic aneurysm wall. *J Vasc Surg* 2003;**38**:1283–1292.
10. Wang DHJ, Makaroun MS, Webster MW, Vorp DA. Effect of intraluminal thrombus on wall stress in patient-specific models of abdominal aortic aneurysm. *J Vasc Surg* 2002;**36**:598–604.
11. O'Leary SA, Kavanagh EG, Grace PA, McGloughlin TM, Doyle BJ. The biaxial mechanical behaviour of abdominal aortic aneurysm intraluminal thrombus: classification of morphology and the determination of layer and region specific properties. *J Biomech* 2014;**47**:1430–1437.
12. Vorp DA, Mandarino WA, Webster MW, Gorcsan J III. Potential influence of intraluminal thrombus on abdominal aortic aneurysm as assessed by a new non-invasive method. *Cardiovasc Surg* 1996;**4**:732–739.
13. Papapanagiotou A, Daskalakis G, Siasos G, Gargalionis A, Papavassiliou A G. The role of platelets in cardiovascular disease: molecular mechanisms. *Curr Pharm Des* 2016;**22**:4493–4505.
14. Busch A, Bleichert S, Ibrahim N, Wortmann M, Eckstein HH, Brostjan C, Wagenhäuser MU, Goergen CJ, Maegdefessel L. Translating mouse models of abdominal aortic aneurysm to the translational needs of vascular surgery. *JVS Vasc Sci* 2021;**2**:219–234.
15. Owens AP, Edwards TL, Antoniak S, Geddings JE, Jahangir E, Wei WQ, Denny JC, Boulaftali Y, Bergmeier W, Daugherty A, Sampson UKA, MacKman N. Platelet inhibitors reduce rupture in a mouse model of established abdominal aortic aneurysm. *Arterioscler Thromb Vasc Biol* 2015;**35**:2032.
16. Dai J, Louedec L, Philippe M, Michel JB, Houard X. Effect of blocking platelet activation with AZD6140 on development of abdominal aortic aneurysm in a rat aneurysmal model. *J Vasc Surg* 2009;**49**:719–727.
17. Touat Z, Ollivier V, Dai J, Huisse MG, Bezeaud A, Sebbag U, Palombi T, Rossignol P, Meilhac O, Guillin MC, Michel JB. Renewal of mural thrombus releases plasma markers and is involved in aortic abdominal aneurysm evolution. *Am J Pathol* 2006;**168**:1022.
18. Lindholt JS, Bjorck M, Michel JB. Anti-platelet treatment of middle-sized abdominal aortic aneurysms. *Curr Vasc Pharmacol* 2013;**11**:305–313.
19. Touat Z, Lepage L, Ollivier V, Nataf P, Hvass U, Labreuche J, Jandrot-Perrus M, Michel JB, Jondeau G. Dilation-dependent activation of platelets and prothrombin in human thoracic ascending aortic aneurysm. *Arterioscler Thromb Vasc Biol* 2008;**28**:940–946.
20. Mackay CDA, Jadli AS, Fedak PWM, Patel VB. Adventitial fibroblasts in aortic aneurysm: unraveling pathogenic contributions to vascular disease. *Diagnostics (Basel)* 2022;**12**:871.
21. Maguire EM, Pearce SWA, Xiao R, Oo AY, Xiao Q. Matrix metalloproteinase in abdominal aortic aneurysm and aortic dissection. *Pharmaceuticals* 2019;**12**:118.
22. Furman MI, Benoit SE, Barnard MR, Valeri CR, Borbone ML, Becker RC, Hechtman HB, Michelson AD. Increased platelet reactivity and circulating monocyte-platelet aggregates in patients with stable coronary artery disease. *J Am Coll Cardiol* 1998;**31**:352–358.
23. Trip MD, Cats VM, van Capelle FJ, Vreeken J. Platelet hyperreactivity and prognosis in survivors of myocardial infarction. *N Engl J Med* 1990;**322**:1549–1554.
24. Zeller JA, Tschoepe D, Kessler C. Circulating platelets show increased activation in patients with acute cerebral ischemia. *Thromb Haemost* 1999;**81**:373–377.
25. Reusswig F, Polzin A, Klier M, Dille MA, Ayhan A, Benkhoff M, Lersch C, Prinz A, Gorressen S, Fischer JW, Kelm M, Elvers M. Only acute but not chronic thrombocytopenia protects mice against left ventricular dysfunction after acute myocardial infarction. *Cells* 2022;**11**:3500.
26. Morrell CN, Mix D, Aggarwal A, Bhandari R, Godwin M, Owens P, Lyden SP, Doyle A, Krauel K, Rondina MT, Mohan A, Lowenstein CJ, Shim S, Stauffer S, Josyula VP, Ture SK, Yule DI, Wagner LE, Ashton JM, Elbadawi A, Cameron SJ. Platelet olfactory receptor activation limits platelet reactivity and growth of aortic aneurysms. *J Clin Invest* 2022;**132**:e152373.
27. Robless PA, Okonko D, Lintott P, Mansfield AO, Mikhailidis DP, Stansby GP. Increased platelet aggregation and activation in peripheral arterial disease. *Eur J Vasc Endovasc Surg* 2003;**25**:16–22.

Downloaded from https://academic.oup.com/cardiovascres/article/120/4/417/7425469 by guest on 04 July 2024

28. Faull RJ, Ginsberg MH. Dynamic regulation of integrins. *Stem Cells* 1995;**13**:38–46.
29. Milne AA, Adam DJ, Murphy WG, Ruckley C V. Effects of asymptomatic abdominal aortic aneurysm on the soluble coagulation system, platelet count and platelet activation. *Eur J Vasc Endovasc Surg* 1999;**17**:434–437.
30. Arnaoutoglou E, Kouvelos G, Papa N, Karamoutsios A, Bouris V, Vartholomatos G, Matsagkas M. Platelet activation after endovascular repair of abdominal aortic aneurysm. *Vascular* 2016;**24**:287–294.
31. Li J, Tong D, Chen F, Song B, Wang Y, Liu Y, Zhang X, Liu N, Xu Y, Li Y, Yin X, Liu W. Inflammatory cytokines enhance procoagulant activity of platelets and endothelial cells through phosphatidylserine exposure in patients with essential hypertension. *J Thromb Thrombolysis* 2021;**51**:933–940.
32. Sundermann AC, Saum K, Conrad KA, Russell HM, Edwards TL, Mani K, Björck M, Wanhainen A, Phillip Owens A. Prognostic value of D-dimer and markers of coagulation for stratification of abdominal aortic aneurysm growth. *Blood Adv* 2018;**2**:3088–3096.
33. Wallinder J, Bergqvist D, Henriksson AE. Haemostatic markers in patients with abdominal aortic aneurysm and the impact of aneurysm size. *Thromb Res* 2009;**124**:423–426.
34. Liu O, Jia L, Liu X, Wang Y, Wang X, Qin Y, Du J, Zhang H. Clopidogrel, a platelet P2Y12 receptor inhibitor, reduces vascular inflammation and angiotensin II induced-abdominal aortic aneurysm progression. *PLoS One* 2012;**7**:e51707.
35. Liu X, Chen X, Xu C, Lou J, Weng Y, Tang L. Platelet protects angiotensin II-driven abdominal aortic aneurysm formation through inhibition of inflammation. *Exp Gerontol* 2022;**159**:111703.
36. Meijer C A, Stijnen T, Wasser MNJM, Hamming JF, Van BJ, Lindeman JHN. Doxycycline for stabilization of abdominal aortic aneurysms: a randomized trial. *Ann Intern Med* 2013;**159**:815–823.
37. Sillesen H, Eldrup N, Hultgren R, Lindeman J, Bredahl K, Thompson M, Wanhainen A, Wingren U, Swedenborg J. Randomized clinical trial of mast cell inhibition in patients with a medium-sized abdominal aortic aneurysm. *Br J Surg* 2015;**102**:894–901.
38. Wanhainen A, Mani K, Kullberg J, Svensjö S, Bersztel A, Karlsson L, Holst J, Gottsäter A, Linné A, Gillgren P, Langenskiöld M, Hultgren R, Roy J, Gilgen NP, Ahlström H, Lederle FA, Björck M. The effect of ticagrelor on growth of small abdominal aortic aneurysms-a randomized controlled trial. *Cardiovasc Res* 2020;**116**:450–456.
39. Hannawa KK, Cho BS, Sinha I, Roelofs KJ, Myers DD, Wakefield TJ, Stanley JC, Henke PK, Upchurch GR. Attenuation of experimental aortic aneurysm formation in P-selectin knockout mice. *Ann N Y Acad Sci* 2006;**1085**:353–359.
40. Lok ZSY, Lyle AN. Osteopontin in vascular disease. *Arterioscler Thromb Vasc Biol* 2019;**39**:613–622.
41. Lund SA, Giachelli CM, Scatena M. The role of osteopontin in inflammatory processes. *J Cell Commun Signal* 2009;**3**:311–322.
42. Isoda K, Nishikawa K, Kamezawa Y, Yoshida M, Kusuhara M, Moroi M, Tada N, Ohsuzu F. Osteopontin plays an important role in the development of medial thickening and neointimal formation. *Circ Res* 2002;**91**:77–82.
43. Mi T, Nie B, Zhang C, Zhou H. The elevated expression of osteopontin and NF-κB in human aortic aneurysms and its implication. *J Huazhong Univ Sci Technolog Med Sci* 2011;**31**:602–607.
44. Bruemmer D, Collins AR, Noh G, Wang W, Territo M, Arias-Magallona S, Fishbein MC, Blaschke F, Kintscher U, Graf K, Law RE, Hsueh WA. Angiotensin II-accelerated atherosclerosis and aneurysm formation is attenuated in osteopontin-deficient mice. *J Clin Invest* 2003;**112**:1318–1331.
45. Schultz G, Tedesco MM, Sho E, Nishimura T, Sharif S, Du X, Myles T, Morser J, Dalman RL, Leung LLK. Enhanced abdominal aortic aneurysm formation in thrombin-activatable procarboxypeptidase B-deficient mice. *Arterioscler Thromb Vasc Biol* 2010;**30**:1363–1370.
46. Seizer P, May AE. Platelets and matrix metalloproteinases. *Thromb Haemost* 2013;**110**:903–909.
47. Balceniuk MD, Trakimas LE, Aghaie C, Mix D, Rasheed K, Ellis J, Glocker R, Doyle A, Stoner MC. Aspirin use is associated with decreased radiologically-determined thrombus sac volume in abdominal aortic aneurysms. *Vascular* 2018;**26**:440–444.
48. Wang Y, Liu Z, Ren J, Xiang M-X. Pharmacological therapy of abdominal aortic aneurysm: an update. *Curr Vasc Pharmacol* 2018;**16**:114–124.

Translational perspective

Abdominal aortic aneurysm (AAA) is a severe cardiovascular disease with high mortality. Since the role of platelets is unclear, we explored platelet-mediated processes in the pathogenesis of AAA. Results from platelet depleted mice and patients with AAA revealed that platelets modulate inflammatory and stiffness-related gene expression of macrophages and fibroblasts. Further, platelets induce the release of osteopontin important for the recruitment of platelets to the aortic wall and to the intraluminal thrombus. Consequently, platelet depletion significantly reduced aneurysm growth. Thus, therapeutic targeting of platelet activation might be crucial for the treatment of patients to reduce AAA formation and progression.

Downloaded from https://academic.oup.com/cardiovascres/article/120/4/417/7425469 by guest on 04 July 2024

Manuscript CVR-2023-0335

Interaction of platelets with macrophages and fibroblasts aggravates inflammation, aortic wall stiffening and osteopontin release in abdominal aortic aneurysm

Wagenhäuser MU*[1], Mulorz J*[1], Krott KJ*[1], Ehrenberg A*[1], Feige T[1], Rhee YH[1], Chatterjee M[2], Petzold N[1], Böddeker C[1], Ibing W[1], Krüger I[1], Popovic AM[1], Spin JM[3,4], Tsao PS[3,4], Roseman A[3], Schelzig H#[1], Elvers M#§[1]

* contributed equally
# contributed equally
§ corresponding author

[1] Department of Vascular- and Endovascular Surgery, University Hospital Düsseldorf, Heinrich-Heine University, Düsseldorf, Germany

[2] Department of Pharmacology, Experimental Therapy and Toxicology, University Hospital Tübingen, Tübingen, Germany

[3] VA Palo Alto Health Care System, Palo Alto, CA, United States

[4] Stanford University, Department of Cardiovascular Medicine, Stanford, CA, United States

E-Mail of Corresponding author: Margitta Elvers, Ph.D., margitta.elvers@med.uni-duesseldorf.de

1. Supplementary Methods

1.1 Cell culture of human cell lines. Human aortic fibroblasts (hAoF, PromoCell®, #C-12380), human aortic smooth muscle cells (hASMC, PromoCell®, #C-12533) and THP-1 (ATCC, #TIB-202) cell lines were cultured in T-75 flasks in 15 mL of their respective media (hAoF, fibroblast growth medium, Sigma-Aldrich, #C23010; hASMC, DMEM medium Gibco™, #11500416; THP-1, RPMI 1640 medium Gibco™, #21875034). THP-1, hASMC and hAoFs medium including 10% fetal bovine serum (FBS) superior (Sigma-Aldrich, #S0615) and 1% penicillin-streptomycin (Gibco™, #15140122). At 70-80% confluence, cells were split 1:5. For this purpose, adherent hAoF were washed twice with DPBS and dissolved with Trypsin-EDTA (Sigma-Aldrich, #T3924). Trypsinization was stopped by addition of medium, and the cell suspension was transferred to a falcon tube and centrifuged at 200 *g* for 5 min. The supernatant was discarded and the cells were resuspended in fresh medium. Non-adherent THP-1 cells do not require trypsinization and were immediately transferred into a falcon tube. Before resuspension in fresh medium the cells were washed once with DPBS by an additional centrifugation step at 200 *g* for 5 minutes. Once resuspended in fresh medium, the cells were ready for cell culture experiments.

For cell culture experiments, cells were seeded into a 24-well plate at 1.5 x 10^5 cells/well. HAoF were incubated for 24 h at 37 °C and 5% CO_2 to allow the cells to become adherent. THP-1 cells were differentiated into macrophages as described elsewhere (1). Therefore, THP-1 cells were differentiated into macrophages by incubation with 150 nM phorbol 12-myristate 13-acetate (PMA, Sigma, #P8139) for 24 hours. After another 24-hour incubation with RPMI medium, the macrophages were polarized into M1 macrophages with 20 ng/ml IFN-γ (R&D System, #285-IF) and 100 ng/ml LPS (Sigma, #8630). These cells were called “differentiated macrophages”. Once hAoF and macrophages became adherent, the platelet supernatant was added and the cells were incubated at 37 °C and 5% CO_2 for 6 h. Afterwards, the supernatant was discarded and the cells were washed twice with ice-cold DPBS. Finally, the cells were detached from wells using TRI Reagent® (Sigma-Aldrich, #T9424).

1.2 Gene expression from human platelets and cell lysates of macrophages and hAoFs. Human platelets were isolated from platelet concentrates using the following protocol. 1-5 x 10^9 of either resting or activated platelets were centrifuged at 2500 *g* for 5 min at 4 °C. The supernatant was discarded and the pellet was resuspended in TRI Reagent®. After transferring the sample into a DNA LoBind Tube (Eppendorf, #30108051), Chloroform (Sigma-Aldrich, #372978) was added at a ratio of 1:5. The samples were shaken thoroughly, incubated for 3 min at RT and centrifuged at 12,000 *g* for 15 min at 4 °C. The aqueous phase was diluted in pure ethanol (3-fold) and mixed with linear acrylamide (1:500) (Invitrogen, #AM9520). After an incubation at 4 °C overnight, the samples were centrifuged at 21,130 *g* at 4 °C. The

supernatant was discarded, and the pellet was washed in ice-cold 80% ethanol and resuspended in 25 µL nuclease free water. Total RNA from cell culture lysates of differentiated macrophages and hAoFs was isolated using the RNeasy Mini Kit (Qiagen, #74106) according to the manufacturer's protocol. RNA content and quality were measured using the BioPhotometer D30 (Eppendorf). All samples were adapted to the same amount of RNA. DNA digestion was performed with DNAse I (Roche, #04716728001) according to the following protocol: 30min/37 °C; 10min/75 °C using a PCR thermocycler (Eppendorf). Subsequent cDNA synthesis was performed using the ImProm- II™ Reverse Transcription System (Promega, #A3800) according to their protocol. For quantification of mRNA levels, fast SYBR™ Green Master Mix (Applied Biosystems, #4385612) was used with following specific oligonucleotide primers: MMP2 (PPH00151B-200), MMP9 (PPH00152E-200), COL1A1 (PPH01299F-200), COL3A1 (PPH00439F-200), SPP1 (PPH00582E-200), and GAPDH (PPH00150F-200) acquired from Qiagen. Following oligonucleotide primers were acquired from Origene: MCP1 (HP 206587), IL-6 (HP 200567), IL-12β (HP 205923), TNF-α (HP 200561), IL-10 (HP 200540) and IL-8 (HP 200551). The IL-1β primer pair (frwd: AGCTTCCTTGTGCAAGTGTCTGAG, rev: TGTTGATGTGCTGCTGCGAGAT) and IL-6 (hAoFs) primer pair (frwd: GGCACTGGCAGAAAACAACC; rev. GCAAGTCTCCTCATTGAATCC) were purchased from Eurofins. Data are normalized to GAPDH and fold changes were calculated using the $^{\Delta\Delta}$Ct method.

1.3 Gene expression of murine aortic tissue. Total RNA was isolated from murine aortae with a TRIzol-based (Invitrogen) RNA isolation protocol. RNA was quantified by NanoDrop (Agilent Technologies), and RNA and miRNA quality were verified with the Agilent 2100 Bioanalyzer (Agilent Technologies). Samples required 260/280 ratios of >1.8 and sample RNA integrity numbers of ≥9 for inclusion. RNA was reverse-transcribed with the TaqMan MicroRNA Reverse Transcription kit (Applied Biosystems) according to the manufacturer's instructions. To quantitate the mRNA levels the TaqMan qRT-PCR assay was used. The following specific oligonucleotide primers were purchased from Thermo Fisher Scientific:

Il-1β (Mm00434228_m1), *Il-6* (Mm00446190_m1), *Il-8* (Mm00441263_m1), *Il-10* (Mm01288386_m1), *Il-12β* (Mm01288989_m1), *Ccl2* (Mm00441242_m1), *Tnf-α* (Mm00443258_m1), *Eln* (Hs00355783_m1), *Mmp2* (Mm00439498_m1), *Mmp9* (Mm00442991_m1), *Col1a1* (Mm00801666_g1), *Col3a1* (Mm01254476_m1), *Spp1* (Mm00436767_m1), *18S* (4319413E). Data were normalized to 18S or GAPDH and all fold changes were calculated using the $^{\Delta\Delta}$Ct method.

1.4 Fragmentation of osteopontin. Fragmentation of recombinant osteopontin (OPN) (PeproTech, #120-35) was performed with thrombin (30 mU/1 µg OPN) (Roche, #10602400001) by incubation at 37 °C for 3 h. Silver staining was used to verify the

concentration of enzymes and the quality of osteopontin fragmentation. Therefore the product was separated via gel electrophoresis and stained using Pierce Silver Stain Kit (Thermo Fisher Scientific, #24612) according to the manufacturer's protocol.

1.5 Adhesion studies. Adhesion experiments were performed to investigate adhesion of human platelets on various protein matrices. For the immobilized osteopontin experiments, full-length osteopontin (fl. OPN, 5 µg/mL) (PeproTech, #120-35) and cleaved osteopontin (cle. OPN, 5 µg/mL) were applied to glass coverslips (24 x 60 mm) in a defined area (10 x 10 mm). For the experiments with soluble osteopontin, the glass coverslips were coated with collagen (200 µg/mL) (Horm®, Takeda Pharmaceutical, #3408075). A matrix of bovine serum albumin (BSA, 1%) was used as negative control and fibrinogen (100 µg/mL) (Sigma-Aldrich, #F3879) was used as a positive control. To generated coated surfaces, glass coverslips were incubated in a humidity chamber at 4 °C overnight and blocked with 1% BSA at RT for 1 h. Human platelets were isolated from the blood of healthy volunteers and treated as required in the following experiments. For the experiments with immobilized osteopontin, platelets were pre-treated with or without an inhibiting $\alpha_v\beta_3$-antibody (30 µg/mL) (Sigma-Aldrich, #MAB1976) at 37 °C for 15 min. Resting, ADP (10 µM; Sigma-Aldrich, Germany, #A2754) and CRP (1 µg/mL; collagen-related peptide, CambCol Laboratories, United Kingdom, #28045457) stimulated platelets (40,000/ µL) were added to the matrices and incubated at 37 °C for 30 min. For the soluble osteopontin experiments, platelets were pre-treated with fl. OPN (1 µg/mL) and cle. OPN (1 µg/mL) at 37 °C for 30 min and then added to a collagen matrix for 5 or 20 min. Finally, unbound platelets were washed off with DPBS, and adhesive platelets were fixed with ice-cold 4% paraformaldehyde for 10 min. Permeabilization with Triton-X100 (0.5%) (Sigma-Aldrich, #T8787) in BSA solution (0.5%) for 10 minutes served as preparation for actin filament staining with rhodamine-phalloidin (1:200) (Invitrogen, #R415) for 40 min. Subsequently, the cover slips were washed with DPBS and covered with the mounting medium Fluoromount-G™ (Sigma-Aldrich, #F4680) and monitored by microscopic. Five pictures from different areas of one biological replicate were taken (platelets: 400 x total magnification; Axio Observer.D1, Carl Zeiss). The total number of adherent platelets was counted using ZEN 3.3. (blue edition) software.

Spreading experiments were performed as described previously (2-4). For spreading analysis of isolated murine platelets the adherent platelets were rinsed, fixed and covered as described above. The samples were imaged using Microscope Axio Observer.D1 (Objective Plan Apochromat 100x/1.40 Oil DIC M27) for differential interference contrast (DIC) imaging resulting in at least 5 representative visual field pictures per slide for 1 sample per mouse. The whole visual field was counted by marking the different spreading stages in Carl Zeiss Software ZEN 3.3 (blue edition). Platelets that show only filopodia were counted as filopodia forming

cells, platelets that start to form lamellipodia and fully spread platelets were counted as lamellipodia forming platelets and landing and attached platelets were counted as adherent cells according to Aslan and McCarty, 2012 (5). Users were blinded to treatment.

For immunofluorescence staining of OPN on adherent platelets, 4.9 x 10^5 platelets were placed on matrices coated with collagen and fibrinogen. After fixation with 2% paraformaldehyde and permeabilization of platelets, nonspecific binding was blocked with goat serum (5%) (Thermo Fisher Scientific, #01-6201) in Tris-buffered saline with 0.1% Tween® 20 detergent (TBS-T) buffer for 1 h. The primary antibodies (20 µg/mL) (abcam, OPN #ab181440, rb IgG #ab27478) were incubated at 4 °C overnight. Secondary antibodies (Invitrogen, 20 ng/mL, goat anti-rabbit 488 #A11008; 3U rhodamine-phalloidin) were incubated at RT for 1 hour. After the staining and mounting with Fluoromount-G™, images were captured using a Leica DMi8 confocal microscope.

1.6 Thrombus formation under flow using the *ex vivo* flow chamber system. Glass cover slips (24 x 60 mm) were coated with collagen (200 µg/mL) or a combination of collagen (200 µg/mL) and fl. OPN (100 µg/ml) (Peprotech, #120-35) at 4 °C overnight. On the next day, spare collagen was removed and cover slips were blocked with BSA (1%) at RT for at least 1 hour. Human whole blood was perfused over both matrices through the flow chamber (diameter: 50 µm x 5 mm) at a shear rate of 1,700 s^{-1} using a pulse-free electric pump. After 3 min, blood perfusion was stopped and Tyrode's buffer was pumped through the flow chamber using the same shear rate. Five pictures were taken (400 x total magnification; Axio Observer.D1, Carl Zeiss) from different areas. The surface coverage was analyzed using ImageJ-win64 software.

1.7 Histology. For the analysis of murine or human aortic tissue (aortic wall), 5-7-micron sections of paraffin-embedded tissue were prepared. Additionally, cryopreserved human thrombus samples (intraluminal thrombus, ILT) were prepared by embedding the tissue into Tissue-Tek® O.C.T.™ compound. Sections were cut using the Leica Biosystems (CM1950 Cryostat). Hematoxylin and eosin staining was performed using a common HE-staining protocol (2). For quantification of the intima/media thickness 2 fields per cross section were analysed by measuring media thickness at 10 distinct locations within each cross section using the ZEN 3.3. (blue edition) software. The modified Elastin Verhoeff van Gieson staining (VVG) was conducted according to manufacturer's protocol (abcam, elastic stain kit #ab150667). Elastin fragmentation was determined as elastin fragments / media lamellar units via ZEN 3.3. (blue edition) software. The number of these breaks were counted in both thoracic and abdominal aortic segments of naive mice, platelet-depleted PPE-operated mice, and IgG treated PPE mice (controls). For each tissue sample 2 fields per cross section were analyzed.

1.8 Immunofluorescence staining. For immunofluorescence staining of osteopontin (OPN), platelets (CD42b), macrophages (Mac-3) and fibroblasts (Vimentin), sections of human and

murine aortic walls as well as intraluminal thrombi (ILT) of AAA patients were stained. For staining of human and murine aortic wall, paraffin-embedded tissue was used, while staining of human ILT was performed in cryopreserved tissue. Prior to the staining, the paraffin-embedded sections were deparaffinized and hydrated. For antigen unmasking the tissues were microwaved at 360 kW for 10 min. ILT sections were fixed with 4% paraformaldehyde for 10 min before staining. For the blocking of nonspecific binding sites, sections of both, cryopreserved and paraffin-embedded were incubated with DPBS + 0.3 % Triton x-100 and goat serum (5%) at RT for 1 h. The primary antibodies ((anti-osteopontin, 20 µg/mL, abcam, #ab181440), recombinant rabbit IgG (monoclonal [EPR25A] isotype control (20 µg/mL, abcam, #ab172730)), CD42b monoclonal antibody (20 µg/mL, Invitrogen™, #42C01), BD Pharmingen™ purified mouse IgG1 κ isotype control (50 µg/mL, BD Bioscience, #554121), BD Pharmingen™ purified rat anti-mouse Mac-3, unlabeled (3.125 µg/mL, BD Bioscience, #BDB550292), anti-CD68 AA 21-120 (10 µg/mL, antibodies-online GmbH, #ABIN671406), anti-CD68 (10 µg/mL, antibodies-online GmbH, #ABIN6941238), vimentin polyclonal antibody (20 µg/mL, Invitrogen™, #PA5-142829), purified rat anti-mouse GPIbα (CD42b, 10 µg/mL, Emfret Analytics, #M042-0)) were incubated at 4 °C overnight. On the next day, the appropriate secondary antibodies (goat anti-rabbit IgG (H+L) cross-adsorbed secondary antibody, Alexa Fluor™ 555 (20 µg/mL, Invitrogen™, #A-21428), eBioscience™ streptavidin eFluor™ 660 conjugate (10 µg/mL, Invitrogen™, #50-4317-80)) were applied to the tissues at RT for 1 h. Negative controls were generated by omission of the primary antibody. In case of platelet staining with CD42b, an intermediate step of biotinylation was used to enhance the fluorescence signal (goat anti-mouse IgG antibody (H+L), biotinylated, GT (7.5 µg/mL, Vector Laboratories, #VEC- BA-9200), goat anti-rat IgG antibody (H+L), biotinylated (7.5 µg/mL, Vector Laboratories, #BA-9400)). Nuclei were identified using DNA staining with 4, 6 diamidino-2-phenylindole dihydrochloride (DAPI, Roche, 1:3000). Samples were analysed using confocal microscopy (LSM 710, Carl Zeiss, Germany). For quantification of the platelet, macrophage and OPN content within the aortic tissue of PPE-operated mice the mean fluorescence intensity (MFI) of 2 subsequent sections was used. For every cross-section 2 representative fields were analysed. The MFI of specifically stained sections was automatically normalized to the area of total aortic tissue. Determination of the normalized MFI was performed using the Carl Zeiss Software ZEN 3.3 (blue edition). For image generation and quantification users were blinded to the treatment.

1.9 Quantification of plasma levels of OPN, MMP2, MMP9 and IL-6. Circulating OPN in plasma of mice was determined according the manufacturer's protocol using mouse/rat osteopontin (OPN) Quantikine ELISA Kit (R&D Systems, #MOST00). In addition, OPN content was analyzed in human plasma, isolated human platelets (stimulated with 10 µM ADP), and from differentiated macrophage cultures using the osteopontin/SPP1 ELISA kit (Thermo Fisher

Scientific, #EHSPP1) according to manufacturer specified protocol. IL6 concentration of hAoF cultures were determined using the Human IL-6 DuoSet ELISA kit (R&D Systems, #DY206-05) according to the manufacturer protocol. MMP2 (R&D Systems, #DY902) and MMP9 (R&D Systems, #DY911) levels in human plasma were also determined according to the manufacturer's protocol.

1.10 Experimental animals: The Ang-II infused ApoE knockout mouse model.

For angiotensin-II (Ang-II) induced AAA formation, 10-week-old male *ApoE*$^{-/-}$ mice purchased form the Jackson Laboratory were used. Prior implantation the alzet osmotic mini-pumps (model 1004, Durect Corporation) were filed with Ang-II (Sigma-Aldrich, #A92525) or sterile isotonic saline (NaCl, 0.9%) and were primed at 37°C in sterile 0.9% $NaCl_2$ overnight. For the implantation mice were anesthetized with 2-3% isoflurane and additionally received a locally subcutaneous (s.c.) injection of metamizol (200 mg/kg) 30 min before surgery. The osmotic mini-pumps were implanted into a subcutaneous pocket within the dorsal region caudal to the scapula. After implantation the osmotic mini-pumps reach a delivery rate of 1 µg/kg/min over a time period of 28 days. For pain relief, all animals received metamizol via drinking water (1.33 mg/mL) for two days. For platelet depletion Ang-II infused *ApoE*$^{-/-}$ mice received a platelet depletion antibody (Emfret Analytics, polyclonal anti-GPIb alpha #R300) or a corresponding IgG control antibody (Emfret Analytics, #C301) after surgery (days 0 and 5). The mice were sacrificed at day 7 post osmotic mini-pump implantation.

1.11 Ultrasound imaging. Prior either PPE surgery or osmotic mini-pump implantation (baseline) and at days 3, 7, 10, 14, 21 and 28 following surgery, maximal aortic diameters at the aneurysm site were measured using ultrasound. Mice were anaesthetized with 2-3% isoflurane, placed on a 37 °C heated plate and ultrasound imaging was performed using a Vevo 2100® High-Resolution In Vivo Micro-Imaging System (VisualSonics). Inner diameter-measurements were obtained following a standardized imaging algorithm with longitudinal B-Mode images during the systolic phase. PWV was examined to assess aortic stiffness by simultaneous tracking of the ECG and the pulse wave at the aortic bifurcation (bif). The distance from the aortic valve to the bif was measured during sacrifice and was set to 3.98 cm for further calculations. For each mouse, 5 PW Doppler sets were recorded. In each set, 3 measurements from the foot of the R-wave of the ECG to the offspring of the pulse wave at the bif were measured to determine the transit time between these two locations. Global aortic PWV was estimated as a ratio of the distance (d) and time (t) delay of the pulse wave between both locations.

2. Supplemental Figures

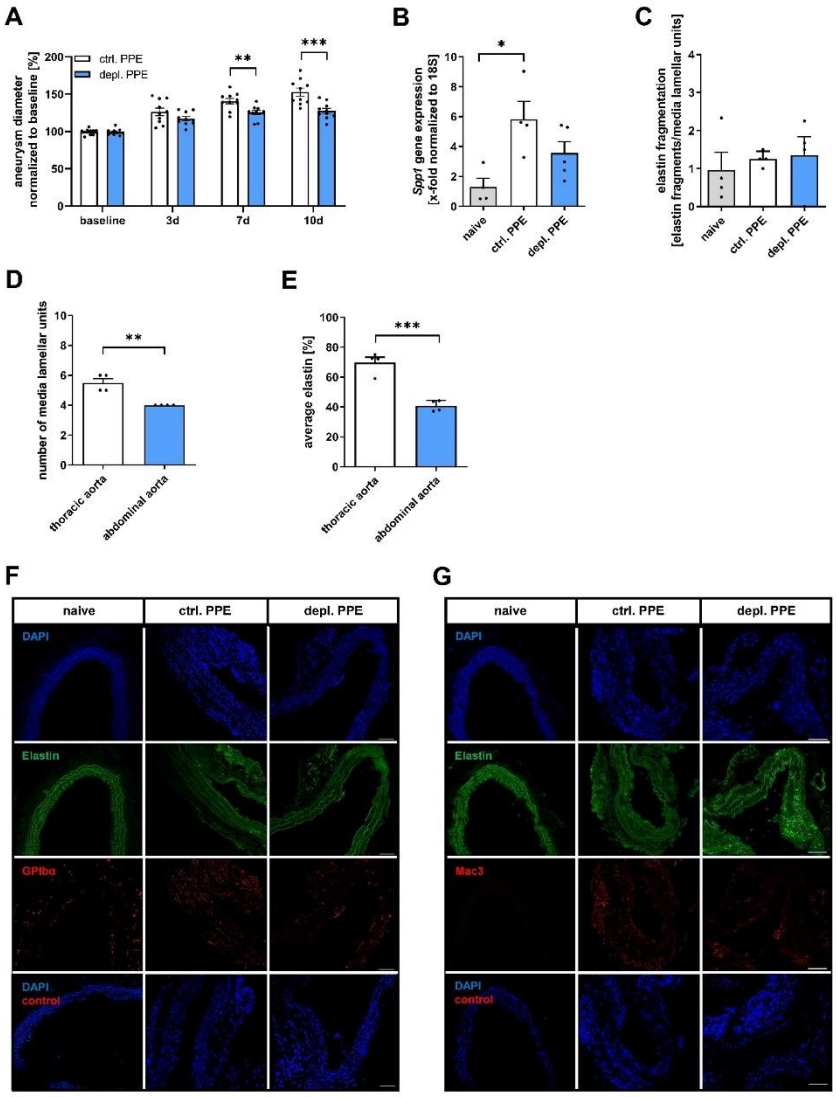


Figure S1. Platelet depletion reveals unaltered elastin degradation within the thoracic aorta in the PPE mouse model. (**A**) Aneurysm diameter of depl. PPE and ctrl. PPE mice was determined by ultrasound measurements at the indicated time points (n = 10). Data were normalized to baseline. (**B**–**E**) Different tissue analysis of thoracic aortae depl. PPE and ctrl. PPE mice. (**B**) *Spp1* gene expression

in thoracic aortic tissue (n = 4–5). (**C**) Elastin fragmentation counted in Verhoeff van Gieson-stained samples from naive and PPE-operated mice (n = 4). (**D**) Number of lamellar units within the thoracic and abdominal aorta segment of naive mice (n = 4). (**E**) Average elastin content of thoracic and abdominal aortic tissue of naive mice as a percentage of whole depicted tissue amount in the sample (n = 4). (**F** and **G**) Representative immunofluorescence (IF) images of (**F**) platelets (CD42b/anti-GPIbα, red) or (**G**) macrophages (anti-Mac3, red), nuclei (DAPI, blue) and elastin (auto fluorescence, green) in aortic tissue sections of depl. PPE and ctrl. PPE at day 3 post-surgery (n = 3–5). Scale bar: 50 µm. Aortic tissue of naive mice served as control (n = 4). Negative controls were achieved by using the respective IgG antibody (control). Data are represented as mean ± SEM. Statistical significances were determined by two-way ANOVA with Sidak's multiple comparison test (**A**), one-way ANOVA with Holm Sidak's multiple comparisons test (**B** and **C**) or unpaired student's t-test (**D** and **E**). $*P < 0.05$, $**P < 0.01$, $***P < 0.001$. Ctrl., control; depl., depletion; PPE, porcine pancreatic elastase (infusion); PWV, pulse wave velocity; *Spp1*, secreted phosphoprotein 1.

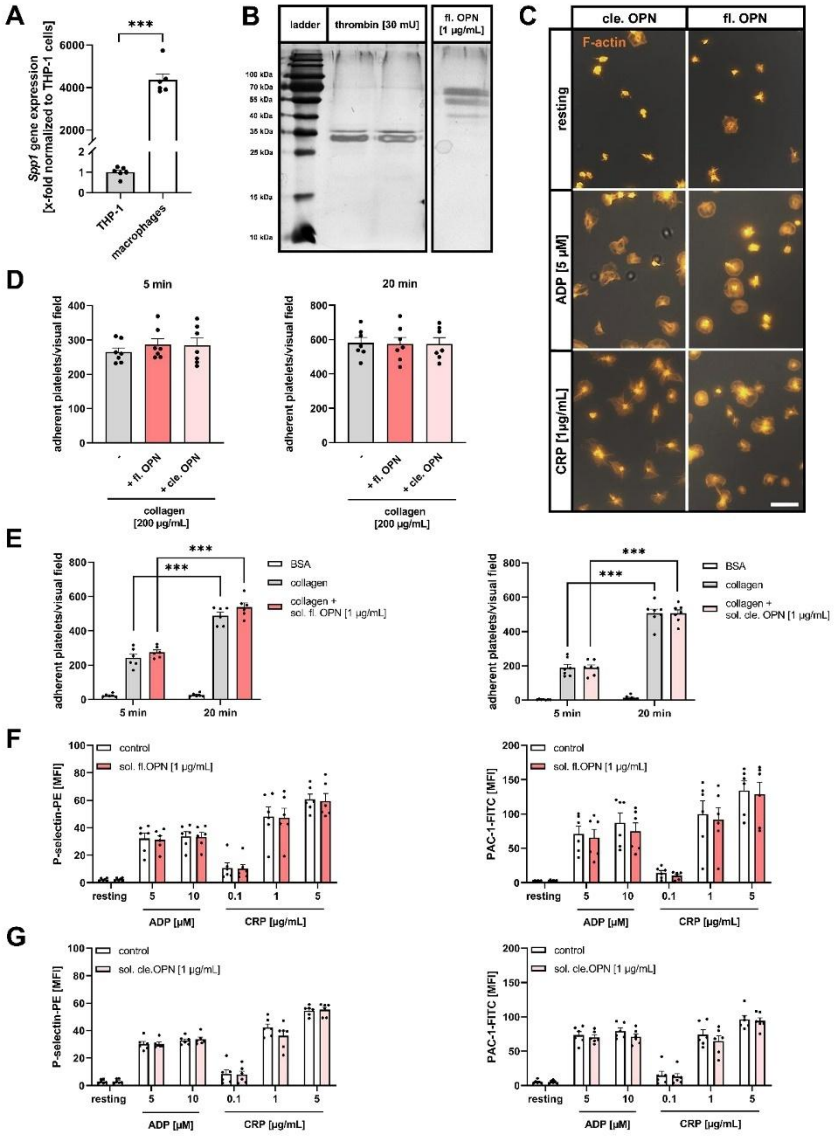


Figure S2. OPN does not modulate adhesion to collagen and platelet activation under static conditions. (**A**) *SPP1* gene expression in THP-1 cells and differentiated macrophages (n = 6). Fold changes were normalized to THP-1 *SPP1* gene expression. (**B**) Full-length OPN was cleaved by thrombin (30 mU/ 1 µg OPN). Silver staining was used to verify the quality of OPN fragmentation. The products were separated via gel electrophoresis and stained using a Pierce Silver Stain Kit. (**C**)

Representative images of filopodia and lamellipodia forming platelets spread on cleaved or full-length osteopontin (5 µg/mL) for 30 minutes. Platelets were stimulated with indicated agonists. Adherent platelets were visualized by rhodamine-phalloidin staining (F-actin, orange) (n = 5). Scale bar: 10 µm. (**D**) Isolated platelets were allowed to adhere on a collagen (200 µg/mL) or collagen/OPN (full-length or cleaved, 5 µg/mL) matrix for 5 and 20 min (n = 7). (**E**) Quantification of adherent human platelets, pre-treated with soluble full-length (fl. OPN, 1 µg/mL) or cleaved (cle. OPN, 1 µg/mL) OPN on a collagen matrix after 5 and 20 min (n = 6–7). BSA served as control. (**F** and **G**) Platelet degranulation (P-selectin-PE) and active integrin $\alpha_{IIb}\beta_3$ externalisation (PAC-1-FITC) of human platelets after incubation with or without (control) full-length or cleaved OPN (1 µg/mL) were determined by flow cytometry (n = 6). Platelets were stimulated with indicated agonists. Data are represented as mean ± SEM. Statistical significances were determined by unpaired student's t-test (**A**), one-way ANOVA with Holm-Sidak's multiple comparisons test (**D**), two-way ANOVA with Tukey's multiple comparisons test (**E**) or multiple t-test (**F** and **G**). ***$P < 0.001$. ADP, adenosine diphosphate; BSA, bovine serum albumin; cle., cleaved; CRP, collagen-related peptide; fl., full-length; OPN, osteopontin; sol., soluble.

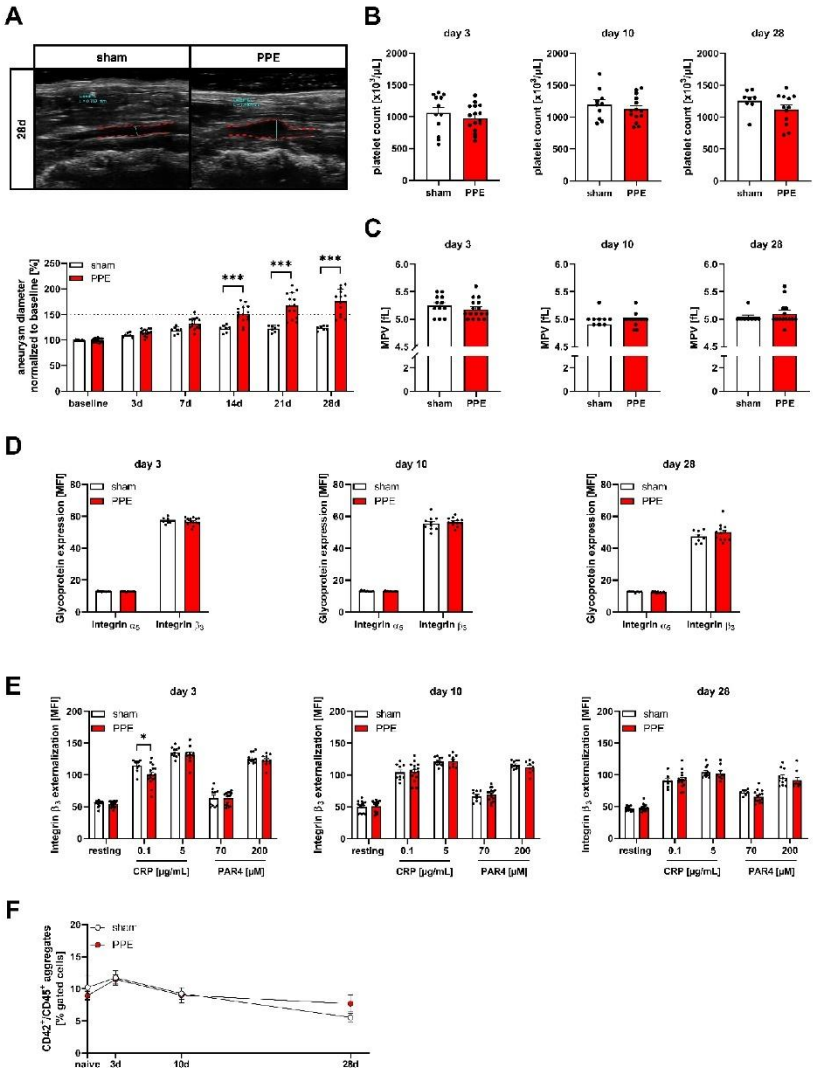


Figure S3. Platelet count, MPV and glycoprotein externalization are not influenced in PPE-operated mice. (**A**) Representative ultrasound images (at day 28) and aortic diameter progression of sham respectively PPE-operated mice over a time-period of 28 days after surgery (n = 8–13). Data were normalized to baseline. (**B**) Platelet count of sham and PPE-operated mice at days 3, 10 and 28 post-surgery (n = 8–16). (**C**) MPV of sham and PPE-operated mice 3, 10 and 28 days post-surgery (n = 8–16). (**D**) Externalization of integrins α_5 and β_3 on the platelet surface in whole blood from mice at days 3, 10 and 28 after sham or PPE surgery (n = 10–12). (**E**) Externalization of integrin β_3 on the platelet

surface in whole blood from mice at days 3, 10 and 28 after sham or PPE surgery after stimulation with indicated agonists (n = 10–12). (**F**) Aggregate formation of platelets ($CD42^+$) and leukocytes ($CD45^+$) in whole blood of naive, sham and PPE-operated mice at days 3, 10 or 28 post-surgery determined by flow cytometry (n = 5–6). Data are represented as mean or percent-gated cells ± SEM. Statistical significances were determined by two-way ANOVA with Sidak's multiple comparison test (**A**), unpaired student's t-test (**B** and **C**), multiple t-test (**D** and **E**) or two-way ANOVA with Sidak's multiple comparison test (**F**). $^*P < 0.05$. CRP, collagen-related peptide; MFI, mean fluorescence intensity; MPV, mean platelet volume; PAR4, protease-activated receptor 4 activating peptide; PPE, porcine pancreatic elastase (infusion).

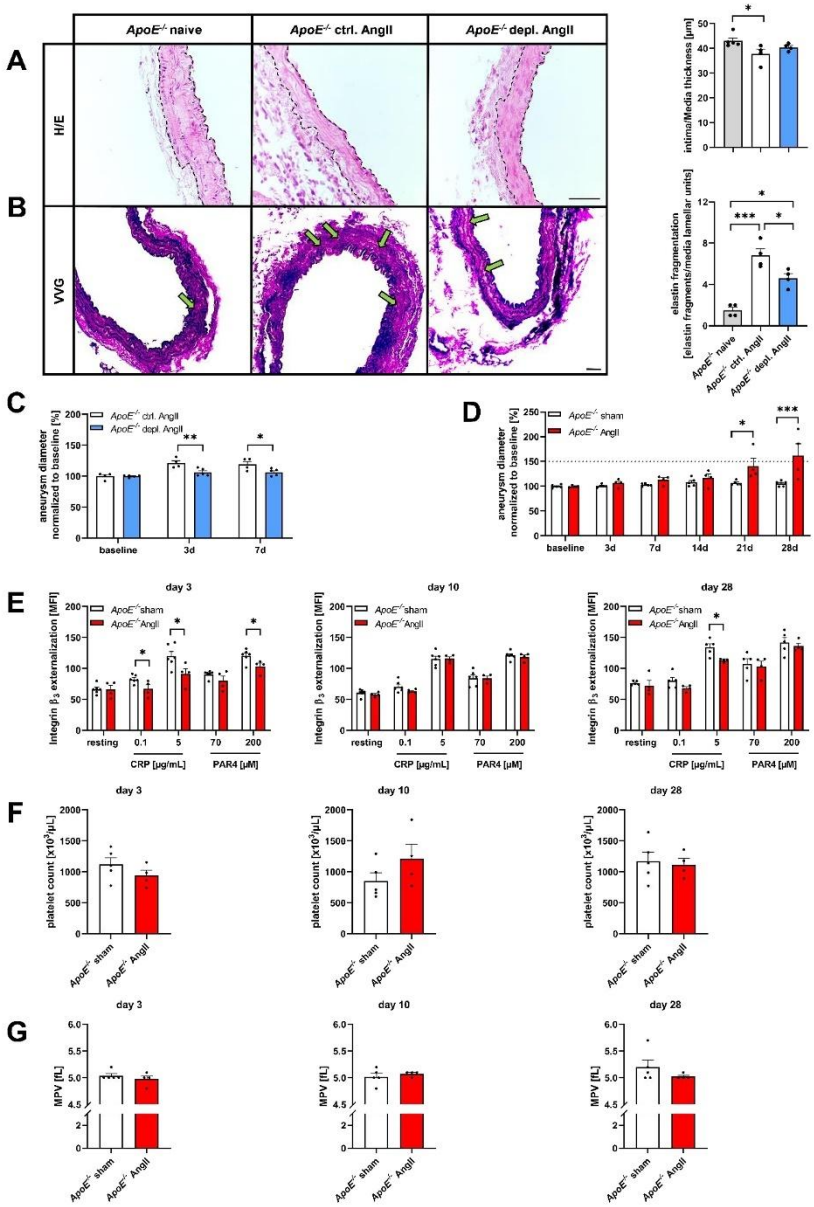


Figure S4. Aortic remodeling, platelet integrin β_3 externalization, platelet counts and MPV in ApoE knockout mice with experimental angiotensin-II induced AAA formation. (**A** and **B**)

Representative images of aortic tissue from depl. *ApoE*$^{-/-}$ and ctrl. *ApoE*$^{-/-}$ mice treated with Ang-II analysed via (**A**) hematoxylin-eosin (H/E) staining and (**B**) Verhoeff van Gieson (VVG) staining. Intima/media thickness was determined after H/E staining (n = 4–5) and elastin fragmentation (breakdowns) was counted after VVG staining (n = 4). Aortic tissue of naïve mice served as control. Scale bars: (**C** and **D**) 50 µm. (**C**) Aortic diameter progression of depl. *ApoE*$^{-/-}$ and ctrl. *ApoE*$^{-/-}$ mice infused with Ang-II for 7 days measured via ultrasound. Data were normalized to baseline (n = 4–5). (**D**) Aortic diameter progression of sham or Ang-II infused *ApoE*$^{-/-}$ mice over a time-period of 28 days determined by ultrasound measurements (n = 4–5). Data were normalized to baseline. (**E**) Externalization of integrin β_3 on the platelet surface in whole blood from mice at days 3, 10 and 28 of sham or Ang-II infused *ApoE*$^{-/-}$ mice after stimulation with indicated agonists (n = 4–5) (**F**) Platelet count of sham or Ang-II infused *ApoE*$^{-/-}$ mice at days 3, 10 and 28 (n = 4–5). (**G**) MPV of sham or Ang-II infused *ApoE*$^{-/-}$ mice 3, 10 and 28 days after osmotic mini-pump implantation (n = 4–5). Data are represented as mean ± SEM. Statistical significances were determined by one-way ANOVA with Holm-Sidak's multiple comparison test (**A** and **B),** two-way ANOVA with Sidak's multiple comparison test (**C** and **D**), multiple t-test (**E**) or unpaired student's t-test (**F** and **G**) or **P* < 0.05, ***P* < 0.01, ****P* < 0.001. Ang-II, angiotensin-II; CRP, collagen-related peptide; ctrl, control; depl., depletion; H/E, hematoxylin-eosin; MFI, mean fluorescence intensity; MPV, mean platelet volume; PAR4, protease-activated receptor 4 activating peptide; VVG, Verhoeff van Gieson.

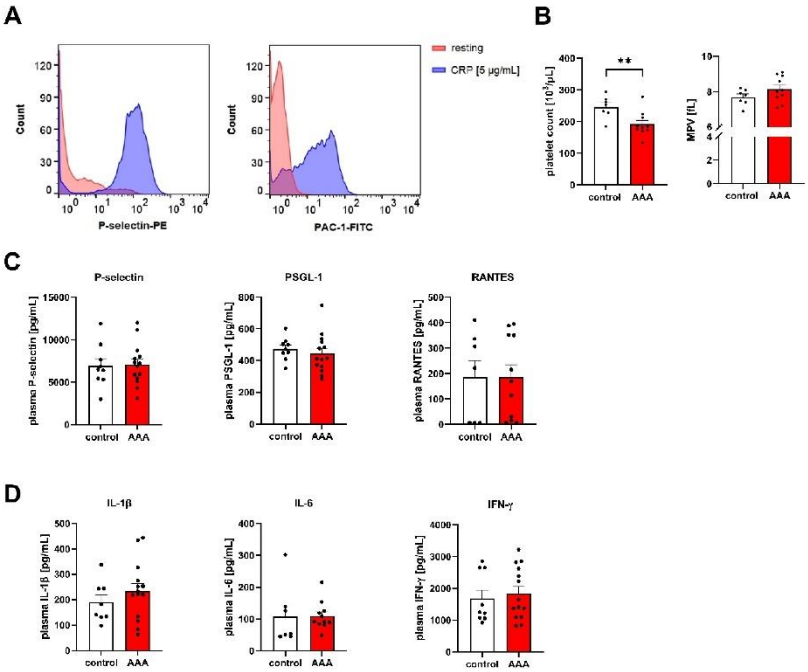
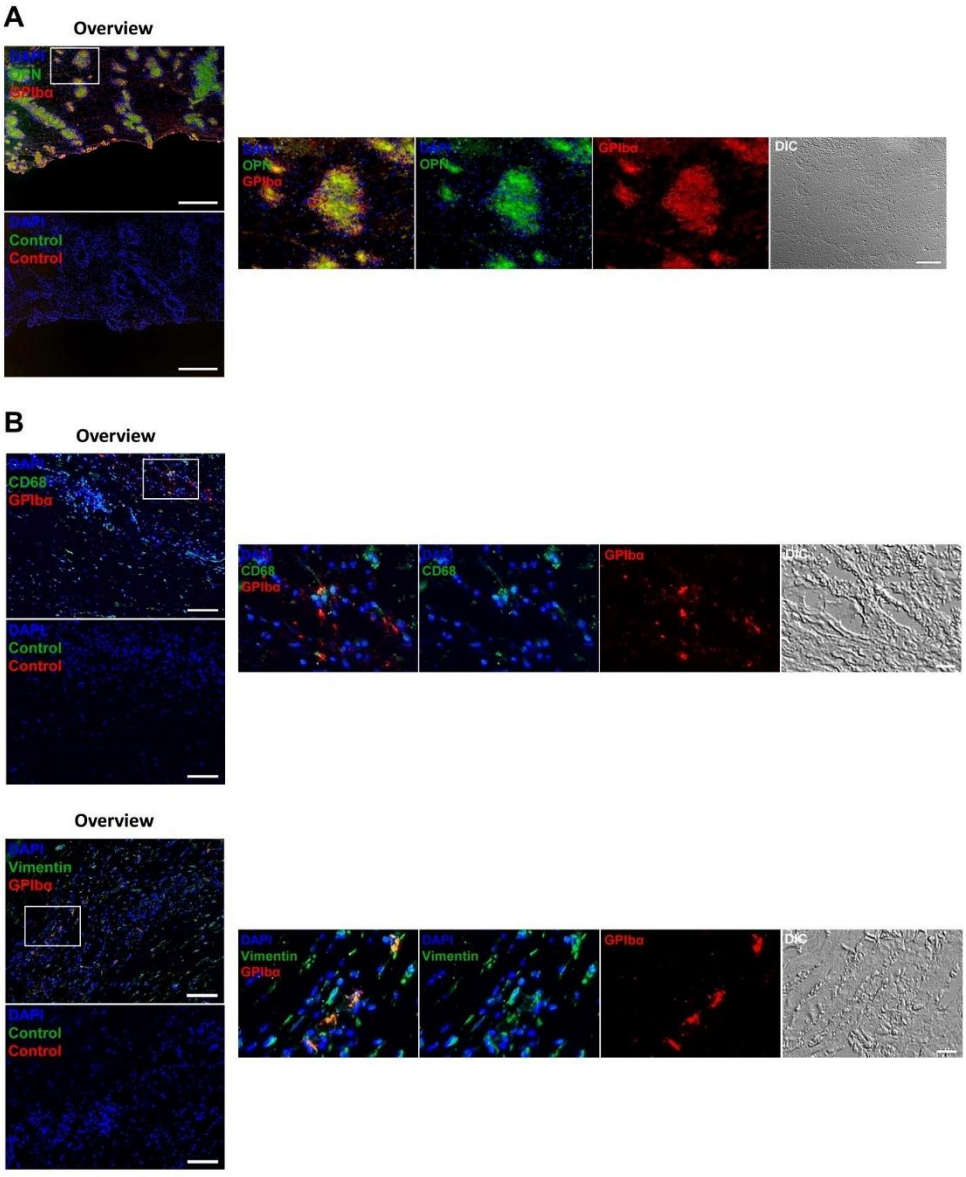


Figure S5. Platelet count, MPV and plasma parameters of AAA patients.

(**A**) Representative histograms for the flow cytometric analysis of P-selectin (left panel) and PAC-1 (right panel) of platelets from AAA patients under resting conditions and after stimulation with 5 µg/mL CRP. (**B**) Platelet count and MPV in AAA patients and age-matched controls (n = 6–10). (**C**) Plasma concentration of P-selectin, PSGL-1 and RANTES in AAA patients and age-matched controls determined by flow cytometric multiplex analysis. (**D**) Plasma concentration of IL-1β, IL6 and IFN-γ in samples of AAA patients and age-matched controls determined by flow cytometric multiplex analysis (n = 7–14). Data are represented as mean ± SEM. Statistical significances were determined by unpaired t-test with Welch's correction (**B**–**D**). $^{**}P < 0.01$. AAA, abdominal aortic aneurysm; CRP, collagen-related peptide; IFN, interferon; IL, interleukin; MPV, mean platelet volume; PSGL, P-selectin glycoprotein ligand; RANTES, regulated on activation, normal T cell expressed and secreted.


A
Overview
DAPI
OPN
GPIbα
DAPI
Control
Control
DAPI
OPN
GPIbα
DAPI
OPN
GPIbα
DIC
B
Overview
DAPI
CD68
GPIbα
DAPI
Control
Control
DAPI
CD68
GPIbα
DAPI
CD68
GPIbα
DIC
Overview
DAPI
Vimentin
GPIbα
DAPI
Control
Control
DAPI
Vimentin
GPIbα
DAPI
Vimentin
GPIbα
DIC

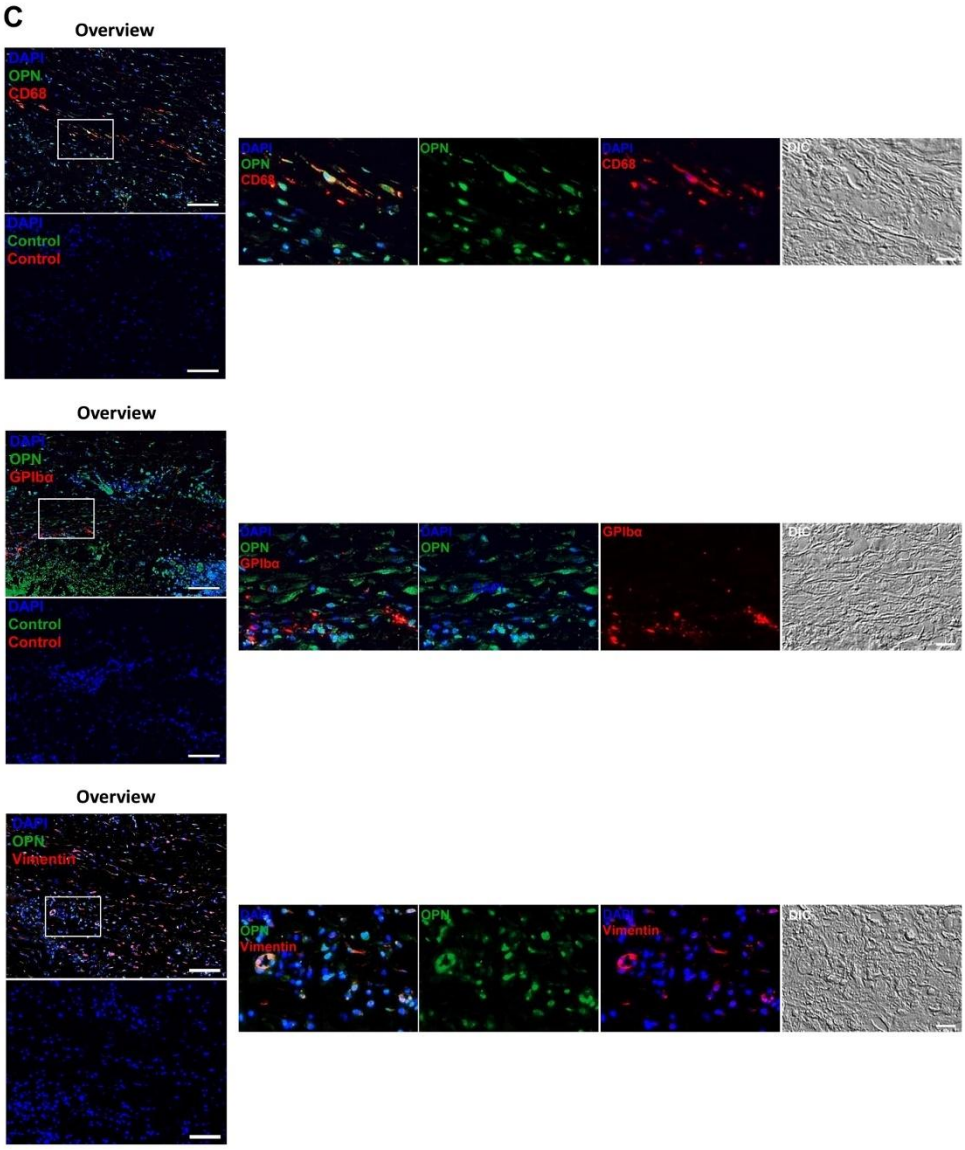


Figure S6. Immunofluorescence staining of aortic vessel walls and intraluminal thrombi from AAA patients. (A+B+C) Immunofluorescence images of **(A)** intraluminal thrombi and **(B+C)** aortic vessel wall together with negative controls were shown in an overview. Individual channels are shown in more detailed magnification. (**A**) Representative differential interference contrast (DIC) microscopy and immunofluorescence images of OPN (anti-OPN, green), platelets (CD42b/anti-GPIbα, red) cell

nuclei (DAPI, blue) in specimens from the luminal layer of intraluminal thrombus (ILT) of AAA patients (n = 5). (**B**) Representative DIC and immunofluorescence images of platelets (anti-CD42b/GPIbα, 2 µg/mL, red), nuclei (DAPI, blue) and macrophages (anti-CD68 AA 21-120, 10 µg/mL, green) respectively fibroblasts (anti-vimentin, 20 µg/mL, green) in the vessel wall of AAA patients (n = 4). (**C**) Representative DIC and immunofluorescence images of osteopontin (anti-OPN, 20 µg/mL, green) and nuclei (DAPI, blue) with macrophages (anti-CD68, 10 µg/mL, red), platelets (anti-CD42b/GPIbα, 2 µg/mL, red) and fibroblasts (anti-vimentin, 20 µg/mL, red) in aortic vessel wall (n = 4). Scale bar: 100 µm (overview) and 20 µM (detail images). Negative controls were achieved by omission of the primary antibody (control). DAPI, 4′, 6-diamidino-2-phenylindole; DIC, differential interference contrast; ILT, intraluminal thrombus; OPN, osteopontin.

3. References

1. Genin M, Clement F, Fattaccioli A, Raes M, and Michiels C. M1 and M2 macrophages derived from THP-1 cells differentially modulate the response of cancer cells to etoposide. *BMC Cancer.* 2015;15:577.
2. Jarre A, Gowert NS, Donner L, Munzer P, Klier M, Borst O, et al. Pre-activated blood platelets and a pro-thrombotic phenotype in APP23 mice modeling Alzheimer's disease. *Cell Signal.* 2014;26(9):2040-50.
3. Gowert NS, Klier M, Reich M, Reusswig F, Donner L, Keitel V, et al. Defective Platelet Activation and Bleeding Complications upon Cholestasis in Mice. *Cell Physiol Biochem.* 2017;41(6):2133-49.
4. Krueger I, Gremer L, Mangels L, Klier M, Jurk K, Willbold D, et al. Reelin Amplifies Glycoprotein VI Activation and AlphaIIb Beta3 Integrin Outside-In Signaling via PLC Gamma 2 and Rho GTPases. *Arteriosclerosis, Thrombosis, and Vascular Biology.* 2020;40(10):2391-403.
5. Aslan JE, and McCarty OJ. Rho GTPases in platelet function. *J Thromb Haemost.* 2013;11(1):35-46.

3.2 GPVI-mediated platelet activation and procoagulant activity aggravate inflammation and aortic wall remodelling in abdominal aortic aneurysm

Feige T[1]*, Bosbach A[1]*, Krott KJ[1]*, Mulorz J[1], Chatterjee M[2], Ortscheid J[1], Krüger E[1], Krüger I[1], Salehzadeh N[1], Goebel S[4], Ibing W[1], Grandoch M[3], Münch G[4], Wagenhäuser MU[1], Schelzig H[1], Elvers M[1]

* contributed equally

[1]Department of Vascular and Endovascular Surgery, University Hospital Duesseldorf, Heinrich-Heine University, Duesseldorf, Germany

[2]Department of Pharmacology, Experimental Therapy and Toxicology, University Hospital Tuebingen, Tuebingen, Germany

[3]Institute of Translational Pharmacology, University Hospital Duesseldorf, Heinrich-Heine University, Duesseldorf, Germany

[4]AdvanceCOR GmbH, Martinsried, Germany

Published in: *Arteriosclerosis, Thrombosis, and Vascular Biology (ATVB)* in 2024

Impact Factor: 7.4 (2024)

License number for republishing: According to the Copyright © 2024, Wolters Kluwer Health policy, no special permission license for the reuse of this publication –published in ATBV– within this thesis is needed.

Own contribution to publication: Ultrasound measurements (WT vs *Gp6*$^{-/-}$ PPE and ePPE mice, ctrl. vs α-GPVI ab treated ePPE mice). Histological staining of murine tissue. Flow cytometric analysis of mice: platelet activation, PS exposure, glycoprotein surface expression VWF-binding, integrin β_3 externalisation and platelet-leukocyte aggregate formation. Immunofluorescence staining of: neutrophils, platelets, macrophages, citrullinated histone-3, OPN, α-smooth muscle actin, cleaved caspase3, elastin, collagen I and collagen IV. Analysis of *ex vivo* neutrophils. ELISA of murine plasma samples including: neutrophil elastase, citH3, MMP2, MMP9, OPN and sGPVI; ELISA of human AAA samples including: sGPVI and fibrin. Flow chamber experiments of murine (sham vs ePPE) and human AAA whole blood samples. GPVI surface exposition of platelets from human AAA samples. Flow cytometric analysis of GPVI shedding in humans. Compilation of AAA patient data. Study design, investigation, data analysis, statistical analysis, figure visualisation. Co-writing of the manuscript.

Check for updates

Arteriosclerosis, Thrombosis, and Vascular Biology

BASIC SCIENCES

GP VI–Mediated Platelet Activation and Procoagulant Activity Aggravate Inflammation and Aortic Wall Remodeling in Abdominal Aortic Aneurysm

Tobias Feige,* Agnes Bosbach,* Kim J. Krott,* Joscha Mulorz, Madhumita Chatterjee, Julia Ortscheid, Evelyn Krüger, Irena Krüger, Niloofar Salehzadeh, Silvia Goebel, Wiebke Ibing, Maria Grandoch, Götz Münch, Markus U. Wagenhäuser, Hubert Schelzig, Margitta Elvers

BACKGROUND: Platelets play an important role in cardiovascular and cerebrovascular diseases. Abdominal aortic aneurysm (AAA) is a highly lethal, atherosclerosis-related disease with characteristic features of progressive dilatation of the abdominal aorta and degradation of the vessel wall, accompanied by chronic inflammation. Platelet activation and procoagulant activity play a decisive role in the AAA pathology as they might trigger AAA development in both mice and humans.

METHODS: The present study investigated the impact of the major platelet collagen receptor GP (platelet glycoprotein) VI in pathophysiological processes underlying AAA initiation and progression. For experimental AAA induction in mice, PPE (porcine pancreatic elastase) and the external PPE model were used.

RESULTS: Genetic deletion of GP VI offered protection of mice against aortic diameter expansion in experimental AAA. Mechanistically, GP VI deficiency resulted in decreased inflammation with reduced infiltration of neutrophils and platelets into the aortic wall. Furthermore, remodeling of the aortic wall was improved in the absence of GP VI, as indicated by reduced MMP (matrix metalloproteinase)-2/9 and OPN (osteopontin) plasma levels and an enhanced α-SMA (α-smooth muscle actin) content within the aortic wall, accompanied by reduced cell apoptosis. Consequently, an elevation in intima/media thickness and elastin content was observed in GP VI–deficient PPE mice, resulting in a significantly reduced aortic diameter expansion and reduced aneurysm incidence. In patients with AAA, enhanced plasma levels of soluble GP VI and fibrin, as well as fibrin accumulation within the intraluminal thrombus might serve as new biomarkers to detect AAA early. Moreover, we hypothesize that GP VI might play a role in procoagulant activity and thrombus stabilization via binding to fibrin.

CONCLUSIONS: In conclusion, our results emphasize the potential need for a GP VI–targeted antiplatelet therapy to reduce AAA initiation and progression, as well as to protect patients with AAA from aortic rupture.

GRAPHIC ABSTRACT: A graphic abstract is available for this article.

Key Words: aortic aneurysm, abdominal ■ aortic rupture ■ blood platelets ■ dilatation ■ inflammation

Downloaded from http://ahajournals.org by on June 17, 2025

Atherosclerotic diseases are a leading cause of cardiovascular-related deaths worldwide.[1] Abdominal aortic aneurysm (AAA) is an atherosclerosis-related disease with a high mortality rate without treatment. The prevalence of AAA, defined as an aortic diameter of ≥3 cm, is age dependent. Further, well-known risk factors are male sex, a family history of AAA,

See accompanying editorial on page 2318

Correspondence to: Margitta Elvers, PhD, University Hospital Duesseldorf, Heinrich-Heine University, Moorenstreet 5, 40225 Duesseldorf, Germany. Email margitta.elvers@med.uni-duesseldorf.de
*T. Feige, A. Bosbach, and K.J. Krott contributed equally.
Supplemental Material is available at https://www.ahajournals.org/doi/suppl/10.1161/ATVBAHA.123.320615.
For Sources of Funding and Disclosures, see page 2315.
© 2024 American Heart Association, Inc.
Arterioscler Thromb Vasc Biol is available at www.ahajournals.org/journal/atvb

Nonstandard Abbreviations and Acronyms

α-SMA	α-smooth muscle actin
AAA	abdominal aortic aneurysm
Ang II	angiotensin II
Casp3	caspase 3
citH3	citrullinated histone H3
Col I	collagen I
Col III	collagen III
Col IV	collagen IV
CRP	collagen-related peptide
DAPI	4′,6-diamidine-2′-phenylindole dihydrochloride
ePPE	external porcine pancreatic elastase
GM-CSF	granulocyte-macrophage colony-stimulating factor
GP	platelet glycoprotein
IL	interleukin
ILT	intraluminal thrombus
INF	interferon
MMP	matrix metalloproteinase
NET	neutrophil extracellular trap
OPN	osteopontin
PAR4	protease activated receptor 4
PPE	porcine pancreatic elastase
PS	phosphatidylserine
RT	room temperature
sGP VI	soluble platelet glycoprotein VI
VWF	von Willebrand factor
WT	wild-type

Highlights

- Genetic deletion of GP (platelet glycoprotein) VI offered protection of mice against abdominal aortic aneurysm formation, indicated by a significantly reduced aortic diameter expansion and reduced aneurysm incidence in experimental abdominal aortic aneurysm.
- GP VI deficiency resulted in decreased inflammation mediated by reduced infiltration of neutrophils and platelets into the aneurysm segment and decreased neutrophil extracellular trap formation.
- Aortic wall remodeling was improved in the absence of GP VI, indicated by reduced MMP (matrix metalloproteinase) 2/9 and OPN (osteopontin) plasma levels, as well as enhanced α-SMA (α-smooth muscle actin) content within the aortic tissue.
- Administration of a GP VI antibody into mice is the first promising therapeutic approach to protect against abdominal aortic aneurysm.
- Analysis of patients with abdominal aortic aneurysm revealed elevated plasma levels of soluble GP VI and fibrin.

smoking, hypertension, hypercholesterolemia, obesity, and cardiovascular diseases. The global prevalence of AAA is ≈0.92% among individuals aged 30 to 79 years, translating to a total of 35.12 million AAA cases worldwide in 2019.[2] With enhanced abdominal aortic diameter, the risk of fatal rupture increases exponentially, leading to high mortality in AAA. Despite great efforts to understand the underlying pathological mechanisms of AAA, the only treatment option to date is endovascular or open surgical repair, once the aortic diameter exceeds the defined cutoff values. Although there are some promising candidates for noninvasive drug-based therapies, clinical implementation of such therapies is lacking. Moreover, prospective randomized trials have either not demonstrated expected therapeutic efficacy or have not been performed to date.[3–7] The characteristic progressive dilatation of the abdominal aorta is accompanied by degradation, remodeling, and weakening of the vessel wall due to chronic inflammation. This is caused by leukocyte infiltration and extracellular matrix degradation by activation of proteolytic enzymes.[5,6,8,9]

Platelets, besides their primary role in thrombosis, hemostasis, and maintaining vascular integrity, are prompt drivers of inflammation, as they release various cytokines, chemokines, growth factors, and biological modulators upon activation. Thus, platelets contribute to inflammation, angiogenesis, cell survival, as well as vascular and tissue repair/regeneration.[10] In contrast to various cardiovascular diseases, relatively little is known about the role of platelets in the pathological development of AAA. However experimental and clinical data strongly suggest that platelet activation may play a pivotal role in AAA initiation and progression.

Different clinical trials provide evidence for the active contribution of platelet response in the development and progression of AAA in humans. Antiplatelet medication of small-sized AAA in which an intraluminal thrombus (ILT) is rarely present has not shown any significant difference. Nevertheless, other clinical trials with AAA sized above 35 mm, respectively 39 mm, have provided evidence of a beneficial effect of antiplatelet medication with low-dose aspirin. Specifically, decreased aneurysm size and less frequent need for surgical repair were reported.[11] Similarly, in various preclinical animal models such as the Ang II (angiotensin II) and the PPE (porcine pancreatic elastase) infusion model, antiplatelet treatment or genetic ablation of specific platelet proteins has demonstrated a beneficial effect on AAA rupture rates, AAA growth, and inflammation.[12–18]

Recently, we demonstrated the pivotal role of platelet activation in the experimental murine PPE model, suggesting that a cross talk between platelets and different target cells such as macrophages and fibroblasts contributes to inflammation, stiffening of the aortic wall, and AAA growth.[19] In this study, we observed a major role of platelets

Downloaded from http://ahajournals.org by on June 17, 2025

in the inflammatory response and remodeling of the aortic wall in experimental AAA, resulting from enhanced platelet activation and procoagulant activity. Elevated platelet reactivity and procoagulant response have also been documented in patients with AAA, strongly supporting the potential relevance of antiplatelet therapy to reduce AAA progression and rupture patients.[19] Moreover, we reported for the first time a pathophysiological relevance of the platelet-specific GP (platelet glycoprotein) VI. GP VI–mediated platelet activation induced enhanced gene expression of acute-phase cytokines and MMP (matrix metalloproteinase)-9 in macrophages, as well as IL (interleukin)-6 release from aortic fibroblasts. However, elevated platelet activation was due to an increase in GP VI activation at day 28 after elastase infusion in mice.[19] Nevertheless, GP VI has been shown to represent a key receptor in acute coronary syndrome and is a useful biomarker for the early detection of atherosclerotic diseases such as acute coronary syndrome and ischemic stroke. Furthermore, GP VI may be used for risk stratification and prediction of clinical outcome in patients with atherosclerotic diseases. In addition, therapeutic implications of targeting GP VI in mice and humans have been described, for example, Revacept, a GP VI–Fc fusion protein that binds to collagen preventing the binding of platelet GP VI to collagen, or by using GP VI–blocking antibodies.[20–25] Although limited data evaluating the role of GP VI in the context of AAA are available, there is still a significant lack of understanding of how platelets are involved in AAA development and progression, especially how GP VI contributes to these processes. Therefore, more mechanistic insights into the specific role of platelets and GP VI in AAA pathology are urgently needed to facilitate the development of appropriate antiplatelet targets. We have recently reported that platelets strongly affect cellular processes, which promote AAA progression.[19] In the present study, we provide strong evidence that GP VI plays a major role in these processes. Thus, there is a strong need to evaluate GP VI as a potential target for novel drug-based AAA therapies, because according to the European guidelines, there is no drug-based therapy to treat patients with AAA available to date.

MATERIALS AND METHODS

Data Availability

The original contributions presented in the study are included in the article. Further inquiries can be directed to the corresponding author.

Study Approval

For experiments with human blood and tissue samples, all participants provided written informed consent to participate in this study according to the guidelines of the Ethics Committee of the University Hospital of Duesseldorf, Germany (ATLANTA study [Potential Activation Mechanisms and Interactions of Platelets in Degenerative Diseases of the Liver, Brain and Aorta], number: 2018-140-kFogU; biobank study number: 5731R [2018-222_1]; MELENA study [Molecular Biological Impact Factors Influencing the Development and Progression of Aortic Aneurysms], study number: 2018-248-FmB; patients with thrombectomy, study number: 4669R). This study was conducted according to the Declaration of Helsinki and the International Council for Harmonisation Guidelines on Good Clinical Practice. All procedures were approved by the Ethics Committee of the University Hospital of Duesseldorf, Germany.

All animal experiments were conducted according to the Declaration of Helsinki and were approved by the Ethics Committee of the State Ministry of Agriculture, Nutrition, and Forestry State of North Rhine-Westphalia, Germany (permit number: 81-02.05.40.21.041, 81-02.04.2018.A409, and 81-02.04.2021.A429), as well as by the Heinrich-Heine-University Animal Care Committee. All procedures conform to the guidelines from Directive 2010/63/EU of the European Parliament on the protection of animals used for scientific purposes.

Human AAA Samples

Fresh citrate-anticoagulated blood (BD Vacutainer; Becton, Dickinson and Company; No. 367714) was collected from patients with AAA. Blood samples of healthy volunteers with an average age of 60.1±1.47 years served as controls. Control blood samples were obtained from the blood donor center at the University Hospital of Duesseldorf, Germany. Human ILT tissue from patients with AAA and tissue of arterial thrombi from patients with thrombectomy were obtained from patients who underwent surgery in the Department of Vascular and Endovascular Surgery at University Hospital Duesseldorf.

Animals

Pathogen-free mice with GP VI ablation (*Gp*$^{-/-}$) were provided by J. Ware (University of Arkansas for Medical Sciences, Little Rock, AR) and backcrossed to C57BL/6J mice. For external PPE (ePPE) application and GP VI–blocking antibody treatment (α-GP VI ab ePPE), C57BL/6J mice were purchased from Janvier Labs. All experiments were conducted with male mice aged 10 to 12 weeks, as female mice reveal enhanced cyclical hormonal fluctuations, resulting in a reduced inducibility of experimental AAA formation.[26] The mice were maintained in an environmentally controlled room at 22±1 °C and a 12-hour day-night cycle. Mice were housed in Makrolon type III cages with ad libitum access to food (standard laboratory diet) and water.

Experimental AAA Mouse Models

The PPE perfusion model is an experimental mouse model established to study AAA development and progression in vivo by infusion of PPE into the abdominal infrarenal aorta. To induce AAA formation, mice were anesthetized with 2% to 3% isoflurane and received an additional subcutaneous injection of buprenorphine (0.1 mg/kg body weight; Temgesic; Eumedica) 30 minutes before PPE surgery. Thus, anesthesia was continuously maintained and monitored throughout the procedure. The PPE surgery was conducted as described previously.[15,19] In short, the infrarenal aortic segment was infused with elastase at 2.5 U/mL for 5 minutes. After surgery, all mice received an additional subcutaneous injection of buprenorphine (0.1 mg/

Downloaded from http://ahajournals.org by on June 17, 2025

kg body weight) for pain relief every 6 hours during the daylight phase and during the night phase through drinking water (9 µg/mL) for the following 3 days. For tissue collection, mice were euthanized via cervical dislocation under deep isoflurane anesthesia at days 7, 14, and 28 post-PPE surgery.

The ePPE model is an experimental mouse model to analyze AAA development and progression in vivo by the external application of PPE to the abdominal infrarenal aorta. Anesthesia and analgesia were performed as described above. For external elastase application, a laparotomy was conducted and the abdominal aorta was separated from the vena cava. To prevent damage to the surrounding tissue, a shell of parafilm was placed around the infrarenal aorta. External application with 25.5 U/mL elastase was conducted for 5 minutes. Sham-operated mice were treated with heat-deactivated elastase (100 °C, 30 minutes) instead. After incubation, the elastase was removed, and the treated aortic segment was washed with 0.9% NaCl once. The parafilm was removed, and the laparotomy was closed. In addition to external elastase treatment, all mice received 0.1% β-aminopropionitrile via drinking water over the whole 28-day time course, starting 3 days before surgery. β-Aminopropionitrile treatment prevents elastin and collagen cross-linking to mimic the human geriatric condition. For tissue collection, mice were euthanized via cervical dislocation under deep isoflurane anesthesia at day 28 post-ePPE surgery.

In Vivo GP VI Blocking Antibody Application

C57BL/6J mice underwent ePPE surgery (with 0.1% β-aminopropionitrile administration as described in 2.4) and received a GP VI blocking antibody (10 mg/kg body weight, Fab Y020347, α-GP VI ab ePPE) or a respective vehicle control (control ePPE) over a time course of 28 days. Intraperitoneal antibody injection was performed every 2 to 3 days, starting 12 hours before surgery.

Ultrasound Imaging

AAA development and progression in PPE-operated mice was monitored via ultrasound measurements. The maximum dilation of the abdominal aorta within the aneurysm segment was measured before (baseline) and at days 7, 14, 21, and 28 after surgery. For ultrasound imaging, mice were anesthetized with 2% to 3% isoflurane and placed onto a heating plate at 37 °C. All ultrasound measurements were performed using a Vevo 3100 High-Resolution In Vivo Micro-Imaging System (VisualSonics). For monitoring the progressive inner aortic diameter dilation, a standardized imaging algorithm with longitudinal B-mode images of the systolic phase was used.

Flow Cytometry

For flow cytometric analysis of murine platelets, heparinized murine whole blood was washed 3× with Tyrode buffer (137 mmol/L NaCl, 2.8 mmol/L KCl, 12 mmol/L $NaHCO_3$, 0.4 mmol/L NaH_2PO_4, and 5.5 mmol/L glucose, pH 6.5) by centrifugation at 650*g* for 5 minutes. After final washing, the samples were resuspended in murine Tyrode buffer supplemented with 1 mmol/L $CaCl_2$. For measuring platelet activation, a 2-color analysis was performed using specific antibodies for P-selectin (CD62P, Wug.E9-fluorescein isothiocyanate [FITC], No. D200; Emfret Analytics) and active integrin $\alpha_{IIb}\beta_3$ (JON/A-PE, No. D200; Emfret Analytics) in a final ratio of 1:10. Samples were incubated with the indicated agonists (ADP; No. A2754; Sigma-Aldrich), CRP (collagen-related peptide; Richard Farndale, University of Cambridge, Cambridge, United Kingdom), the thromboxane A2 analogue U46619 (No. 1932; Tocris) or PAR4 (protease-activated receptor 4) peptide (No. 3494; Tocris) and the respective antibodies for 15 minutes at 37 °C in the dark. The reaction was stopped by adding 300 µL of PBS to all samples. For analyzing the GP exposure, washed whole blood samples were incubated with specific antibodies against integrin α_5 (CD49e, Tap. A12-FITC, No. M080-1; Emfret Analytics), GP Ibα (CD42b, Xia. G5-PE, No. M040-2; Emfret Analytics), or GP VI (JAQ1-FITC, No. M011-1; Emfret Analytics) in a ratio of 1:10 for 15 minutes at room temperature (RT). To determine upregulation in GP surface expression or VWF (von Willebrand factor) surface exposition, washed blood was specifically labeled for integrin β_3 (CD61, Luc.H11-FITC, No. M031-1; Emfret Analytics), respectively VWF (VWF-FITC, No. P150-1; Emfret Analytics) at a ratio of 1:10 and stimulated with the indicated agonists. To determine phosphatidylserine (PS) exposure on the platelet surface, washed murine whole blood was resuspended in binding buffer (10 µmol/L HEPES, 140 µmol/L NaCl, and 2.5 mmol/L $CaCl_2$, pH 7.4). All samples were labeled with a PS-detecting antibody (Cy5 [Cyanine5] annexin V, No. 559934; BD Biosciences) at a ratio of 1:10. Samples were incubated with the indicated agonists and antibodies for 20 minutes at 37 °C in the dark. The reaction was stopped by adding 300 µL of binding buffer (0.1 M HEPES, 1.4 M NaCl, and 25 mmol/L $CaCl_2$, pH 7.4). All samples were labeled for 15 minutes at RT. To analyze platelet-leukocyte aggregate formation, washed murine whole blood was specifically labeled for the leukocytes (CD45, 30-F11-APC [allophycocyanin], No. 559864; BD Biosciences), neutrophils (Ly6G [lymphocyte antigen 6 complex locus G6D], 1A8-APC, No. 127614; BioLegend), T cells (CD3, 17A2-APC, No. 100235; BioLegend), macrophages, or granulocytes (CD11b, M1/70-APC, No. 553312; BD Biosciences and CD14, Sa14-2-APC, No. 123311; BioLegend) at a ratio of 1:10. GP Ibα (CD42b, Xia.G5-PE, No. M040-2; Emfret Analytics) served as a platelet-specific marker. All samples were labeled for 15 minutes at RT in the dark. For analyzing human platelets, whole blood samples were diluted at a ratio of 1:10 in human Tyrode buffer (137 mmol/L NaCl, 2.8 mmol/L KCl, 12 mmol/L $NaHCO_3$, 0.4 mmol/L NaH_2PO_4, and 5.5 mmol/L glucose, pH 6.5) and specifically stained for 15 minutes at RT using an antibody against GP VI (HY101-PE, No. 565241; BD Pharmingen) at a ratio of 1:10. All samples were analyzed using a BD FACSCalibur flow cytometer.

Flow Cytometry–Based Multiplex Analysis

Plasma levels of the circulating inflammatory cytokines IL-1α, IL-1β, IL-6, IL-10, IL-17A, INF (interferon)-γ, and GM-CSF (granulocyte-macrophage colony-stimulating factor) in PPE-operated mice were determined using a flow cytometry–based bead multiplex analysis (LEGENDplex mouse inflammation panel [13 plex], No. 740150; BioLegend). All measurements were conducted according to the manufacturer's instructions by using a BD FACSLyric flow cytometer.[27]

Immunofluorescence Staining of Murine Aortic Tissue

Paraffin-embedded aortic tissue from PPE-operated mice was sliced into 5-µm sections using an automatic microtome (Microm HM355; Thermo Fisher Scientific). Before staining,

Downloaded from http://ahajournals.org by on June 17, 2025

all sections were deparaffinized and hydrated. For antigen unmasking, the tissue sections were heated at 300 W in citrate buffer (pH 6.0) for 10 minutes. For staining of macrophages and platelets, the aortic tissue sections were blocked for 1 hour at RT with a protein-blocking solution (No. X0909; Dako). After blocking, the sections were specifically stained for macrophages (Mac3 [CD107b], No. 550292; BD Pharmingen; 1:50) or platelets (GP Ibα [CD42b], No. M042-0; Emfret Analytics; 1:50) at 4 °C overnight. The respective IgG primary antibody served as a negative control (No. 559478; BD Pharmingen; 1:800 and No. C301; Emfret Analytics; 1:50). The sections were incubated with a biotinylated secondary antibody (No. BA-9400; Vector; 1:200) for 1 hour at RT and afterward with a streptavidin eFluorTM 660 conjugate (No. 50-4317-80; Thermo Fisher Scientific; 1:20) for 30 minutes at RT. For staining of neutrophils (Ly6G, No. 551459; BD Pharmingen; 1:50), OPN (osteopontin; No. ab181440; Abcam; 1:50), α-SMA (α-smooth muscle actin; No. ab5694; Abcam; 1:50), active Casp3 (caspase 3; cleaved Casp3, No. 9661; Cell Signaling; 1:50), Col I (collagen I; No. ab270993; Abcam; 1:100), Col IV (collagen IV; No. ab6586; Abcam; 1:100), and citrullinated histone H3 (citH3; No. ab219407, 1:100) respectively, the aortic tissue sections were blocked with DPBS (containing 0.3% Triton X-100 and 5% goat serum) for 1 hour at RT. After overnight incubation with the respective primary antibodies at 4 °C, the sections were stained with a highly cross-adsorbed Alexa Fluor Plus 555–conjugated secondary antibody (No. A32794; Invitrogen; 1:200) for 1 hour at RT. For staining of neutrophils a highly cross-adsorbed Alexa Fluor Plus 568–conjugated secondary antibody (No. A11077; Invitrogen; 1:200) was used. The respective IgG antibody served as a negative control (No. 3900S; Cell Signaling). For visualizing nuclei, all tissue sections were stained with DAPI (4′,6-diamidine-2′-phenylindole dihydrochloride; No. 10236276001; Roche; 1:3000). For image generation, the Axio Observer.D1 microscope (Zeiss) or the LSM 880 Airyscan Fast system (Zeiss) was used. Tissue sections of PPE-operated mice were analyzed as percentage of cell content normalized to the total aortic tissue, using Image J (version 1.53t) by applying the preinstalled default threshold. For quantification of the aortic elastin content, the mean fluorescence intensity was determined using the ZEN software (blue edition, version 3.3; Zeiss). The mean fluorescence intensity of each section was normalized to the total area of the aortic tissue.

Histology of Murine Aortic Tissue

Paraffin-embedded aortic tissue from PPE mice was sliced into 5-µm sections using an automatic microtome (Microm HM355; Thermo Fisher Scientific). Hematoxylin/eosin staining of murine aortic tissue was conducted as described elsewhere.[28] The intima/media thickness of PPE-operated mice was analyzed by measuring the aortic media thickness at 10 distinct positions within the aneurysm segment using the ZEN software (blue edition, version 3.3; Zeiss). The modified Verhoeff-van Gieson staining of the murine aortic tissue was performed according to the manufacturer's instructions (elastic stain, No. HT25A-1KT; Sigma-Aldrich). For analyzing elastin fragmentation, the number of elastin breaks was determined using the ZEN software (blue edition, version 3.3; Zeiss). Moreover, picrosirius red staining of the murine aortic tissue was conducted as described elsewhere.[29,30] To determine the collagen composition within the aneurysm segment, the collagen density was analyzed under polarized light using Axio Imager 2 (Zeiss). Collagen content was determined as percentage normalized to the total aortic tissue, using the Image J (version 1.53t) software by applying the preinstalled default threshold. For a modified Martius Scarlet blue staining of murine aortic tissue, paraffin-embedded sections were hydrated and incubated in Bouin solution (No. HT10132; Sigma-Aldrich) for 1 hour at 56 °C. All sections were washed for 10 minutes in tap water and for 5 minutes in 96% ethanol. Afterward, the tissue sections were stained with Naphthol yellow S (No. sc-215544; Santa Cruz Biotechnology) for 5 minutes at RT. After staining, the sections were washed in dH_2O for 5 minutes and subsequently stained using a crystal scarlet solution for 10 minutes at RT. For differentiation, all sections were incubated in 1% phosphotungstic acid (No. 100583; Merck Millipore) for 10 minutes at RT. Tissue sections were washed once in dH_2O and for 10 s in 1% acetic acid. Subsequently, the tissue sections were dehydrated and embedded using a Roti-Histokitt mounting medium. Fibrin content was determined as percentage normalized to the total aortic tissue, using the Image J (version 1.53t) software by applying the preinstalled default threshold.

Analysis of Ex Vivo Neutrophils

Neutrophils of PPE-operated WT (wild-type) and *Gp6*$^{-/-}$ mice were isolated from citrate-anticoagulated peripheral blood at day 7 post-surgery using a disconctinous density gradient–based isolation method as described elsewhere.[31] To analyze AAA-related neutrophil adhesion, 1.8×10^6 neutrophils in 1× RPMI 1640 (supplemented with 10% fetal bovine serum and 1% penicillin/streptomycin) were seeded in chamber slides (No. 178599; Thermo Fisher Scientific) for 3 hours at 37 °C (5% CO_2). After incubation, nonadherents were removed by washing twice with PBS. Adherent neutrophils were fixated with 4% PFA for 15 minutes at RT. After fixation, cells were blocked with 5% BSA supplemented with 0.3% Triton for 1 hour at RT. To analyze AAA-related neutrophil adhesion and neutrophil extracellular trap (NET) formation, cells were specifically stained for neutrophils (Ly6G, No. 551459; BD Pharmingen; 1:50) and citH3 (No. ab219407; 1:50), respectively. After overnight incubation with the respective primary antibodies at 4 °C, the adherent cells were stained with a highly cross-adsorbed Alexa Fluor Plus 568–conjugated secondary antibody (No. A11077; Invitrogen; 1:200) and a highly cross-adsorbed Alexa Fluor Plus 555–conjugated secondary antibody (No. A32794; Invitrogen; 1:200) for 1 hour at RT. For visualizing nuclei, cells were stained with DAPI (No. 10236276001; Roche; 1:3000). To investigate the impact of GP VI on AAA-related neutrophil adhesion, neutrophils from PPE-operated WT mice isolated at day 7 post-surgery were incubated with isolated platelets from naive WT and *Gp6*$^{-/-}$ mice. Murine platelet isolation was conducted as described elsewhere.[32] Subsequently, 1.8×10^6 neutrophils of WT PPE mice in 1× RPMI 1640 (supplemented with 10% fetal bovine serum and 1% penicillin/streptomycin) were incubated with 5×10^6 WT and *Gp6*$^{-/-}$ platelets for 3 hours at 37 °C (5% CO_2). Platelets were stimulated with 1 µg/mL CRP (Richard Farndale, University of Cambridge, Cambridge, United Kingdom). Unstimulated platelets served as control. To visualize adhesion, cells were specifically stained for neutrophils (Ly6G, No. 551459; BD Pharmingen; 1:50) as described above. In addition platelets were specifically stained for GP IX

Downloaded from http://ahajournals.org by on June 17, 2025

(No. orb167288; Biorbyt; 1:50). For image generation, the Axio Observer.D1 microscope was used.

Histology of Human Thrombus Tissue

For Martius Scarlet blue staining of human thrombus tissue, paraffin-embedded sections were hydrated and incubated in Bouin solution (No. HT10132; Sigma-Aldrich) for 1 hour at 56 °C. All sections were washed for 10 minutes in tap water and for 5 minutes in 96% ethanol. Afterward, the tissue sections were stained with Naphthol yellow S (No. sc-215544; Santa Cruz Biotechnology) for 5 minutes at RT. After staining, the sections were washed in dH_2O for 5 minutes and subsequently stained using a crystal scarlet solution for 10 minutes at RT. For differentiation, all sections were incubated in 1% phosphotungstic acid (No. 100583; Merck Millipore) for 10 minutes at RT, followed by an incubation with methyl blue (No. M5528; Sigma-Aldrich) for 15 minutes at RT. Tissue sections were washed once in dH_2O and for 10 s in 1% acetic acid. Subsequently, the tissue sections were dehydrated and embedded using a Roti-Histokitt mounting medium. For immunohistochemical staining of platelets in human thrombus tissue, paraffin-embedded sections were deparaffinized and hydrated. For antigen unmasking, the tissue sections were heated at 300 W in citrate buffer (pH 6.0) for 10 minutes. The sections were washed 3× in Tris-buffered saline supplemented with 0.1% Tween 20 for 5 minutes at RT. Tissue sections were blocked for 1 hour at RT with a protein-blocking solution (No. X0909; Dako). After blocking, the sections were specifically stained for platelets (GP Ibα [CD42b], No. MA5-11642; Invitrogen; 1:100) at 4 °C overnight. The respective IgG primary antibody served as control (No. 5415S; Cell Signaling Technology; 1:1250). For endogenous peroxidase activity blocking, the sections were incubated with 0.3% hydrogen peroxide for 15 minutes at RT. Afterward, the sections were incubated with a biotinylated secondary antibody (No. BA-9200; Vector Laboratories; 1:300) for 30 minutes at RT, followed by an incubation with an avidin-biotinylated horseradish peroxidase enzyme complex (No. PK-6100; Vector Laboratories) for 30 minutes at RT. For antigen detection, the tissue sections were incubated with a VIP peroxidase substrate (No. SK-4600; Vector Laboratories) for 2 minutes at RT. Nuclei were visualized by incubation with methyl green (No. H-3402; Vector Laboratories) for 10 minutes at 60 °C. After washing in dH_2O, the sections were dehydrated and mounted using Roti-Histokitt mounting medium. Tissue sections of human thrombus samples were analyzed as percentage content normalized to the total thrombus tissue, using the Image J (version 1.53t) software by applying the preinstalled default threshold.

ELISA

For the analysis of murine plasma samples, ELISA for OPN (No. DY441; R&D Systems), neutrophil elastase (ELA2 [neutrophil elastase 2]; No. DY4517-05; R&D Systems), MMP2 (No. MMP200; R&D Systems), MMP9 (No. MMPT90; R&D Systems), citH3 (No. MBS7273794; MyBioSource), and soluble GP VI (sGP VI; No. MBS109240; MyBioSource) was performed. Plasma samples from patients with AAA were analyzed using a human fibrin (No. MBS265263; MyBioSource) and a human sGP VI (No. MBS9390142; MyBioSource) ELISA. All ELISAs were conducted according to the manufacturer's instructions.

Thrombus Formation Under Flow Ex Vivo (Flow Chamber Experiments)

Rectangular glass coverslips (24×60 mm) were coated with 200 µg/mL collagen (Horm collagen reagent, No. 1130630; Takeda Austria GmbH) at 4 °C overnight. After coating, the coverslips were blocked with 1% BSA (in PBS) for 1 hour at RT. Fresh citrate-anticoagulated human blood was preincubated with with 10 µmol/L mepacrine (Sigma-Aldrich) and 8.5 µg/mL AF546 fibrinogen (No. F13192; Invitrogen) for 10 minutes at RT. For murine thrombus formation, citrate-anticoagulated blood was incubated with 0.5 µg/mL 3,3′-dihexyloxacarbocyanine iodide (No. D273; Sigma-Aldrich) and 8.5 µg/mL AF546 fibrinogen (No. F13192; Invitrogen) for 10 minutes at RT. Prelabeled whole blood samples were perfused over the precoated coverslips using a flow chamber system (50 µm×5 mm) under a shear rate of 1700 s^{-1} (12.75 mL/h). After flow, coverslips were fixated with 4% PFA for 15 minutes at RT. Afterward, slides were stained with AF647 annexin V (No. A23204; Invitrogen) diluted 1:20 in binding buffer (10 µmol/L HEPES, 140 µmol/L NaCl, and 2.5 mmol/L $CaCl_2$, pH 7.4). Five representative images were taken using the Axio Observer.D1 microscope. Thrombus formation, thrombus volume, fibrin/fibrinogen content, and PS exposure of murine and human thrombi were analyzed by using Image J (version 1.53t).

Statistical Analysis

Data are presented as the arithmetic mean±SEM. Statistical analyses were performed using GraphPad Prism 8 (version 8.4.3). The indicated sample size for each experiment reflects the number of independent biological replicates. The statistical analysis was conducted based on the assumption of normality, due to the use of inbred mice strains, as well as due to low numbers of independent biological replicates for in vivo experiments. For patient data, check for normality was performed using the Shapiro-Wilk test. Statistical differences between 2 groups were determined using an unpaired multiple *t* test, an unpaired Student *t* test, or a Mann-Whitney *U* test for nonparametric data. For the analysis between >2 groups, an ordinary 1-way ANOVA or 2-way ANOVA, followed by the recommended post hoc test, was performed. For comparing 2 groups during a time course at 1 time point (aortic diameter progression, platelet-leukocyte aggregates), an ordinary 2-way ANOVA with a Sidak multiple comparison post hoc test was used; when comparing 2 groups and multiple time points, a Tukey multiple comparisons post hoc test was performed. For correlation, the nonparametric Spearman correlation was used, due to low numbers of independent biological replicates in in vivo experiments. For evaluation of animal survival rates of in vivo experiments, a log-rank (Mantel-Cox) model was used. To analyze AAA incidence in mice, a Fisher exact test was conducted. $P<0.05$ was considered as statistically significant.

RESULTS

GP VI–Deficient Mice Are Protected Against Experimental AAA Progression

We induced experimental murine AAA in GP VI–deficient and control mice utilizing the PPE model to investigate

Downloaded from http://ahajournals.org by on June 17, 2025

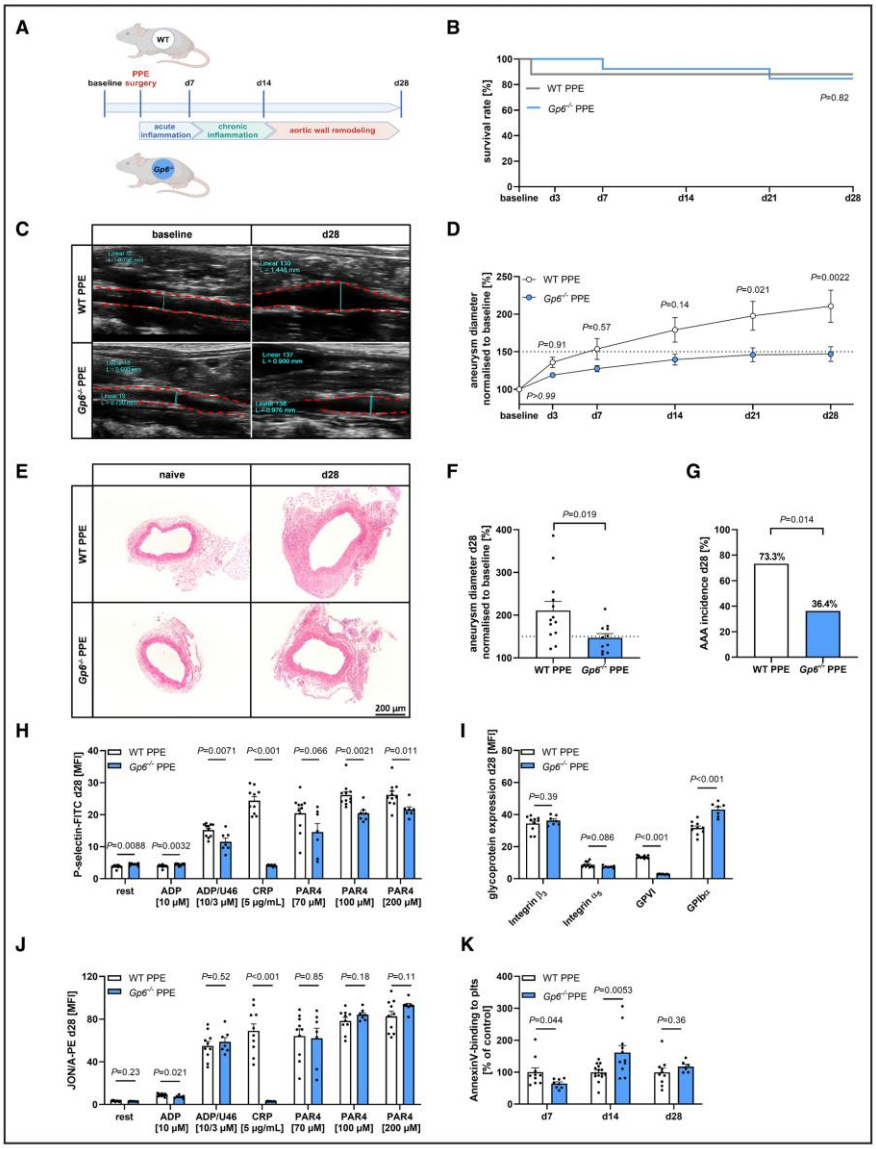


Figure 1. GP (platelet glycoprotein) VI–deficient mice are protected against experimental abdominal aortic aneurysm (AAA) progression.

A, Schematic overview of experimental procedure: C57BL/6J WT (wild-type) and GP VI–deficient (*Gp6*$^{-/-}$) PPE (porcine pancreatic elastase) mice underwent PPE surgery. Operated mice were euthanized and analyzed at day 7 (d7), day 14 (d14), and day 28 (d28) after surgery. **B**, Survival rate of PPE-operated WT (n=17) and *Gp6*$^{-/-}$ (n=16) mice over a time period of 28 days. **C**, Representative ultrasound images of WT (n=13) and *Gp6*$^{-/-}$ (n=11) PPE mice before (baseline) and 28 days after surgery. **D**, Aortic diameter progression of WT (n=13) and *Gp6*$^{-/-}$ (n=11) PPE mice over a time period of 28 days, analyzed via ultrasound measurements. Data were normalized to baseline. **E**, Representative overview images of H/E-stained aortic tissue from WT (n=6) and *Gp6*$^{-/-}$ (n=5) PPE mice at d28. Aortic tissue from naive WT (*Continued*)

Downloaded from http://ahajournals.org by on June 17, 2025

whether the genetic loss of GP VI affects different cellular processes associated with the initiation and progression of AAA (Figure 1A). While the overall survival rate was unaltered between the groups (Figure 1B), we detected significantly attenuated aortic diameter progression of AAA over a 28-day time period by ultrasound tracking (Figure 1C, 1D, and 1F; Figure S1A). Reduced aortic diameter in GP VI–deficient mice was confirmed by hematoxylin/eosin staining at the end of the observation period of 28 days (Figure 1E). Furthermore, AAA incidence was reduced, with only 36.4% of GP VI–deficient mice displaying an AAA. The AAA incidence is thereby defined as an inner aortic diameter of ≥150% at the end time point of 28 days, compared with baseline. In contrast, 73.3% of the WT PPE controls showed AAA development (Figure 1G). In regard to body weight, platelet count, and mean platelet volume at baseline and at different time points after elastase infusion, no differences were observed (Figure S1B through S1D).

Since platelet activation and procoagulant activity of platelets are crucial for AAA progression,[19] we analyzed platelet activation, GP expression, and procoagulant activity of platelets in GP VI–deficient and WT mice over a 28-day time period after elastase infusion. At day 28, reduced platelet activation in response to ADP and the thromboxane A2 analogue U46619, CRP, and PAR4 peptide that activates the thrombin receptor PAR4 has been observed as reflected by reduced P-selectin exposure while integrin $\alpha_{IIb}\beta_3$ activation was reduced following stimulation of platelets with ADP and CRP (Figure 1H and 1J). In addition to the absence of GP VI on the surface of GP VI ablated mice (control experiment), the analysis of GP exposure on the platelet surface showed elevated GP Ibα exposure at the membrane of GP VI–deficient platelets at day 28 compared with WT PPE controls (Figure 1I). Basal procoagulant activity of nonstimulated GP VI–deficient platelets, as shown by annexin V binding, was reduced at day 7 but not at later time points (Figure 1K).

The analysis of naive (unoperated) mice revealed no alterations in platelet activation and procoagulant activity (apart from GP VI–dependent platelet activation; Figures S2A and S3A). In addition, we analyzed platelet activation and procoagulant activity of platelets at early time points following elastase infusion. We detected reduced P-selectin exposure and reduced integrin $\alpha_{IIb}\beta_3$ activation only in response to CRP, whereas activation following stimulation of platelets with agonists that activate G-protein–coupled receptors was unaltered at day 7 after elastase infusion (Figure S2B). In contrast, at day 14, reduced P-selectin exposure of GP VI–deficient platelets was not only limited to stimulation with CRP but also evident, when platelets were stimulated with ADP and the thromboxane A2 analogue U46619. In contrast, integrin $\alpha_{IIb}\beta_3$ activation was reduced at day 14 following stimulation of platelets with ADP alone (Figure S2C). Furthermore, platelet activation with CRP and PAR4 peptide resulted in reduced procoagulant activity of GP VI–deficient platelets at day 7, whereas alterations at later time points were observed only after CRP stimulation (Figure S3A). In addition to the absence of GP VI on the surface of GP VI ablated mice (control experiment), the analysis of GP exposure on the platelet surface showed elevated GP Ibα exposure on the membrane of GP VI–deficient platelets at day 14 compared with WT PPE controls (Figure S3B). Thereby, VWF binding to platelets (via GP Ibα) was reduced in GP VI–deficient mice only after CRP stimulation, under naive conditions and at different time points after elastase infusion (Figure S3C). The externalization of integrin β_3 was reduced after CRP stimulation but not in resting or PAR4 activated GP VI–deficient platelets (Figure S3D). In contrast to elevated GP Ibα exposure at day 14 and day 28 on the membrane of GP VI–deficient platelets, GP exposure of platelets in naive mice was unaltered. However, GP VI was absent in GP VI–deficient mice at all time points and under naive conditions, confirming the genetic deletion of GP VI in these mice (Figure 1I; Figure S3B).

Genetic Deletion of Platelet GP VI Impairs Inflammation by Affecting Neutrophil Infiltration

To determine the effect of GP VI on platelet-mediated inflammation in experimental AAA (Figure 2A), we first determined the plasma levels of different proinflammatory cytokines at the early time point of 7 days post-PPE. The results revealed partly reduced acute-phase cytokines, such as IL-1β, IL-6, and IFN-γ, whereas levels of anti-inflammatory IL-10 showed a tendency of increase (Figure 2B). This might be due to the fact that thromboinflammatory interactions between GP VI activated platelets and leukocytes may foster inflammatory release

Figure 1 Continued. (n=6) and *Gp6*$^{-/-}$ (n=5) mice served as control. Scale bar, 200 µm. **F**, Aneurysm diameter of WT (n=13) and *Gp6*$^{-/-}$ (n=11) mice at d28 post-PPE surgery. Data were normalized to baseline. **G**, AAA incidence of WT (n=13) and *Gp6*$^{-/-}$ (n=11) PPE mice revealing an aortic diameter of ≥150% at 28 days post-surgery. **H** through **K**, Washed murine whole blood from PPE-operated WT and *Gp6*$^{-/-}$ mice was analyzed via flow cytometry. Platelet degranulation (P-selectin–fluorescein isothiocyanate [FITC]; **H**), platelet surface exposure of integrin β_3, integrin α_5, GP VI, and GP Ibα (**I**), and active integrin $\alpha_{IIb}\beta_3$ (JON/A-PE; WT [n=10–11] and *Gp6*$^{-/-}$ [n=7]; **J**). Platelets were stimulated with indicated agonists. **K**, Phosphatidylserine (PS) exposure of platelets (annexin V–Cy5 [Cyanine5]) at d7, d14, and d28 post-surgery (WT [n=10–15] and *Gp6*$^{-/-}$ [n=6–11]). Data are represented as mean±SEM. Statistical analysis was performed using (**B**) a log-rank (Mantel-Cox) test, (**D**) 2-way ANOVA with a Sidak multiple comparisons post hoc test, (**F**) an unpaired Student *t* test, (**G**) a Fisher exact test, and (**H**–**K**) an unpaired multiple *t* test. CRP indicates collagen-related peptide; d3, day 3; d21, day 21; H/E, hematoxylin-eosin; L, lumen; MFI, mean fluorescence intensity; PAR4, protease-activated receptor 4 activating peptide; Plts, platelets; rest, resting; and U46, thromboxane A_2 analogue U46619.

Downloaded from http://ahajournals.org by on June 17, 2025

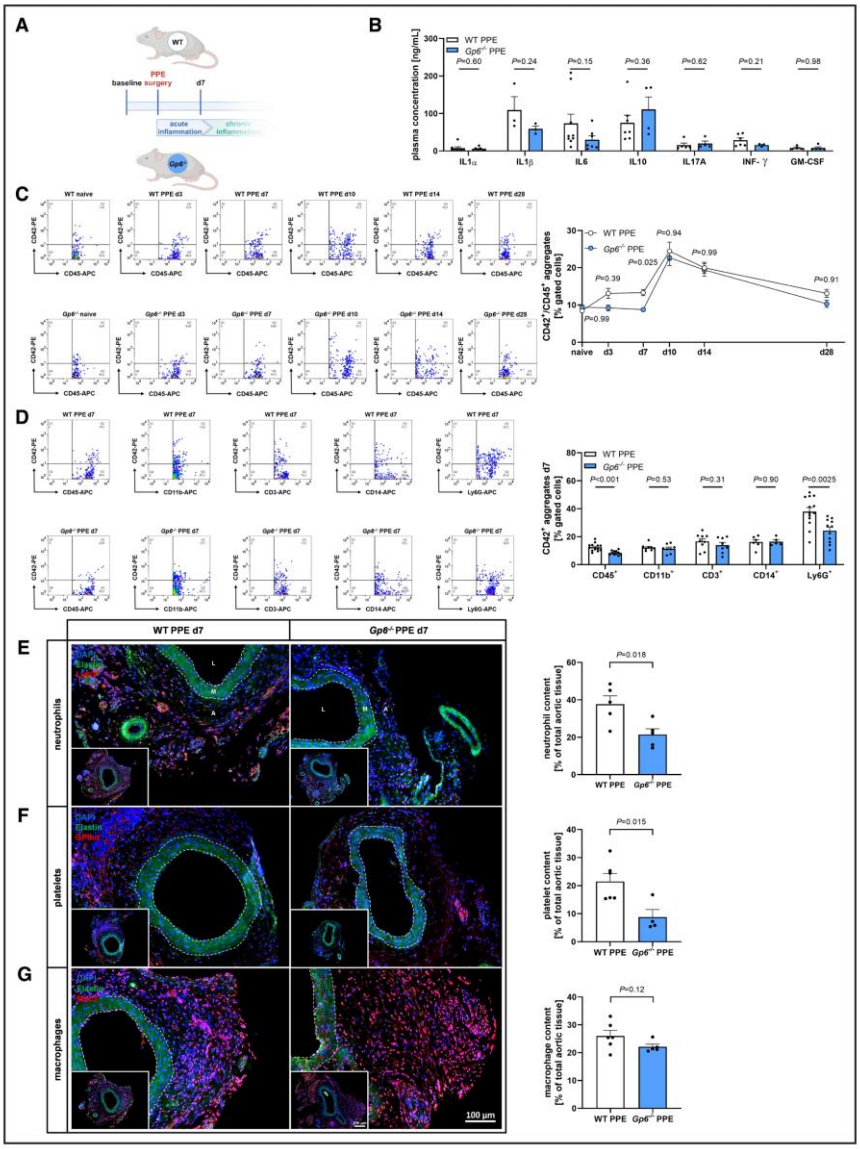


Figure 2. Genetic deletion of platelet GP (platelet glycoprotein) VI impairs inflammation by affecting neutrophil infiltration.
A, Schematic overview of experimental procedure: PPE (porcine pancreatic elastase)-operated C57BL/6J WT (wild-type) and GP VI–deficient (*Gp6*$^{-/-}$) PPE mice were euthanized and analyzed at day 7 (d7). **B**, Plasma concentration of inflammatory cytokines in WT (n=3–8) and *Gp6*$^{-/-}$ (n=3–7) PPE mice at d7 post-surgery, determined by multiplex analysis using a cytometric bead array. **C**, Platelet-leukocyte aggregate formation was analyzed in whole blood samples of PPE-operated WT (n=6–15) and *Gp6*$^{-/-}$ (n=6–12) mice at day 0 (naive), day 3 (d3), d7, day 14 (d14), and day 28 (d28) post-surgery. Aggregate formation was determined as double-positive events for CD42b (platelet maker, GP Ibα) and CD45 (leukocyte marker) via flow cytometry. **D**, Aggregate formation of platelets with different leukocyte subtypes in WT (n=6–14) and *Gp6*$^{-/-}$ (n=5–11) PPE mice at d7 post-surgery, analyzed via flow cytometry. **E** through **G**, Representative immunofluorescence (*Continued*)

Downloaded from http://ahajournals.org by on June 17, 2025

from the latter. However, genetic ablation of platelet GP VI may not entirely block the release of these mediators. Further, we analyzed platelet-leukocyte conjugates in the circulation of PPE mice at different time points. As shown in Figure 2C, we detected reduced platelet-leukocyte conjugates at the early time point of day 7 (Figure 2C and 2D). In contrast, no differences were observed in the extent of different platelet-leukocyte conjugates in naive mice or at 14 days after elastase infusion (Figure S4). A detailed analysis revealed that reduced conjugates of platelets with CD45-positive cells were preferentially of neutrophil origin, as indicated by the reduced number of platelet-neutrophil conjugates in GP VI–deficient mice compared with controls at day 7 (Figure 2D), which was not observed at other time points after elastase infusion or in naive mice (Figure S4C). The reduced number of platelet-neutrophil conjugates was accompanied by reduced migration of neutrophils and platelets into the aortic wall of GP VI–deficient AAA mice (Figure 2E and 2F). In contrast, the migration of macrophages into the aneurysm segment was unaltered (Figure 2G).

Platelet GP VI Affects NET Formation in Early Experimental AAA

The impact of GP VI in NET formation was analyzed at day 7 (Figure 3A). In line with the reduced presence of neutrophils in the aortic wall, the plasma level of neutrophil elastase—an indicator of neutrophil activation and degranulation—was reduced in GP VI–deficient mice (Figure 3B). The impact of neutrophil activation and degranulation on AAA-related aortic diameter progression in GP VI–deficient mice was reflected by a strong correlation (as indicated by the Spearman correlation coefficient) of the neutrophil elastase plasma content with the aneurysm diameter at day 7 post-elastase infusion (Figure 3C).

Moreover, we analyzed NET formation by citH3 in experimental AAA mice. Quantification of NET formation revealed a significant increase in plasma levels of citH3 in WT mice at day 7 compared with naive mice. In GP VI–deficient mice, we detected reduced citH3 in the aortic tissue and in the plasma at day 7 post-elastase infusion with a strong correlation of plasma citH3 and the aneurysm diameter (Figure 3D through 3G). Furthermore, we isolated neutrophils from WT and GP VI–deficient mice at day 7 post-elastase infusion and analyzed neutrophil adhesion. Neutrophils were stained for Ly6G and citH3 to quantify adherent Ly6G and citH3-postivie neutrophils. Thereby, a reduced number of adherent neutrophils isolated from GP VI–deficient mice compared with WT controls was detected (Figure 3H and 3I). Further, the number of citH3-positive neutrophils of GP VI–deficient mice was significantly reduced compared with control mice 7 days post-elastase infusion (Figure 3H and 3J). To analyze the impact of platelets on neutrophil adhesion, we isolated neutrophils from WT mice at day 7 post-elastase infusion and incubated the cells with platelets from either WT controls or GP VI–deficient mice for 3 hours. Quantification analysis revealed a reduced number of adherent neutrophils when these cells were incubated with CRP-activated platelets from GP VI–deficient mice (Figure 3K and 3L).

Early Effects of Platelet GP VI on Aortic Wall Remodeling by MMP Activation and OPN Deposition

Next, we investigated whether GP VI affects aortic wall remodeling in early AAA development (Figure 4A). First, we analyzed early events such as the presence of MMP2 and MMP9, OPN, or sGP VI in the plasma of control WT PPE mice. Thereby, increased MMP2 and OPN plasma level at day 7 and increased MMP9 plasma level at day 14 were detected. Whereas sGP VI was enhanced at days 7 and 14 post–PPE-induced AAA formation (Figure S5A through S5D). Next, we determined MMP and OPN plasma levels in GP VI–deficient mice at day 7 after elastase infusion. We detected significantly and strongly reduced plasma levels of MMP2 and OPN in the plasma of GP VI–deficient mice, whereas a trend of decrease was observed in MMP9 plasma levels (Figure 4B through 4D). Reduced OPN plasma levels were paralleled by reduced OPN expression in the aortic wall of GP VI–deficient mice compared with WT PPE controls (Figure 4E). Although the α-SMA content—as the marker for the phenotypic switch of fibroblasts to myofibroblasts—was unaltered at this early time point, the presence of active Casp3-positive cells—an indicator of apoptosis—was significantly reduced within the aortic media of GP VI–deficient mice (Figure 4F and 4G).

Modulation of MMP9 Release and Smooth Muscle Cell Content at 14 Days After AAA Induction

Aortic wall remodeling in AAA was also analyzed at day 14 after elastase infusion (Figure 5A). At this time point,

Figure 2 Continued. images and quantification of neutrophil, platelet, and macrophage infiltration into the aneurysm segment of PPE-operated WT (n=5–6) and *Gp6*$^{-/-}$ (n=4–5) mice at d7. The aortic tissue was specifically stained for (**E**) neutrophils (anti-Ly6G [lymphocyte antigen 6 complex locus G6D]/Cy3 [Cyanine3]; red), (**F**) platelets (anti-GP Ibα/Cy5 [Cyanine5]; red) or (**G**) macrophages (anti-Mac3/Cy5; red). Elastin autofluorescence (green) is shown (green) and nuclei were stained with DAPI (4′,6-diamidine-2′-phenylindole dihydrochloride; blue). Scale bars: 100 µm and 200 µm (overview). Data are represented as mean±SEM. Statistical analysis was performed using (**B** and **D**) an unpaired multiple *t* test, (**C**) a 2-way ANOVA with a Sidak multiple comparisons post hoc test, and (**E**–**G**) an unpaired Student *t* test. A indicates adventitia; APC, allophycocyanin; GM-CSF, granulocyte-macrophage colony-stimulating factor; IL, interleukin; INF, interferon; L, lumen; and M, media.

Downloaded from http://ahajournals.org by on June 17, 2025

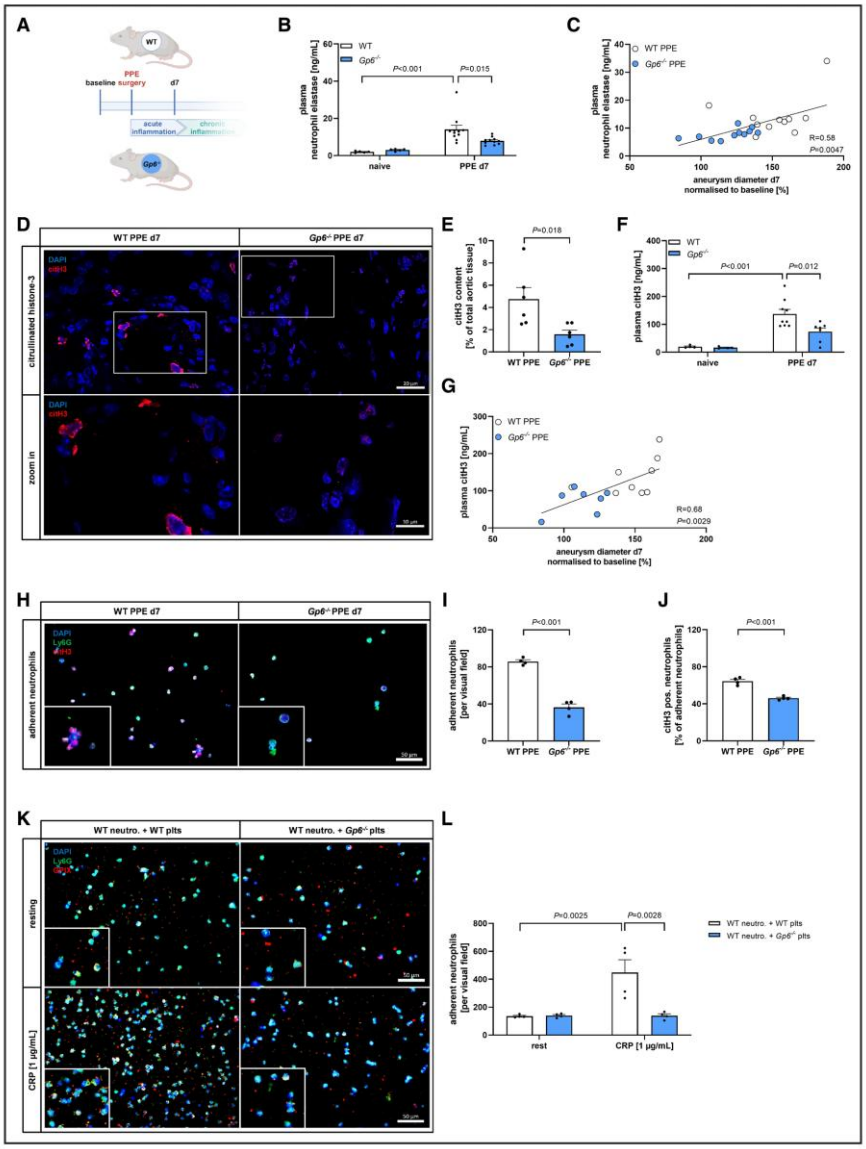


Figure 3. Platelet GP (platelet glycoprotein) VI affects neutrophil extracellular trap (NET) formation in early experimental abdominal aortic aneurysm (AAA).

A, Schematic overview of experimental procedure: PPE (porcine pancreatic elastase)-operated C57BL/6J WT (wild-type) and GP VI–deficient (*Gp6*$^{-/-}$) PPE mice were euthanized and analyzed at day 7 (d7). **B**, Neutrophil elastase plasma concentration at d7 post-surgery in WT (n=11) and *Gp6*$^{-/-}$ (n=11) PPE mice, estimated by ELISA. Naive WT (n=5) and *Gp6*$^{-/-}$ (n=5) mice served as controls. **C**, Spearman correlation between neutrophil elastase plasma concentration and the aneurysm diameter at d7 post-PPE (WT [n=11] and *Gp6*$^{-/-}$ [n=11]). **D** and **E**, Representative immunofluorescence images and quantification of NET formation within the aneurysm segment of PPE-operated WT (n=6) and *Gp6*$^{-/-}$ (n=5) mice at d7. Aortic tissue was specifically stained for citrullinated histone H3 (citH3; anti-citH3/Cy3 [Cyanine3]; red). (*Continued*)

Downloaded from http://ahajournals.org by on June 17, 2025

no differences in MMP2 plasma levels were detected. However, MMP9 and OPN plasma levels were significantly reduced in GP VI–deficient mice (Figure 5B through 5D). Reduced plasma levels of OPN were again paralleled by decreased OPN expression in the aortic wall of GP VI–deficient mice (Figure 5E). In addition, we detected a significantly upregulated percentage of α-SMA–positive cells in the aortic media but comparable Casp3-positive cells in the aortic wall of GP VI–deficient mice (Figure 5F and 5G).

Platelet GP VI Significantly Contributes to Aortic Wall Remodeling in Experimental AAA

Differences in MMP plasma levels, OPN content, and α-SMA–positive cells in GP VI–deficient PPE mice resulted in improved aortic wall remodeling 28 days after elastase infusion, as indicated by increased intima/media thickness, reduced elastin fragmentation, and elevated elastin content (Figure 6A through 6C). Improved aortic wall remodeling in GP VI–deficient mice was reflected by a strong correlation (as indicated by the Spearman correlation coefficient) of intima/media thickness, as well as elastin fragmentation to aneurysm diameter progression at day 28 post-elastase infusion (Figure 6D and 6E). In contrast to the elastin content, we did not observe significant alterations in the average collagen content in GP VI–deficient PPE mice compared with WT PPE controls (Figure 6F). However, a detailed analysis of collagen within the aortic wall revealed an altered collagen composition in GP VI–deficient mice, based on a significantly elevated Col I and reduced Col III (collagen III) content in these mice (Figure 6G), while the Col IV content within the aneurysm segment was unaltered between the genotypes (Figure S6). In control experiments, we provided evidence that no differences were observed in the aortic intima/media thickness, elastin fragmentation, or collagen composition in naive mice from both groups (Figure S7).

GP VI–Deficient Mice Are Protected Against ePPE-Induced AAA Formation

To confirm the importance of GP VI in AAA formation and progression, we utilized another experimental mouse model of AAA, namely the ePPE model, reflecting a promising tool with translational value (Figure 7A).[12] The survival rate was not different between WT and GP VI–deficient mice, but we detected significantly reduced aneurysm diameter expansion at intermediate and late time points after elastase application (Figure 7B through 7E; Figure S8A). In contrast to PPE-operated mice, the determination of platelet activation at the end of the observation period of 28 days revealed only a significant reduction after CRP stimulation (Figure 7F and 7H) but no differences in GP exposure while GP VI was absent in these mice as expected (Figure 7G). Procoagulant activity was reduced in resting and CRP-activated platelets after 28 days post-elastase application (Figure 7I). Furthermore, integrin-β_3 externalization and VWF binding was reduced only in response to CRP activation at day 28 post-elastase application (Figure S8B and S8C). Further, no alterations between WT and GP VI–deficient mice have been detected with regard to platelet-leukocyte conjugates, body weight, platelet counts, and mean platelet volume at day 28 of ePPE induction (Figure S8D through S8G).

Reduced GP VI exposure at the membrane of platelets but elevated sGP VI in the plasma of ePPE mice compared with sham-operated controls was detected suggesting that GP VI shedding is altered in ePPE mice (Figure 8A and 8B). Moreover, a significant correlation between plasma sGP VI and the aneurysm diameter was evident as shown in Figure 8C. However, no differences in surface coverage or thrombus volume between sham- and ePPE-operated mice were observed when whole blood was perfused over a collagen-coated surface under a shear rate of 1700 s^{-1} using the flow chamber system (Figure 8D). Furthermore, the fibrin/fibrinogen content of 3-dimensional thrombi and the amount of procoagulant platelets in these thrombi were not altered between sham- and ePPE-operated mice (Figure 8E).

GP VI Blocking Attenuates Aortic Diameter Progression in ePPE-Induced AAA Progression

We next performed the first translational attempt of therapeutic intervention and injected a GP VI–blocking antibody (Fab Y020347, α-GP VI ab ePPE) into

Figure 3 Continued. Nuclei were stained with DAPI (4′,6-diamidine-2′-phenylindole dihydrochloride; blue). Scale bars, 20 and 10 µm (zoom in). **F**, CitH3 plasma concentration at d7 post-surgery in WT (n=9) and *Gp6*$^{-/-}$ (n=7) PPE mice, estimated by ELISA. Naive WT (n=4) and *Gp6*$^{-/-}$ (n=4) mice served as controls. **G**, Spearman correlation between citH3 plasma concentration and the aneurysm diameter at d7 post-PPE (WT [n=9] and *Gp6*$^{-/-}$ [n=7]). **H**, Representative immunofluorescence images of isolated neutrophils of WT (n=4) and *Gp6*$^{-/-}$ (n=4) PPE mice at d7 post-surgery. Adherent neutrophils were specifically stained for Ly6G (lymphocyte antigen 6 complex locus G6D; anti-Ly6G/488; green) and citH3 (anti-citH3/Cy3; red). Nuclei were stained with DAPI (blue). Scale bars, 50 µm. **I** and **J**, Quantification of (**I**) adherent Ly6G-positive and (**J**) citH3-positive neutrophils. **K**, Isolated neutrophils of WT (n=4) PPE mice at d7 were incubated either with isolated WT (n=4) or *Gp6*$^{-/-}$ (n=4) platelets for 3 hours. Adherent cells were specifically stained for neutrophils (anti-Ly6G/488; green) and platelets (anti-GP IX/Cy3; red). Nuclei were stained with DAPI (blue). Scale bars, 50 µm. **L**, Quantification of adherent Ly6G-positive neutrophils after 3 hours of incubation either with WT (n=4) or *Gp6*$^{-/-}$ (n=4) platelets. Data are represented as mean±SEM. Statistical analysis was performed using (**B**, **F**, and **L**) a 2-way ANOVA with a Tukey multiple comparisons post hoc test and (**E**, **I**, and **J**) an unpaired Student *t* test. CRP indicates collagen-related peptide; neutro., neutrophil; Plts, platelets; pos., positive; and rest, resting.

Downloaded from http://ahajournals.org by on June 17, 2025

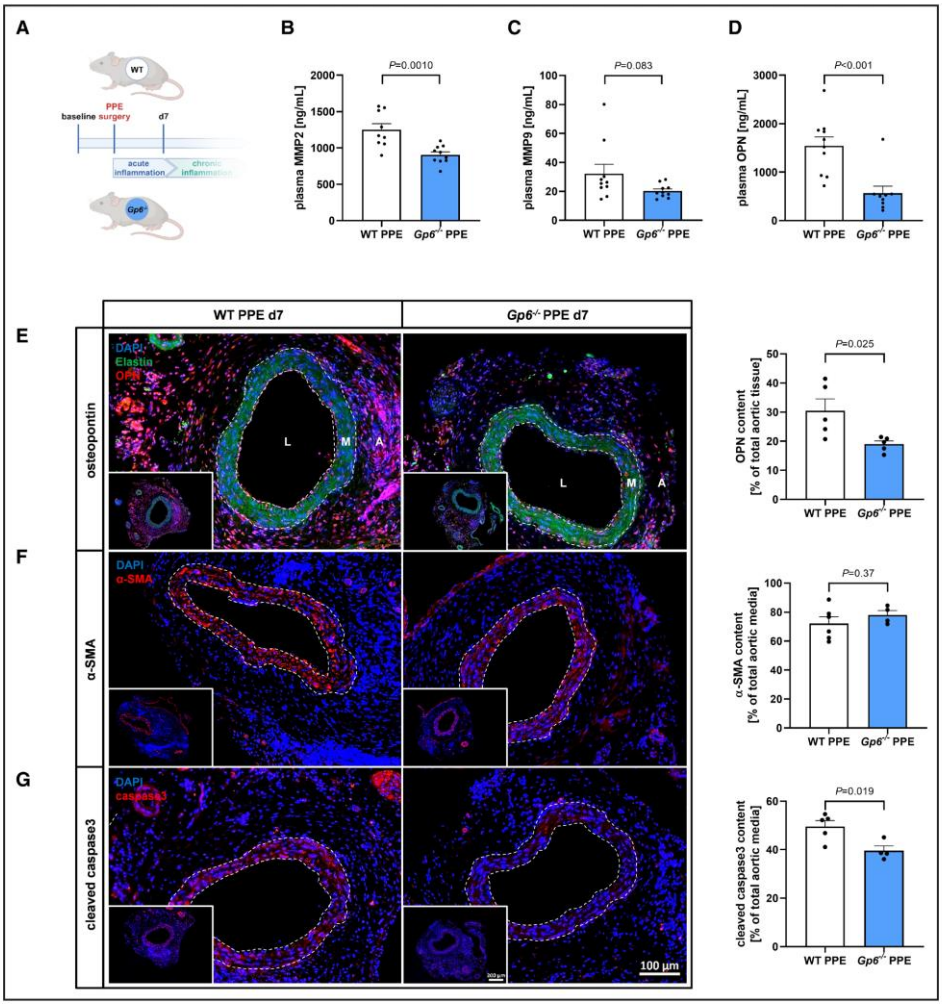


Figure 4. Early interference of GP (platelet glycoprotein) VI on aortic wall remodeling by MMP (matrix metalloproteinase) activation and OPN (osteopontin) deposition.

A, Schematic overview of experimental procedure: PPE (porcine pancreatic elastase)-operated C57BL/6J WT (wild-type) and GP VI–deficient (*Gp6*$^{-/-}$) PPE mice were euthanized and analyzed at day 7 (d7). **B** through **D**, Plasma concentration of (**B**) MMP2, (**C**) MMP9, and (**D**) OPN in PPE-operated WT (n=9–11) and *Gp6*$^{-/-}$ (n=9–10) mice at d7 post-surgery, determined via ELISA. **E** through **G**, Representative immunofluorescence images and quantification of OPN, α-SMA (α-smooth muscle actin), and caspase 3 within the aneurysm segment of WT (n=5–6) and *Gp6*$^{-/-}$ (n=4–5) PPE mice at d7. The aortic tissue was specifically stained for (**E**) OPN (anti-OPN/Cy3 [Cyanine3]; red), (**F**) α-SMA (anti-α-SMA/Cy3; red), or (**G**) active caspase 3 (anti-cleaved caspase 3/Cy3; red). Elastin autofluorescence (green) is shown, and nuclei were stained with DAPI (4′,6-diamidine-2′-phenylindole dihydrochloride; blue). Scale bars, 100 and 200 µm (overview). Data are represented as mean±SEM. Statistical analysis was performed using (**B**–**G**) an unpaired Student *t* test.

ePPE-operated mice, starting 12 hours before surgery (Figure 9A). Again, no differences were detected with regard to survival rates in both groups (Figure 9B). Aneurysm diameter expansion was significantly reduced at intermediate and late time points post-elastase application (Figure 9C through 9E; Figure S9A). The

Downloaded from http://ahajournals.org by on June 17, 2025

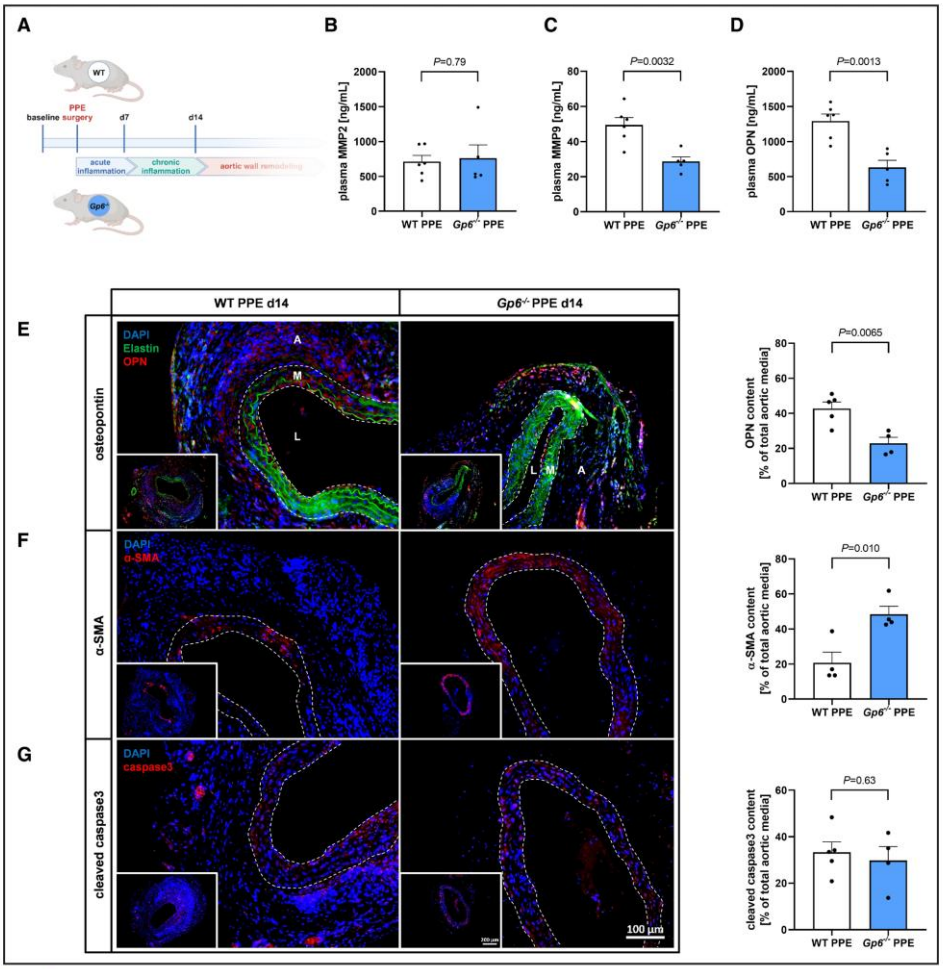


Figure 5. Modulation of MMP (matrix metalloproteinase) 9 release and smooth muscle cell content at day 14 (d14) after abdominal aortic aneurysm (AAA) induction.

A, Schematic overview of experimental procedure: PPE (porcine pancreatic elastase)-operated C57BL/6J WT (wild-type) and GP (platelet glycoprotein) VI–deficient (*Gp6*$^{-/-}$) PPE mice were euthanized and analyzed at d14. **B** through **D**, Plasma concentration of (**B**) MMP2, (**C**) MMP9, and (**D**) OPN (osteopontin) in PPE-operated WT (n=6) and *Gp6*$^{-/-}$ (n=5) mice at d14 post-surgery, analyzed via ELISA. **E** through **G**, Representative immunofluorescence images and quantification of OPN, α-SMA, and caspase 3 within the aneurysm segment of WT (n=4–5) and *Gp6*$^{-/-}$ (n=4) PPE mice at d14. The aortic tissue was specifically stained for (**E**) OPN (anti-OPN/Cy3 [Cyanine3]; red), (**F**) α-SMA (α-smooth muscle actin; anti-α-SMA/Cy3; red), or (**G**) active caspase 3 (anti-cleaved caspase 3/Cy3; red). Elastin autofluorescence (green) is shown, and nuclei were stained with DAPI (4′,6-diamidine-2′-phenylindole dihydrochloride; blue). Scale bars, 100 and 200 µm (overview). Data are represented as mean±SEM. Statistical analysis was performed using (**B**–**G**) an unpaired Student *t* test. d7 indicates day 7.

body weight of both groups was unaltered following antibody injection over a time course of 28 days (Figure S9B). The analysis of platelet activation at day 28 post-elastase application revealed no response to CRP stimulation, neither with regard to P-selectin exposure (Figure 9F) nor to integrin activation (Figure 9H), confirming complete inhibition of GP VI activation in antibody-treated mice. However, antibody treatment

Downloaded from http://ahajournals.org by on June 17, 2025

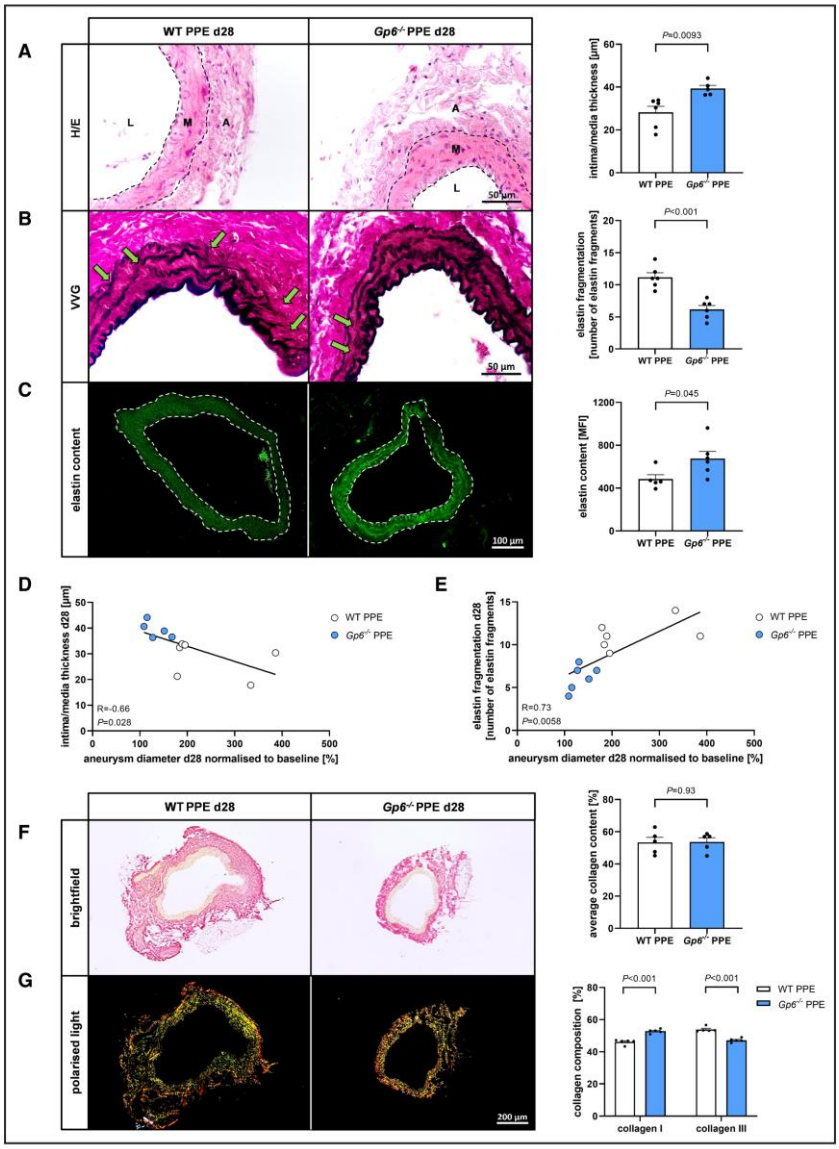


Figure 6. Platelet GP (platelet glycoprotein) VI significantly contributes to aortic wall remodeling in abdominal aortic aneurysm (AAA).

A through **C**, Representative images and quantification of the aortic tissue from PPE (porcine pancreatic elastase)-operated WT (wild-type) and *Gp6*$^{-/-}$ mice at day 28 (d28) post-surgery. **A**, The intima/media thickness was analyzed using hematoxylin/eosin (H/E) staining of WT (n=6) and *Gp6*$^{-/-}$ (n=5) PPE mice. Scale bar, 50 µm. **B**, Quantification of elastin fragmentation within the aortic media of WT (n=6) and *Gp6*$^{-/-}$ (n=6) PPE mice via Verhoeff-van Gieson (VVG) staining. Scale bar, 50 µm. **C**, Elastin content of WT (n=4) and *Gp6*$^{-/-}$ (n=6) PPE mice was determined by analyzing the elastin autofluorescence within the aortic media. Scale bar, 100 µm. **D** and **E**, Spearman correlation between (**D**) intima/media thickness, (**E**) elastin fragmentation, and the aneurysm diameter at d28 post-PPE. **F** and **G**, Collagen content and (*Continued*)

Downloaded from http://ahajournals.org by on June 17, 2025

does not affect GP VI exposure at the platelet surface. Thus, no differences in the exposure of different GPs at the platelet membrane were detected (Figure 8G). Moreover, the externalization of integrin-β_3 was reduced after stimulation of platelets with CRP and with the PAR4 peptide while VWF binding to platelets was only reduced in response to CRP (Figure S9C and S9D). Annexin V binding reflecting procoagulant activity of platelets was significantly reduced in antibody-treated mice at the resting state and following CRP stimulation of platelets (Figure 9I). However, no differences were observed between control and antibody-treated mice with regard to different platelet-leukocyte conjugates, platelet counts, and mean platelet volume at day 28 post-elastase application (Figure S9E through S9G).

Elevated Plasma Levels of sGP VI and Enhanced Deposition of Fibrin in the ILT and in the Plasma of Patients With AAA

To study the relevance of platelet GP VI in AAA pathology among patients, we first determined the levels of sGP VI in the plasma and surface expression of GP VI on the platelet surface of patients with AAA. We detected increased sGP VI plasma levels, while the abundance of GP VI on the platelet surface was not significantly altered compared with healthy controls (Figure 10A and 10B; Figure S12A). The plasma level of fibrin, a newly identified GP VI ligand, important for GP VI–mediated thrombus stabilization[33] was elevated in patients with AAA compared with healthy controls (Figure 10C). Moreover, the platelet content within the ILT of patients with AAA was reduced compared with arterial thrombi of different origin, isolated from patients who underwent thrombectomy (Figure 10D; Figure S13B). Increased fibrin plasma levels were paralleled by elevated fibrin deposition in the ILT of patients with AAA compared with arterial thrombi of patients with thrombectomy (Figure 10E). Furthermore, thrombus formation using peripheral blood samples in the ex vivo flow chamber system revealed no differences between patients with AAA and controls in thrombus formation or thrombus volume on a collagen matrix under dynamic arterial flow conditions (Figure 10F). The analysis of these 3-dimensional thrombi with regard to the fibrin/fibrinogen content showed no differences between AAA patient and control samples (Figure 10G). However, we detected elevated PS exposure of platelets that have been incorporated into the thrombi confirming recently published results showing enhanced procoagulant activity of circulating platelets from patients with AAA (Figure 10G). Following recently published data showing OPN accumulation in the ILT and the aortic wall,[19] we anaylzed whether OPN is able to shed GP VI from the platelet surface. In contrast to the snake venom convulxin that activates and sheds GP VI from the platelet surface, we here provide the first evidence that soluble OPN is not able to shed GP VI from the surface of human platelets (Figure S14). Clinical parameters of the here analyzed AAA and thrombectomy patient cohorts are summarized in Table S1.

DISCUSSION

In this study, we found that genetic deletion of the major platelet collagen receptor GP VI protects mice against aortic diameter expansion in experimental AAA. These protective effects are attributed to reduced inflammation due to decreased platelet-neutrophil aggregate formation, neutrophil activation, and infiltration into the aortic wall. In addition, GP VI promotes aortic wall remodeling, as indicated by reduced MMP2/9 and OPN plasma levels but elevated α-SMA content within the aortic tissue, accompanied by reduced cell apoptosis. Consequently, enhanced intima/media thickness and elevated elastin content were observed in GP VI–deficient PPE mice, leading to significantly reduced aortic diameter expansion and reduced aneurysm incidence. Importantly, patients with AAA showed elevated plasma levels of sGP VI and fibrin, accompanied by massive fibrin accumulation within the ILT, suggesting that platelet GP VI might be a crucial mediator in thromboinflammatory processes. Moreover, sGP VI may serve as a potential biomarker for AAA development, as in other cardiovascular atherothrombotic diseases.

AAA is an atherosclerosis-related disease with multifactorial causes. Characteristic hallmarks are chronic inflammation and ECM degradation within the abdominal aortic wall, often accompanied by the formation of an ILT in patients with AAA. Abnormal platelet activation has been described for many atherosclerotic and cardiovascular diseases leading to an increased risk of thromboembolic events.[34] In AAA, elevated platelet activation has been described as a major pathological feature in experimental mice (PPE mouse model) and in patients with AAA. Specifically, platelet hyperresponsiveness/hyperreactivity has been described in both mice and patients with AAA,[19] whereby platelet GP VI collagen/fibrinogen/fibrin interactions may trigger AAA initiation and progression. In

Figure 6 Continued. composition in the aortic tissue of PPE-operated WT (n=5) and *Gp6*$^{-/-}$ (n=5) mice at d28. **F**, Representative bright-field images and quantification of the average collagen content using picrosirius red staining. **G**, Representative images and quantification of the aortic collagen composition (collagen type I, red-yellow, and collagen type III, green) using polarized light. Aortic tissue was stained using picrosirius red. Scale bar, 200 µm. Data are represented as mean±SEM. Statistical analysis was performed using (**A**–**C** and **F**) an unpaired Student *t* test and (**G**) a 2-way ANOVA with a Sidak multiple comparisons post hoc test. A indicates adventitia; L, lumen; M, media; and MFI, mean fluorescence intensity.

Downloaded from http://ahajournals.org by on June 17, 2025

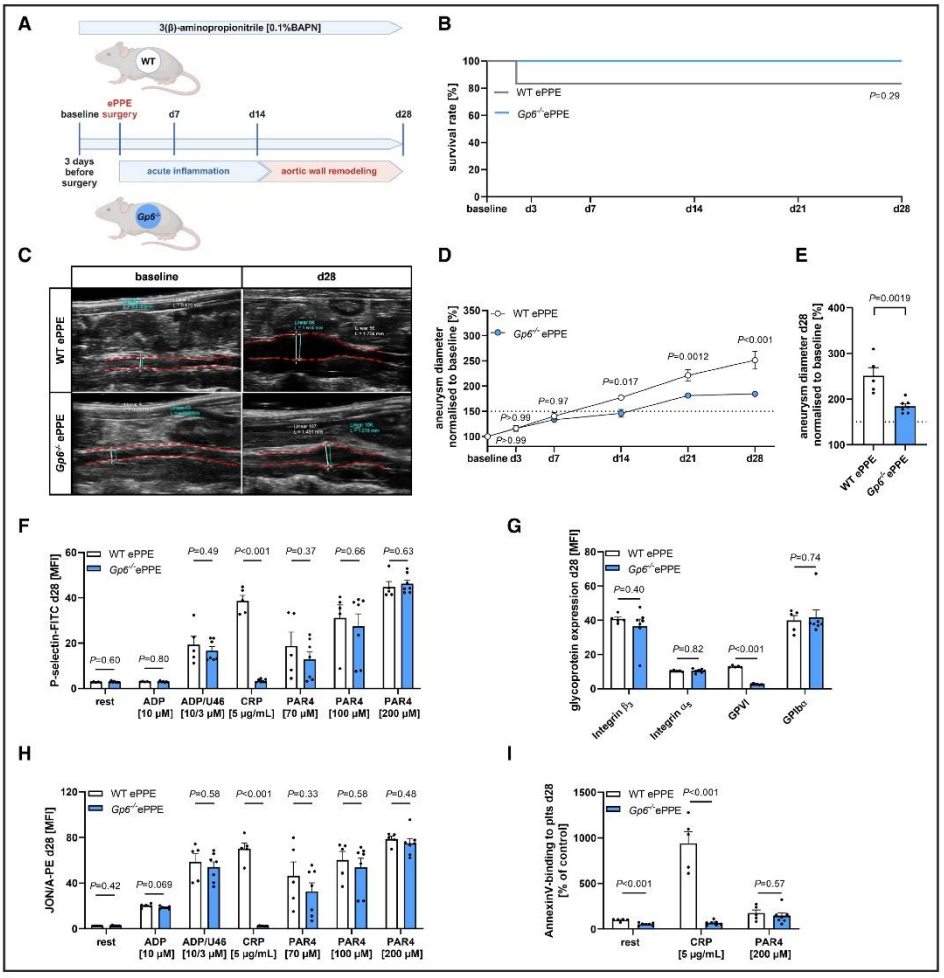


Figure 7. GP (platelet glycoprotein) VI–deficient mice are protected against external porcine pancreatic elastase (ePPE)–induced experimental abdominal aortic aneurysm (AAA) formation.

A, Schematic overview of experimental procedure: C57BL/6J WT (wild-type) and GP VI–deficient (*Gp6*$^{-/-}$) ePPE mice underwent ePPE surgery. Operated mice were analyzed at day 28 (d28) post-surgery. **B**, Survival rate of ePPE-operated WT (n=6) and *Gp6*$^{-/-}$ (n=7) mice over a time period of 28 days. **C**, Representative ultrasound images of WT (n=5) and *Gp6*$^{-/-}$ (n=7) ePPE mice before (baseline) and 28 days after surgery. **D**, Aortic diameter progression of WT (n=5) and *Gp6*$^{-/-}$ (n=7) ePPE mice over a time period of 28 days, analyzed via ultrasound measurements. Data were normalized to baseline. **E**, Aneurysm diameter of WT (n=5) and *Gp6*$^{-/-}$ (n=7) mice at d28 post-ePPE surgery. Data were normalized to baseline. **F** through **I**, Washed murine whole blood from ePPE-operated WT and *Gp6*$^{-/-}$ mice was analyzed via flow cytometry. Platelet degranulation (P-selectin–fluorescein isothiocyanate [FITC]; **F**); platelet surface exposure of integrin β_3, integrin α_6, GP VI, and GP Ibα (**G**), active integrin $\alpha_{IIb}\beta_3$ (JON/A-PE) and phosphatidylserine (PS) exposure (annexin V–Cy5 [Cyanine5]; WT [n=5] and *Gp6*$^{-/-}$ [n=7]; **H**). Platelets were stimulated with indicated agonists. Data are represented as mean±SEM. Statistical analysis was performed using (**B**) a log-rank (Mantel-Cox) test, (**D**) a 2-way ANOVA with a Sidak multiple comparisons post hoc test, (**E**) an unpaired Student *t* test, and (**F–I**) an unpaired multiple *t* test. BAPN indicates β-aminopropionitrile; CRP, collagen-related peptide; d3, day 3; d7, day 7; d14, day 14; d21, day 21; L, lumen; MFI, mean fluorescence intensity; PAR4, protease-activated receptor 4 activating peptide; Plts, platelets; rest, resting; and U46, thromboxane A_2 analogue U46619.

Downloaded from http://ahajournals.org by on June 17, 2025

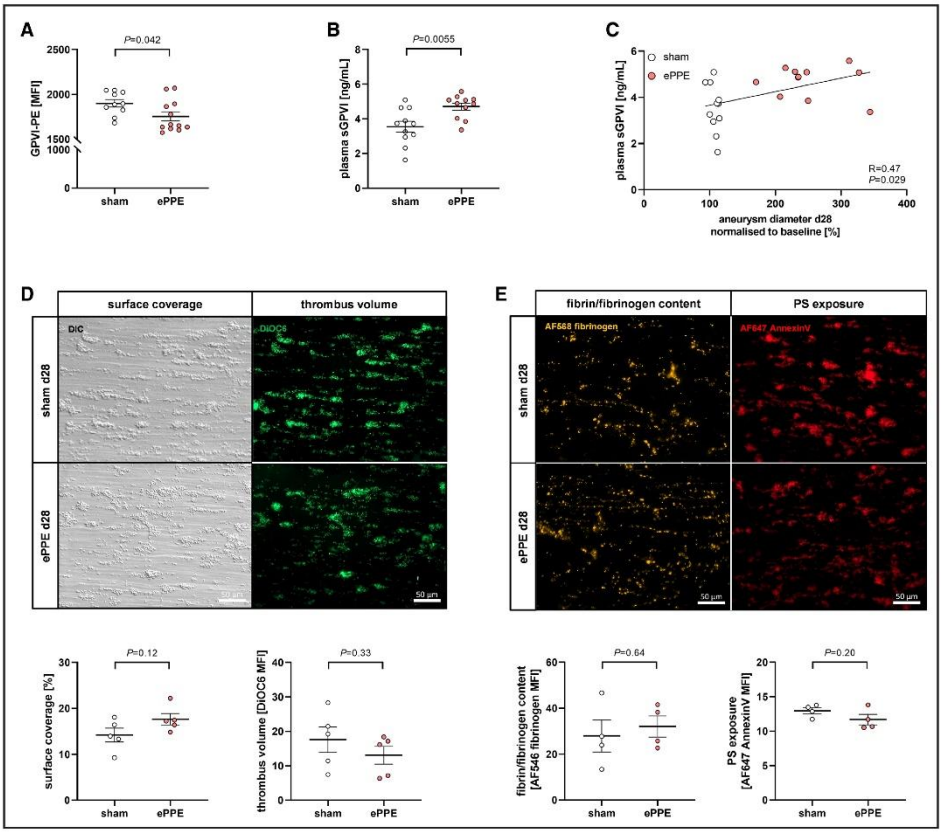


Figure 8. External porcine pancreatic elastase (ePPE)–operated mice reveal enhanced plasma levels of soluble GP (platelet glycoprotein) VI and reduced GP VI surface exposition.
A, GP VI surface exposition on platelets of sham (n=10) and ePPE (n=12) mice. **B**, Plasma concentration of soluble GP VI (sGP VI) of sham-operated (n=11) and ePPE-operated (n=11) mice at day 28 (d28) post-surgery. **C**, Spearman correlation between sGP VI plasma concentration and aneurysm diameter at d28 post-ePPE surgery. **D** and **E**, Representative fluorescence images and quantification of ex vivo flow chamber experiments. Murine whole blood samples of sham (n=4–5) and ePPE (n=4–5) mice were perfused over a collagen matrix (200 µg/mL) under an arterial shear rate of 1700 s^{-1}. **D**, Analysis of surface coverage and thrombus volume of murine thrombi. Platelets were prelabeled with 3,3′-dihexyloxacarbocyanine iodide (DiOC6; green). Scale bar, 50 µm. **E**, Fibrin/fibrinogen content and phosphatidylserine (PS) exposure of murine thrombi after flow. Murine whole blood samples were preincubated with 8.5 µg/mL AF546 fibrinogen (orange). For PS exposure analysis, murine thrombi were stained with AF647 annexin V after flow (red). Scale bar, 50 µm. Data are represented as mean±SEM. Statistical analysis was performed using (**A**, **B**, **D**, and **E**) an unpaired Student *t* test. DIC indicates differential interference contrast; and MFI, mean fluorescence intensity.

addition, another study provided evidence for enhanced activation after stimulation of platelets with thrombin and thromboxane.[16] In the present study, we detected reduced platelet activation and procoagulant activity in response to the PAR4 peptide (PS and P-selectin exposure), which may be responsible—at least in part—for the reduced aortic diameter expansion in GP VI–deficient mice. Notably, reduced procoagulant activity was detected in GP VI–deficient platelets at all time points during the 28-day observation period in response to GP VI stimulation, as well as in resting and PAR4-stimulated platelets at early time points (day 7). It has already been shown that GP VI activation is able to directly support thrombin-induced platelet activation. Remarkably, this process is independent of Syk and Src kinases.[35] GP VI indirectly enhances thrombin-mediated platelet activation by triggering PS exposure to provide a procoagulant surface at the platelet membrane, leading to thrombin generation.[36,37]

Downloaded from http://ahajournals.org by on June 17, 2025

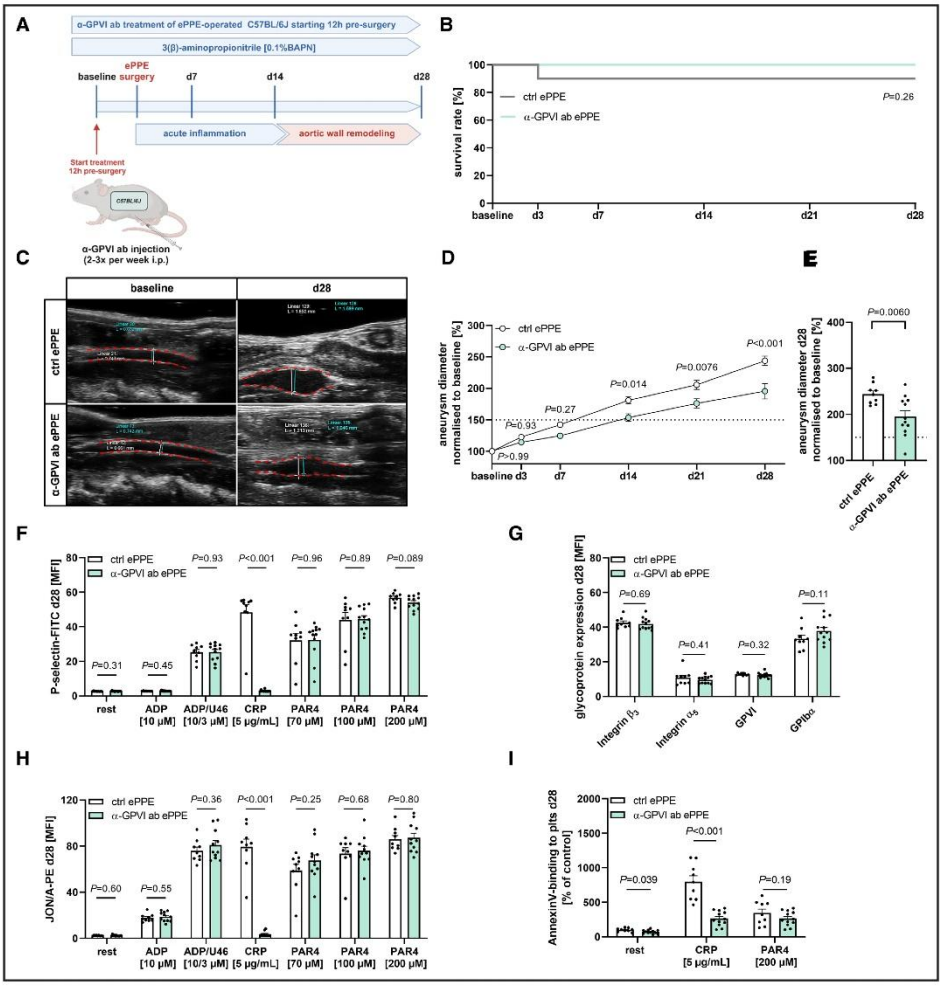


Figure 9. GP (platelet glycoprotein) VI blocking attenuates aortic diameter progression in external porcine pancreatic elastase (ePPE)–induced abdominal aortic aneurysm (AAA) progression.

A, Schematic overview of experimental procedure: C57BL/6J mice underwent ePPE surgery and received a GP VI–blocking antibody (10 mg/kg body weight, Fab Y020347, α-GP VI ab ePPE) or a respective vehicle control (ctrl ePPE) over a time course of 28 days. The GP VI–blocking antibody was injected every 2 to 3 days, starting 12 hours before surgery. Operated mice were analyzed at day 28 (d28) post-surgery. **B**, Survival rate of ePPE-operated ctrl (n=10) and α-GP VI antibody–treated (n=12) mice over a time period of 28 days. **C**, Representative ultrasound images of ctrl (n=9) and α-GP VI antibody–treated (n=12) ePPE mice before (baseline) and 28 days after surgery. **D**, Aortic diameter progression of ctrl (n=9) and α-GP VI antibody–treated (n=12) ePPE mice over a time period of 28 days, analyzed via ultrasound measurements. Data were normalized to baseline. **E**, Aneurysm diameter of ctrl (n=9) and α-GP VI antibody–treated (n=12) mice at d28 post-ePPE surgery. Data were normalized to baseline. **F** through **I**, Washed murine whole blood from ePPE-operated ctrl and α-GP VI antibody–treated mice was analyzed via flow cytometry. Platelet degranulation (P-selectin–FITC; **F**); platelet surface exposure of integrin β_3, integrin α_5, GP VI, and GP Ibα (**G**); active integrin $\alpha_{IIb}\beta_3$ (JON/A-PE) and phosphatidylserine (PS) exposure (annexin V–Cy5 [Cyanine5]; ctrl [n=9] and α-GP VI ab [n=12]; **H**). Platelets were stimulated with indicated agonists. Data are represented as mean±SEM. Statistical analysis was performed using (**B**) a log-rank (Mantel-Cox) test, (**D**) 2-way ANOVA with a Sidak multiple comparisons post hoc test, (**E**) an unpaired Student *t* test, and (**F–I**) an unpaired multiple *t* test. ab indicates antibody; BAPN, β-aminopropionitrile; CRP, collagen-related peptide; ctrl, control; i.p., intraperitoneal; MFI, mean fluorescence intensity; PAR4, protease-activated receptor 4 activating peptide; Plts, platelets; rest, resting; and U46, thromboxane A_2 analogue U46619.

Downloaded from http://ahajournals.org by on June 17, 2025

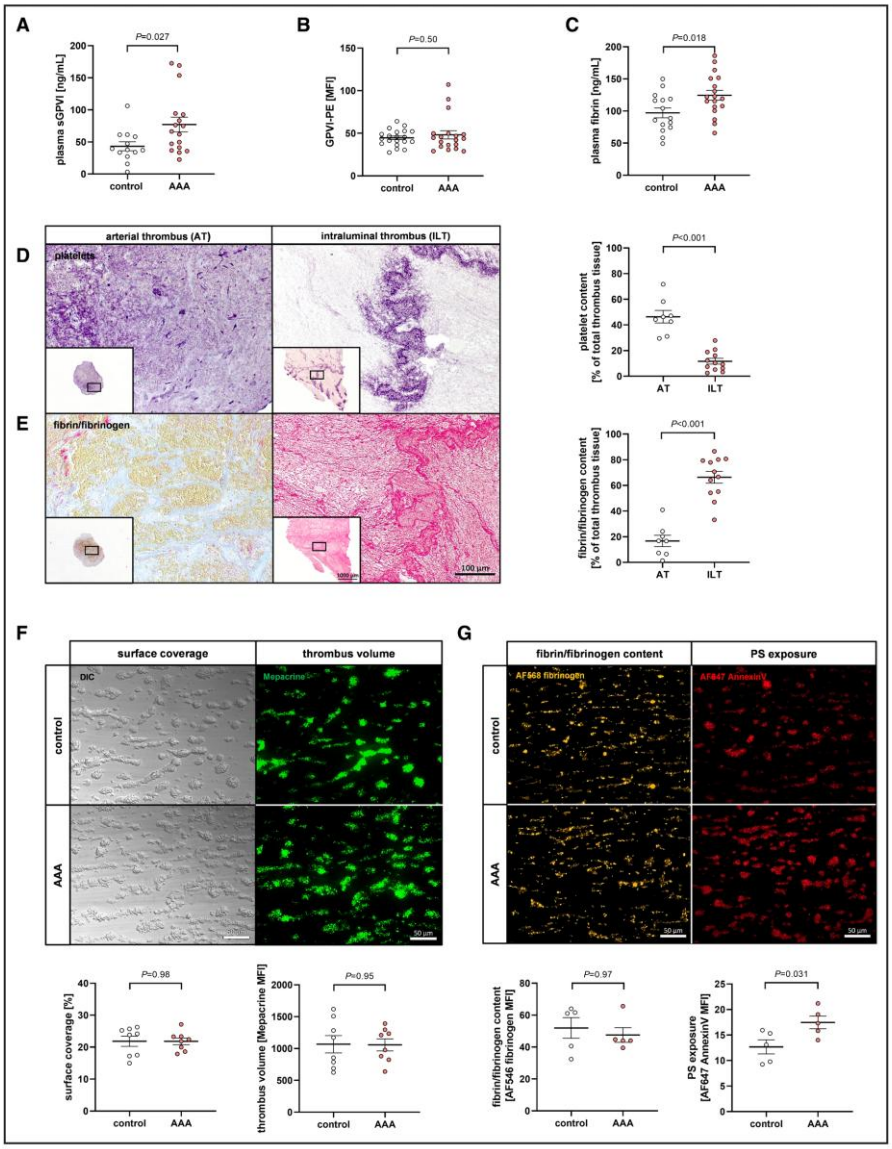


Figure 10. Elevated plasma levels of soluble GP (platelet glycoprotein) VI and enhanced deposition of fibrin in the intraluminal thrombus (ILT) and in the plasma of patients with abdominal aortic aneurysm (AAA).

A, Plasma concentration of soluble GP VI (sGP VI) in samples of AAA (n=18), analyzed via ELISA. Samples of healthy volunteers served as controls (n=13). **B**, Platelet surface GP VI exposure of patients with AAA (n=19), determined in whole blood samples by flow cytometry. Healthy volunteers served as controls (n=20). **C**, Fibrin plasma concentration in samples of AAA (n=18), analyzed via ELISA. Samples of healthy volunteers served as controls (n=15). **D** and **E**, Representative images and quantification of ILT tissue samples from patients with AAA (n=12). Arterial thrombus (AT) tissue from patients with thrombectomy (n=8) served as control. **D**, Thrombus sections were immunohistochemically stained specifically for platelets (anti-GP Ibα). **E**, Histological Martius Scarlet blue (MSB) staining of (*Continued*)

Downloaded from http://ahajournals.org by on June 17, 2025

Downloaded from http://ahajournals.org by on June 17, 2025

Reduced procoagulant activity of GP VI–deficient platelets may have resulted from decreased platelet activation. Elevated thrombin plasma levels in patients with AAA may occur as a consequence of the enhanced procoagulant activity of platelets, which is a characteristic feature of AAA.[38,39] Thus, we believe that, together with reduced platelet activation and procoagulant activity, GP VI–deficient platelets account for reduced aortic diameter expansion in these mice. Furthermore, our previously mentioned study provided strong evidence for platelets to trigger OPN expression and release from macrophages via GP VI, indicating that OPN not only plays a role in inflammatory and remodeling processes in AAA but may also modulate recruitment of platelets to the aortic wall and the ILT. Thus, it is plausible that the reduced OPN protein levels in the plasma and within the aortic wall of GP VI–deficient mice resulted in reduced accumulation and infiltration of platelets at day 7 after PPE induction.[19]

To date, only a small number of studies that mainly utilized the Ang II infusion model of experimental AAA have analyzed the role of platelets. Blocking of the platelet ADP receptor P2Y12 (purinergic P2Y, G-protein–coupled 12 receptor) by clopidogrel was shown to prevent AAA formation by protecting the elastic lamina of the mouse aorta and by reducing inflammation and MMP2 expression.[40] Recently, we have shown that platelet depletion by antibody treatment protects mice from aortic diameter expansion,[19] suggesting a dominant role of platelets in Ang II and elastase-induced AAA formation in mice. Other investigators have explored the role of platelets in the ePPE mouse model.[16] The authors detected elevated platelet activation in mice and patients with a role for P-selectin because P-selectin knockout mice showed attenuated AAA.[14]

Platelet GP VI has been previously shown to affect inflammatory responses and vascular integrity. Strong evidence for an impact of GP VI in neutrophil activation was provided by Burkard et al[41] who showed that GP VI plays a pivotal role in neutrophil recruitment and NET formation in acute lung injury. Furthermore, Denorme et al[42] found a role of necrotic platelets in the interaction with neutrophils leading to elevated brain injury during ischemic stroke. In line with these results, we here demonstrated that GP VI is also important for neutrophil activation and NET formation at early time points in AAA (Figure 3), suggesting that GP VI triggers neutrophil-mediated inflammatory responses in different diseases. Besides neutrophil activation, Boilard et al[43] identified GP VI to trigger microparticle production and amplify inflammation in arthritis. Moreover, GP VI has been shown to contribute to local host defense during pneumonia-driven sepsis by triggering leukocyte activation.[44] During cutaneous inflammation, GP VI promotes the inflammatory response of macrophages.[45] Notably, platelet recruitment to the site of inflammation is mediated—at least in part—by GP VI, as shown in a model of glomerulonephritis.[46]

In addition to the impact of platelet GP VI on inflammation, an important role of this collagen receptor has been shown in various cerebrovascular and cardiovascular diseases, both in patients and in experimental rodent models.[24,33,47,48] Furthermore, GP VI also represents a useful biomarker for the early detection of these diseases and has great potential for strategizing an efficacious antithrombotic therapy.[47] To date, the translation of experimental findings into therapeutic implications for AAA has been challenging. Several trials for different drugs and therapeutic strategies have failed to demonstrate a clinical benefit.[49–51] There were also different trials that analyzed the benefit of antiplatelet therapies.[11,51–53] However, it remains an open question, which patients with AAA could benefit most from antiplatelet therapy. Notably, major differences in the efficacy of antiplatelet therapy have been linked to the aneurysm size as patients with small-size aneurysms often did not benefit from antiplatelet therapies, whereas beneficial effects have been demonstrated for patients with large aneurysms.[11,51,52] Therapeutic benefits of antiplatelet drugs in enlarged AAAs may be due to the fact that these patients develop an ILT that is only rarely present in patients with small AAA.[11] Different experimental studies showed beneficial effects by blocking GP VI in acute myocardial infarction or stroke in mice or by the treatment of mice with the recombinant dimeric collagen receptor GP VI–Fc (Revacept).[22,24,48,54] In phase I clinical trials, Revacept and GP VI Fab ACT017 (glenzocimab) offered specific and efficient inhibition of collagen-induced platelet aggregation.[55–57] In phase II clinical trials, a beneficial effect of Revacept has been shown for patients with internal carotid artery stenosis.[58] In contrast, in the randomized, double-blind, placebo-controlled ISAR-PLASTER phase II trial (Intracoronary Stenting and Antithrombotic Regimen: Lesion Platelet Adhesion as Selective Target of Endovenous Revacept) in which patients with stable ischemic heart disease underwent elective percutaneous coronary intervention, Revacept, given on top of standard

Figure 10 Continued. thrombus sections to visualize fibrin depositions. Scale bars, 100 and 1000 µm (overview). **F** and **G**, Representative fluorescence images and quantification of ex vivo flow chamber experiments. Whole blood samples of patients with AAA (n=5–8) were perfused over a collagen matrix (200 µg/mL) under an arterial shear rate of 1700 s^{-1}. Whole blood samples of healthy volunteers served as controls (n=5–8). **F**, Analysis of surface coverage and thrombus volume of thrombi from patients with AAA. Platelets were prelabeled with mepacrine (green). Scale bar, 50 µm. **G**, Fibrin/fibrinogen content and phosphatidylserine (PS) exposure of thrombi after flow. Human whole blood samples were preincubated with 8.5 µg/mL AF546 fibrinogen (orange). For PS exposure analysis, human thrombi were stained with AF647 annexin V after flow (red). Scale bar, 50 µm. Data are represented as mean±SEM. Statistical analysis was performed using (**A**) a Mann-Whitney *U* test and (**B**–**G**) an unpaired Student *t* test. DIC indicates differential interference contrast; and MFI, mean fluorescence intensity.

antithrombotic therapy, did not reduce myocardial injury in patients.[21] In a randomized double-blind, placebo-controlled phase IIa trial (ACTIMIS [Acute Ischemic Stroke Interventional Study]), glenzocimab (1000 mg) was well tolerated when given to patients with acute ischemic stroke in addition to alteplase (with or without mechanical thrombectomy). All-cause deaths were lower with glenzocimab while symptomatic intracranial hemorrhage was not detected. However, the authors conclude that glenzocimab might reduce serious adverse events, intracranial hemorrhage, and mortality but suggest that these first results need further research to confirm that glenzocimab in combination with alteplase is a potential therapeutic option for patients with acute ischemic stroke.[59] These first data from different groups together with the here presented results, therefore, indicate that antiplatelet therapy targeting GP VI may be an available option to treat patients with (cardiovascular and cerebrovascular) diseases including AAA. However, there is a need for further studies that carefully investigate whether the blocking of platelet GP VI function is beneficial for these patients. However, the idea of GP VI as a novel therapeutic target in AAA is emphasized by the results from PPE mice treated with a GP VI–blocking antibody (Figure 9) and patients with AAA (Figure 10) demonstrating elevated levels of sGP VI suggesting that a multipanel of biomarkers including sGP VI might be beneficial to detect early and late stages of AAA in patients. One potent marker within this panel might be the thrombus burden ratio as shown recently.[60] Besides increased levels of sGP VI, we detected elevated levels of fibrin in the plasma and increased fibrin deposition in the ILT of patients with AAA. Fibrin is a GP VI ligand that is able to stabilize thrombus formation under dynamic conditions,[61] trigger procoagulant activity, and affect clot structure.[36,62] Thus, it is tempting to speculate that the GP VI–fibrin axis contributes to elevated procoagulant activity and clot formation by increasing thrombin generation and by stabilizing the ILT in AAA. Impairment of the GP VI–fibrin axis may lead to destabilization of the ILT, resulting in an increased aneurysm rupture risk. Therefore, the impact of the GP VI–fibrin axis on ILT formation and clot structure during AAA development awaits future investigation.

In conclusion, the present findings support the potential role of antiplatelet therapy to reduce AAA progression with platelet GP VI as a new therapeutic target in AAA.

ARTICLE INFORMATION

Received December 20, 2023; accepted August 14, 2024.

Affiliations

Department of Vascular and Endovascular Surgery (T.F., A.B., K.J.K., J.M., J.O., E.K., I.K., N.S., W.I., M.U.W., H.S., M.E.) and Institute of Translational Pharmacology (M.G.), University Hospital Duesseldorf, Heinrich-Heine University, Germany. Department of Pharmacology, Experimental Therapy and Toxicology, University Hospital Tuebingen, Germany (M.C.). AdvanceCOR GmbH, Martinsried, Germany (S.G., G.M.).

Acknowledgments

The authors thank Martina Spelleken and Annika Zimmermann for excellent technical assistance. PPE (porcine pancreatic elastase) surgeries were conducted by Julia Odendahl (Department of Cardiology, Pulmonology and Vascular Medicine, University Hospital Duesseldorf; S1 Project TRR259). The authors acknowledge the Center for Advanced Imaging at Heinrich-Heine University, Düsseldorf, for providing access to the Zeiss LSM 880 Airyscan Fast system (DFG-INST 208/746-1 FUGG) and especially for providing support during imaging and analysis. All graphic abstracts were generated with BioRender.com. M. Elvers and T. Feige designed the study. T. Feige, A. Bosbach, K.J. Krott, J. Mulorz, M. Chatterjee, J. Ortscheid, E. Krüger, I. Krüger, and N. Salehzadeh performed experiments. T. Feige, K.J. Krott, M. Chatterjee, and M. Elvers analyzed and interpreted the data. T. Feige and M. Elvers wrote the manuscript with all authors providing feedback. T. Feige, A. Bosbach, and K.J. Krott contributed equally to this study.

Sources of Funding

This work was supported by Deutsche Forschungsgemeinschaft (German Research Foundation), Collaborative Research Centre TRR259 (Aortic Disease; grant No. 397484323: TP A07 to H. Schelzig and M. Elvers, TP B08 to M. Grandoch, and TP C03 to M.U. Wagenhäuser), and RTG 2816 (grant No. 464254052: to M. Chatterjee).

Disclosures

None.

Supplemental Material

Supplemental Methods
Table S1
Figures S1–S14
Major Resources Table
ARRIVE Guidelines

REFERENCES

1. Firnhaber JM, Powell CS. Arterial atherosclerosis: vascular surgery interventions. *Am Fam Physician.* 2022;105:65–72.
2. Song P, He Y, Adeloye D, Zhu Y, Ye X, Yi Q, Rahimi K, Rudan I; Global Health Epidemiology Research Group (GHERG). The global and regional prevalence of abdominal aortic aneurysms: a systematic review and modelling analysis. *Ann Surg.* 2022;277:912–919. doi: 10.1097/SLA.0000000000005716
3. Cameron SJ, Russell HM, Owens AP 3rd. Antithrombotic therapy in abdominal aortic aneurysm: beneficial or detrimental? *Blood.* 2018;132:2619–2628. doi: 10.1182/blood-2017-08-743237
4. Golledge J, Morris DR, Pinchbeck J, Rowbotham S, Jenkins J, Bourke M, Bourke B, Norman PE, Jones R, Moxon JV. Editor's choice - metformin prescription is associated with a reduction in the combined incidence of surgical repair and rupture related mortality in patients with abdominal aortic aneurysm. *Eur J Vasc Endovasc Surg.* 2019;57:94–101. doi: 10.1016/j.ejvs.2018.07.035
5. Karrowni W, Dughman S, Hajj GP, Miller FJ Jr. Statin therapy reduces growth of abdominal aortic aneurysms. *J Investig Med.* 2011;59:1239–1243. doi: 10.2130/JIM.0b013e31823548e8
6. Kunath A, Unosson J, Friederich-Persson M, Bjarnegård N, Becirovic-Agic M, Björck M, Mani K, Wanhainen A, Wågsäter D. Inhibition of angiotensin-induced aortic aneurysm by metformin in apolipoprotein E-deficient mice. *JVS Vasc Sci.* 2021;2:33–42. doi: 10.1016/j.jvssci.2020.11.031
7. Sutton SS, Magagnoli J, Cummings TH, Hardin JW. Association between metformin and abdominal aortic aneurysm in diabetic and non-diabetic US veterans. *J Investig Med.* 2020;68:1015–1018. doi: 10.1136/jim-2019-001177
8. Sakalihasan N, Limet R, Defawe OD. Abdominal aortic aneurysm. *Lancet.* 2005;365:1577–1589. doi: 10.1016/S0140-6736(05)66459-8
9. Shimizu K, Mitchell RN, Libby P. Inflammation and cellular immune responses in abdominal aortic aneurysms. *Arterioscler Thromb Vasc Biol.* 2006;26:987–994. doi: 10.1161/01.ATV.0000214999.12921.4f
10. Gawaz M, Vogel S. Platelets in tissue repair: control of apoptosis and interactions with regenerative cells. *Blood.* 2013;122:2550–2554. doi: 10.1182/blood-2013-05-468694
11. Lindholt JS, Björck M, Michel JB. Anti-platelet treatment of middle-sized abdominal aortic aneurysms. *Curr Vasc Pharmacol.* 2013;11:305–313. doi: 10.2174/1570161111311030005
12. Busch A, Bleichert S, Ibrahim N, Wortmann M, Eckstein HH, Brostjan C, Wagenhäuser MU, Goergen CJ, Maegdefessel L. Translating mouse models

Downloaded from http://ahajournals.org by on June 17, 2025

of abdominal aortic aneurysm to the translational needs of vascular surgery. *JVSVasc Sci.* 2021;2:219–234. doi: 10.1016/j.jvssci.2021.01.002
13. Dai J, Louedec L, Philippe M, Michel JB, Houard X. Effect of blocking platelet activation with AZD6140 on development of abdominal aortic aneurysm in a rat aneurysmal model. *J Vasc Surg.* 2009;49:719–727. doi: 10.1016/j.jvs.2008.09.057
14. Hannawa KK, Cho BS, Sinha I, Roelofs KJ, Myers DD, Wakefield TJ, Stanley JC, Henke PK, Upchurch GR. Attenuation of experimental aortic aneurysm formation in P-selectin knockout mice. *Ann NY Acad Sci.* 2006;1085:353–359. doi: 10.1196/annals.1383.014
15. Metz LM, Feige T, de Biasi L, Ehrenberg A, Mulorz J, Toska LM, Reusswig F, Quast C, Gerdes N, Kelm M, et al. Platelet pannexin-1 channels modulate neutrophil activation and migration but not the progression of abdominal aortic aneurysm. *Front Mol Biosci.* 2023;10:1111108. doi: 10.3389/fmolb.2023.1111108
16. Morrell CN, Mix D, Aggarwal A, Bhandari R, Godwin M, Owens P 3rd, Lyden SP, Doyle A, Krauel K, Rondina MT, et al. Platelet olfactory receptor activation limits platelet reactivity and growth of aortic aneurysms. *J Clin Invest.* 2022;132:e152373. doi: 10.1172/JCI152373
17. Owens AP 3rd, Edwards TL, Antoniak S, Geddings JE, Jahangir E, Wei WQ, Denny JC, Boulaftali Y, Bergmeier W, Daugherty A, et al. Platelet inhibitors reduce rupture in a mouse model of established abdominal aortic aneurysm. *Arterioscler Thromb Vasc Biol.* 2015;35:2032–2041. doi: 10.1161/ATVBAHA.115.305537
18. Touat Z, Ollivier V, Dai J, Huisse MG, Bezeaud A, Sebbag U, Palombi T, Rossignol P, Meilhac O, Guillin MC, et al. Renewal of mural thrombus releases plasma markers and is involved in aortic abdominal aneurysm evolution. *Am J Pathol.* 2006;168:1022–1030. doi: 10.2353/ajpath.2006.050868
19. Wagenhauser MU, Mulorz J, Krott KJ, Bosbach A, Feige T, Rhee YH, Chatterjee M, Petzold N, Böddeker C, Ibing W, et al. Crosstalk of platelets with macrophages and fibroblasts aggravates inflammation, aortic wall stiffening, and osteopontin release in abdominal aortic aneurysm. *Cardiovasc Res.* 2024;120:417–432. doi: 10.1093/cvr/cvad168
20. Gröschel K, Uphaus T, Loftus I, Poppert H, Diener HC, Zobel J, Münch G. Revacept, an inhibitor of platelet adhesion in symptomatic carotid artery stenosis: design and rationale of a randomized phase II clinical trial. *TH Open.* 2020;4:e393–e399. doi: 10.1055/s-0040-1721078
21. Mayer K, Hein-Rothweiler R, Schüpke S, Janisch M, Bernlochner I, Ndrepepa G, Sibbing D, Gori T, Borst O, Holdenrieder S, et al. Efficacy and safety of revacept, a novel lesion-directed competitive antagonist to platelet glycoprotein VI, in patients undergoing elective percutaneous coronary intervention for stable ischemic heart disease: the randomized, double-blind, placebo-controlled ISAR-PLASTER phase 2 trial. *JAMA Cardiol.* 2021;6:753–761. doi: 10.1001/jamacardio.2021.0475
22. Pachel C, Mathes D, Arias-Loza AP, Heitzmann W, Nordbeck P, Deppermann C, Lorenz V, Hofmann U, Nieswandt B, Frantz S. Inhibition of platelet GPVI protects against myocardial ischemia-reperfusion injury. *Arterioscler Thromb Vasc Biol.* 2016;36:629–635. doi: 10.1161/ATVBAHA.115.305873
23. Rout A, Tantry US, Novakovic M, Sukhi A, Gurbel PA. Targeted pharmacotherapy for ischemia reperfusion injury in acute myocardial infarction. *Expert Opin Pharmacother.* 2020;21:1851–1865. doi: 10.1080/14656566.2020.1787987
24. Schönberger T, Ziegler M, Borst O, Konrad I, Nieswandt B, Massberg S, Ochmann C, Jürgens T, Seizer P, Langer H, et al. The dimeric platelet collagen receptor GPVI-Fc reduces platelet adhesion to activated endothelium and preserves myocardial function after transient ischemia in mice. *Am J Physiol Cell Physiol.* 2012;303:C757–C766. doi: 10.1152/ajpcell.00060.2012
25. Wichaiyo S, Parichatikanond W, Rattanavipanon W. Glenzocimab: a GPVI (glycoprotein VI)-targeted potential antiplatelet agent for the treatment of acute ischemic stroke. *Stroke.* 2022;53:3506–3513. doi: 10.1161/STROKEAHA.122.039790
26. Lu G, Su G, Davis JP, Schaheen B, Downs E, Roy RJ, Ailawadi G, Upchurch GR. A novel chronic advanced stage abdominal aortic aneurysm murine model. *J Vasc Surg.* 2017;66:232–242.e4. doi: 10.1016/j.jvs.2016.07.105
27. Cebo M, Dittrich K, Fu X, Manke MC, Emschermann F, Rheinlaender J, von Eysmondt H, Ferreirós N, Sudman J, Witte A, et al. Platelet ACKR3/CXCR7 favors antiplatelet lipids over an atherothrombotic lipidome and regulates thromboinflammation. *Blood.* 2022;139:1722–1742. doi: 10.1182/blood.2021013097
28. Jarre A, Gowert NS, Donner L, Münzer P, Klier M, Borst O, Schaller M, Lang F, Korth C, Elvers M. Pre-activated blood platelets and a prothrombotic phenotype in APP23 mice modeling Alzheimer's disease. *Cell Signal.* 2014;26:2040–2050. doi: 10.1016/j.cellsig.2014.05.019
29. Reusswig F, Polzin A, Klier M, Dille MA, Ayhan A, Benkhoff M, Lersch C, Prinz A, Gorressen S, Fischer JW, et al. Only acute but not chronic thrombocytopenia protects mice against left ventricular dysfunction after acute myocardial infarction. *Cells.* 2022;11:3500. doi: 10.3390/cells11213500
30. Reusswig F, Dille M, Kruger E, Ortscheid J, Feige T, Gorressen S, Fischer JW, Elvers M. Platelets modulate cardiac remodeling via the collagen receptor GPVI after acute myocardial infarction. *Front Immunol.* 2023;14:1275788. doi: 10.3389/fimmu.2023.1275788
31. Swamydas M, Luo Y, Dorf ME, Lionakis MS. Isolation of mouse neutrophils. *Curr Protoc Immunol.* 2015;110:3.20.1–3.20.15. doi: 10.1002/0471142735.im0320s110
32. Donner L, Toska LM, Kruger I, Groniger S, Barroso R, Burleigh A, Mezzano D, Pfeiler S, Kelm M, Gerdes N, et al. The collagen receptor glycoprotein VI promotes platelet-mediated aggregation of beta-amyloid. *Sci Signal.* 2020;13:eaba9872. doi: 10.1126/scisignal.aba9872
33. Bigalke B, Stellos K, Geisler T, Kremmer E, Seizer P, May AE, Lindemann S, Melms A, Luft A, Gawaz M. Expression of platelet glycoprotein VI is associated with transient ischemic attack and stroke. *Eur J Neurol.* 2010;17:111–117. doi: 10.1111/j.1468-1331.2009.02754.x
34. Papapanagiotou A, Daskalakis G, Siasos G, Gargalionis A, Papavassiliou AG. The role of platelets in cardiovascular disease: molecular mechanisms. *Curr Pharm Des.* 2016;22:4493–4505. doi: 10.2174/1381612822666160607064118
35. Hughan SC, Hughes CE, McCarty OJT, Schweighoffer E, Soultanova I, Ware J, Tybulewicz VLJ, Watson SP. GPVI potentiation of platelet activation by thrombin and adhesion molecules independent of Src kinases and Syk. *Arterioscler Thromb Vasc Biol.* 2007;27:422–429. doi: 10.1161/01.ATV.0000252826.96134.21
36. Mammadova-Bach E, Ollivier V, Loyau S, Schaff M, Dumont B, Favier R, Freyburger G, Latger-Cannard V, Nieswandt B, Gachet C, et al. Platelet glycoprotein VI binds to polymerized fibrin and promotes thrombin generation. *Blood.* 2015;126:683–691. doi: 10.1182/blood-2015-02-629717
37. Leo L, Di Paola J, Judd BA, Koretzky GA, Lentz SR. Role of the adapter protein SLP-76 in GPVI-dependent platelet procoagulant responses to collagen. *Blood.* 2002;100:2839–2844. doi: 10.1182/blood-2002-04-1234
38. Sundermann AC, Saum K, Conrad KA, Russell HM, Edwards TL, Mani K, Björck M, Wanhainen A, Owens AP. Prognostic value of D-dimer and markers of coagulation for stratification of abdominal aortic aneurysm growth. *Blood Adv.* 2018;2:3088–3096. doi: 10.1182/bloodadvances.2017013359
39. Wallinder J, Bergqvist D, Henriksson AE. Haemostatic markers in patients with abdominal aortic aneurysm and the impact of aneurysm size. *Thromb Res.* 2009;124:423–426. doi: 10.1016/j.thromres.2009.01.016
40. Liu O, Jia L, Liu X, Wang Y, Wang X, Qin Y, Du J, Zhang H. Clopidogrel, a platelet P2Y12 receptor inhibitor, reduces vascular inflammation and angiotensin II induced-abdominal aortic aneurysm progression. *PLoS One.* 2012;7:e51707. doi: 10.1371/journal.pone.0051707
41. Burkard P, Schonhart C, Vogtle T, Kohler D, Tang L, Johnson D, Hemmen K, Heinze KG, Zarbock A, Hermanns HM, et al. A key role for platelet GPVI in neutrophil recruitment, migration, and NETosis in the early stages of acute lung injury. *Blood.* 2023;142:1463–1477. doi: 10.1182/blood.2023019940
42. Denorme F, Manne BK, Portier I, Eustes AS, Kosaka Y, Kile BT, Rondina MT, Campbell RA. Platelet necrosis mediates ischemic stroke outcome in mice. *Blood.* 2020;135:429–440. doi: 10.1182/blood.2019002124
43. Boilard E, Nigrovic PA, Larabee K, Watts GF, Coblyn JS, Weinblatt ME, Massarotti EM, Remold-O'Donnell E, Farndale RW, Ware J, et al. Platelets amplify inflammation in arthritis via collagen-dependent microparticle production. *Science.* 2010;327:580–583. doi: 10.1126/science.1181928
44. Claushuis TAM, de Vos AF, Nieswandt B, Boon L, Roelofs J, de Boer OJ, van 't Veer C, van der Poll T. Platelet glycoprotein VI aids in local immunity during pneumonia-derived sepsis caused by gram-negative bacteria. *Blood.* 2018;131:864–876. doi: 10.1182/blood-2017-06-788067
45. Pierre S, Linke B, Suo J, Tarighi N, Del Turco D, Thomas D, Ferreiros N, Stegner D, Frölich S, Sisignano M, et al. GPVI and thromboxane receptor on platelets promote proinflammatory macrophage phenotypes during cutaneous inflammation. *J Invest Dermatol.* 2017;137:686–695. doi: 10.1016/j.jid.2016.09.036
46. Devi S, Kuligowski MP, Kwan RY, Westein E, Jackson SP, Kitching AR, Hickey MJ. Platelet recruitment to the inflamed glomerulus occurs via an alphallbbeta3/GPVI-dependent pathway. *Am J Pathol.* 2010;177:1131–1142. doi: 10.2353/ajpath.2010.091143
47. Bigalke B, Elvers M, Schönberger T, Gawaz M. Platelet and soluble glycoprotein VI - novel applications in diagnosis and therapy. *Curr Drug Targets.* 2011;12:1821–1830. doi: 10.2174/138945011797635867

Downloaded from http://ahajournals.org by on June 17, 2025

48. Kleinschnitz C, Pozgajova M, Pham M, Bendszus M, Nieswandt B, Stoll G. Targeting platelets in acute experimental stroke: impact of glycoprotein Ib, VI, and IIb/IIIa blockade on infarct size, functional outcome, and intracranial bleeding. *Circulation.* 2007;115:2323–2330. doi: 10.1161/CIRCULATIONAHA.107.691279
49. Meijer CA, Stijnen T, Wasser MN, Hamming JF, van Bockel JH, Lindeman JH; Pharmaceutical Aneurysm Stabilisation Trial Study Group. Doxycycline for stabilization of abdominal aortic aneurysms: a randomized trial. *Ann Intern Med.* 2013;159:815–823. doi: 10.7326/0003-4819-159-12-201312170-00007
50. Sillesen H, Eldrup N, Hultgren R, Lindeman J, Bredahl K, Thompson M, Wanhainen A, Wingren U, Swedenborg J; AORTA Trial Investigators. Randomized clinical trial of mast cell inhibition in patients with a medium-sized abdominal aortic aneurysm. *Br J Surg.* 2015;102:894–901. doi: 10.1002/bjs.9824
51. Wanhainen A, Mani K, Kullberg J, Svensjö S, Bersztel A, Karlsson L, Holst J, Gottsäter A, Linné A, Gillgren P, et al. The effect of ticagrelor on growth of small abdominal aortic aneurysms-a randomized controlled trial. *Cardiovasc Res.* 2020;116:450–456. doi: 10.1093/cvr/cvz133
52. Balceniuk MD, Trakimas LE, Aghaie C, Mix D, Rasheed K, Ellis J, Glocker R, Doyle A, Stoner MC. Aspirin use is associated with decreased radiologically-determined thrombus sac volume in abdominal aortic aneurysms. *Vascular.* 2018;26:440–444. doi: 10.1177/1708538118762214
53. Wang YD, Liu ZJ, Ren J, Xiang MX. Pharmacological therapy of abdominal aortic aneurysm: an update. *Curr Vasc Pharmacol.* 2018;16:114–124. doi: 10.2174/1570161115666170413145705
54. Goebel S, Li Z, Vogelmann J, Holthoff HP, Degen H, Hermann DM, Gawaz M, Ungerer M, Münch G. The GPVI-Fc fusion protein Revacept improves cerebral infarct volume and functional outcome in stroke. *PLoS One.* 2013;8:e66960. doi: 10.1371/journal.pone.0066960
55. Voors-Pette C, Lebozec K, Dogterom P, Jullien L, Billiald P, Ferlan P, Renaud L, Favre-Bulle O, Avenard G, Machacek M, et al. Safety and tolerability, pharmacokinetics, and pharmacodynamics of ACT017, an antiplatelet GPVI (glycoprotein VI) Fab. *Arterioscler Thromb Vasc Biol.* 2019;39:956–964. doi: 10.1161/ATVBAHA.118.312314
56. Ungerer M, Rosport K, Bultmann A, Piechatzek R, Uhland K, Schlieper P, Gawaz M, Münch G. Novel antiplatelet drug revacept (dimeric glycoprotein VI-Fc) specifically and efficiently inhibited collagen-induced platelet aggregation without affecting general hemostasis in humans. *Circulation.* 2011;123:1891–1899. doi: 10.1161/CIRCULATIONAHA.110.980623
57. Lebozec K, Jandrot-Perrus M, Avenard G, Favre-Bulle O, Billiald P. Design, development and characterization of ACT017, a humanized Fab that blocks platelet's glycoprotein VI function without causing bleeding risks. *mAbs.* 2017;9:945–958. doi: 10.1080/19420862.2017.1336592
58. Uphaus T, Richards T, Weimar C, Neugebauer H, Poli S, Weissenborn K, Imray C, Michalski D, Rashid H, Loftus I, et al. Revacept, an inhibitor of platelet adhesion in symptomatic carotid stenosis: a multicenter randomized phase II trial. *Stroke.* 2022;53:2718–2729. doi: 10.1161/STROKEAHA.121.037006
59. Mazighi M, Kohrmann M, Lemmens R, Lyrer PA, Molina CA, Richard S, Toni D, Plétan Y, Sari A, Meilhoc A, et al; ACTIMIS Study Group. Safety and efficacy of platelet glycoprotein VI inhibition in acute ischaemic stroke (ACTIMIS): a randomised, double-blind, placebo-controlled, phase 1b/2a trial. *Lancet Neurol.* 2024;23:157–167. doi: 10.1016/S1474-4422(23)00427-1
60. Mulorz J, Mazrekaj A, Sehl J, Arnautovic A, Garabet W, Krott KJ, Schelzig H, Elvers M, Wagenhäuser MU. Relative thrombus burden ratio reveals overproportioned intraluminal thrombus growth-potential implications for abdominal aortic aneurysm. *J Clin Med.* 2024;13:962. doi: 10.3390/jcm13040962
61. Alshehri OM, Hughes CE, Montague S, Watson SK, Frampton J, Bender M, Watson SP. Fibrin activates GPVI in human and mouse platelets. *Blood.* 2015;126:1601–1608. doi: 10.1182/blood-2015-04-641654
62. Gauer JS, Duval C, Xu RG, Macrae FL, McPherson HR, Tiede C, Tomlinson D, Watson SP, Ariëns RAS. Fibrin-glycoprotein VI interaction increases platelet procoagulant activity and impacts clot structure. *J Thromb Haemost.* 2023;21:667–681. doi: 10.1016/j.jtha.2022.09.004

Downloaded from http://ahajournals.org by on June 17, 2025

Supplemental Material

GPVI-mediated platelet activation and pro-coagulant activity aggravate inflammation and aortic wall remodelling in abdominal aortic aneurysm

Feige T[1]*, Bosbach A[1]*, Krott KJ[1]*, Mulorz J[1], Chatterjee M[2], Ortscheid J[1], Krüger E[1], Krüger I[1], Salehzadeh N[1], Goebel S[4], Ibing W[1], Grandoch M[3], Münch G[4], Wagenhäuser MU[1], Schelzig H[1], Elvers M[§1]

* contributed equally
§ corresponding author

[1]Department of Vascular- and Endovascular Surgery, University Hospital Duesseldorf, Heinrich-Heine University, Duesseldorf, Germany

[2]Department of Pharmacology, Experimental Therapy and Toxicology, University Hospital Tuebingen, Tuebingen, Germany

[3]Institute of Translational Pharmacology, University Hospital Duesseldorf, Heinrich-Heine University, Duesseldorf, Germany

[4]AdvanceCOR GmbH, Martinsried, Germany

E-Mail of Corresponding Author: Margitta Elvers, Ph.D., margitta.elvers@med.uni-duesseldorf.de

1. Supplemental Methods

1.1 Human plasma preparation. For plasma preparation, citrate-anticoagulated human blood samples were centrifuged at 1,000 x *g* for 10 min at RT. After centrifugation, the platelet-free plasma (PFP) was collected and stored at -70 °C until use.

1.2 Murine blood collection and plasma preparation. Murine whole blood was collected in 300 µL heparin solution (20 U/mL). For murine *ex vivo* flow chamber experiments citrate-anticoagulated blood was used. Blood cell counts, including platelet count and mean platelet volume (MPV), were analysed using a hematology analyzer (Sysmex KX21N, Norderstedt). For plasma preparation, blood was collected into EDTA-coated Microvettes® (#20.1341, Sarstedt). Samples were centrifuged at 2,500 x *g* for 5 min at 4 °C. Plasma samples were stored at -70 °C until use.

1.3 Preparation of murine aortic tissue. Mice were euthanised via cervical dislocation under deep isoflurane anaesthesia at days 7, 14, and 28 post PPE surgery. After euthanasia, the thorax was opened, and the heart was punctured with a butterfly cannula at the apex cordis of the left ventricle. The vascular system was subsequently perfused under constant pressure with approximately 20 mL of cold heparin solution (20 U/mL, 4 °C, #2047217, Braun) to prevent clot formation. Subsequently, the abdominal aorta was removed and fixed in 4% paraformaldehyde (PFA, #P087.5, Carl Roth) for 24 h at 4 °C. After dehydration in an ethanol gradient, the aortic tissue was incubated for at least 12 h in Roti®Histol (#6640.4, Carl Roth) at RT and embedded in paraffin (#P3558, Sigma-Aldrich).

1.4 Flow cytometric analysis of GPVI shedding. For investigating the impact of recombinant OPN on GPVI shedding citrate-anticoagulated blood (BD–Vacutainer®; Becton, Dickinson and Company; #367714) of healthy volunteers was diluted at a ratio of 1:10 in human Tyrode's buffer (137 mM NaCl, 2.8 mM KCl, 12 mM $NaHCO_3$, 0.4 mM NaH_2PO_4, and 5.5 mM glucose; pH 6.5). All samples were specifically stained for 15 min at RT using an antibody against GPVI (HY101-PE, #565241, BD Pharmingen™) at a ratio of 1:10 and subsequently incubated with the indicated agonists (collagen-related peptide (CRP; Richard Farndale, University of Cambridge, Cambridge, UK), osteopontin (OPN, #120-35,PeproTech), PAR4 peptide (PAR4; #3494, Tocris)) and the respective antibodies for 15 min and 1h at 37 °C in the dark. Stimulation with Convulxin (Cvx, #ALX-350-100-C050, Enzo Life Sciences) served as positive control. The reaction was stopped by adding 300 µL of PBS. All samples were analysed using a BD FACSCalibur™ flow cytometer.

2. Supplemental Figures and Legends

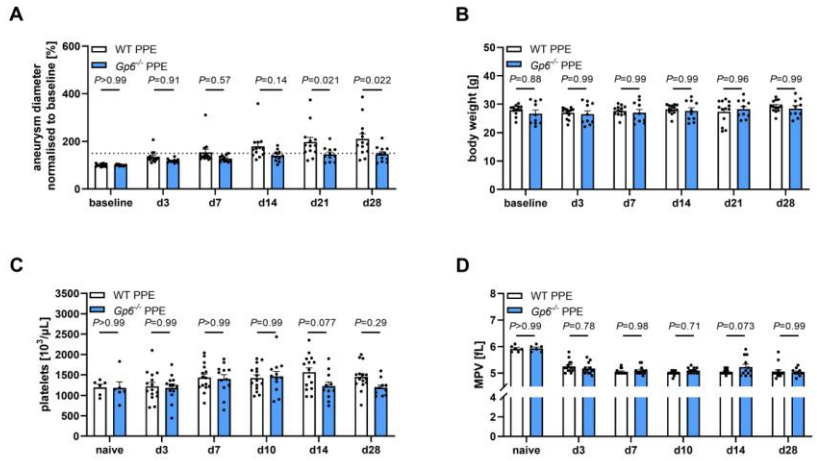


Figure S1. Aortic diameter, body weight and platelet count of GPVI deficient mice in PPE induced AAA progression. (**A**) Aortic diameter progression of WT (*n* = 13) and *Gp6*$^{-/-}$ (*n* = 11) PPE mice over a time period of 28 days, analysed by ultrasound measurements. Data were normalised to baseline. (**B**) Body weight of PPE operated WT (*n* = 13) and *Gp6*$^{-/-}$ (*n* = 11) mice prior (baseline) and at day 3, 7, 14, 21, 28 post surgery. (**C** and **D**) Platelet count and MPV of naive (WT (*n* = 6) and *Gp6*$^{-/-}$ (*n* = 6)) and PPE operated (WT (*n* = 13) and *Gp6*$^{-/-}$ (*n* = 11) mice at day 7, 14 and 28 post surgery. (Data are represented as mean values ± SEM. Statistical analysis was performed using (**A**–**D**) a two-way ANOVA with a Sidak's multiple comparisons post-hoc test. AAA = Abdominal aortic aneurysm; MPV = Mean platelet volume; PPE = Porcine pancreatic elastase (infusion).

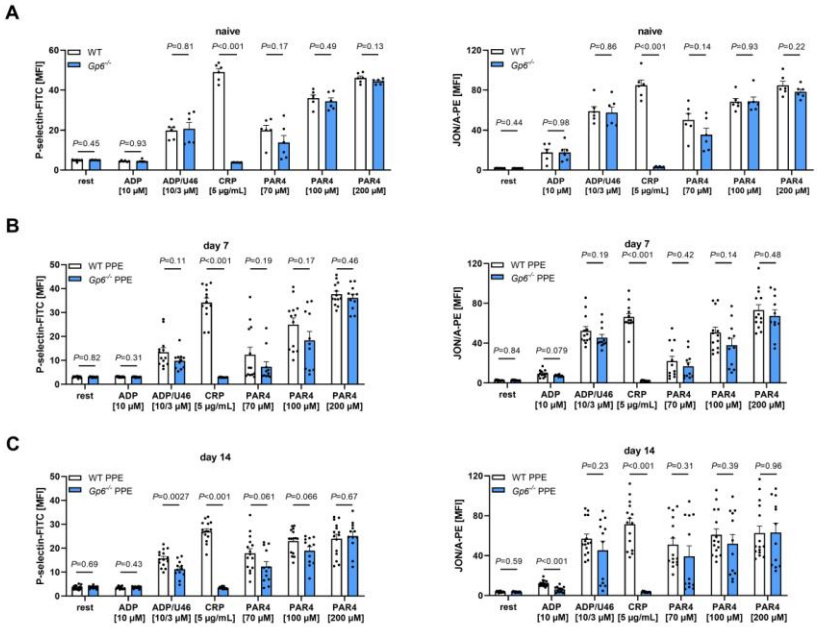


Figure S2. Platelet degranulation and integrin $\alpha_{IIb}\beta_3$ activation of GPVI deficient mice in PPE induced AAA progression. (**A**–**C**) Platelet degranulation (P-selectin-FITC) and active integrin $\alpha_{IIb}\beta_3$ (JON/A-PE) of washed murine whole blood from (**A**) naive (n = 6) and PPE operated WT (n = 13–15) and *Gp6*$^{-/-}$ (n = 11–12) mice at (**B**) day 7 and (**C**) day 14 was analysed by flow cytometry. Platelets were stimulated with indicated agonists. Data are represented as mean values ± SEM. Statistical analysis was performed using (**A**–**C**) an unpaired multiple t-test. ADP = Adenosine diphosphate; CRP = Collagen-related peptide; MFI = Mean fluorescence intensity; PAR4 = Protease-activated receptor 4 activating peptide; PS = Phosphatidylserine; PPE = Porcine pancreatic elastase (infusion); U46619 (U46) = Thromboxane A_2 analogue.

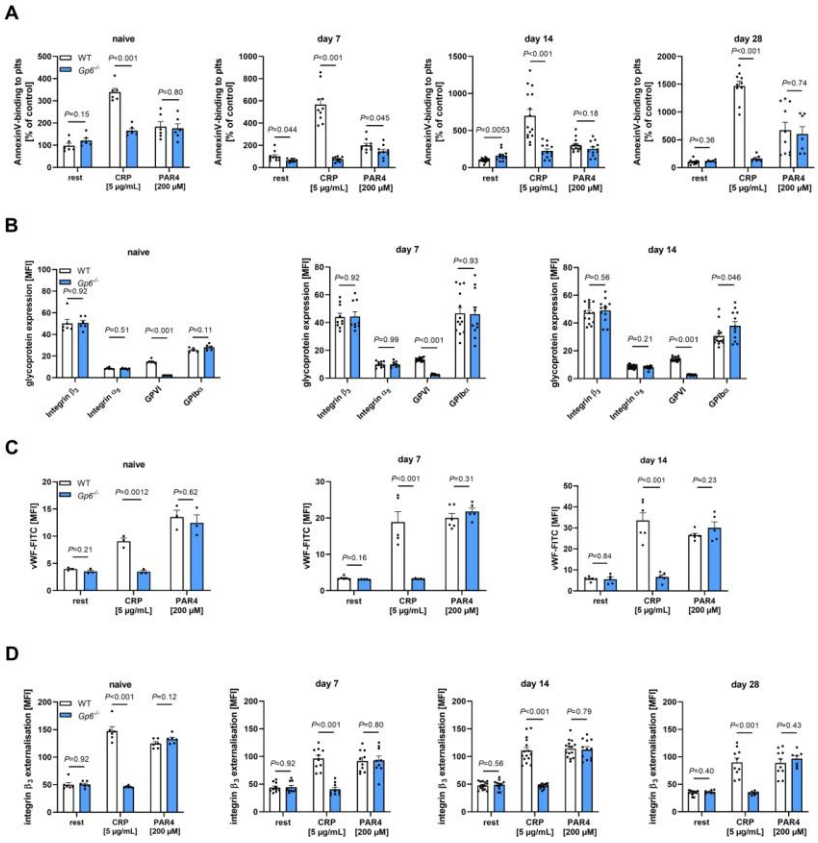


Figure S3. PS-exposure, platelet glycoprotein expression, vWF binding to platelets and integrin β3 externalisation of GPVI deficient mice during PPE-induced AAA development. Washed murine whole blood of naive and PPE operated WT and *Gp6*$^{-/-}$ mice at days 7, 14 and 28 were analysed by flow cytometry. (**A**) PS-exposure (Annexin V-Cy5) of platelets from naive (WT (*n* = 6) and *Gp6*$^{-/-}$ (*n* = 6)) and PPE operated (WT (*n* = 8–14) and *Gp6*$^{-/-}$ (*n* = 9–12)) mice at day 7, 14 and 28 post surgery. Platelets were stimulated with indicated agonists. (**B**) Platelet surface expression of integrin β_3, integrin α_5, GPVI and GPIbα under resting conditions in naïve (WT (*n* = 6) and *Gp6*$^{-/-}$ (*n* = 6)) and PPE operated (WT (*n* = 10–15) and *Gp6*$^{-/-}$ (*n* = 9–12)) mice at day 7 and 14 post surgery. (**C**) VWF binding to platelets from naive (WT (*n* = 3) and *Gp6*$^{-/-}$ (*n* = 3)) and PPE operated (WT (*n* = 5-6) and *Gp6*$^{-/-}$ (*n* = 5)) mice at day 7 and 14 post surgery. Platelets were stimulated with indicated agonists. (**D**) Integrin β_3 externalisation in naive WT (n = 6) and *Gp6*$^{-/-}$ (*n* = 6)

and PPE operated (WT (n = 10–15) and *Gp6*$^{-/-}$ (n = 7–12)) mice at day 7, 14 and 28 post surgery. Platelets were stimulated with indicated agonists. Data are represented as mean values ± SEM. Statistical analysis was performed using (**A**–**D**) an unpaired multiple t-test. CRP = Collagen-related peptide; MFI = Mean fluorescence intensity; PAR4 = Protease-activated receptor 4 activating peptide; Plts = Platelets; PPE = Porcine pancreatic elastase (infusion); vWF = von Willebrand factor.

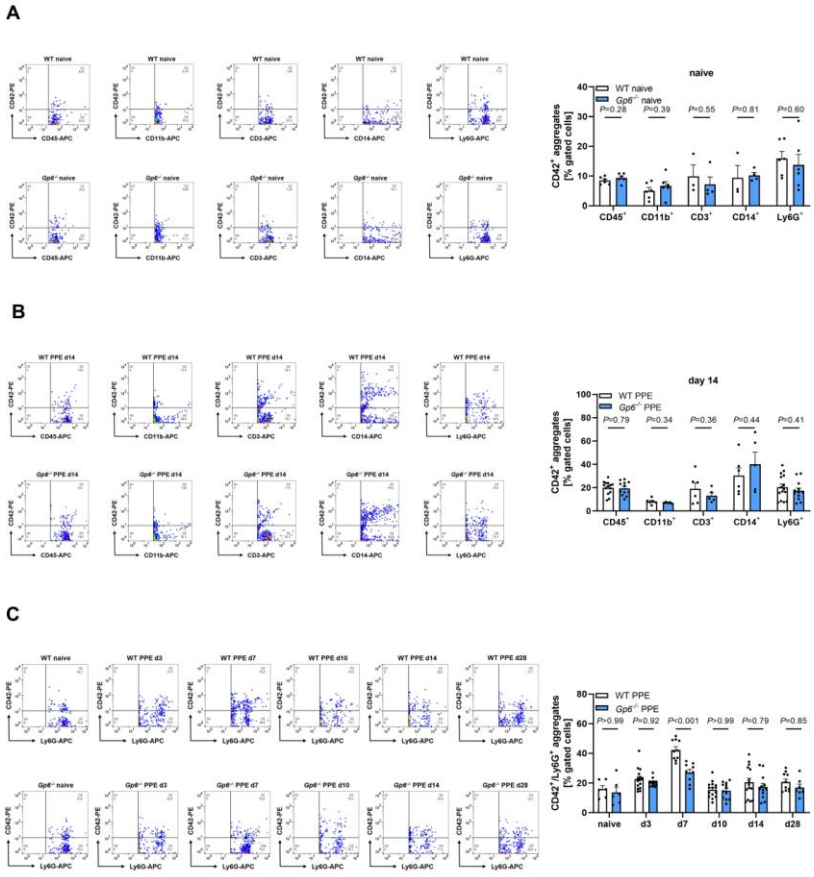


Figure S4. Platelet-leukocyte aggregates in naive and PPE operated GPVI deficient mice. (**A** and **B**) Aggregate formation of platelets with different leukocyte subtypes in (**A**) naive (WT (n = 3–6) and *Gp6*$^{-/-}$ (n = 3–6)) and (**B**) PPE operated (WT (n = 6–14) and *Gp6*$^{-/-}$ (n = 5–12)) mice at day 14 post surgery, analysed by flow cytometry. (**C**) Platelet-neutrophil aggregate formation was analysed in PPE operated WT (n = 6–15) and *Gp6*$^{-/-}$ (n = 6–12) mice at day 0 (naive) 3, 7, 14, 28 post surgery. Aggregate formation was determined as double positive events for CD42b (platelet maker, GPIbα) and CD45 (WBC marker) by flow cytometry. Data are represented as mean values ± SEM. Statistical analysis was performed using (**A** and **B**) an unpaired multiple t-test and (**C**) a two-way ANOVA with a Sidak's multiple comparisons post-hoc test. PPE = Porcine pancreatic elastase (infusion).

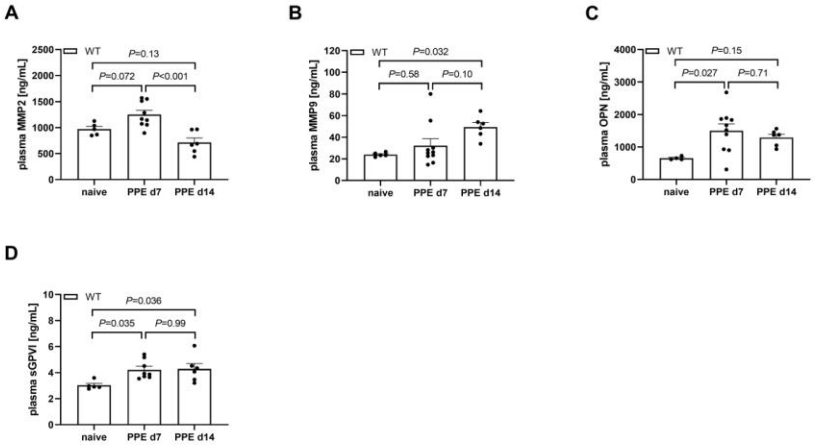


Figure S5. MMP, OPN and sGPVI plasma level during experimental AAA progression. (**A**–**D**) Plasma concentration of (**A**) MMP2, (**B**) MMP9, (**C**) OPN and (**D**) sGPVI of PPE operated WT (*n* = 6–10) mice at day 7 and 14 post surgery, analysed by ELISA. Naive WT (*n* = 4–5) mice served as control. Data are represented as mean values ± SEM. Statistical analysis was performed using (**A**–**D**) an one-way ANOVA with a Tukey's multiple comparisons post-hoc test. MMP = Matrix metalloproteinase; OPN = Osteopontin; PPE = Porcine pancreatic elastase (infusion); sGPVI = soluble GPVI.

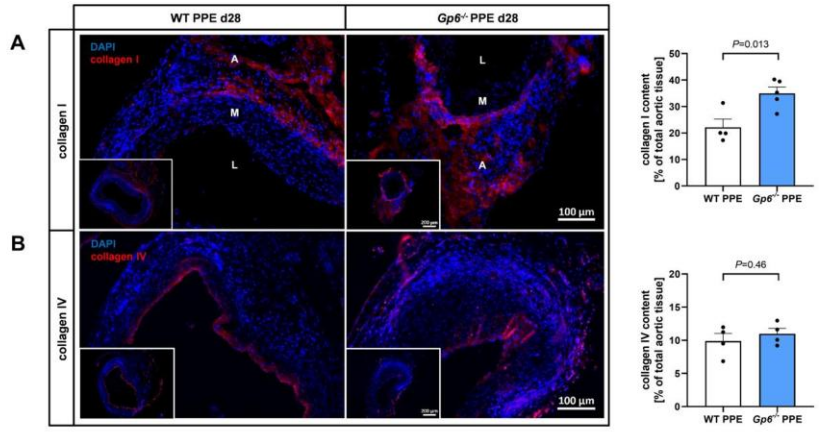


Figure S6. Collagen I and IV content within the aortic tissue of PPE operated GPVI deficient mice. (**A** and **B**) Representative immunofluorescence images and quantification of collagen content within the aneurysm segment of PPE operated WT (n = 4) and *Gp6*$^{-/-}$ (n = 4–5) mice at day 28. Aortic tissue was specifically stained for (**A**) collagen I (anti-collagen I /Cy3; red) and (**B**) collagen IV (anti-collagen IV/Cy5; red). Nuclei were stained with DAPI (blue). Scale bars: 100 µm and 200 µm (overview). Data are represented as mean values ± SEM. Statistical analysis was performed using (**A** and **B**) an unpaired student's t-test. A = Adventitia; L = Lumen; M = Media; PPE = Porcine pancreatic elastase (infusion).

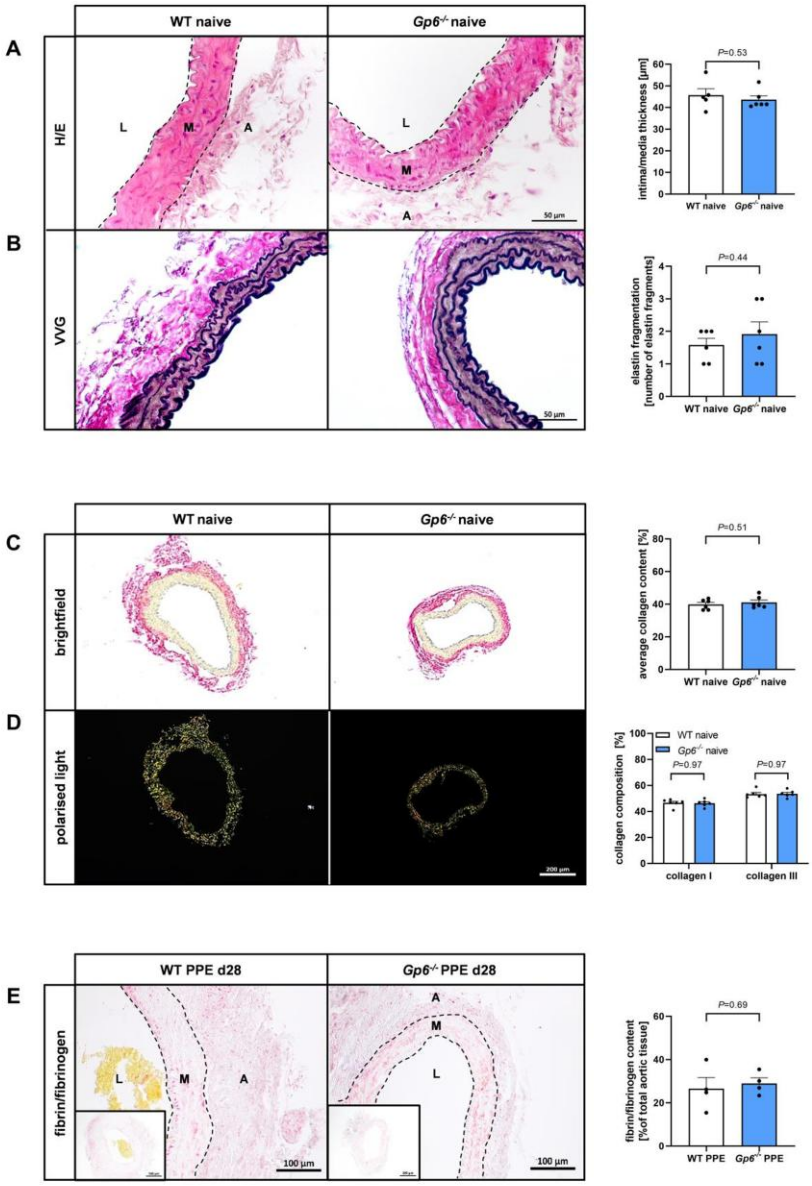


Figure S7. Aortic intima/media thickness, elastin fragmentation and collagen composition in naive GPVI deficient mice. (**A**–**D**) Representative images and quantification of aortic tissue from naive (unoperated) WT and *Gp6*$^{-/-}$ mice. (**A**) Intima/media thickness was

analysed by using H/E staining of naive WT (*n* = 5) and *Gp6*$^{-/-}$ (*n* = 6) mice. Scale bar: 50 µm. (**B**) Quantification of elastin fragmentation within the aortic media of naive WT (*n* = 6) and *Gp6*$^{-/-}$ (*n* = 6) mice by VVG staining. Scale bar: 50 µm. (**C**) Representative brightfield images and quantification of the average collagen content using picrosirius red staining. (**G**) Representative images and quantification of the aortic collagen composition using polarized light (collagen type I, red-yellow and collagen type III, green). Aortic tissue was stained using picrosirius red. Scale bar: 200 µm. (**E**) Histological MSB staining to visualise fibrin deposits within the aortic tissue of PPE operated WT (*n* = 4) and *Gp6*$^{-/-}$ (*n* = 4) mice at day 28 post surgery. Scale bars: 100 µm and 200 µm (overview). Data are represented as mean values ± SEM. Statistical analysis was performed using (**A**–**C, E**) an unpaired student's t-test and (**D**) a two-way ANOVA with a Sidak's multiple comparisons post-hoc test; A = Adventitia; H/E = Haematoxylin-eosin; L = Lumen; M = Media; MSB = Martius scarlet blue; PPE = Porcine pancreatic elastase (infusion); VVG = Verhoeff-van Gieson.

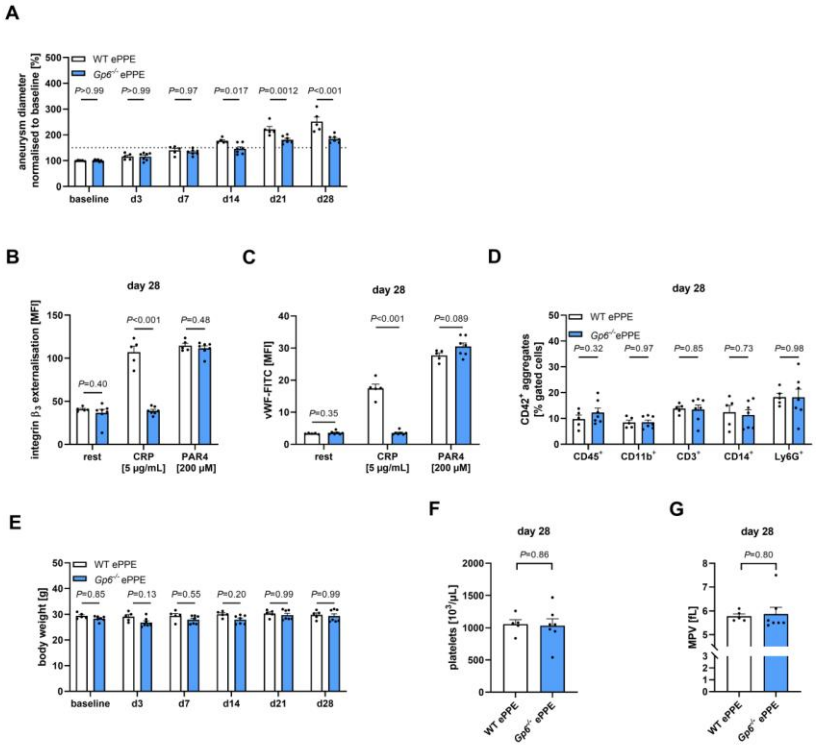


Figure S8. Integrin β_3 externalisation, vWF binding to platelets, body weight and, platelet count of GPVI deficient mice during ePPE induced AAA development. (**A**) Aortic diameter progression of WT (*n* = 5) and *Gp6*$^{-/-}$ (*n* = 7) ePPE mice over a time period of 28 days, analysed by ultrasound measurements. Data were normalised to baseline. (**B**) Integrin β_3 externalisation in ePPE operated WT (*n* = 5) and *Gp6*$^{-/-}$ (*n* = 7) mice at day 28 post surgery. Platelets were stimulated with indicated agonists. (**C**) VWF binding to platelets of ePPE-operated WT (*n* = 5) and *Gp6*$^{-/-}$ (*n* = 7) mice at day 28 post surgery. Platelets were stimulated with indicated agonists. (**D**) Aggregate formation of platelets with different leukocyte subtypes in ePPE operated WT (*n* = 5) and *Gp6*$^{-/-}$ (*n* = 7) mice at day 28 post surgery, analysed by flow cytometry. (**E**) Body weight of ePPE operated WT (*n* = 5) and *Gp6*$^{-/-}$ (*n* = 7) mice prior (baseline) and at day 3, 7, 14, 21, 28 post surgery. (**F** and **G**) Platelet count and MPV of WT (*n* = 5) and *Gp6*$^{-/-}$ (*n* = 7) ePPE mice at day 28. Data are represented as mean values ± SEM. Statistical analysis was performed using (**A** and **E**) a two-way ANOVA with a Sidak's multiple comparisons post-hoc test, (**B**–**D**) an unpaired multiple t-test and (**F** and **G**) an unpaired student's t-test. AAA = Abdominal aortic aneurysm; CRP = Collagen-related peptide; ePPE = External porcine

pancreatic elastase (application); MFI = Mean fluorescence intensity; MPV = Mean platelet volume; PAR4 = Protease-activated receptor 4 activating pepetide; vWF = von Willebrand factor.

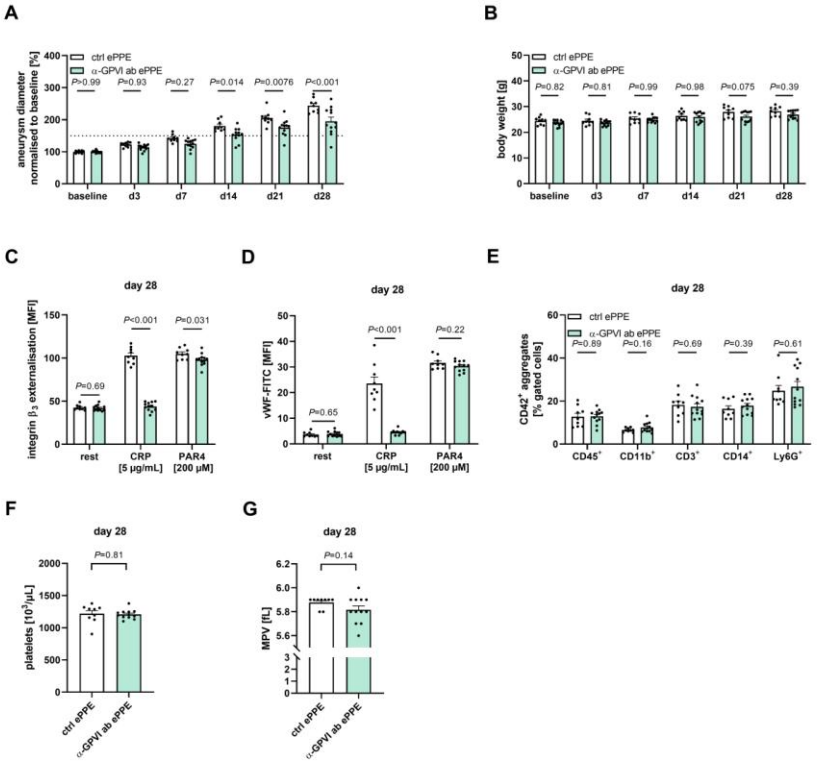
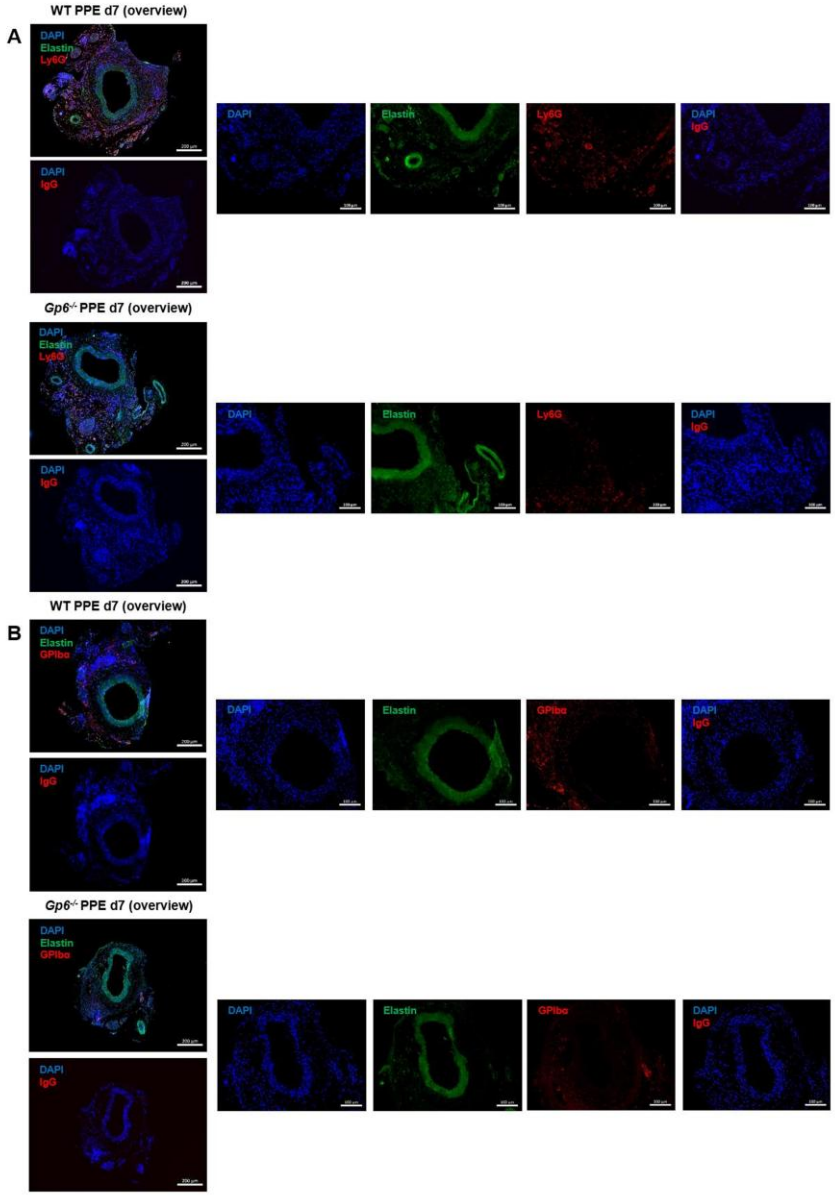


Figure S9. Body weight, platelet count, integrin β$_3$ externalisation and vWF binding to platelets of α-GPVI antibody treated mice during ePPE induced AAA development. (**A**) Aortic diameter progression of ctrl (*n* = 9) and α-GPVI antibody (10 mg/kg body weight, Fab Y020347, α-GPVI ab ePPE) treated (*n* = 12) ePPE mice over a time period of 28 days, analysed via ultrasound measurements. Data were normalised to baseline. (**B**) Body weight of of ctrl (*n* = 9) and α-GPVI ab (*n* = 12) ePPE mice prior (baseline) and at day 3, 7, 14, 21 and 28 post surgery. (**C**) Platelet integrin β$_3$ externalisation of ctrl (*n* = 9) and α-GPVI antibody treated (*n* = 12) ePPE mice at day 28 post surgery. Platelets were stimulated with indicated agonists. (**D**) VWF binding to platelets of ctrl (*n* = 9) and α-GPVI ab (*n* = 12) ePPE mice at day 28 post surgery. Platelets were stimulated with indicated agonists. (**E**) Aggregate formation of platelets with different leukocyte subtypes in ctrl (*n* = 9) and α-GPVI ab (*n* = 12) ePPE mice at day 28 post surgery, analysed by flow cytometry. (**F** and **G**) Platelet count and MPV of ctrl (*n* = 9) and α-GPVI antibody treated (*n* = 12) ePPE mice at day 28. Data are represented as mean values ± SEM. Statistical analysis was performed using (**A** and **B**) a two-way ANOVA

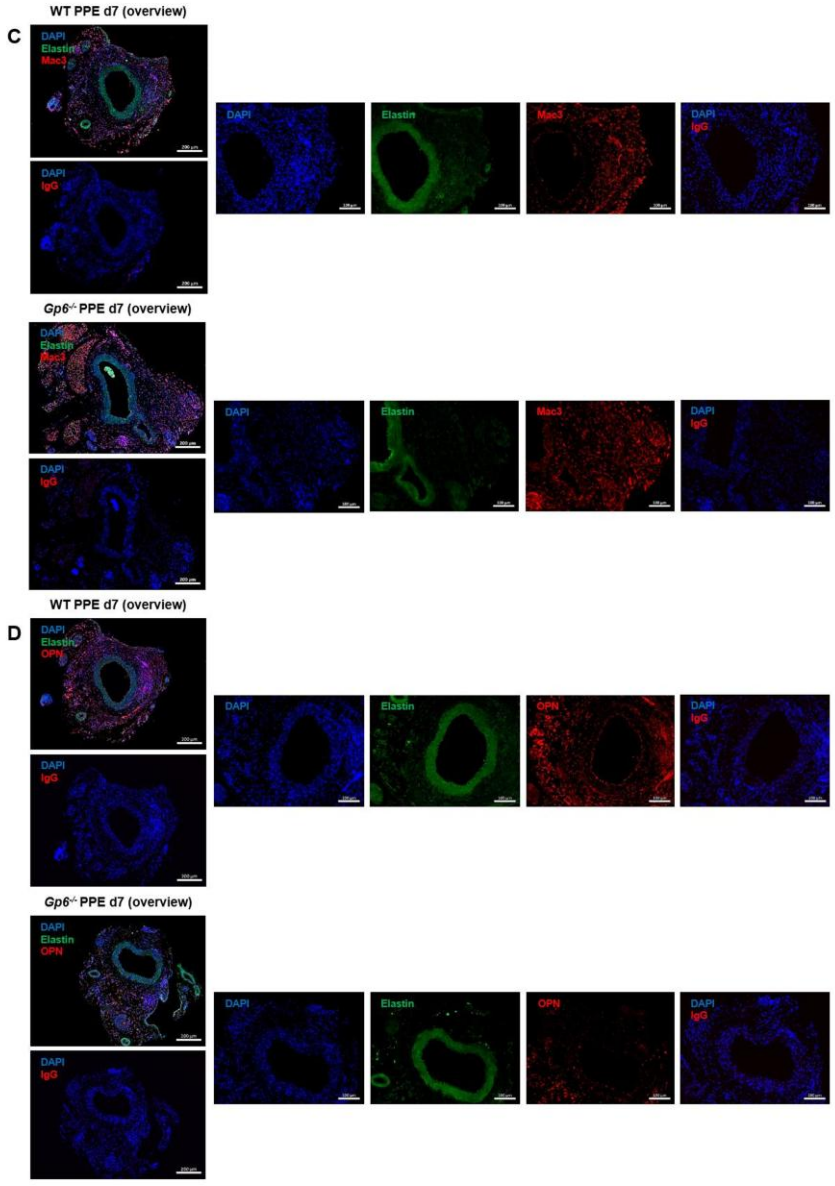
with a Sidak's multiple comparisons post-hoc test, (**C**–**E**) an unpaired multiple t-test and (**F** and **G**) an unpaired student's t-test. AAA = Abdominal aortic aneurysm; Ab = antibody; CRP = Collagen-related peptide; ePPE = External porcine pancreatic elastase (application); MFI = Mean fluorescence intensity; MPV = Mean platelet volume; PAR4 = Protease-activated receptor 4 activating peptide; vWF = von Willebrand factor.

GPVI in inflammation and ECM remodelling in AAA



16

GPVI in inflammation and ECM remodelling in AAA



17

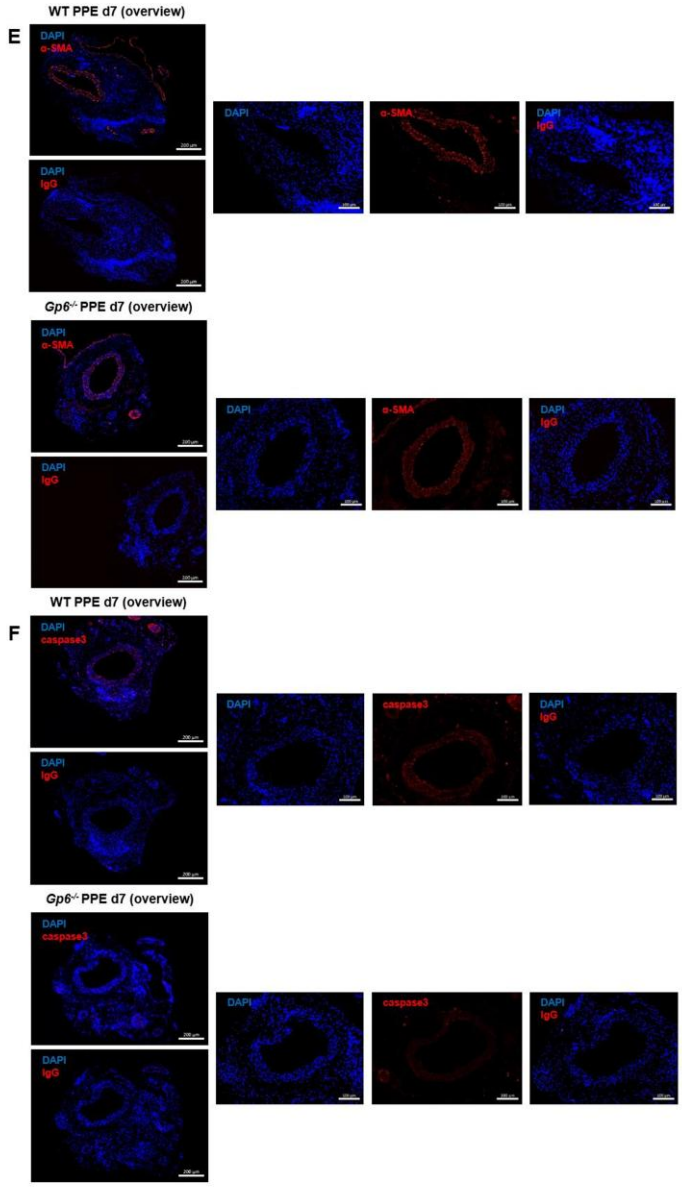


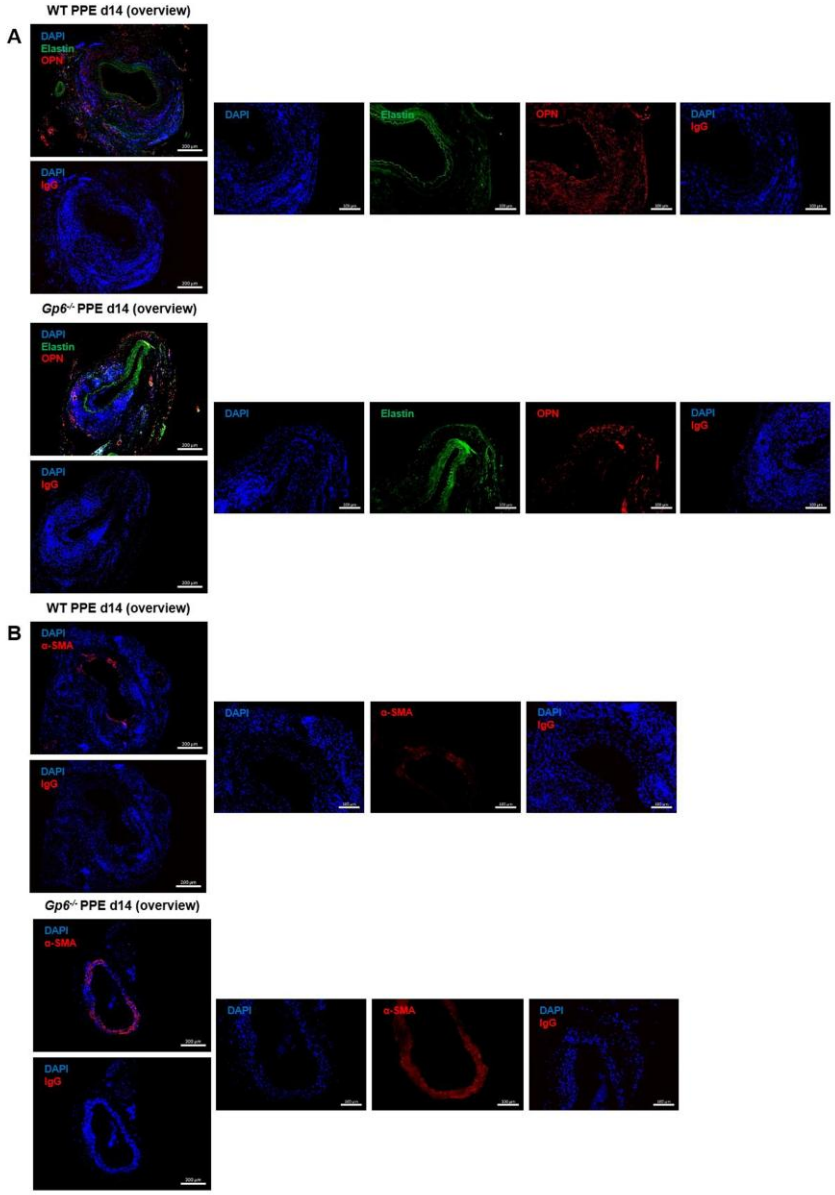
Figure S10. Immunofluorescence images of murine aortic tissue 7 days after experimental AAA induction. (**A**–**F**) Representative immunofluorescence overview (left) and single-channel images (right) with respective IgG controls of murine aortic tissue from

18

GPVI in inflammation and ECM remodelling in AAA

PPE operated WT (n = 5–6) and *Gp6*$^{-/-}$ (n = 4–5) mice at day 7. Aortic tissue was specifically stained for (**A**) neutrophils (anti-Ly6G/Cy3; red), (**B**) platelets (anti-GPIbα/Cy5; red), (**C**) macrophages (anti-Mac3/Cy5; red), (**D**) OPN (anti-OPN/Cy3; red), (**E**) α-SMA (anti-α-SMA/Cy3; red) or (**F**) active caspase3 (anti-cleaved caspase3/Cy3; red). Elastin autofluorescence (green) is shown, and nuclei were stained with DAPI (blue). Scale bars: 200 µm (overview) and 100 µm. OPN = Osteopontin; PPE = Porcine pancreatic elastase (infusion); SMA = Smooth muscle actin.

GPVI in inflammation and ECM remodelling in AAA



20

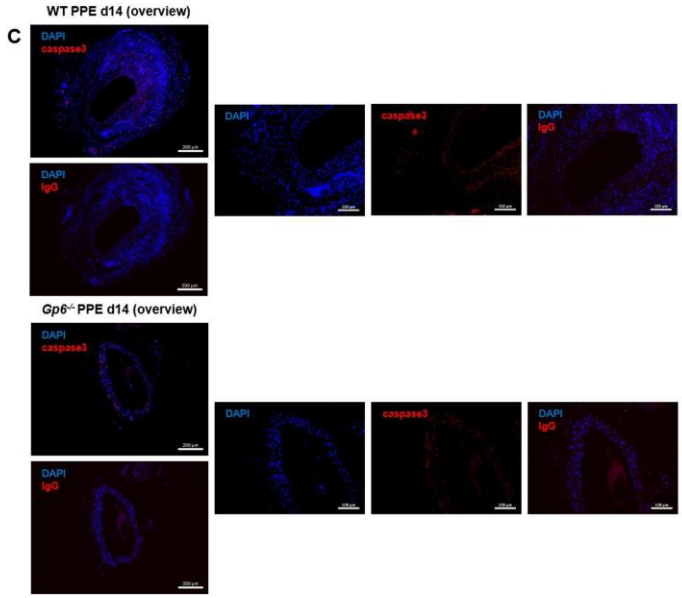


Figure S11. Immunofluorescence images of murine aortic tissue 14 days after experimental AAA induction. (**A**–**C**) Representative immunofluorescence overview (left) and single-channel images (right) with respective IgG controls of murine aortic tissue obtained from PPE operated WT (*n* = 5–6) and *Gp6*$^{-/-}$ (*n* = 4–5) mice at day 14. Aortic tissue was specifically stained for (**A**) OPN (anti-OPN/Cy3; red), (**B**) α-SMA (anti-α-SMA /Cy3; red) or (**C**) active caspase3 (anti-cleaved caspase3/Cy3; red). Elastin autofluorescence (green) is shown, and nuclei were stained with DAPI (blue). Scale bars: 200 µm (overview) and 100 µm. OPN = Osteopontin; PPE = Porcine pancreatic elastase (infusion); SMA = Smooth muscle actin.

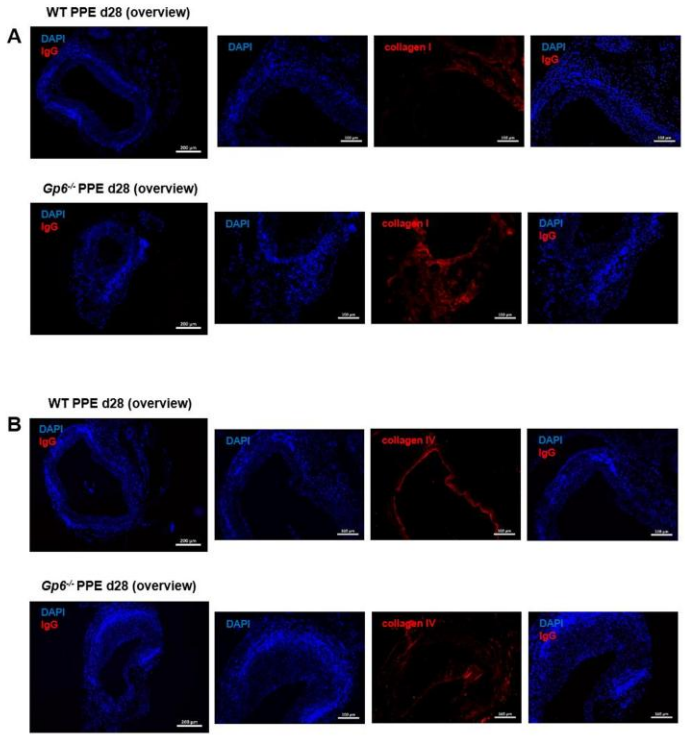


Figure S12. Immunofluorescence images of murine aortic tissue 28 days after experimental AAA induction. (**A** and **B**) Representative immunofluorescence overview (left) and single-channel images (right) with respective IgG controls of murine aortic tissue obtained from PPE operated WT ($n = 4$) and *Gp6*$^{-/-}$ ($n = 4–5$) mice at day 28. Aortic tissue was specifically stained for (**A**) collagen I (anti-collagen I/Cy3; red) and (**B**) collagen IV (anti-collagen IV/Cy3; red). Nuclei were stained with DAPI (blue). Scale bars: 200 µm (overview) and 100 µm. PPE = Porcine pancreatic elastase (infusion)

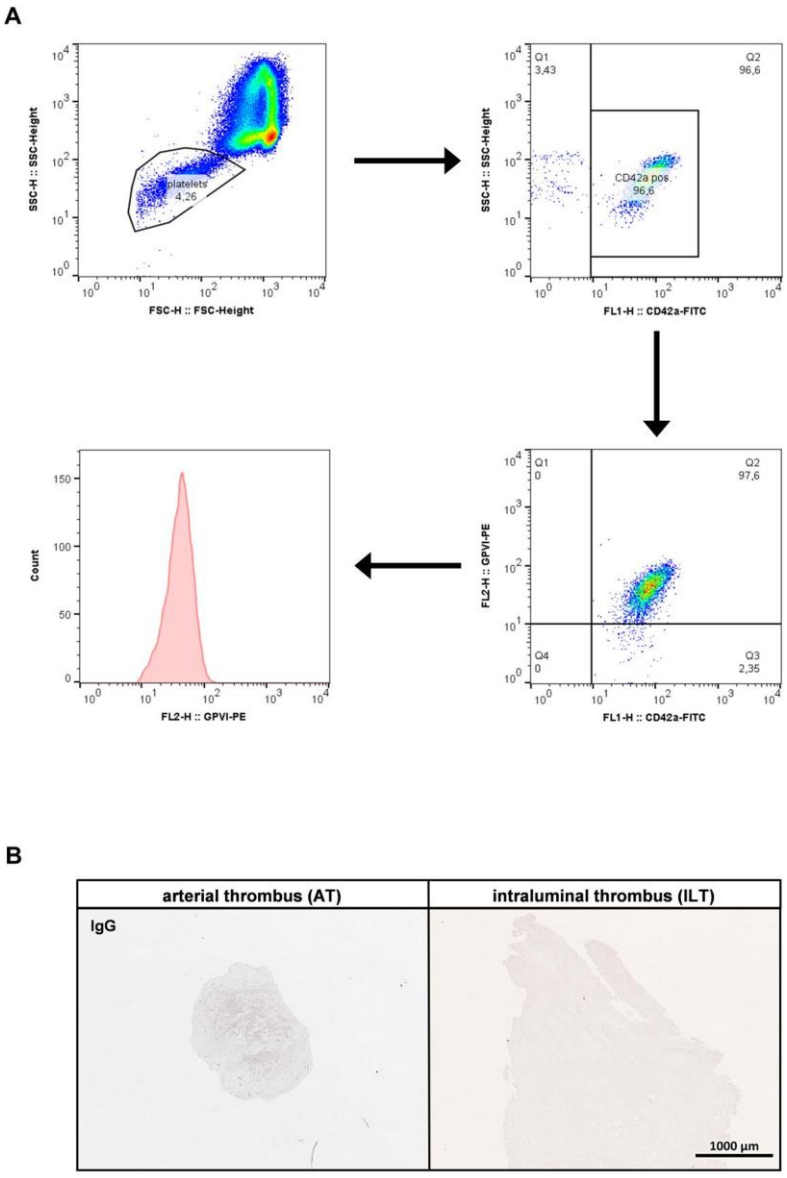


Figure S13. Gating strategy for flow cytometric analysis of AAA patients. (**A**) Gating strategy for analysing GPVI expression on platelets of AAA patients. Whole blood samples

were first gated on platelets according to their specific FSC/SSC profile. In addition, the platelet population was gated using the platelet specific marker GPIbα (CD42a) and a representative histogram for the GPVI expression on the platelet surface after gating is provided. (**B**) Representative images of IgG controls of immunohistochemically stained (platelets, anti-GPIbα) arterial thrombus (AT) tissue from thrombectomy patients (n = 8), respectively intraluminal thrombus (ILT) tissue samples from AAA patients (n = 12) samples. Scale bar: 1000 µm.

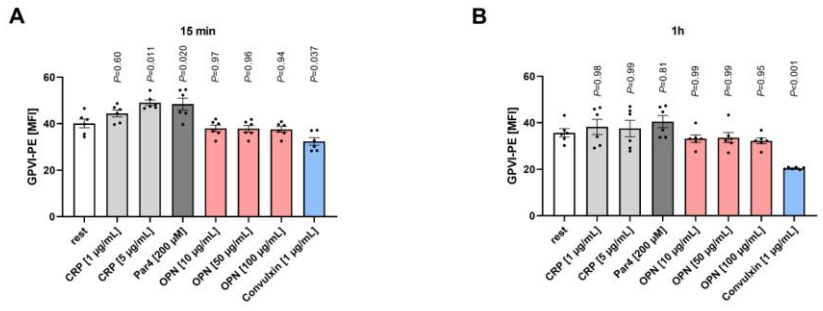


Figure S14. Full-length OPN does not induce GPVI shedding on platelets. (**A** and **B**) Platelet surface GPVI exposure in human whole blood samples after stimulation with different agonists (**A**) for 15 min and (**B**) for 1h, determined by flow cytometry (*n* = *6*). Data are represented as mean values ± SEM. Statistical analysis was performed using (**A** and **B**) a one-way ANOVA with a Tukey's multiple comparisons post-hoc test. *P*-values compared to resting. CRP = Collagen-related peptide; MFI = Mean fluorescence intensity; OPN = Osteopontin; PAR4 = Protease-activated receptor 4 activating peptide.

Table S1. Clinical parameter of AAA and thrombectomy patients. Continuous data are represented as mean ± SEM. Dichotomous data are represented as absolute frequency with percentage (%).

	Age [years]	Male sex	History of smoking	CHD	aHT	T2D	Obesity	Statins	SAPT	Antihypertensive drugs
AAA	78.0	87.5%	37.5 %	33.3 %	83.3 %	16.7 %	20.8 %	83.3 %	95.8 %	91.7 %
(n =24)	± 1.70	(21)	(9)	(8)	(20)	(4)	(5)	(20)	(23)	(22)
AT	74.1	37.5 %	25.0 %	62.5%	100 %	37.5%	12.5 %	62.5 %	75.0 %	100 %
(n =8)	± 2.65	(3)	(2)	(5)	(8)	(3)	(1)	(5)	(6)	(8)

AAA = abdominal aortic aneurysm; aHT = arterial hypertension; CHD = coronary heart disease; AT = Arterial thrombi (thrombectomy patients); SAPT = single anti-platelet therapy; T2D: type 2 diabetes.

Control whole blood samples were collected from anonymised healthy donors (average age: 60.1 ± 1.47 years) from the blood bank of the University Hospital Duesseldorf.

3. Major Resources Table

Animals (*in vivo* studies)

Species	Vendor or Source	Background Strain	Sex	Persistent ID / URL
Mouse	J. Ware (University of Arkansas for Medical Sciences, Little Rock, USA)/own breeding strain (animal facility of the Heinrich-Heine University Duesseldorf, Germany)	C57BL/6J;129-Gp6tm1ware	male	
Mouse	Janvier Labs	C57BL/6J	male	

Genetically Modified Animals

	Species	Vendor or Source	Background Strain	Other Information	Persistent ID / URL
Parent - Male	Mouse	J. Ware (University of Arkansas for Medical Sciences, Little Rock, USA)/own breeding strain (animal facility of the Heinrich-Heine University Duesseldorf, Germany)	C57BL/6J;129-Gp6tm1ware		
Parent - Female	Mouse	J. Ware (University of Arkansas for Medical Sciences, Little Rock, USA)/own breeding strain (animal facility of the Heinrich-Heine University Duesseldorf, Germany)	C57BL/6J;129-Gp6tm1ware		

Antibodies

Target antigen	Vendor or Source	Catalog #	Working concentration	Lot # (preferred but not required)	Persistent ID / URL
Active integrin $\alpha_{IIb}\beta_3$ (JON/A-PE)	Emfret Analytics	D200	1:10	IG	
Alexa Fluor™ Plus 555 conjugated secondary antibody	Invitrogen™	A32794	10 µg/mL	YH376319	
Alexa Fluor™ Plus 568 conjugated secondary antibody	Invitrogen™	A11077	10 µg/mL	2540882	
Biotinylated secondary antibody	Vector Laboratories	BA-9400	1:200	ZB1216	
Biotinylated secondary antibody	Vector Laboratories	BA-9200	1:300	ZH0318	
Caspase3 (casp3)	Cell Signaling	9661	1 µg/mL	47	
CD11b (M1/70-APC)	BD Biosciences	553312	20 µg/mL	2154242	
CD14 (Sa14-2-APC)	BioLegend	123311	20 µg/mL	B368460	
CD3 (17A2-APC)	BioLegend	100235	20 µg/mL	B402451	
CD45 (30-F11-APC)	BD Biosciences	559864	20 µg/mL	1145631	
Citrullinated histone H3 (citH3)	abcam	ab219407	4.4 µg/mL	1000318-10	

Collagen I (Col I)	abcam	ab270993	5.8 µg/mL	1007081-32	
Collagen IV (Col IV)	abcam	ab6586	11.7 µg/mL	1034101-8	
GPIbα (CD42b, Xia.G5-PE)	Emfret Analytics	M040-2	1:10	0402-C	
GPIbα (CD42b)	Emfret Analytics	M042-0	10 µg/mL	0420-B	
GPIbα (CD42b)	Invitrogen™	MA5-11642	2 µg/mL	WC3211061	
GPIX (GP9)	biorbyt	orb167288	1:50	V2116	
GPVI (Fab Y020347)	AdvanceCOR GmbH	n/a	10 mg/kg body weight	n/a	
GPVI (JAQ1-FITC)	Emfret Analytics	M011-1	1:10	0111-C	
GPVI (HY101-PE)	BD Pharmingen™	565241	10 µg/mL	1271934	
Integrin α_5 (CD49e, Tap.A12-FITC)	Emfret Analytics	M080-1	1:10	0801-B	
integrin β_3 (CD61, Luc.H11-FITC)	Emfret Analytics	M031-1	1:10	0311-C	
Ly6G (1A8-APC)	BioLegend	127614	20 µg/mL	B322683	
Ly6G (1A8)	BD Pharming™	551459	10 µg/mL	6021908	
Mac3 (CD107b)	BD Pharmingen™	550292	0.6 µg/mL	2182319	
Mouse IgG isotype control	Cell Signaling Technology	5415S	2 µg/mL	10	
Osteopontin (OPN)	abcam	ab181440	20 µg/mL	GR3401503-2	
PS exposure (Cy™ 5 AnnexinV)	BD Bioseciences	559934	6 µg/mL	3261734	
PS exposure (AF647 AnnexinV)	Invitrogen™	A23204	1:20	2604401	
P-selectin (CD62P, Wug.E9-FITC)	Emfret Analytics	D200	1:10	IG	
Rabbit IgG isotype control	Cell Signaling	3900S	5 µg/mL	7131507	
Rat IgG isotype control	Emfret Analytics	C301	10 µg/mL	301-N	
Smooth muscle actin (αSMA)	abcam	ab5694	4 µg/mL	GR3356867-3	
Streptavidin eFluorTM 660 conjugate	Thermo Fisher Scientific	50-4317-80	10 µg/mL	2547666	
vWF-FITC	Emfret Analytics	P150-1	1:10	1501-A	

DNA/cDNA Clones

Clone Name	Sequence	Source / Repository	Persistent ID / URL
None			

Cultured Cells

Name	Vendor or Source	Sex (F, M, or unknown)	Persistent ID / URL
None			

Data & Code Availability

Description	Source / Repository	Persistent ID / URL
None		

Other

Description	Source / Repository	Persistent ID / URL
Adenosine diphosphate (ADP)	Sigma-Aldrich	A2754
AF546 fibrinogen	Invitrogen™	F13192
avidin-biotinylated HRP enzyme complex	Vector Laboratories	PK-6100
Bouin's Solution	Sigma-Sldrich	HT10132
Collagen (Horm® collagen reagent)	Takeda Austria GmbH	1130630
Collagen-related peptide (CRP)	Richard Farndale, University of Cambridge, Cambridge, UK	N/A
Convulxin (Cvx)	Enzo Life Sciences	ALX-350-100-C050
DAPI (4′, 6-Diamidine-2′-phenylindole dihydrochloride)	Roche	10236276001
DiCO6	Sigma-Aldrich	D273
Elastase from porcine pancreas	Sigma-Aldrich	E1250-100MG
Flow cytometry-based bead multiplex analysis (LEGENDplex™ Mouse Inflammation panel [13-plex])	BioLegend	740150
heparin solution,	Braun	2047217
Human fibrin ELISA	MyBioSource	MBS265263
Human soluble GPVI ELISA	MyBioSource	MBS9390142
Mepacrine	Sigma-Aldrich	N/A
Methyl blue	Sigma-Aldrich	M5528
Methyl green	Vector Laboratories	H-3402
Murine citH3 ELISA	MyBioSource	MBS7273794
Murine MMP2 ELISA	R&D Systems	MMP200
Murine MMP9 ELISA	R&D Systems	MMPT90
Murine neutrophil elastase (ELA2) ELISA	R&D Systems	DY4517-05
Murine OPN ELISA	R&D Systems	DY441
Murine sGPVI ELISA	MyBioSource	MBS109240
Naphthol yellow S	anta Cruz Biotechnology	sc-215544
Osteopontin (OPN)	PeproTech	120-35,
PAR4 peptide (PAR4)	Tocris	3494
paraffin	Sigma-Aldrich	P3558
Phosphotungstic acid	Merck Millipore	100583
Protein blocking solution	Dako	X0909
Roti®-Histokitt mounting medium	Sigma-Aldrich	M5528
thromboxane A2 analogue U46619 (U46)	Tocris	1932
Verhoeff-van Gieson (Elastic stain)	Sigma-Aldrich	HT25A-1KT
VIP peroxidase substrate	Vector Laboratories	SK-4600
β-Aminopropionitrile (BAPN)	Sigma-Aldrich	A3134-25G

4. ARRIVE GUIDELINES

The ARRIVE guidelines (https://arriveguidelines.org/) are a checklist of recommendations to improve the reporting of research involving animals. Key elements of the study design should be included below to better enable readers to scrutinize the research adequately, evaluate its methodological rigor, and reproduce the methods or findings.

Study Design

Groups	Sex	Age	Number (prior to experiment)	Number (after termination)	Littermates (Yes/No)	Other description
Gp6$^{+/+}$ (WT) PPE	male	10-12 weeks	38	32	No	
Gp6$^{-/-}$ PPE	male	10-12 weeks	37	27	No	
Gp6$^{+/+}$ (WT) ePPE	male	10-12 weeks	6	5	No	
Gp6$^{-/-}$ ePPE	male	10-12 weeks	7	7	No	
sham (C57BL/6J)	male	10-12 weeks	16	16	No	
ePPE (C57BL/6J)	male	10-12 weeks	20	17	No	
Ctrl ePPE (C57BL/6J)	male	10-12 weeks	10	9	No	
α-GPVI ePPE (C57BL/6J)	male	10-12 weeks	12	12	No	

Sample Size: Please explain how the sample size was decided Please provide details of any a *prior* sample size calculation, if done.

Statistical analysis was performed on 5-17 biological replicates per condition. No sample size calculation was conducted prior experimental procedures.

Inclusion Criteria

N/A

Exclusion Criteria

N/A

Randomization

For *in vivo* studies all animals were randomly allocated into the different experimental groups

Blinding

For data analysis and evaluation, as well as the generation of *in vivo* data, all users were blinded to the treatment

3.3 Revacept (GPVI-FC) treatment attenuates experimental induced abdominal aortic aneurysm formation in mice

Since the AAA pathology is mainly driven by the asymptomatic, progressive dilation of the abdominal aorta, the risk of a fatal aortic rupture increases over time. When the aortic diameter progression exceeds pre-defined clinical threshold values, surgical intervention —either by OAR or EVAR— represents the only available treatment option. To date no drug-based therapy targeting aneurysm growth and thereby AAA progression is available. Although several promising candidates for potential drug-based approaches have been evaluated throughout the last years. However, their clinical translation is still lacking and remains challenging. Different clinical trials of drug-based therapies failed, as the primary endpoint of effectively targeting AAA growth and progression was not reached. Therefore, testing of potential candidates in *in vivo* animal models of experimental induced AAA formation is still of great importance, in order to identify novel targets for the development of pharmacological therapies targeting AAA progression [124].

As previously described (**Section 3.2**), a first translational approach by targeting GPVI-signalling in platelets via a GPVI-blocking antibody *in vivo* revealed a beneficial effect on experimental induced AAA formation in mice [248]. Based on these findings, we next focused on another promising candidate targeting GPVI-signalling by investigating the potential of Revacept to effectively address aneurysm growth *in vivo*. Revacept is a dimeric fusion protein consisting of a Fc fragment fused to endogenous platelet GPVI (GPVI-Fc). Mechanistically, after a vessel wall injury Revacept binds to the exposed collagen, thus preventing GPVI-binding to collagen and therefore GPVI-mediated platelet activation, aggregation and platelet recruitment (**Figure 11**). Besides collagen, Revacept is capable of binding additional extracellular matrix proteins including vitronectin, laminin and fibronectin. In addition, Revacept prevents VWF-binding to collagen, thereby avoiding GPIb-mediated platelet activation [78, 79, 250-252].

Since Revacept exclusively binds to exposed ECM proteins and not to platelet surface receptors, platelet function seems to be unaffected. An initial clinical phase I study (trial registration: NCT01042964) revealed no notable off target effects following Revacept application in healthy volunteers [253]. However, platelet aggregation was sufficiently targeted, while haemostasis, platelet counts as well as bleeding time were unaltered. Beyond this, in randomised phase II clinical trials Revacept showed a beneficial effect in symptomatic carotid artery stenosis patients (trial registration: NCT01645306) [116, 120], while no improvement in stable coronary heart disease patients was observed (trial registration: NCT 03315285) [254, 255]. In order to evaluate the potential of Revacept as a novel antiplatelet therapy targeting AAA progression in a

preclinical setting, Revacept was analysed in regard to aneurysm growth and platelet function in experimental induced AAA formation, utilising the ePPE mouse model.

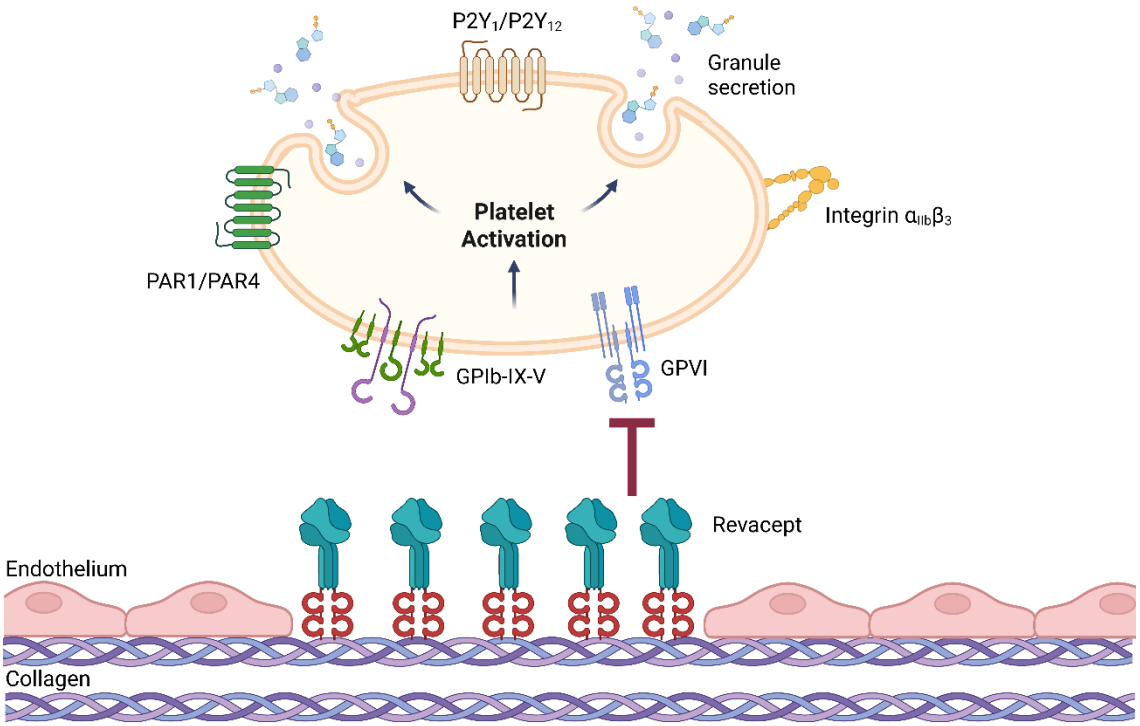


Figure 11. Revacept: Mechanism of action. Revacept is a fusion protein consisting of a Fc fragment fused to endogenous platelet GPVI (GPVI-Fc). GPVI represents the main collagen receptor on the platelet surface. Revacept binds to the exposed collagen of the ECM, thus preventing GPVI-binding to collagen and therefore GPVI-mediated platelet activation, aggregation and platelet recruitment. Beside collagen, Revacept binds further ECM proteins including vitronectin, laminin and fibronectin. In addition, Revacept prevents VWF-binding to collagen, thereby avoiding GPIb-mediated platelet activation. Since Revacept exclusively binds to exposed ECM proteins and not to platelet surface receptors, platelet function is unaffected. ECM = Extracellular matrix; GP = Glycoprotein; Par = Protease-activated receptor; VWF = Von Willebrand factor (created with BioRender.com).

3.3.1 Humanised GPVI mice revealed an unaltered aortic diameter under naive conditions

For analysing the potential of Revacept as a novel antiplatelet therapy targeting AAA in a preclinical setting, humanised (*h*)*Gp6*$^{+/+}$ mice were used. These mice exhibit the human GPVI receptor on the platelet surface and were analysed in the following experiments in order to reflect the situation in human AAA patients as close as possible. Therefore, this mouse line was characterised in a first step in regard to basal platelet function, as well as *ex vivo* thrombus formation. C57BL/6N mice, exhibiting the murine GPVI receptor on the platelet surface, served as WT controls. Data revealed unaltered platelet, RBC and white blood cell (WBC) counts

(**Section 6.1, Figure S2**) and only minor differences in platelet degranulation (**Section 6.1, Figure S3A**, P-selectin), respectively integrin $\alpha_{IIb}\beta_3$ activation (**Section 6.1, Figure S3B**, JON/A) upon GPVI stimulation with low-dose of CRP. In addition, *hGp6*$^{+/+}$ mice showed an increased procoagulant activity, indicated by an enhanced AnnexinV-binding, under resting conditions and after CRP stimulation (**Section 6.1, Figure S4A**). The glycoprotein exposition on the platelet surface of *hGp6*$^{+/+}$ mice revealed no major differences compared to the respective WT controls. However, the GPIX receptor, part of the GPIb-V-IX complex, was found to be slightly elevated in *hGp6*$^{+/+}$ mice (**Section 6.1, Figure S5A**). Flow cytometric analysis further revealed unaltered CD40L exposition, as well as VWF-binding to platelets from *hGp6*$^{+/+}$ mice (**Section 6.1, Figure S6A**). In addition, *ex vivo* thrombus formation analysed via flow chamber experiments showed no significant differences in surface coverage or thrombus volume (**Section 6.1, Figure S7A**). However, thrombi from *hGp6*$^{+/+}$ mice revealed an enhanced procoagulant activity for incorporated cells compared to WT mice, matching the enhanced PS exposure of resting platelets in these mice analysed via flow cytometry (**Section 6.1, Figure S4A** and **S7B**).

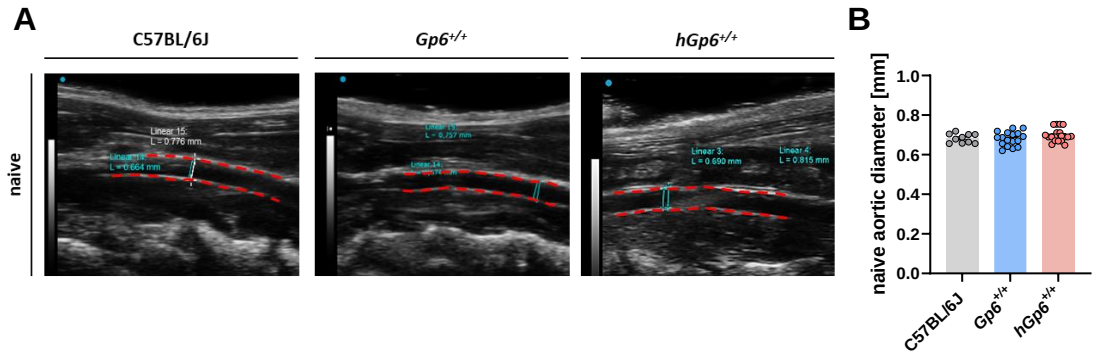


Figure 12. Humanised GPVI mice revealed an unaltered aortic diameter under naive conditions. (**A**) Representative ultrasound images of naive (unoperated) C57BL/6J and *Gp6*$^{+/+}$ (both exhibiting murine GPVI on the platelet surface), respectively humanised (*h*)*Gp6*$^{+/+}$ mice. (**B**) Aortic diameter of naive C57BL/6J (*n* = 10), *Gp6*$^{+/+}$ (*n* = 17) and *hGp6*$^{+/+}$ (n = 21) mice, analysed via ultrasound measurements. Data are represented as mean values ± SEM. Statistical analysis was performed using (**B**) a one-way ANOVA with a Tukey's multiple comparison post-hoc test.

Prior to investigating the effect of Revacept on aortic diameter progression in experimental induced AAA formation, the aortic diameter of naive *hGp6*$^{+/+}$ mice was analysed, in order to secure unaffected naive aortic diameter after genetically induced human GPVI expression. Therefore, naive *hGp6*$^{+/+}$ mice were compared to C57BL/6J and *Gp6*$^{+/+}$ which both exhibit the murine GPVI receptor on the platelet surface (**Figure 12**). Ultrasound measurements

(**Figure 12A**) revealed an unaltered inner aortic diameter of *hGp6*$^{+/+}$ mice in comparison to both control groups of C57BL/6J, respectively *Gp6*$^{+/+}$ mice (**Figure 12B**).

3.3.2 Revacept treatment attenuates aortic diameter progression in ePPE induced AAA formation

In order to evaluate whether Revacept has the potential to act as a novel drug-based therapy targeting AAA progression, experimental AAA formation was induced using the ePPE mouse model. For this first translational approach, *hGp6*$^{+/+}$ mice underwent ePPE surgery and subsequently received a Revacept injection (GPVI-Fc, ePPE Revacept) every 2–3 days over a time course of 28 days, starting 12 h prior surgery. Mice that received a vehicle control (ePPE ctrl.) served as a control group (**Figure 13A**).

The overall survival rate over the whole observation period of 28 days revealed no significant differences between Revacept treated and control ePPE mice (**Figure 13B**). This indicates, that long-term *in vivo* Revacept application does not negatively affect the survival probability after experimental AAA induction in mice. To investigate whether Revacept treatment attenuates the aneurysm growth, the aortic diameter expansion was monitored once a week over the whole observation period of 28 days via ultrasound measurements (**Figure 13C**). Thereby, Revacept treatment resulted in a significantly reduced dilation of the inner aortic diameter at days 21 and 28 post ePPE surgery (**Figure 13D** and **E**). However, the AAA incidence, showed only a moderate but not significant decrease to 88.8% in Revacept treated mice. In comparison, 100% of ePPE operated mice that received the vehicle control developed an aneurysm at day 28. (**Figure 13F**) Thereby, the AAA incidence is defined by an inner aortic diameter of ≥ 150% at the observation endpoint of 28 days. However, analysis of the AAA severity at day 28 revealed that ePPE operated control mice showed moderate (200-250% of aortic diameter expansion) or severe aneurysms (250–300% of aortic diameter expansion), while Revacept treated mice predominantly exhibited mild (150–200% of aortic diameter expansion) and to a lower extent moderate (200–250% of aortic diameter) aneurysms (**Figure 13G** and **H**).

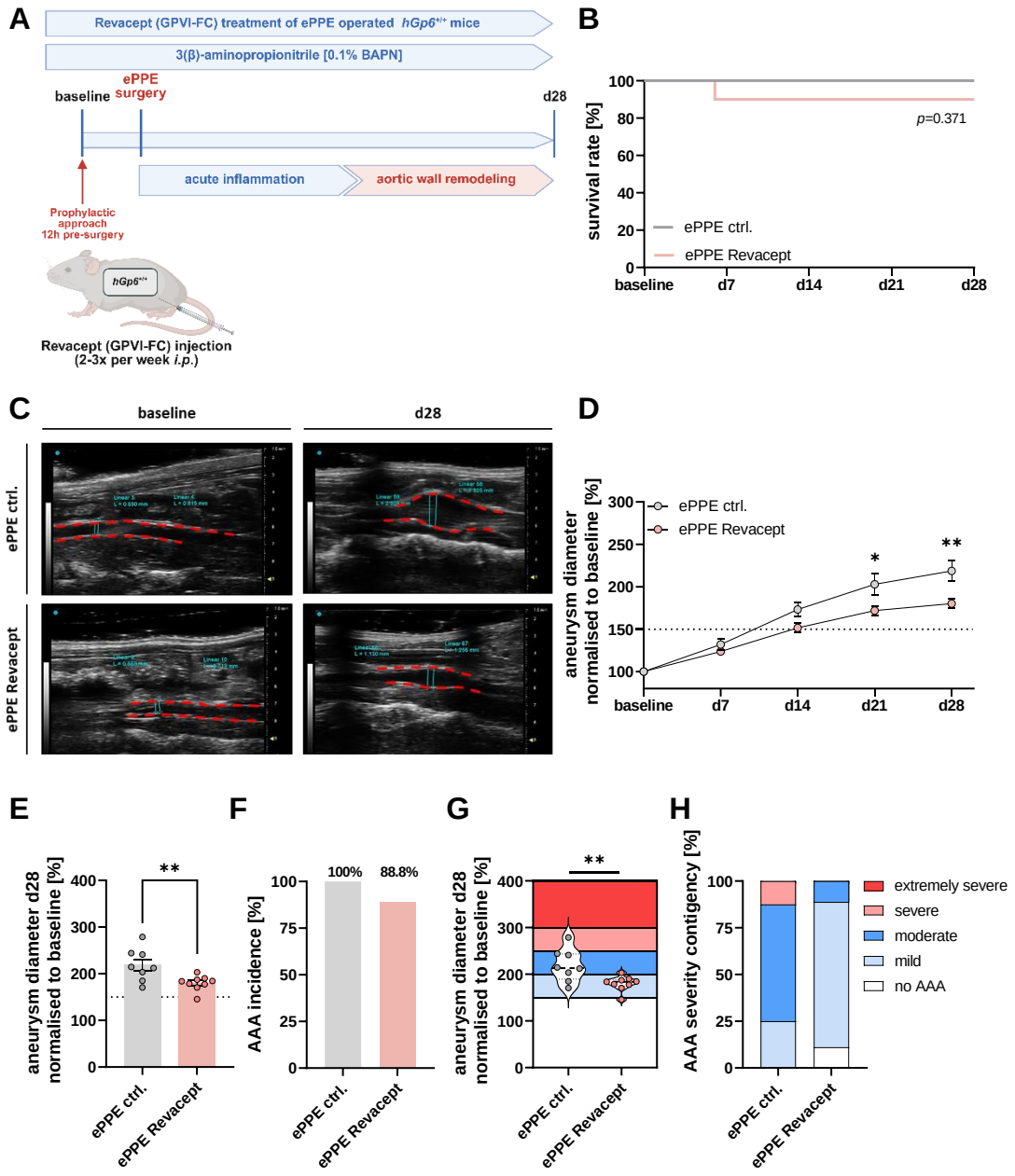


Figure 13. Revacept treatment attenuates aortic diameter progression in ePPE induced AAA progression. (**A**) Schematic overview of experimental procedure: humanised (*h*)*Gp6*$^{+/+}$ mice underwent ePPE surgery and received Revacept (10 mg/kg body weight, GPVI-Fc, ePPE Revacept) or a respective vehicle control (ePPE ctrl) over a time course of 28 days. Mice were injected every 2–3 days, starting 12 h before surgery. (**B**) Survival rate of ePPE operated ctrl (n = 8) and Revacept treated (n = 10) mice over a time period of 28 days. (**C**) Representative ultrasound images of ctrl (n = 8) and Revacept treated (n = 9) ePPE mice before (baseline) and 28 days after surgery. (**D**) Aortic diameter progression of ctrl (n = 8) and Revacept treated (n = 9) ePPE mice over a time period of 28 days. Data were normalised to baseline. (**E**) Aneurysm diameter of ePPE ctrl (n = 8) and Revacept treated (n = 9) mice at day 28. Data were normalised to baseline. (**F**) AAA incidence of ctrl (n = 8) and Revacept treated (n = 9) ePPE mice revealing an aortic diameter of ≥ 150% at day 28. (**G** and **H**) AAA severity contingency of ctrl (n = 8) and Revacept treated (n = 9) ePPE mice at day 28. Data are represented as mean values ± SEM. Statistical analysis was performed using (**B**) a Log-rank (Mantel-Cox) test, (**D**) RM two-way ANOVA with a Sidak's multiple comparison post-hoc test, (**E** and **G**) an unpaired student's t-test and (**F**) a Fisher's exact-test. *p < 0.05, **p < 0.01. AAA = Abdominal aortic aneurysm; ctrl = Control; ePPE = External porcine pancreatic elastase (application); *i.p.* = Intraperitoneal.

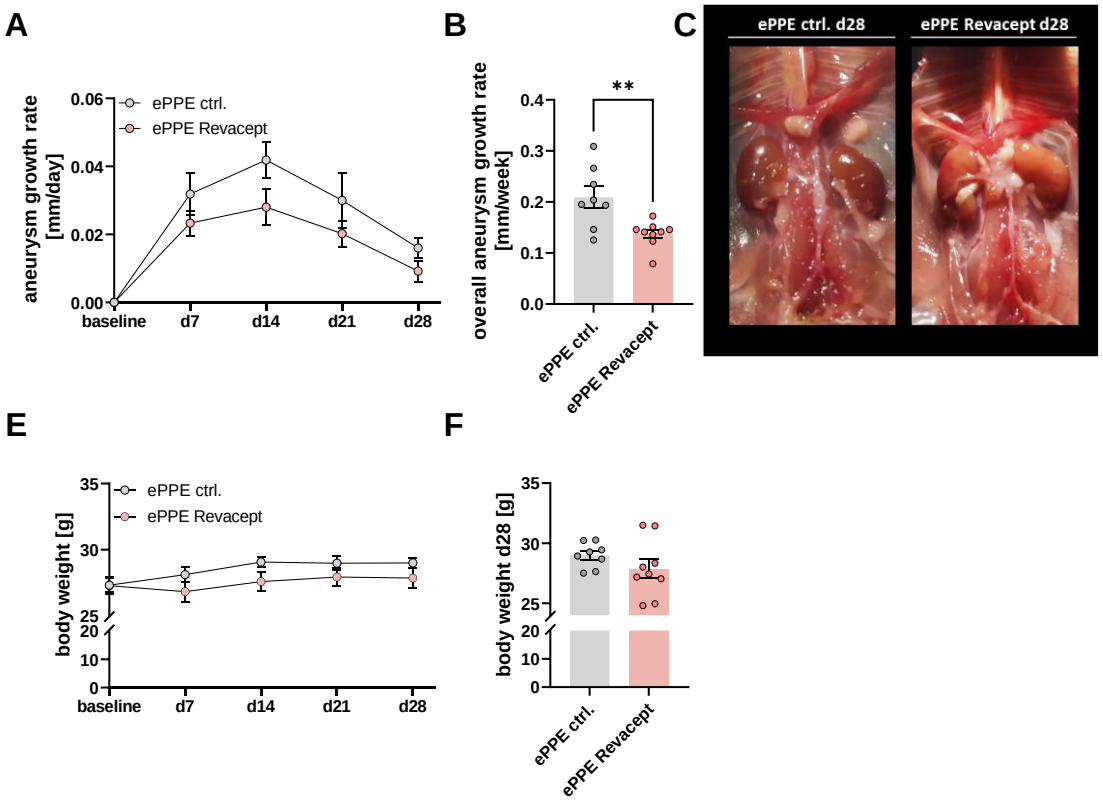


Figure 14. Revacept treatment leads to reduced aneurysm growth rates in ePPE induced AAA progression. (**A**) Aneurysm growth rate (mm/day) of ctrl (*n* = 8) and Revacept treated (*n* = 9) ePPE mice over a time period of 28 days, analysed via ultrasound measurements. (**B**) Overall aneurysm growth rate (mm/week) ctrl (*n* = 8) and Revacept treated (*n* = 9) mice. Data were normalised to baseline. (**C**) Representative images of the aortic tissue of ctrl (*n* = 8) and Revacept treated (*n* = 9) ePPE mice at day 28. (**E**) Body weight progression of ctrl (*n* = 8) and Revacept treated (*n* = 9) ePPE mice over a time course of 28 days. (**F**) Body weight of ctrl (*n* = 8) and Revacept treated (*n* = 9) ePPE mice at day 28. Data are represented as mean values ± SEM. Statistical analysis was performed using (**A** and **E**) a RM two-way ANOVA with a Sidak's multiple comparison post-hoc test, (**B** and **F**) an unpaired student's t-test. ***p* < 0.01. AAA = Abdominal aortic aneurysm; ctrl = Control; ePPE = External porcine pancreatic elastase (application).

However, the body weight progression of ePPE operated mice was not affected by Revacept over a time course of 28 days, when compared to the control group (**Figure 14E** and **F**). Additionally, the blood cell counts of circulating cells were analysed in Revacept treated ePPE mice at day 28 post surgery (**Figure 14**).

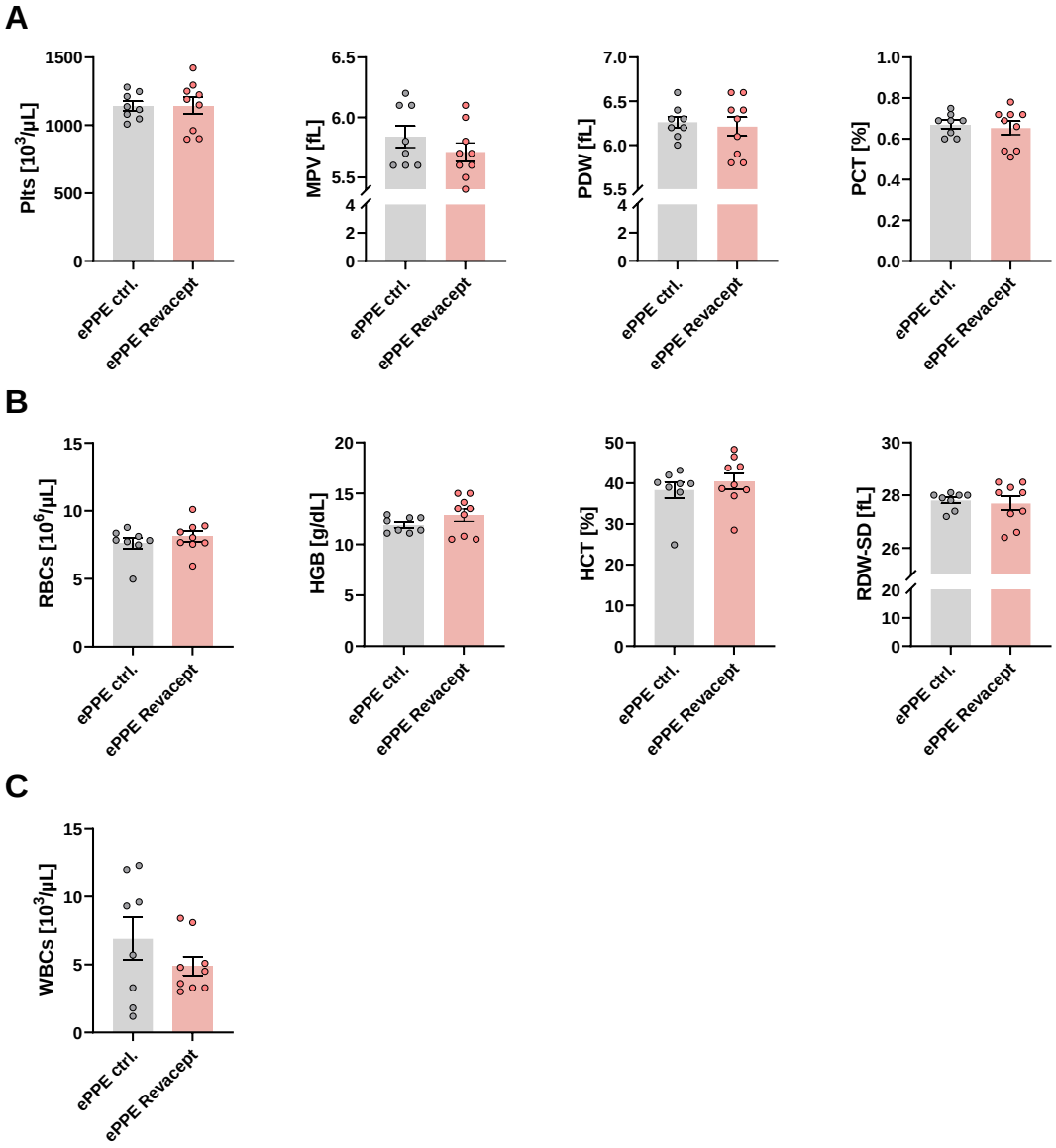


Figure 15. Platelet, RBC and WBC counts of Revacept treated mice are unaltered at day 28 post ePPE surgery. (**A**) Platelet counts and platelet specific blood parameters of whole blood samples from of ctrl (*n* = 8) and Revacept treated (*n* = 9) ePPE mice at day 28 post surgery. (**B**) RBC counts and RBC specific blood parameters of ctrl (*n* = 8) and Revacept treated (*n* = 9) ePPE mice at day 28 post surgery. (**C**) WBC counts of ctrl (*n* = 8) and Revacept treated (*n* = 9) ePPE mice at day 28. Data are represented as mean values ± SEM. Statistical analysis was performed using (**A**–**C**) an unpaired student's t-test. AAA = Abdominal aortic aneurysm; ctrl = Control; ePPE = External porcine pancreatic elastase (application); HCT = Haematocrit; HGB = Haemoglobin; MPV = Mean platelet volume; PCT = Plateletcrit; PDW = Platelet distribution width; Plts = Platelets; RBCs = Red blood cells; WBCs = White blood cells; RDW = Red blood cell distribution width.

Thereby, neither platelet count, nor platelet-related blood parameters, including the mean platelet volume (MPV), platelet distribution width (PDW) and the plateletcrit (PCT) were altered at day 28 in Revacept treated ePPE mice, compared to the respective control mice (**Figure 15A**). However, this finding is in line with the results from the previously mentioned initial clinical

phase I study, where no effects of Revacept on the platelet count in healthy volunteers was reported [253]. Moreover, the number of circulating RBCs and the RBC-related parameters including Haematocrit (HCT), Haemoglobin (HGB) Red blood cell distribution width (RDW) were unaltered (**Figure 15B**). In line with these results, the WBC counts of Revacept treated ePPE mice were unaffected in, when compared to the control group as well (**Figure 15C**).

3.3.3 Revacept does not affect platelet degranulation and integrin $\alpha_{IIb}\beta_3$ activation in experimental AAA formation

As recently published by Wagenhäuser *et al*., platelet activation was shown to be affected during AAA formation and progression in both human and mice. Thereby, platelet from AAA patients revealed a pre-activated state under resting conditions, as well as an enhanced activation profile after GPVI stimulation with low-doses of CRP. These findings of an enhanced GPVI-mediated platelet activation were also reflected in murine platelets, which underwent PPE surgery [256]. In order to investigate whether Revacept application affects the platelet activation profile in mice after experimental AAA induction, platelet degranulation (**Figure 16A**, P-selectin) as well as integrin $\alpha_{IIb}\beta_3$ activation (**Figure 16B**, JON/A) were analysed at day 28 post ePPE surgery. Flow cytometric analysis revealed no significant differences in regard to platelet degranulation (**Figure 16A**) and integrin $\alpha_{IIb}\beta_3$ activation (**Figure 16B**) in Revacept treated ePPE mice after platelet stimulation with various agonists. Thereby, GPVI-mediated platelet activation, as well as G-protein coupled receptor signalling via $P2Y_{12}$ or PAR4 were unaltered 28 days after AAA induction between both groups. These results indicate, that Revacept treatment does not negatively affect platelet activation during AAA formation, which results in a normal haemostasis *in vivo*.

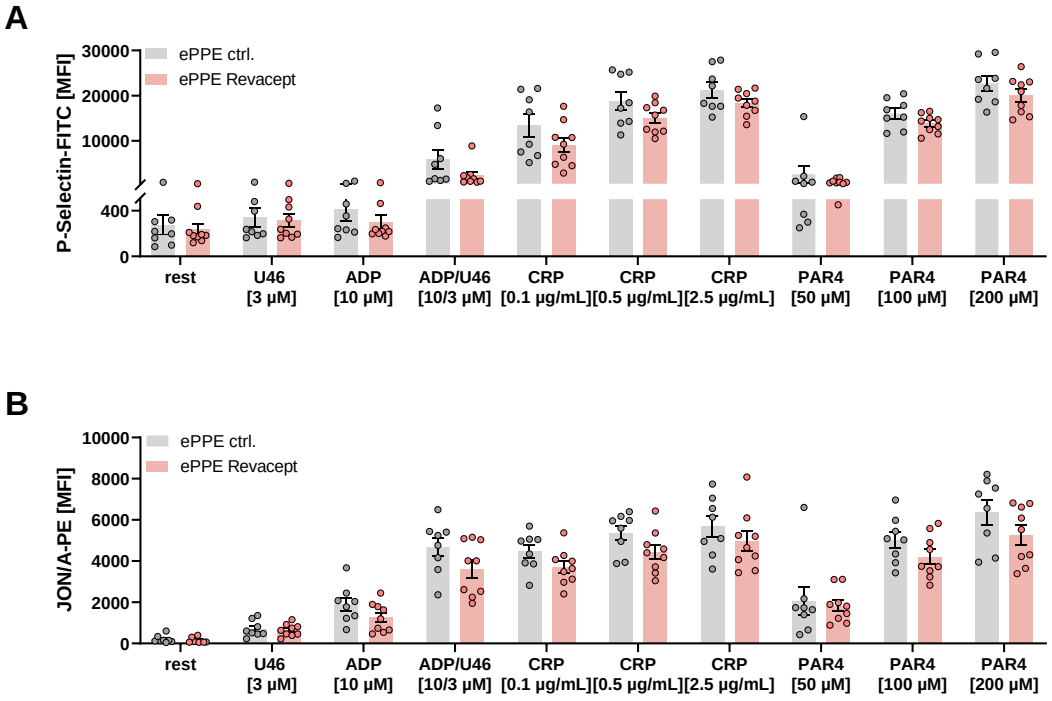


Figure 16. Treatment with Revacept leads to unaltered platelet activation in ePPE operated mice. (**A** and **B**) Washed murine whole blood from ePPE operated ctrl and Revacept treated mice was analysed via flow cytometry. (**A**) Platelet degranulation (P-selectin-FITC) and (**B**) active integrin $\alpha_{IIb}\beta_3$ (JON/A-PE) of ctrl (*n* = 8) and Revacept treated (*n* = 9) ePPE mice at day 28 post surgery. Platelets were stimulated with indicated agonists. Data are represented as mean values ± SEM. Statistical analysis was performed using (**A** and **B**) an unpaired multiple t-test. ADP = Adenosine diphosphate; CRP = Collagen-related peptide; ctrl = Control; ePPE = External porcine pancreatic elastase (application); MFI = Mean fluorescence intensity; PAR4 = Protease-activated receptor 4 activating peptide; U46619 (U46) = Thromboxane A_2 analogue; rest = resting.

Next, the glycoprotein exposition on the platelet surface at day 28 after experimental induced AAA formation was analysed via flow cytometry. Thereby, Revacept treated ePPE mice revealed a significantly reduced GPVI exposition on the platelet surface, compared to the respective control mice (**Figure 17A** and **E**). As integrins play a pivotal role within the process of haemostasis by mediating platelet activation, adhesion and aggregation, the integrin surface exposition in Revacept treated ePPE mice was analysed additionally. Thereby, the integrin $\alpha_{IIb}\beta_3$ only showed a moderate reduction by trend, which did not reach significance (p=0.078), while exposition of the integrins α_2, α_5 and the integrin β_3 subunit was unaltered (**Figure 17A**). As described previously, the GPIb-V-IX complex, consisting of four subunits, mediates the initial adhesion of platelets to the damaged blood vessel wall via the interaction to collagen-bound VWF [24]. Flow cytometric analysis of the receptor subunits in Revacept treated ePPE mice revealed no major differences of the GPIbα, GPIbβ, GPV or GPIX surface exposition, compared to the respective control group (**Figure 17A**).

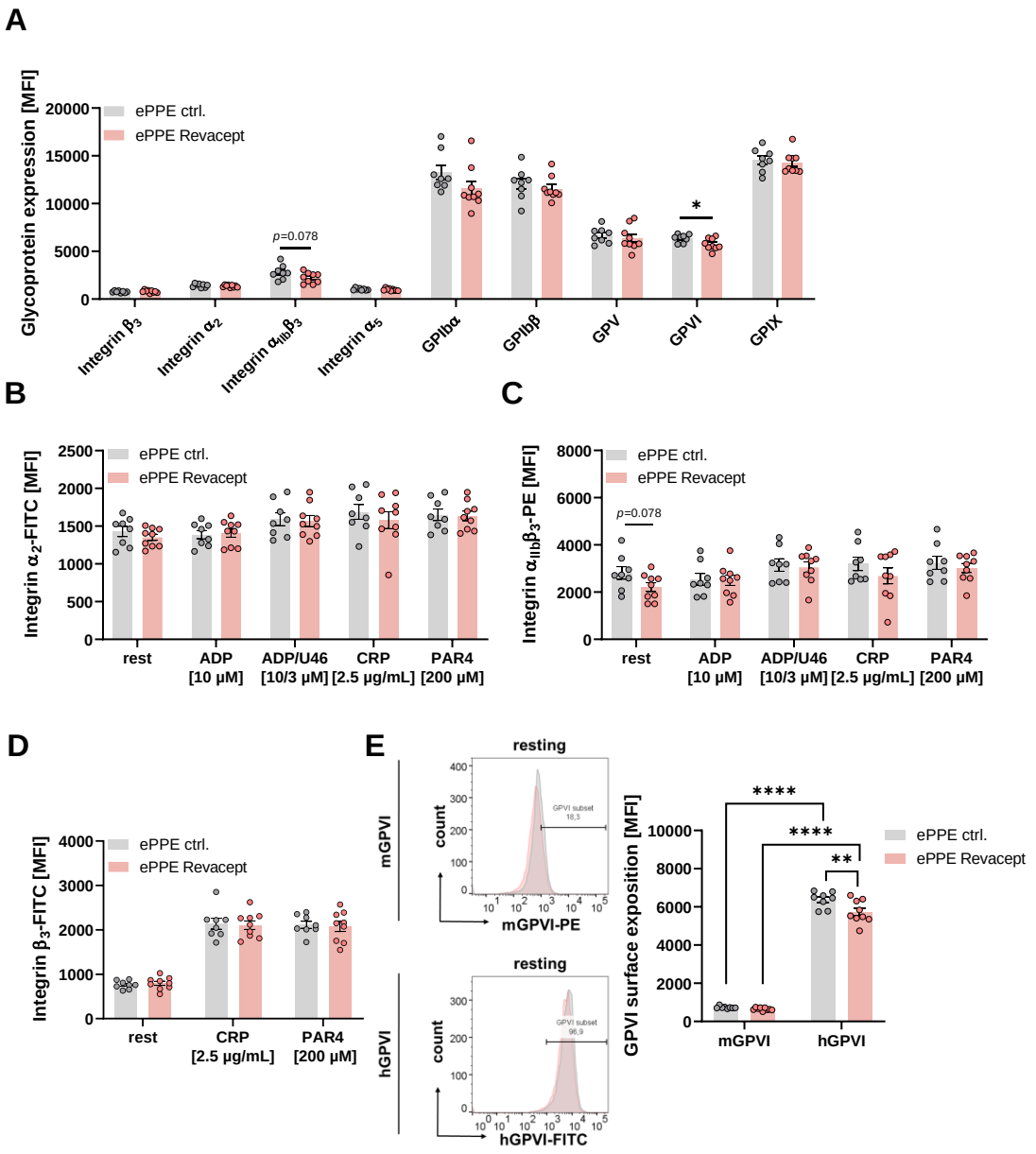


Figure 17. Platelet glycoprotein exposition in Revacept treated mice at day 28 post ePPE surgery. (**A**-**E**) Washed murine whole blood from ePPE operated ctrl and Revacept treated mice was analysed via flow cytometry. (**A**) Platelet surface exposure of integrin β_3, integrin α_2, integrin α_5, integrin $\alpha_{IIb}\beta_3$, GPIbα, GPIbβ, GPV, GPVI and GPIX in ctrl (*n* = 8) and Revacept treated (*n* = 9) ePPE mice at day 28 post surgery. (**B**–**D**) Externalisation of (**B**) Integrin α_2 (CD49b), (**C**) integrin $\alpha_{IIb}\beta_3$ (CD41/61) and (**D**) integrin β_3 (CD61) on the platelet surface of ctrl (*n* = 8) and Revacept treated (*n* = 9) ePPE mice. Platelets were stimulated with indicated agonists. (**E**) Exposition of murine (m) and human (h) GPVI on the platelet surface of ctrl (*n* = 8) and Revacept treated (*n* = 9) *hGp6*$^{+/+}$ ePPE mice. Representative histograms are shown. Data are represented as mean values ± SEM. Statistical analysis was performed using (**A**–**D**) an unpaired multiple t-test or (**E**) a two-way ANOVA with a Tukey's multiple comparison post-hoc test; $^{**}p < 0.01$, $^{****}p < 0.0001$. ADP = Adenosine diphosphate; CRP = Collagen-related peptide; ctrl = Control; ePPE = External porcine pancreatic elastase (application); MFI = Mean fluorescence intensity; PAR4 = Protease-activated receptor 4 activating peptide; U46619 (U46) = Thromboxane A_2 analogue; rest = resting.

In addition to that, further analysis of the integrin α_2 (**Figure 17B**), total integrin $\alpha_{IIb}\beta_3$ (**Figure 17C**) and the integrin β_3 subunit (**Figure 17D**) showed no significant alterations in receptor externalisation on the platelet surface, upon platelet activation with different agonists. However, an additional flow cytometric analysis regarding GPVI confirmed the absence of the murine GPVI receptor in both groups, thereby ensuring the genetically induced replacement of the murine GPVI receptor by its human analogue (**Figure 17E**).

3.3.4 Reduced procoagulant activity of platelets derived from Revacept treated ePPE mice

The exposure of phosphatidylserine (PS) on the surface of activated platelets is a crucial process to ensure the formation of stable three-dimensional thrombi, in order to prevent excessive blood loss due to a vascular wall injury. Thereby, PS exposure on the platelet membrane provides a procoagulant surface, leading to the formation of the prothrombinase complex, which in turn facilitates the cleavage of prothrombin into thrombin. Local thrombin generation results in activation and recruitment of circulating platelets, which directly contributes to thrombus formation and stabilisation at sites of vascular injury [23, 58]. As recently published by Wagenhäuser *et al*., the procoagulant activity of platelets was reported to be enhanced during AAA formation in both humans and mice. In this context, PS exposure of platelets was found to be highly correlated with the progressive aortic diameter expansion in the PPE model for experimental induced AAA formation in mice [256]. Besides other platelet signalling pathways, GPVI-signalling has been shown to promote procoagulant activity via PS exposure on the platelet membrane, thus contributing to local thrombin generation [83]. Therefore, it is not surprising that *in vivo* GPVI-blocking resulted in a significantly reduced procoagulant activity of platelets under resting conditions and after GPVI stimulation in experimental induced AAA formation in mice (**Section 3.1**).

In order to analyse the effect of Revacept on the procoagulant activity of platelets, PS exposure of Revacept treated ePPE mice at day 28 post surgery was analysed. Flow cytometric analysis revealed a significantly reduced PS exposure, indicated by a decrease in AnnexinV-binding to platelets derived from Revacept injected ePPE mice under resting conditions (**Figure 18A**). However, PS exposure after platelet activation either by CRP or PAR4 was unaltered, compared to the respective control group (**Figure 18A**). Again, the procoagulant activity of platelets was strongly correlated with the aneurysm size at day 28 post AAA induction, as indicated by the Spearman's correlation coefficient (R=0.5428) (**Figure 18B**). As Klatt *et al*. demonstrated, platelets are capable of inducing PS exposure on RBCs by direct cell-cell interaction via the

FasL/FasR signalling pathway, resulting in RBC-mediated local thrombin generation [58]. Therefore, PS exposure on the RBC membrane was analysed next, in order to determine whether Revacept treatment affects the procoagulant activity of RBCs during AAA formation. In contrast to the results obtained from platelets, PS exposure of RBCs was unaltered between both groups (**Figure 18C**).

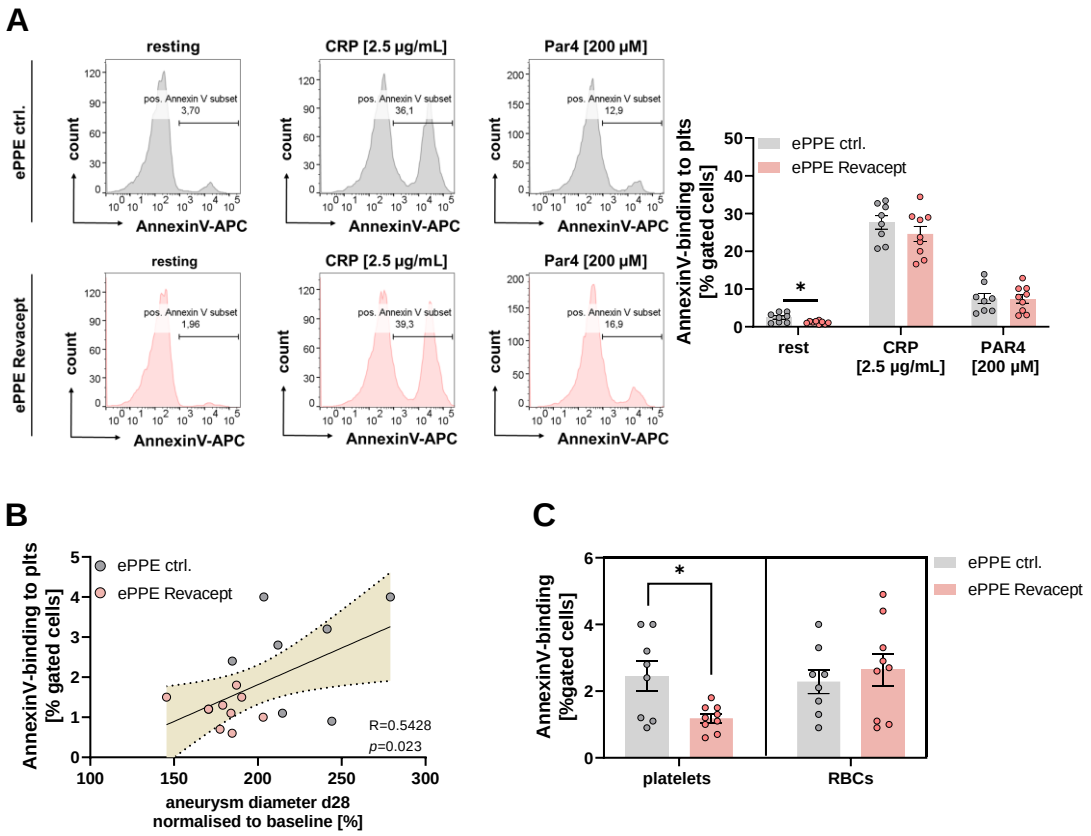


Figure 18. Reduced procoagulant activity of platelets derived from Revacept treated ePPE mice. (**A**-**C**) Washed murine whole blood from ePPE operated ctrl and Revacept treated mice was analysed via flow cytometry. (**A**) AnnexinV-binding to platelets from ctrl (*n* = 8) and Revacept treated (*n* = 9) ePPE mice at day 28 post surgery. Platelets were stimulated with indicated agonists. Representative histograms are shown. (**B**) Spearman's correlation between AnnexinV-binding to platelets and the aneurysm diameter at day 28 post ePPE of ctrl. (*n* = 8) and Revacept (*n* = 9) mice. (**C**) AnnexinV-binding to platelets and RBCs under resting conditions from ePPE ctrl (*n* = 8) and Revacept treated (*n* = 9) mice. Data are represented as mean values ± SEM. Statistical analysis was performed using (**A** and **C**) an unpaired multiple t-test; **p* < 0.05. CRP = Collagen-related peptide; ctrl = Control; ePPE = External porcine pancreatic elastase (application); PAR4 = Protease-activated receptor 4 activating peptide; Plts = platelets; U46619 (U46); rest = resting.

As the direct interaction of platelets with RBCs, via the FasL/FasR axis, plays an important role for the local thrombin generation and subsequent thrombus formation, the FasL exposition on the platelet surface was determined via flow cytometry. Thereby, control mice exhibited a

significantly enhanced FasL exposition on their platelet surface, compared to Revacept injected mice (**Figure 19A**). This was paralleled by a moderate positive correlation between platelet FasL externalisation and aneurysm size at day 28 post ePPE surgery (R=0.4296) (**Figure 19B**).

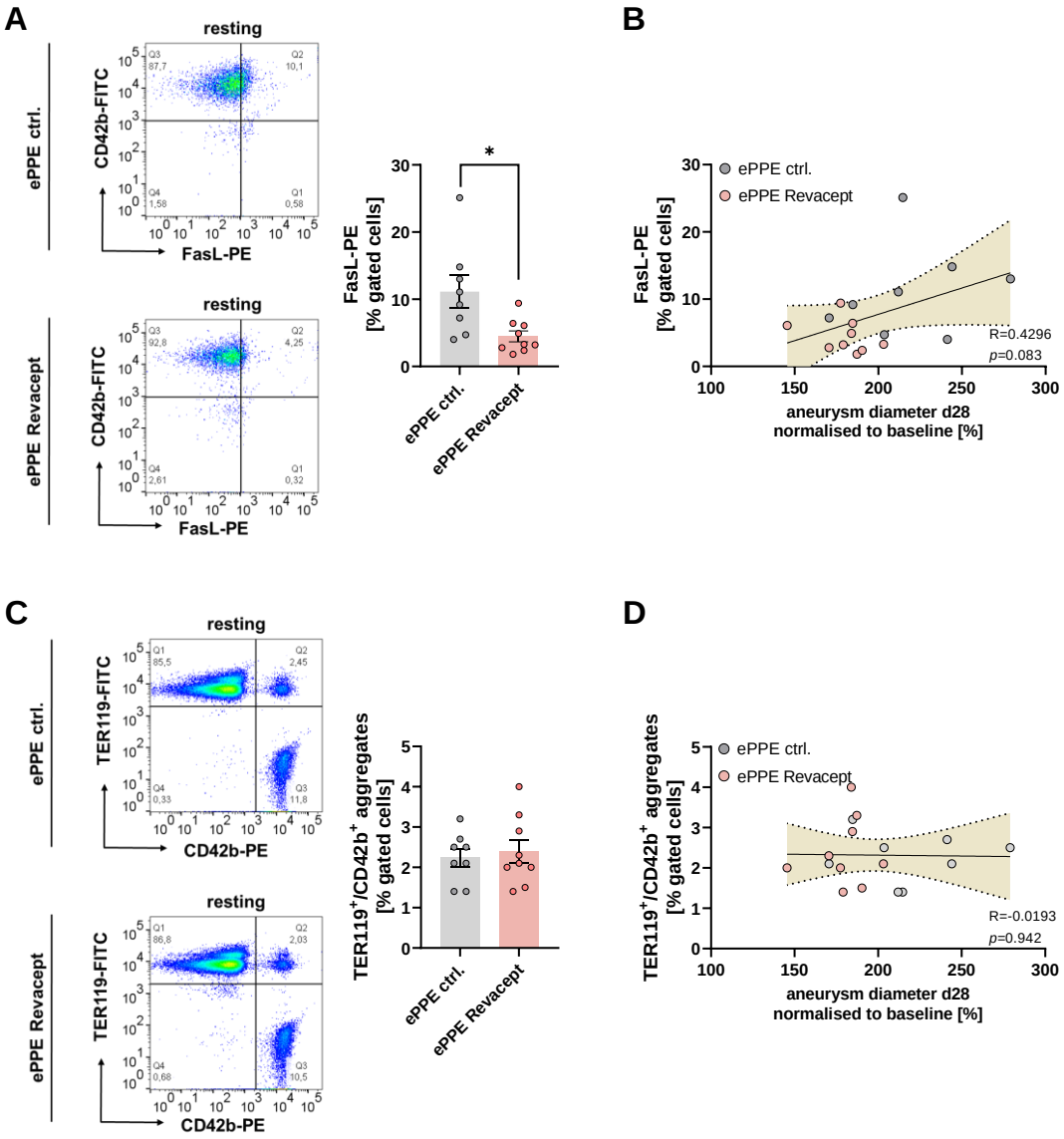


Figure 19. Platelets from Revacept treated ePPE mice revealed a reduced FasL surface exposition at day 28 post surgery. (**A** and **C**) Washed murine whole blood from ePPE operated ctrl and Revacept treated mice was analysed via flow cytometry. (**A**) Frequency of FasL positive platelets from ctrl (*n* = 8) and Revacept treated (*n* = 9) ePPE mice at day 28 post surgery. Representative histograms are shown. (**B**) Spearman's correlation between FasL positive platelets and the aneurysm diameter at day 28 post ePPE of ctrl. (*n* = 8) and Revacept (*n* = 9) mice. (**C**) Platelet-RBC aggregate formation from ePPE ctrl (*n* = 8) and Revacept treated (*n* = 9) mice was determined as double-positive events for CD42b (platelet maker, GPIbα) and TER119 (RBC marker, glycophorin A). (**D**) Spearman's correlation between platelet-RBC aggregates and the aneurysm diameter at day 28 post ePPE of ctrl. (*n* = 8) and Revacept (*n* = 9) mice. Data are represented as mean values ± SEM. Statistical analysis was performed using (**A** and **C**) an unpaired student's t-test; *$p < 0.05$. ctrl = Control; ePPE = External porcine pancreatic elastase (application).

However, this decrease in FasL exposition did not culminate into an altered platelet-RBC aggregate formation via the FasL/FasR axis (**Figure 19C**), as indicated by the constant percentage of CD42b (platelet marker, GPIbα) and TER119 (RBC marker, glycophorin A) double-positive events measured by flow cytometry, when comparing both groups (**Figure 19C**). As a result, no correlation of platelet-RBC aggregate formation and the aneurysm size at day 28 was observed (R=-0.0193) (**Figure 19D**).

As described previously, GPVI was shown to directly modulate platelet-mediated inflammation in early PPE induced AAA formation (day 7) by affecting the number of circulating platelet-leukocyte aggregates, especially of those with neutrophils (**Section 3.2**). In order to determine whether Revacept treatment affects the platelet-related inflammatory response the aggregate formation of platelets with different leukocyte subtypes was analysed at the observation endpoint at day 28 after ePPE surgery.

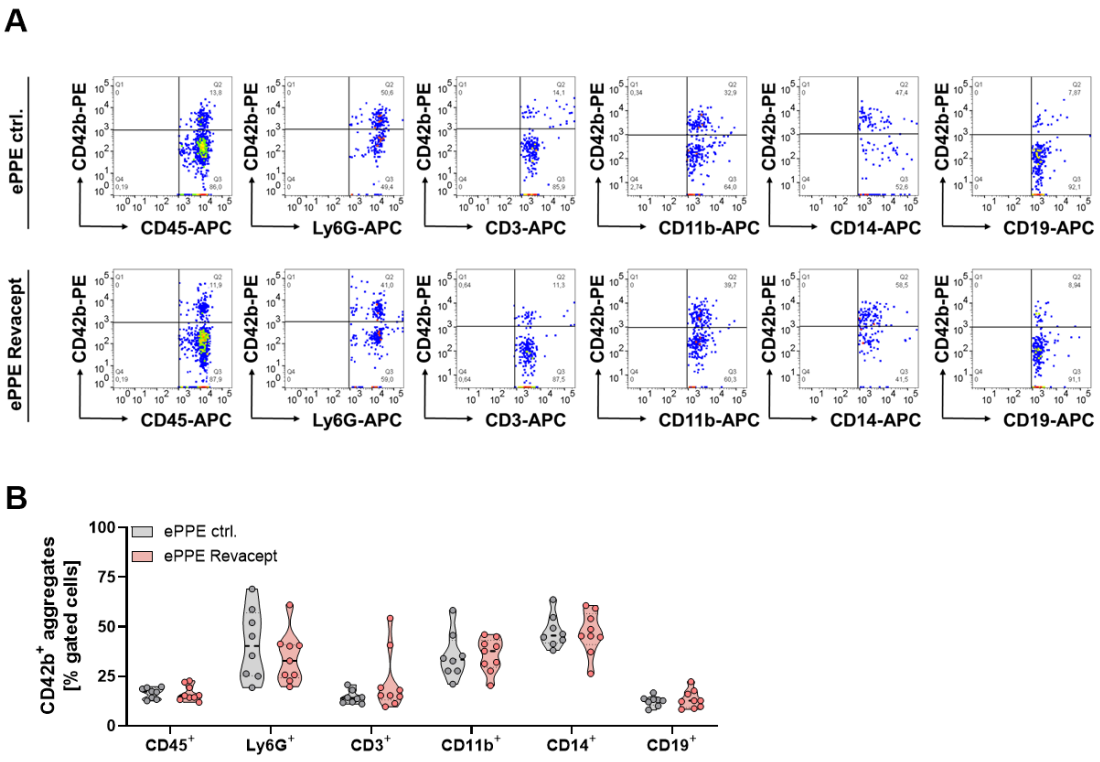


Figure 20. The formation of circulating platelet-leukocyte aggregates is unaffected by Revacept treatment at day 28 after ePPE induced AAA formation. (**A** and **B**) Washed murine whole blood from ePPE operated ctrl and Revacept treated mice was analysed via flow cytometry. (**A**) Representative histograms of platelet-leukocyte aggregate formation. (**B**) Platelet-leukocyte aggregate formation in ePPE operated ctrl (*n* = 8) and Revacept treated (*n* = 9) mice at day 28 post surgery. Aggregate formation of platelets with different leukocyte subtypes was determined as double-positive events for CD42b (platelet maker, GPIbα) and the respective leukocyte marker. Data are represented as mean values ± SEM. Statistical analysis was performed using (**B**) an unpaired multiple t-test. ctrl = Control; ePPE = External porcine pancreatic elastase (application).

Therefore, murine whole blood samples were analysed using flow cytometry to determine double-positive events of platelets (CD42b, GPIbα) with leukocytes (CD45), neutrophils (Ly6G), T cells (CD3), and B cells (CD19), respectively macrophages or granulocytes (CD14 and CD11b) (**Figure 20A**). However, the evaluation of platelet-leukocyte aggregate formation revealed no major differences in the aggregate formation of platelets with the different leukocyte subtypes in Revacept treated ePPE mice at day 28, compared to the control group (**Figure 20B**). These results are in line with the previously described data of GPVI-deficient mice which also showed an unaltered platelet-leukocyte aggregate formation at day 28 after PPE induced AAA formation (**Section 3.1**). These findings Indicate that the platelet-mediated inflammatory response is mainly promoted via GPVI in the early phase of experimental induced AAA formation.

As noted previously (**Section 3.2**), platelet GPVI has been identified to modulate the inflammatory response in early AAA formation by affecting platelet-neutrophil aggregate formation, neutrophil activation and migration, as well as the formation of NETs within the aneurysm. Thereby, the direct interaction of platelets and neutrophils is facilitated at least partially by the CD40L/CD40 axis. In this context platelet derived CD40L plays a crucial role in the modulation of the innate and adaptive immune response by promoting neutrophil activation and recruitment via binding to CD40 [257-259]. Therefore, CD40L exposition on the platelet surface of Revacept treated ePPE mice at day 28 post experimental AAA induction was assessed. The flow cytometric analysis revealed no significant differences in CD40L exposition between both groups under resting conditions and after platelet activation with different agonists. However, an upregulation of CD40L on the platelet surface could be observed after GPVI activation via high dose of CRP. Stimulation of the thrombin receptor PAR4 using the PAR4 activating peptide, revealed an enhanced CD40L externalisation only by trend, without reaching statistical significance (p=0.089) (**Figure 21A**).

As described previously, binding of VWF to the GPIb-V-IX complex represents the first crucial step in the process of platelet recruitment at the site of vessel wall injury. Thereby, the GPIb/VWF axis facilitates the firm adhesion of platelets to the vascular wall, followed by the subsequent binding of GPVI to the exposed collagen, which is needed to initiate platelet activation, adhesion and aggregation [22]. Thus, VWF-binding to platelet surface via GPIbα was analysed via flow cytometry. VWF binding at day 28 post ePPE surgery was found to be unaffected after Revacept treatment under resting conditions and after CRP, respectively PAR4 induced platelet activation (**Figure 21B**). In line with the observed upregulation of CD40L, an enhanced binding of VWF to the platelet surfaces was detected after platelet activation. Thereby, both CRP-mediated GPVI activation, as well as PAR4 activation led to a strongly

enhanced VWF binding to GPIbα. This increase in VWF binding was independent of Revacept treatment, as it was also observed also in the control mice (**Figure 21B**).

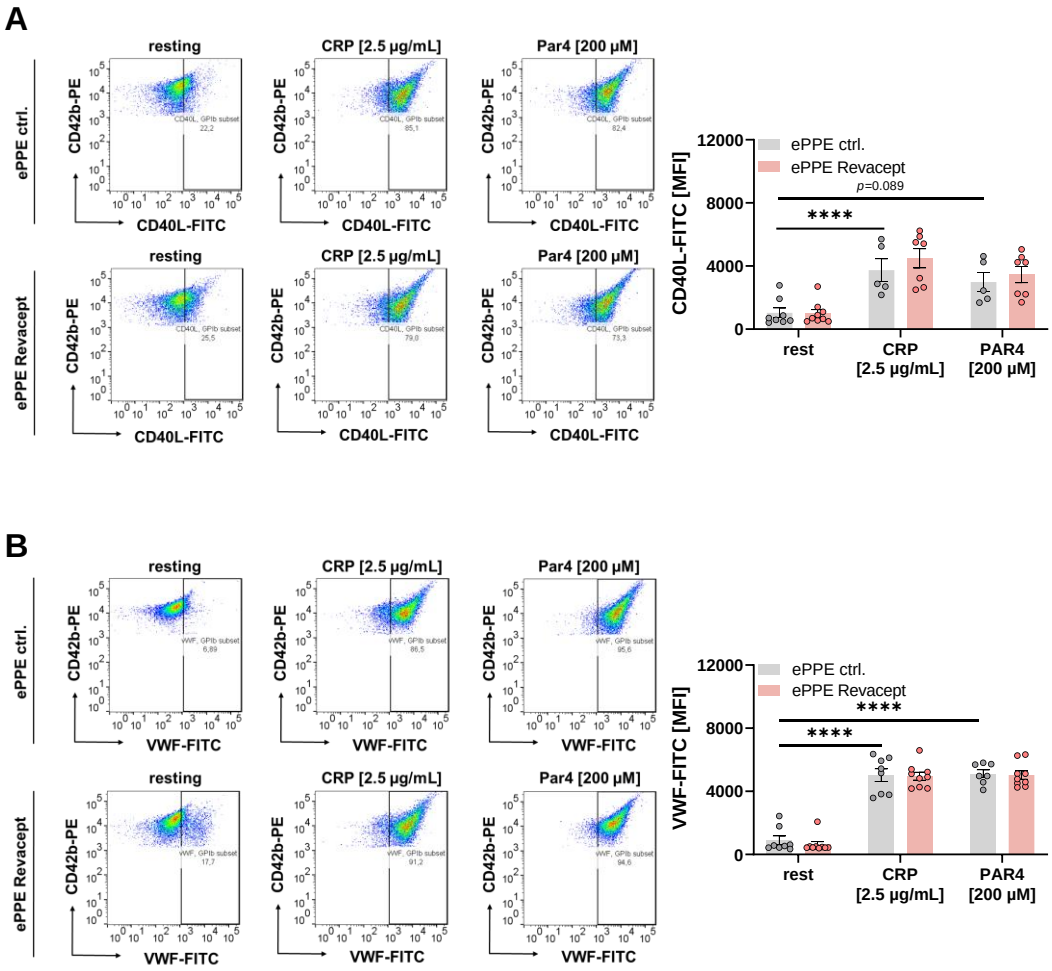


Figure 21. CD40L surface externalisation and VWF-binding to platelets were unaltered in Revacept treated ePPE operated mice at day 28. (**A** and **B**) Washed murine whole blood from ePPE operated ctrl and Revacept treated mice was analysed via flow cytometry. (**A**) CD40L surface externalisation of platelets from ctrl (*n* = 8) and Revacept treated (*n* = 9) ePPE mice at day 28 post surgery. Platelets were stimulated with indicated agonists. Representative histograms are shown. (**B**) VWF-binding to platelets from ctrl (*n* = 8) and Revacept treated (*n* = 9) ePPE mice at day 28 post surgery. Platelets were stimulated with indicated agonists. Representative histograms are shown. Data are represented as mean values ± SEM. Statistical analysis was performed using (**A** and **B**) a two-way ANOVA with a Tukey's multiple comparison post-hoc test; ****$p < 0.0001$. ctrl = Control; ePPE = External porcine pancreatic elastase (application); VWF= Von Willebrand factor.

In conclusion, these first translational preclinical data indicate, that Revacept has the potential to act as a novel drug-based therapy targeting AAA formation by attenuating aortic diameter progression, while the basal platelet function is unaffected.

4 Discussion

4.1 Crosstalk of platelets with macrophages and fibroblasts aggravates inflammation, aortic wall stiffening, and osteopontin release in abdominal aortic aneurysm

Beyond their essential role in haemostasis, accumulating evidence has emerged indicating that dysregulated platelet function and activity are key mediators for the onset and progression of a broad spectrum of CVDs, such as stroke, atherosclerosis, and myocardial infarction [6, 107, 233-235]. Throughout the last years, several preclinical studies reported beneficial effects of antiplatelet therapies with regard to the AAA pathology, by effectively attenuating aneurysm growth and rupture risk across different experimental animal models for AAA formation [241].

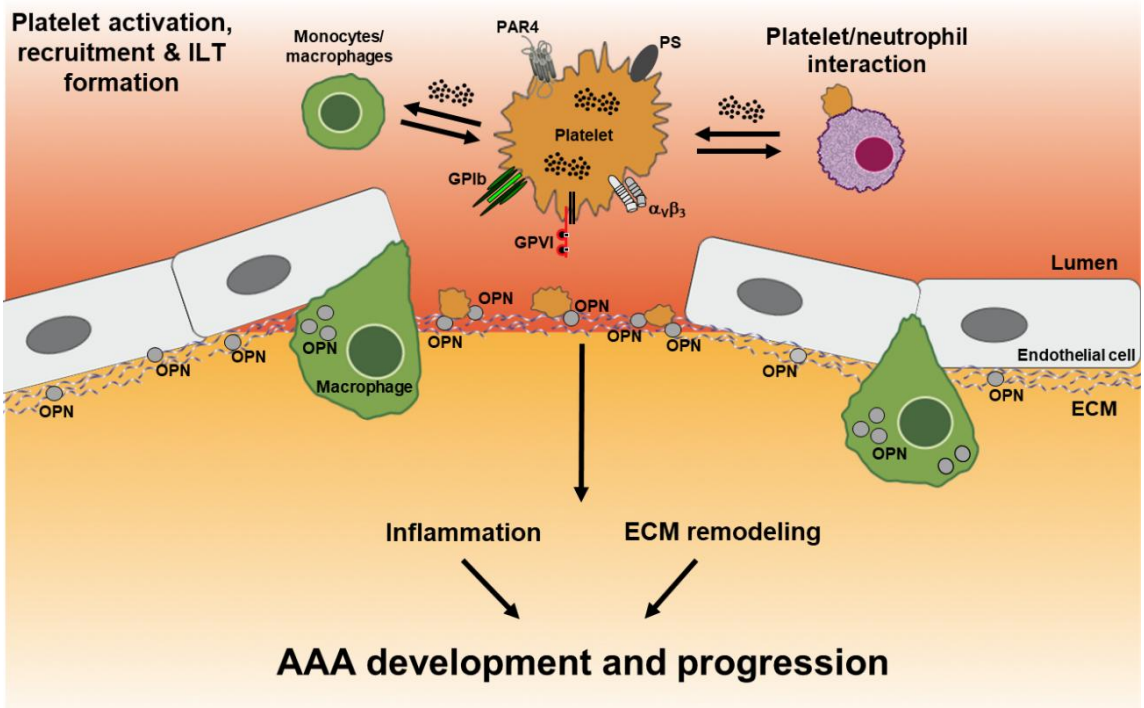


Figure 22. Mechanistical contribution of platelet function to the AAA pathogenesis. Platelets play a pivotal role in the initiation and progression of AAA by facilitating vascular inflammation, as well as progressive degradation of the ECM, thus compromising the aortic wall integrity within the aneurysmal segment. Specifically, platelets were shown to induce the upregulation of *SPP1* (OPN), as well as inflammatory and stiffness-related gene expression in macrophages and aortic tissue, thereby promoting inflammatory responses and ECM remodelling. This is paralleled by a reinforced adhesion and migration of platelets into both the aortic vessel wall and the ILT. Moreover, elevated platelet activation and procoagulant activity in AAA patients were found to represent additional pathological hallmarks for aneurysm formation and progression. AAA = Abdominal aortic aneurysm; ECM = Extracellular matrix; ILT = Intraluminal thrombus; OPN = Osteopontin. Taken from [256].

However, the underlying mechanisms by which platelets may contribute to aneurysm initiation, progression, and rupture remain incompletely understood. Therefore, the present study investigated the underlying effect of platelet function and activity on the pathophysiological mechanisms of AAA formation and progression. Thereby, platelets were identified as crucial mediators of the AAA pathology by reinforcing both the inflammatory response and the progressive remodelling of the aortic wall (**Figure 22**). Platelet-depletion during experimental induced AAA formation using the PPE mouse model resulted in markedly attenuated expression of key inflammatory (*Spp1, Il1b, Il6, Il8, Il10, Il12, Ccl2,* and *Tnf-a*) and matrix remodelling genes (*Mmp9* and *Col1a1*) within the aneurysmal tissue culminating into a significantly restricted aortic diameter progression. Mechanistically, platelets were shown to promote vascular inflammation by reinforcing AAA-related gene expression of differentiated macrophages. Thereby, platelets were shown to upregulate both the inflammatory (*SPP1*, *IL1B, IL6, Il8, IL10, IL12b,* and *TNFA*) and matrix remodelling-related gene expression (*MMP9* and *COL1A1*) in these cell types *in vitro*. In addition, initial experimental data provided evidence for a novel mechanism by which platelet recruitment into both the aneurysmal vessel wall and the ILT is mediated via the expression and deposition of the proinflammatory cytokine OPN (*SPP1*) (**Figure 22**). Beyond this, patient data revealed a hyperactive platelet activation profile in patients diagnosed with AAA, which was accompanied by a markedly elevated procoagulant activity. These data were paralleled by preclinical *in vivo* data in mice utilising the PPE mouse model for experimental induced AAA formation. These data highlight the therapeutic potential of antiplatelet therapies by targeting platelet hyperreactivity in order to effectively restrict aneurysm growth in patients with AAA.

4.1.1 Persistent platelet hyperreactivity as a novel pathological hallmark in patients diagnosed with AAA

Over the recent years, multiple studies have reported reduced circulating platelet counts in patients with AAA, with platelet numbers inversely correlating with aneurysm size [236, 237]. This persistent thrombocytopenia has been linked to a consumption coagulopathy driven by sustained platelet hyperreactivity, as evidenced by enhanced P-selectin exposure on the platelet surface following stimulation of either PAR1 or the thromboxane receptor. Consistently, circulating levels of soluble P-selectin were markedly elevated in the plasma of patients diagnosed with AAA [181, 238, 239, 260]. This is paralleled by a substantially pronounced spontaneous platelet aggregation in patients with AAA, underscoring a persistent hyperreactivity of platelets in the AAA pathology under resting conditions [261]. These findings are further substantiated by the present study, as clinical data revealed a pronounced

hyperreactive phenotype of platelets derived from AAA patients not only after platelet activation but also under resting conditions, as indicated by enhanced P-selectin surface exposure as well as integrin $\alpha_{IIb}\beta_3$ activation (**Section 3.1, Figure 7A**). Conversely, Morrell *et al*. recently reported unaltered platelet activation in AAA patients under resting conditions, as evidenced by comparable P-selectin surface exposure in relation to the corresponding control cohort. However, these controverse data may be attributable to differences in the composition of the respective control cohort. Whereas Morrell *et al.* included control subjects across a broad age range, the control group in the present study was strictly age-matched (65.4 years ± 1.59) relative to the analysed patient cohort (75.5 years ± 2.20) [260]. Given that aging is a well-established modulator of platelet function by promoting a hyperreactive platelet phenotype, the use of age-matched controls emerged to be essential for a valid interpretation of platelet activation profiles [262-266]. In this context, Gnanenthiran *et al*. clearly demonstrated an aging-dependent increase in platelet activation in three distinct age cohorts of healthy individuals. Thereby, both P-selectin surface exposure and integrin $\alpha_{IIb}\beta_3$ activation were significantly enhanced in elderly subjects (79.5 ± 7.3 years), compared to young (25 ± 3.1 years) and middle aged (45.8±6.7 years) individuals [267]. These data underscore the need for age-matched control cohorts for a more comprehensive analysis of platelet-specific data in patients with AAA. Besides the hyperreactive state under resting conditions, the present study additionally revealed a pronounced responsiveness of platelets due to GPVI-mediated activation using low-dose of CRP (**Section 3.1, Figure 7A**). The observed reduced platelet activation threshold upon GPVI stimulation in this study was further confirmed by preclinical *in vivo* data using the PPE mouse model for experimental induced AAA formation (**Section 3.1, Figure 5**). This experimental mouse model was shown to exclusively mimic the human AAA pathology in terms of platelet hyperactivity in comparison to a further commonly used AngII mouse model (**Section 3.1, Figure 6**). Beyond a hyperreactive platelet profile, increased PS exposure on the platelet surface —reflecting enhanced procoagulant activity— has emerged as a novel platelet-specific characteristic of the AAA pathology. This sustained procoagulant phenotype likely arises from the aforementioned persistent platelet hyperreactivity and was observed in both the experimental PPE mouse model (**Section 3.1, Figure 5E**) and in patients with AAA (**Section 3.1, Figure 7A**). However, PS exposure on platelets serves as a critical mediator of thrombus formation by providing a procoagulant surface that amplifies local thrombin generation. Consequently, enhanced PS exposure of platelets in the context of the AAA pathology may directly reinforce platelet activation and the subsequent recruitment of platelets to the aneurysm wall and the ILT. [268-270]. In detail, preclinical data presented in this work demonstrated that this pronounced procoagulant activity within the AAA pathology is —at least

partially— mediated in a GPVI-dependent manner, as pharmacological blocking of GPVI resulted in a markedly attenuated PS exposure of platelets in experimental induced AAA formation *in vivo*, using the ePPE mouse model (**Section 4.3**) [248]. Therefore, the excessive recruitment of platelets from the circulation into the ILT may contribute to the decline in platelet counts observed in AAA patients. Thus, the persistent platelet hyperreactivity, as well as the reinforced recruitment of platelets into the aneurysmal tissue highlight the potential contribution of dysregulated platelet function to a prothrombotic phenotype observed in the AAA pathology, potentially acting as a prompt driver for the disease progression [181, 240, 271].

4.1.2 Platelet depletion attenuates vascular inflammation and aortic wall remodelling in experimental induced AAA formation

Despite this accumulating clinical and experimental evidence, the precise mechanistic pathways by which platelets drive aneurysm formation and progression were still unclear. In this context, the present experimental study provides first mechanistical insights by identifying platelets as critical mediators of the AAA pathogenesis, driving both vascular inflammation (**Section 3.1, Figure 1**) and progressive remodelling of the aortic wall (**Section 3.1, Figure 2**). In detail, platelet depletion during the early phase of PPE-induced experimental AAA formation resulted in a pronounced downregulation of key inflammatory (*Spp1, Il1b, Il6, Il8, Il10, Il12, Ccl2,* and *Tnf-a*) and ECM remodelling genes (*Mmp9* and *Col1a1*) within the aneurysmal tissue, thus amplifying an AAA-promoting transcriptional profile. This was paralleled by a markedly attenuated macrophages infiltration into the aneurysm segment in the absence of platelets, culminating into a significantly attenuated aortic diameter progression in early experimental induced aneurysm formation (**Section 3.1, Figure 1C**–**F**). Collectively, these initial mechanistical findings emphasise platelet activity as a potent driver of the AAA pathogenesis and identify its targeting as a promising therapeutic strategy. Accordingly, antiplatelet therapies emerge as potential pharmacological intervention in order to effectively restrict aneurysm growth and, ultimately, improve clinical the outcome of AAA patients.

Over recent years, multiple experimental studies have consistently demonstrated protective effects of different antiplatelet therapies on aneurysm growth and rupture risk in different preclinical settings [241]. In detail, pharmacological inhibition of ADP-dependent platelet activation using clopidogrel, a selective $P2Y_{12}$ receptor antagonist, significantly attenuated aortic diameter expansion in the AngII-induced murine model of AAA [242]. Notably, Owens *et al.* demonstrated that, in mice with established aneurysms, treatment with either clopidogrel or ASA substantially reduced rupture-associated mortality in the same experimental AAA mouse

model [243]. These beneficial effects of antiplatelet therapies in experimental AAA were further strengthened by additional preclinical evidence. Liu *et al.* demonstrated that dual antiplatelet therapy with ASA and the $P2Y_{12}$ inhibitor ticagrelor significantly attenuated aortic diameter expansion in mice with established aneurysms in the AngII mouse model, supporting the clinical potential of antiplatelet therapies in this context [241]. Collectively, these experimental findings underscore the critical contribution of platelet activation and function to the AAA pathology, thereby highlighting the potential of antiplatelet therapies in order to effectively attenuate aneurysm growth and rupture risk. Despite this compelling preclinical evidence, translation of these experimental findings into clinical routine remains challenging. Antiplatelet therapies, such as low-dose of ASA, are widely prescribed in various CVDs, including AAA, to reduce mortality due to secondary thrombotic events. However, their ability of effectively target aneurysm growth is still highly debated [244, 272].

In this context, clinical evidence for the use of low-dose ASA in patients with AAA may suggest a that the therapeutic efficiency is linked to aneurysm progression in a size–dependent manner. Thereby, randomised controlled trials using low-dose ASA revealed no beneficial effects in individuals with small-size aneurysms —exhibiting an aortic diameter of < 40 mm— and were even associated with increased post-rupture mortality in some cohorts [156, 245]. Conversely, other clinical studies demonstrated that treatment with low-dose ASA is capable of effectively restricting aortic diameter progression of small-size aneurysm with an initially aortic diameter of 35 mm, respectively 39 mm [246]. In line, pharmacological intervention with ASA in AAA patients with mid-size aneurysms of 40–49 mm provided evidence to be associated with an attenuated aortic diameter expansion [245]. These findings highlight the relevance of an aneurysm size-based stratification of AAA patients suggesting that antiplatelet therapies may provide a therapeutical benefit in the appropriate AAA patient cohort. However, this emphasises the urgent need for further clinical studies to optimise treatment strategies. Therefore, it remains critical to further evaluate which subgroups of AAA patients are most likely to derive therapeutic benefit from antiplatelet therapies, in particular with respect to the limitation of aneurysm growth and rupture risk. The variable outcomes of antiplatelet therapies observed in clinical trials further emphasise the relevance of further preclinical investigation of the AAA pathology for the identification of novel platelet-specific therapeutic targets via the use of *in vivo* animal models of experimental AAA induction [241]. Especially due to its central role in platelet activation pharmacological targeting of the main platelet collagen receptor GPVI may represent a promising approach for the development of a novel antiplatelet therapy in the context of the AAA pathology (**Section 4.2**) [248].

4.1.3 GPVI-mediated platelet activation amplifies the OPN-dependent vascular inflammatory response in the AAA pathology

Beyond its contribution to different physiological processes —such as wound healing, cell adhesion, chemotaxis, and the regulation of cell survival and apoptosis—, the multifunctional glycoprotein OPN has emerged as a key mediator in a broad spectrum of pathological conditions, including atherosclerosis, stenosis, or cardiac hypertrophy [273-275]. Notably, multiple studies have indicated a prominent role of OPN in the pathogenesis of myocardial infarction, by promoting immune cell recruitment and amplifying local cytokine expression at the site of cardiac inflammation, thus exacerbating tissue injury and adverse cardiac remodelling [276-279]. Given its dual function as proinflammatory cytokine and ECM protein different studies reported a potential underlying impact of OPN on the AAA pathology in both experimental animal models as well as human disease. In this context, preclinical data from Bruemmer *et al.* demonstrated that genetic deletion of OPN markedly restricted aneurysm growth *in vivo*, using the AngII model for experimental AAA induction in mice, highlighting the profound contribution of OPN to aneurysm progression and vascular remodelling [280]. Beyond this, a recent study reported significantly elevated levels of circulating OPN —as also reported in the present study (**Section 3.1, Figure 7F**)— paralleled by a pronounced OPN deposition in the aneurysmal aortic wall of patients diagnosed with AAA. These findings suggest that this persistently enhanced OPN content may contribute to the chronic proinflammatory environment within the aneurysmal tissue, thus facilitating the adverse aortic wall remodelling in patients [281]. Notably, Golledge *et al.* identified a positive correlation of circulating OPN serum levels and the risk factor adjusted aneurysm growth in patients with small-size aneurysms (aortic diameter of 34.0 ± 3.8 mm), highlighting OPN as a potential biomarker for predicting AAA [282].

In this context, the present study provided first evidence that the sustained platelet hyperreactivity —as implicated in the AAA pathology— amplifies the pronounced expression and deposition of OPN within the growing aneurysm. Specifically, platelet depletion during the early phase of PPE-induced experimental AAA formation resulted in a markedly downregulation of the *Spp1* expression (the OPN encoding gene) in aneurysmal wall *in vivo* (**Section 3.1, Figure 1F**). This attenuated transcriptional profile ultimately culminated into a significantly reduced level of circulating OPN in the plasma of platelet-depleted mice (**Section 3.1, Figure 1G**). Mechanistically, OPN has already shown to be abundantly expressed by macrophages, functioning as a key mediator for the macrophage-mediated proinflammatory response by reinforcing immune cell adhesion, migration, and cytokine expression [281, 283, 284]. Accordingly, the suppressed OPN gene expression of platelet-depleted mice can be primarily attributed to the significantly reduced presence of macrophages within the

aneurysmal tissue, due to abolished direct and/or indirect platelet–macrophage interactions (**Section 3.1, Figure 1G** and **H**). This mechanism was further validated in *in vitro* experiments, demonstrating that the treatment with the supernatant of activated platelets amplified OPN gene expression (*SPP1*) in differentiated macrophages. These findings indicate that the indirect crosstalk of platelets and macrophages reinforces a chronic proinflammatory environment via macrophage-derived OPN, thus contributing to the adverse aortic wall remodelling within the AAA pathology. Notably, the upregulated OPN gene expression was —at least partially— mediated via GPVI-induced platelet activation, implying a potential crosstalk of OPN and platelet GPVI (**Section 3.1, Figure 3F**). In this context, genetic deletion of GPVI resulted in a significant reduction in both levels of circulating as well as deposited OPN within the aortic tissue following PPE-induced experimental AAA induction. These findings indicate the profound contribution of GPVI-mediated platelet activation to the local OPN abundance within the growing aneurysm (**Section 3.2, Figure 4** and **Figure5**) [248]. In this context, static adhesion as well as platelet activation via GPVI were shown to be unaffected in the presence of both cleaved and full-length OPN (**Section 3.1, Figure S2D**–**G**). However, flow chamber experiments revealed a markedly enhanced *ex vivo* thrombus formation on a collagen matrix in the presence of immobilised OPN under high arterial shear rates (1,700 s^{-1}), indicating a functional crosstalk between GPVI and OPN, especially under dynamic conditions (**Section 3.1, Figure S4D**). Given the established ability of OPN to bind to various components of the ECM, including collagen, this potentially shear-dependent interplay may amplify the GPVI-mediated thrombus formation on collagen under high shear —as evident within the aneurysmal segment— in an OPN-dependent manner [285-287]. Consequently, the persistently pronounced OPN content observed in the AAA pathology may reinforce the GPVI-mediated recruitment of platelets to the aneurysmal site, thereby facilitating ILT formation and growth.

In conclusion, the findings from this study demonstrate the profound impact of dysregulated platelet function on both the onset and progression of the AAA pathology, highlighting the great potential of antiplatelet therapies as a therapeutic intervention for patients diagnosed with AAA. Mechanistically, the data presented in this study revealed that platelet hyperreactivity —as manifested in the AAA pathology— reflects a key driver of the disease progression by promoting both vascular inflammation and adverse remodelling at the site of aneurysm formation. Nevertheless, it remains essential to further evaluate which patient subgroups are most likely to derive therapeutic benefit from antiplatelet therapies, in particular with respect to the limitation of aneurysm growth and rupture risk. The contrary outcomes of antiplatelet therapies observed in clinical trials emphasise the need for further preclinical investigations of the AAA pathology in order to identify novel platelet-specific therapeutic targets [241, 256].

4.2 GPVI-mediated platelet activation and procoagulant activity aggravate inflammation and aortic wall remodelling in abdominal aortic aneurysm

Given its pivotal role in platelet activation, the main platelet collagen receptor GPVI has emerged as a promising therapeutic target for the development of novel antithrombotic therapies. GPVI-signalling has been implicated in the onset and progression of various CVDs, including myocardial infarction and stroke [79, 117, 235]. Accordingly, this study investigated the impact of GPVI-mediated platelet activation on AAA formation and progression to determine whether GPVI represents a suitable target in order to effectively limit aneurysm growth. Therefore, the underlying mechanisms of GPVI-mediated platelet activation on AAA formation and progression were investigated by analysing GPVI-deficient mice in two independent *in vivo* mouse models for experimental induced AAA formation —the PPE and ePPE model— over a time course of 28 days.

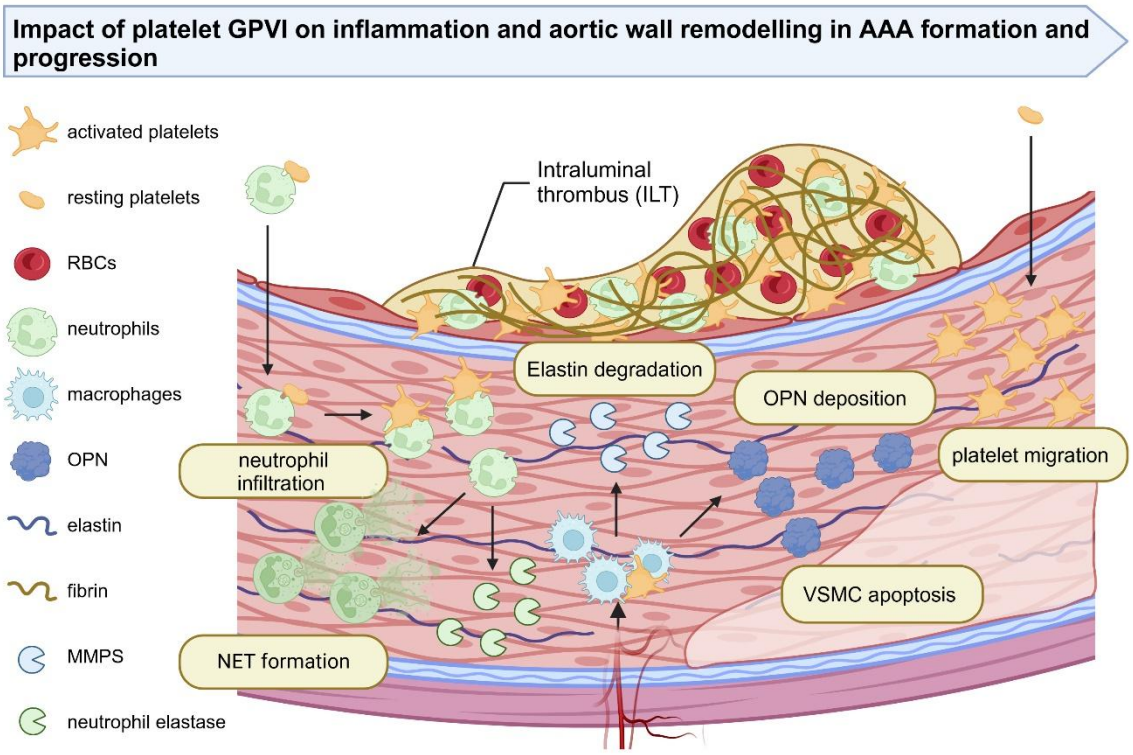


Figure 23. Impact of platelet GPVI on inflammation and aortic wall remodelling in AAA formation and progression. Platelet GPVI contributes to the pathophysiology of AAA by modulating neutrophil and platelet recruitment to the aortic wall, as well as NET formation during early stages of aneurysm development. In addition, GPVI promotes elastin degradation and VSMC apoptosis within the medial layer. Thus, GPVI-signalling results in a compromised aortic wall integrity, reinforcing the progressive dilation of the abdominal aorta. Furthermore, deposition of the pro-inflammatory and remodelling-associated cytokine OPN is increased in a GPVI-dependent manner. AAA = Abdominal aortic aneurysm; ECM = Extracellular matrix; GP = Glycoprotein; MMP = Matrix metalloproteinase; NET= Neutrophil extracellular trap; OPN = Osteopontin; RBC = Red blood cell; VSMC = Vascular smooth muscle cell. Taken from [248].

Thereby, GPVI-deficient mice showed protection against experimental induced AAA formation in both *in vivo* models, indicated by a significantly restricted aortic diameter progression within the observation period of 28 days. Mechanistically, genetic deletion of GPVI resulted in an attenuated vascular inflammation, reflected by a diminished neutrophil infiltration into the aneurysmal tissue, accompanied by a reduced release of neutrophil-derived elastase, as well as NET formation. This was paralleled by a preserved aortic wall integrity in the absence of GPVI, as indicated by decreased plasma MMP levels and an increased VSMC content within the aortic media, due to reduced cellular apoptosis (**Figure 23**). Thus, GPVI-deficient mice exhibited increased intima/media thickness and preserved elastin integrity, resulting in significantly attenuated aortic expansion. These findings were confirmed by an initial translational approach as administration of a GPVI-blocking antibody was capable of effectively restricting aneurysm growth in the ePPE mouse model.

4.2.1 Genetic deletion of platelet GPVI impairs inflammation by affecting neutrophil infiltration and NET formation in early AAA

As outlined above, the AAA pathology is closely associated with a sustained inflammatory response, characterised by the extensive infiltration of immune cells into both the aortic wall and the ILT [124, 288]. Within the aneurysmal tissue recruited immune cells actively promote aneurysm formation by the release of pro-inflammatory cytokines and chemokines, generation of ROS, and the secretion of ECM degrading proteases, such as MMPs. Collectively, these processes establish a chronic proinflammatory environment, amplifying immune cell recruitment in a feed-forward loop, thus reinforcing aortic wall degradation and aneurysm growth [145, 200]. Thereby, both innate immune cells —such as macrophages, neutrophils, natural killer cells, mast cells, and dendritic cells— as well as adaptive immune cell populations, including T and B lymphocytes, are abundantly present within the aneurysmal tissue and have been mechanistically implicated in driving AAA initiation and progression [198, 204-209, 211, 289]. The present study demonstrated that platelets directly contribute to the inflammatory response and vascular integrity during early experimental induced AAA formation by specifically affecting neutrophil activation and recruitment in a GPVI-dependent manner (**Section 3.2, Figure 2**).

Within the AAA pathology neutrophils were found to be present, alongside with other immune cell subpopulations, in both in the aortic vessel wall and ILT. This is paralleled by an increase in neutrophil-derived effector molecules, such as MPO and neutrophil elastase in the circulation and aortic tissue of patients diagnosed with AAA [224, 290-292]. Consistent with these

observations, preclinical studies utilising distinct murine models for experimental induced AAA formation (the AngII, PPE, and ePPE mouse models) revealed, that neutrophil infiltration into the aneurysmal segment reflects a hallmark of the early phase of aneurysm initiation and progression [247, 293-295]. In this context, a preclinical study by Eliason *et al*. highlighted the pivotal contribution of neutrophil driven inflammation to the AAA pathogenesis as neutrophil depletion in experimental induced AAA formation was linked to a markedly attenuated aortic diameter progression *in vivo*. In addition, this was paralleled by a reduced AAA incidence upon antibody-mediated depletion of neutrophils, further establishing neutrophils as critical drivers of aneurysm formation [206]. Mechanistically, the present study revealed that genetic deletion of GPVI markedly attenuated vascular inflammation via limiting neutrophil activation, as indicated by reduced release of neutrophil-derived elastase (**Section 3.2, Figure 3B** and **C**), as well as a restricted formation of circulating platelet-neutrophil aggregates (**Section 3.2, Figure 2C** and **D**). Consequently, both platelet and neutrophil migration into the aortic tissue was significantly reduced in GPVI-deficient mice (**Section 3.2, Figure 2E** and **F**). Thereby, different studies already underlined a critical role of GPVI-mediated platelet activation for the vascular inflammatory response in the context of different pathological conditions including arthritis, stroke, sepsis, glomerulonephritis or myocardial infarction [296-300]. However, the here reported novel mechanistic insights were supported by a recent study from Burkard *et al*., identifying platelet GPVI as crucial mediator for the neutrophil-driven thrombo-inflammation in a model for LPS-induced acute lung injury. Thereby, pharmacological targeting of GPVI-dependent platelet activation via administration of the immunodepleting anti-GPVI antibody JAQ1 resulted in a markedly restricted pulmonary inflammation, due to a reduction in platelet-neutrophil aggregate formation, as well as a significantly attenuated migration of neutrophils into the affected lung tissue [118]. In conclusion, these findings highlight GPVI as a central mediator of neutrophil-mediated inflammation, supporting that pharmacological targeting of GPVI may constitute a promising approach to effectively restrict the inflammatory response within the AAA pathology. Accordingly, pharmacological inhibition of GPVI may culminate in a preserved aortic wall integrity by offering protection against neutrophil elastase promoted ECM degradation.

Beyond this, excessive activation and transmigration of neutrophil within the aneurysmal segment is linked to a reinforced NET formation, which has emerged as an additional pathological hallmark of the AAA-related inflammatory response. NETs consist of an extracellular chromatin network interspread with histones —most notably citH3— as well as neutrophil elastase, MMP9, and MPO, thereby directly providing a persistent proinflammatory environment within the aortic tissue, which in turn amplifies the immune cell recruitment into

the growing aneurysm [221-223]. In regard to this, Eilenberg *et al*. already reported, that patients diagnosed with AAA revealed markedly increased burden of NETs within both the aortic vessel wall and the ILT, as indicated by significantly elevated circulating and tissue levels of citH3, a potent marker for NET formation [224, 301]. Consistently, a high density of citH3-positive neutrophils has been identified in aneurysmal aortic tissue, indicating pronounced NET formation within the AAA pathology [224]. In a recent experimental study pharmacological targeting of NET formation by blocking of downstream effectors, such as protein arginine deiminase 4 (PADI4) —facilitating histone citrullination— was found to effectively restrict aneurysm growth *in vivo*. These preclinical data highlight the profound impact of NET formation as an additional mechanistic key driver for AAA development and progression, identifying NET-associated pathways as potential targets for novel therapeutic interventions [302]. In regard to this, the present study provides the first direct evidence that platelet GPVI critically contributes to the reinforced NET formation observed within the AAA pathology. Genetic deletion of GPVI markedly restricted NET formation within the aortic tissue in experimental induced aneurysm formation, indicated by significantly reduced circulating and tissue citH3 levels, thus identifying a GPVI-dependent interplay of platelets and neutrophils as a central mechanism for NET-mediated aortic inflammation (**Section 3.2, Figure 3**). These findings were paralleled by the previously mentioned study by Burkard *et al*., as JAQ1-mediated blocking of GPVI resulted in a significantly attenuated NET formation *in vivo*, leading to a restricted pulmonary inflammation in an experimental mouse model for LPS-induced acute lung injury [118].

Collectively, the present study provided novel mechanistic insights by which platelets critically modulate the inflammatory response during early aneurysm formation in a GPVI-dependent manner by affecting neutrophil activation, infiltration, as well as NET formation [248]. Accordingly, pharmacological targeting of GPVI-dependent platelet activation may emerge as a promising translational strategy in order to restrict neutrophil-mediated vascular inflammation during early aneurysm formation, potentially limiting aneurysm growth and thus may improving the clinical outcome of AAA patients.

4.2.2 Platelet GPVI significantly contributes to progressive aortic wall remodelling in experimental induced AAA formation

As described previously, genetic deletion of GPVI offered protection against experimental induced AAA formation, evidenced by a markedly attenuated aortic diameter progression and a reduced AAA incidence at day 28 after PPE surgery (**Section 3.2, Figure 1C**–**G**). These findings

were independently validated in a second experimental AAA model (the ePPE mouse model), confirming that the observed effects of GPVI-mediated platelet activation on aortic diameter progression are independent from the selected *in vivo* model (**Section 3.2, Figure 7C**–**E**). Within the AAA pathophysiology, proteolytic degradation of elastin fibres within the tunica media constitutes a key mechanism for the onset of aneurysm growth, by compromising the aortic architecture. Thereby, the loss of the medial elastin, is considered as a central driver for the progressive and irreversible dilation of the aortic diameter, observed in patients diagnosed with AAA [124, 303-305].

As recently published, Wagenhäuser *et al*. (**Section 3.1**) provided first experimental evidence that platelets directly contribute to the AAA pathology by affecting aortic wall integrity via the reinforcement of elastin fragmentation. In this context, platelet depletion was shown to preserve the medial elastin content during the early phase of PPE-induced experimental AAA formation (day 10) (**Section 3.1, Figure 2D**) [256]. Based on these findings, the present study demonstrated, that the platelet-driven proteolytic degradation of elastin within the aneurysmal segment is —at least partially— mediated via the main collagen receptor GPVI. From a pathophysiological perspective, genetic deletion of GPVI resulted in a preserved elastin content within the aneurysmal tissue, due to a significant reduction in elastin fragmentation (**Section 3.2, Figure 6B** and **C**). Mechanistically, the proteolytic degradation of the medial elastin is primarily driven by increased MMP activity in the aortic wall, resulting from a disruption of the tightly regulated balance between MMPs and their physiological inhibitors the so-called TIMPs [185-187]. Notably**,** TIMP1 and TIMP2 expression was shown to be markedly downregulated in aortic tissue from AAA patients with aneurysms exhibiting an aortic diameter exceeding 55 mm [186]. This reduction in TIMP expression is linked to a pronounced upregulation of MMP1, MMP2, MMP9, MMP12 and MMP14 within the aneurysmal tissue of AAA patients [185, 187-191]. Moreover, elevated expression of MMP8 in mesenchymal cells, such as macrophages or VSMCs, alongside an enhanced MMP13 abundance has been implicated in the pathophysiological progression of AAA [306, 307]. Consistent with the well-established role of MMP expression and activity in AAA initiation and progression, we here provided evidence that platelets amplify proteolytic elastin fragmentation via a GPVI-dependent regulation of circulating MMP levels. Notably, loss of GPVI resulted in a marked attenuation of plasma MMP2 concentrations during the early inflammatory phase at day 7 following PPE-induced AAA formation (**Section 3.2, Figure 4B**), accompanied by reduced MMP9 levels during the remodelling phase at day 14 (**Section 3.2, Figure 5C**). Thus, this GPVI-mediated biphasic modulation of the circulating MMP content directly culminated into a preserved elastin structure and content detected in GPVI-deficient mice at the observation end time-point at

day 28 (**Section 3.2, Figure 6b** and **C**). Supporting their critical involvement in the AAA pathology, constitutive genetic deletion of either MMP2 or MMP9 has been shown to limit aortic diameter expansion across distinct experimental AAA mouse models, highlighting the critical contribution of MMPs to aneurysm growth *in vivo* [308, 309]. In line with these experimental results, clinical data revealed an elevated concentration of MMP2 within both plasma and aortic tissue of patients diagnosed with AAA [189, 310, 311]. Accordingly, MMP9 plasma and tissue levels were found to be consistently enhanced in AAA patients compared to healthy controls, accompanied by a significantly enhanced MMP9 activity in both the aortic vessel wall and the ILT. Beyond its mechanistic role, MMP9 has emerged as a potential biomarker of the disease severity, as patients revealed enhanced MMP9 levels after aortic rupture, when compared with individuals exhibiting an intact AAA. Consistently, this was paralleled by a postoperative decline of circulating MMP9 following surgical intervention [188, 260, 312-315].

Over the past decades, accumulating evidence has emerged that platelets themselves contain a broad spectrum of MMPs, and their endogenous inhibitors, the so-called TIMPs. Specifically, MMP1, MMP2, MMP3, MMP9, MMP12, and MMP14, together with TIMP1, TIMP2, and TIMP3, have been identified within platelets, localised either in the cytosol or stored within granules [260, 316-325]. Upon platelet activation, these proteolytic mediators are released and exert regulatory effects on platelet function under both physiological and pathophysiological conditions. Notably, platelet-derived MMP activity has been implicated in modulating key aspects of platelet function, including priming, activation, adhesion, aggregation, intracellular Ca^{2+} mobilisation, and thrombus formation [319-321, 326-329]. In detail, platelet-derived MMP2 is involved in platelet priming, activation, as well as thrombus formation. Thereby, MMP2 is shown to reinforce the platelet reactivity to various agonists, suggesting its involvement in the modulation of different intracellular platelet signalling pathways [326, 330, 331]. Mechanistically, upon platelet activation, the inactive precursor pro-MMP2 is translocated from the cytoplasm to the platelet surface where it undergoes proteolytic cleavage into its active form (MMP2), followed by its subsequent release into the circulation. In this context, the release of platelet-derived MMP2 was shown to be, at least partially, dependent on GPVI-signalling, as collagen-induced platelet activation markedly enhanced MMP2 secretion [319, 326, 331]. In addition to that, MMP2 amplifies collagen-dependent platelet activation and thrombus formation under shear stress, implicating a potential interplay with the main collagen receptor GPVI [332]. This interaction appears to be particularly relevant under high-shear conditions *in vivo*, as those present within the aneurysmal segment of AAA patients. Thus, platelet-derived MMP2 may not only contribute to the proteolytic degradation of structural components of the

aortic vessel wall, but also reinforce the GPVI-mediated recruitment of circulating platelets into the aneurysmal tissue and the ILT.

In contrast to the reported amplifying effects of MMP2 on platelet function platelet-derived MMP9 was shown to negatively regulate platelet reactivity by attenuating intracellular Ca^{2+} mobilisation and, consequently, platelet activation [327, 328, 333]. However, a recent study by Morrel *et al.* reported a significantly enhanced MMP9 activity in platelets from AAA patients, in comparison with healthy controls. This was paralleled by a markedly downregulated expression of the endogenous MMP9 inhibitor TIMP1, indicating a direct contribution of platelets to the MMP/TIMP-imbalance observed in the AAA pathology [260]. Collectively, these findings suggest that a reduced release of platelet-derived MMPs may account —at least in part– for the attenuated MMP2 and MMP9 plasma levels in GPVI-deficient mice observed during the inflammatory (day 7), respectively remodelling phase (day 14) in experimental induced AAA formation. This may provide first evidence supporting a potential role of GPVI-mediated platelet activation in regulating the release of platelet-derived MMPs under pathological conditions in the context of AAA progression. Especially by considering that experimental data already demonstrated that GPVI-signalling is implicated in the release of platelet-derived MMP2 [331]. In line with these findings, the administration of antiplatelet therapy in an experimental *in vivo* model of AAA formation either via ASA (COX1 inhibitor) or clopidogrel ($P2Y_{12}$ inhibitor), sufficiently reduced both MMP2 content as well as MMP2 and MMP9 activity within the aortic tissue in mice [243]. This indicates that dysregulated platelet activation, as observed in AAA patients (**Section 3.1, Figure 7A** and **B**) directly contributes to the adverse aortic wall remodelling by enhancing both MMP content and activity in the aneurysmal segment. Therefore, a systematic assessment of platelet MMP2 and MMP9 expression, respectively enzymatic activity in GPVI-deficient mice across distinct stages of AAA development (inflammatory and remodelling phase) could reflect a promising future approach in order to further elucidate the mechanistic role of GPVI-signalling for aortic wall remodelling. Due to their prominent role within the AAA pathogenesis, inhibiting MMP expression or activity has already emerged as a promising translational approach in order to restrict aneurysm growth. For instance, the antibiotic agent doxycycline was shown to effectively restrict aneurysm progression in different *in vivo* models for experimental induced AAA formation by the unspecific inhibition of MMP expression and activity [334]. However, clinical evaluation has produced inconsistent outcomes in different randomised trials with respect to the ability of doxycycline to attenuate aortic diameter expansion in AAA patients [335-338]. Thus, the clinical translation of MMP inhibition in the context of AAA pathogenesis remains challenging, largely due to the persistent lack of inhibitor specificity and the prevalence of off-target and

respectively side effects [339]. Therefore, targeting platelet GPVI via specific blocking antibodies may represent a promising novel target in order to attenuate MMP-mediated elastin fragmentation by reducing circulating MMP2 and MMP9 level in AAA patients. In this context, the GPVI Fab fragment inhibitor Glenzocimab (ACT017) represents a potential candidate, as Glenzocimab administration in a phase 1 clinical study revealed no bleeding complications in healthy individuals, supporting the absence of off-target effects [114].

Alongside elastin, collagen fibres are another structural key component of the aortic ECM, by providing tensile strength and stiffness in order to withstand the physiological biomechanical forces, thus preserving aortic vessel wall integrity. Within the aortic wall, type I and type III represent the most abundant collagen subtypes, collectively accounting for 80–90% of the total collagen content. The remaining 10–20% are attributed to the collagen types IV, V, VI, and VII [125, 334, 340, 341]. In the AAA pathology, collagen type I and IV are predominantly localised within the tunica intima and tunica media, whereas collagen type III is most abundantly present in the tunica adventitia [342-344]. Mechanistically, dysregulations of collagen turnover and crosslinking —essential for tissue repair and regeneration of the aortic wall— as well as collagen composition have been linked to multiple pathological conditions, including the development of AAA [345-347]. In this context, analysis of GPVI-deficient mice at day 28 after experimental induced AAA formation with regard to the aortic collagen content revealed no alterations in the overall collagen abundance within the aortic tissue as indicated by Sirius red staining (**Section 3.2, Figure 6F**). However, a detailed analysis using polarised light revealed an altered collagen composition. Thereby, loss of GPVI resulted in a shifted collagen type I/III ratio within the aneurysmal segment towards collagen type I (**Section 3.2, Figure 6G**), while collagen composition in naive mice was unaltered (**Section 3.2, Figure S7F** and **D**). However, in AAA patients, an enhanced collagen type I and III content, accompanied by a reinforced crosslinking of collagen fibres has been reported, resulting in an augmented aortic stiffness at the site of aneurysm formation. Notably, the persistent ratio of collagen type I to type III in the aortic wall is proposed to play a crucial role in AAA development, as a sustained balance in the collagen content is essential for preserving aortic integrity and function [347]. In particular, an elevated synthesis of type III procollagen was reported in the aneurysmal tissue of AAA patients [348]. Thereby, newly synthesised collagen type III is more vulnerable to proteolytic degradation by MMPs due to a lower degree of fibre crosslinking, which may contribute to the attenuated tensile strength of the aortic vessel wall observed in the AAA pathology [348-350]. Therefore, platelet GPVI may contribute to the aortic diameter progression by promoting deposition of collagen type III, resulting in a compromised tensile strength of the aortic wall due to enhanced elasticity of the aneurysmal segment. In line with these findings, Reusswig *et al.* recently

reported a comparable phenotype, in which the cardiac remodelling after acute myocardial infarction is modulated in a GPVI-dependent manner at least partially via a shifted collagen type I/III ratio towards collagen type I within the heart tissue of GPVI-deficient mice, resulting in reduced scar formation and improved cardiac output. In addition, the analysis of cardiac tissue in these mice revealed a significantly reduced *Col1a1*, as well as *Col3a1* gene expression 21 days after acute myocardial infarction in the absence of GPVI [235]. Thus, these data highlight the profound impact of GPVI-signalling on collagen-related remodelling processes in different CVDs, such as myocardial infarction and AAA. Strikingly, platelet depletion during the early remodelling phase of experimentally induced AAA (day 10) resulted in a significant reduction in *Col1a1* expression, whereas *Col3a1* expression remained unaltered within the aortic tissue of PPE-operated mice (**Section 3.1, Figure 2E**). Collectively, these findings indicate that platelet- and GPVI-mediated effects on collagen type III (*Col3a1*) synthesis and deposition emerge predominantly at later stages of AAA progression, as evidenced by reduced collagen III abundance in established aneurysms of GPVI-deficient mice at day 28. (**Section 3.2, Figure 6F**). These findings suggest that platelet, respectively GPVI-mediated alterations with regard to synthesis and deposition of collagen type III culminate during later stages of aneurysm development, as collagen type III in GPVI-deficient mice was found to be reduced at day 28 post PPE-induced AAA formation.

4.2.3 GPVI-mediated platelet activation reinforces VSMC loss in experimental induced AAA formation

Besides proteolytic degradation and reorganisation of structural key components of the aortic ECM, VSMC dysfunction and loss reflect an additional pathological hallmark of the progressive remodelling process of the aortic vessel wall observed during AAA formation [125, 351]. Under physiological conditions, VSMCs play an essential role in vascular homeostasis by regulating vascular tone, thereby maintaining blood pressure in order to ensure a sufficient blood circulation, which is mainly facilitated by their contractile phenotype [352-354]. Moreover, VSMCs directly contribute to vascular repair, remodelling and preservation of vessel wall integrity by the tightly regulated synthesis and organisation of major ECM components, such as collagen and elastin [355, 356]. Under pathological conditions, VSMCs exhibit profound functional dysregulation characterised by phenotypic switching as well as reprogramming, apoptosis, ROS generation, the release of proinflammatory cytokines (e.g. IL1β, IL6, and MCP-1), ECM degrading enzymes (e.g. MMP2 and MMP9), and impaired autophagy [193, 197, 357-363]. These maladaptive responses collectively undermine vessel wall integrity

and are recognised as key drivers of AAA development and progression. Therefore, the underlying effects of platelet GPVI on VSMC loss within the inflammatory (day 7) and remodelling phase (day 14) of experimental induced AAA formation were further investigated by analysing α-SMA expression —a widely used marker for VSMCs and myofibroblasts— in the aortic media of GPVI-deficient mice. In contrast to the inflammatory phase, in which the α-SMA expression remained unaltered (**Section 3.2, Figure 4F**), loss of GPVI was associated with a significant increase in the proportion of α-SMA content within the aneurysmal segment during the remodelling phase at day 14 (**Section 3.2, Figure 5F**). This enhanced α-SMA content may reflect either a reinforced transdifferentiation of aortic fibroblasts into myofibroblasts, or a preservation of VSMC survival by preventing augmented apoptotic activity in the aneurysmal segment. In line with this finding, GPVI-deficient mice displayed a pronounced reduction in the number of active caspase3-positive cells within the aortic media during early AAA formation at day 7 (**Section 3.2, Figure 4G**). Thereby, this attenuated apoptotic response strongly suggests that the increased α-SMA abundance observed at day 14 is mainly attributed to a diminished loss of VSMCs in the absence of GPVI. Mechanistically, several studies have identified that activation of the extrinsic apoptotic pathway via the FasR/FasL-axis plays a role in programmed cell death of VSMCs in the AAA pathology [364-366]. While the FasR (CD95) is broadly expressed across different cell types, its physiological membrane-bound ligand FasL (CD95L) is predominantly restricted to inflammatory cells, including T lymphocytes, natural killer cells, T cells, B cells, and macrophages [367-376]. Expression of FasR and FasL have been detected within the vascular tissue in both physiological and pathological conditions, where FasR-mediated activation of the extrinsic apoptotic pathways has been implicated in multiple vascular pathologies, such as atherosclerosis [377-382]. Upon FasL binding, FasR activation facilitates an intracellular signalling cascade, leading to the oligomerisation and activation of caspase8 and caspase10. This resulting initiator caspase-complex in turn promotes downstream activation of effector caspases, including caspase3, caspase6, and caspase7, ultimately driving chromatin degradation and subsequent apoptosis [368, 383]. Importantly, Schleicher *et al*. demonstrated that besides inflammatory cells, platelets are capable of inducing FasR-mediated apoptosis of different target cells by exposing FasL on their surface upon platelet activation. Moreover, it was shown that the activity of caspase3 and caspase7 in target cells is regulated in a platelet-dependent manner [384]. In line with these results, Klatt *et al.* reported that this upregulation upon platelet activation is at least partially promoted via GPVI, as stimulation with CRP resulted in a significantly enhanced FasL exposure on the platelet surface in the presence of WBCs [58]. However, a more detailed analysis of GPVI-deficient mice with regard to platelet FasL-mediated VSMCs loss revealed a markedly reduced FasL exposure on platelets during inflammatory phase

(day 7) of experimental induced AAA formation in the absence of GPVI (**Section 6.1, Figure S1B**). This was accompanied by a modest, though not statistically significant, reduced FasL abundance within the aortic tissue of these mice (**Section 6.1, Figure S1A**), which may be dedicated to the attenuated migration of platelets into the aneurysmal segment observed upon GPVI deficiency (**Section 3.2, Figure 2F**). Collectively, these findings highlight a potential GPVI dependency of platelet-derived FasL in driving extrinsic apoptotic signalling within the aneurysmal vessel wall, thus reinforcing VSMCs loss and ultimately compromising aortic wall integrity and stability.

In conclusion, we here demonstrated that GPVI-mediated platelet activation has a profound impact on AAA formation and progression by reinforcing different pathophysiological key mechanisms for the onset of the progressive aortic wall remodelling. Mechanistically, platelet GPVI promotes proteolytic degradation of elastin fibres by MMPs, alterations in aortic collagen composition and VSMC apoptosis, culminating in a substantially compromised aortic wall integrity, thus facilitating aortic diameter expansion in the AAA pathology.

4.2.4 GPVI as potential translational target for the development of novel pharmacological therapies in AAA formation and progression

Based on the previously described mechanistic interplay of platelet GPVI and the onset and progression of AAA, we next focused on a first translational approach by targeting GPVI-signalling *in vivo*. The present study aimed to evaluate whether GPVI represents a potential candidate as novel platelet-specific target for the development of a pharmacological therapy, in order to restrict aneurysm growth in patients with AAA. Due to its central role in platelet activation, GPVI has emerged as a therapeutically relevant target for the development of novel antithrombotic strategies. Pharmacological inhibition of GPVI-signalling is therefore under intensive investigation and may represent a promising novel antithrombotic therapy in order to prevent cardiovascular events [106, 113-116]. Throughout the last years several experimental studies have demonstrated beneficial effects via the pharmacological inhibition of GPVI-mediated platelet activation on multiple cardiovascular pathologies, including arterial thrombosis, myocardial infarction, ischaemic stroke, and acute lung injury [79, 117, 118, 299]. Notably, a recent study by Navarro *et al*. reported that targeting of GPVI-signalling using the novel humanised platelet GPVI Fab inhibitor EMA601 offered robust protection against arterial thrombosis and ischaemic stroke in mice [117]. Similarly, administration of the immunodepleting anti-GPVI antibody JAQ1 resulted in a markedly attenuated development of ischaemic stroke development in a murine cerebral artery occlusion model [119]. In line with these results, Kleinschnitz *et al.* demonstrated a significantly improved outcome after

experimental induced transient cerebral ischaemia in mice that received anti-GPVI treatment via JAQ1 application [300]. These results from experimental studies highlight the great potential of targeting GPVI-signalling *in vivo* as a novel therapeutic intervention in CVDs. However, data on pharmacological inhibition of GPVI-signalling in the context of the AAA pathology are lacking. Therefore, a first translational approach targeting GPVI-mediated platelet activation in the ePPE mouse model for experimental AAA induction was performed within this work. Notably, prophylactic application of the novel GPVI-blocking antibody Fab Y020347 resulted in a significantly attenuated aortic diameter progression over a time course of 28 days in the ePPE mouse model (**Section 3.2, Figure 9C**–**E**). These results indicate that pharmacological inhibition of platelet GPVI is capable of effectively restricting aneurysm growth *in vivo*. Thereby, confirming the profound effect of GPVI on aortic diameter progression, which was observed upon genetic deletion in GPVI-deficient mice (**Section 3.2, Figure 1C**–**F** and **Figure 7C**–**E**). In line with these results, Benson *et al*. recently reported that the therapeutic application of the immunodepleting anti-GPVI antibody JAQ1 in presence of an established AAA effectively attenuated the progressive aortic diameter expansion in two different *in vivo* models —the AngII and ePPE mouse model— of experimental induced AAA formation [385]. These findings demonstrate that pharmacological targeting of platelet GPVI not only offers protection against AAA formation in a prophylactic approach, but also may effectively limit aneurysm progression in patients with a pre-existing AAA. Accordingly, GPVI-blocking antibodies emerge as compelling therapeutic candidates capable of attenuating aneurysm growth and ultimately may reducing AAA-related mortality due to aortic rupture. Notably, sustained pharmacological inhibition of GPVI was not accompanied by bleeding complications or off-target effects throughout the whole observation period of 28 days, as reflected by an unaffected survival rate of anti-GPVI treated mice in comparison to the control group (**Section 3.2, Figure 9b**). Therefore, these data provide strong evidence that targeting GPVI-signalling as a novel antiplatelet therapy does not enhance rupture risk or the overall mortality in this preclinical setting. This finding is supported by an initial phase 1 clinical trial evaluating the humanised anti-GPVI monoclonal antibody Glenzocimab (ACT017). Thereby, intravenous infusion of Glenzocimab over a time period of 6 hours was shown to effectively attenuate the collagen-induced aggregation of platelets from healthy volunteers. However, with regard to Glenzocimab administration (62.5–2000 mg) neither bleeding complications, nor enhanced bleeding times were reported. This was paralleled by unaltered platelet counts and normal GPVI surface exposition on platelets derived from healthy volunteers following Glenzocimab infusion [386]. These clinical observations align with previous reports demonstrating, that loss of GPVI in humans is associated, at most, with a mild bleeding phenotype, while genetic deletion in mice even results in unaffected bleeding times.

Collectively, these findings indicate that platelet GPVI is not essentially required or normal haemostatic function, thus pharmacological inhibition offers a promising approach for antithrombotic strategies while avoiding bleeding complications, which are associated with conventional antiplatelet therapies [387-391]. In this context, a randomised double-blind phase 1b/2a clinical trial (ACTIMIS [Acute Ischemic Stroke Interventional Study] trial registration: NCT03803007) reported, that Glenzocimab (1000 mg) administration as an add-on therapy in combination with a recombinant tissue plasminogen activator (rt-PA, alteplase) treatment was linked to reduced intracerebral haemorrhage, as well as an overall improved mortality rate in patients with acute ischaemic stroke [114]. As Glenzocimab has already proven safety and efficacy in clinical trials, it represents the most promising candidate among the currently available GPVI-blocking agents for further translational investigations in the context of the AAA pathology [115]. Therefore, especially given promising preclinical evidence GPVI-targeting strategies —either via Fab Y020347 or JAQ1— preclinical evaluation of Glenzocimab using a murine *in vivo* AAA mouse model would constitute a valuable step toward the development of a novel platelet-related pharmacological intervention, capable of attenuating aneurysm progression [248, 385].

In conclusion, the experimental evidence presented in this work demonstrates that antiplatelet strategies by targeting GPVI-signalling offer an effective therapeutic approach to restrict the AAA pathogenesis in a preclinical setting. These findings highlight the crucial importance of further clinical testing in order to evaluate whether pharmacological inhibition of platelet GPVI is capable of providing therapeutic benefit in AAA patients as well. In this context, the identification of AAA patient cohorts that are most likely to benefit from antiplatelet therapies is still controversial and highly debated, as contradictory outcomes have been reported throughout the last years [244-246, 272, 392]. However, emerging clinical evidence suggests that therapeutic efficacy of antiplatelet agents is highly dependent on aneurysm size, whereas different studies demonstrated, that especially patients with mid- or large- size aneurysms would benefit from antiplatelet therapies [245, 246, 393, 394]. Notably, it has to be considered that these contradictory outcomes may be due to small patient numbers, as well as composition of the respective cohort, as in the majority of studies predominantly patients with small-size aneurysm were recruited. [156, 245, 246]. Thus, intensifying the clinical evaluation of antiplatelet therapies, particularly with respect to patient cohort size composition, remains of crucial clinical importance in order to effectively evaluate the therapeutic potential of targeting platelet function in the context of AAA formation and progression.

4.2.5 GPVI as potential biomarker for AAA prediction and risk stratification

Given its essential role in platelet activation, GPVI has emerged as a promising therapeutic target for the development of novel antithrombotic strategies. Notably, elevated GPVI expression has been reported in patients with acute coronary syndromes, correlating with enhanced thrombotic risk and thus highlighting GPVI as a potential biomarker for clinical risk stratification [106, 113, 395]. In this context, multiple studies have consistently reported markedly elevated plasma levels of sGPVI under prothrombotic conditions in patients with CVDs, including myocardial infarction, ischaemic stroke, and acute coronary syndromes [72, 106-108]. Collectively, these findings support the notion that sGPVI may serve as a novel clinically relevant biomarker for the identification of patients with increased risk for thrombotic disorders, in order to enable risk stratification and early initiation of therapeutic interventions. In this context, different haemostatic markers were shown to be markedly elevated in the circulation of patients diagnosed with AAA, including platelet factor 4, thrombin-antithrombin (TAT) complex, as well as D-dimer [268-270, 396-398]. In a population-based study, increased D-dimer —reflecting an enhanced fibrinolysis— and circulating TAT complexes were positively linked to aneurysm growth rates, highlighting their potential as independent biomarkers for the prediction of AAA progression [269, 396, 397, 399, 400]. Despite these promising initial data, clinical translation of reliable biomarkers for prediction and risk stratification in the context of the AAA pathology remains leaking. Consequently, systematic clinical evaluation of novel potential circulating predictors for AAA formation and progression is highly relevant. In the present study, a significantly enhanced concentration of sGPVI in the plasma of both mice (**Section 3.2, Figure 8b** and **C**) and humans (**Section 3.2, Figure 10A**) with an established AAA was observed, indicating that sGPVI may serve as a potential biomarker in the AAA pathology. These findings are supported by a recent study by Benson *et al*. in which markedly enhanced levels of sGPVI were reported, which was consistently reproduced across two independent AAA patient cohorts from different countries. Thereby, sGPVI has emerged as a highly predictive biomarker for AAA diagnosis, demonstrating a stronger correlation with aneurysm growth rates in patients with AAA, than D-dimer plasma levels, the currently most established circulating marker for AAA prediction [385, 398, 401]. Collectively, these data underscore the clinical potential of sGPVI as a novel and robust biomarker for the prediction and risk stratification of AAA patients. In this context, Bye *et al*. developed a novel approach for the prediction of prothrombotic events, based on a hyperreactive platelet phenotype. The so-called TRIPLE (Thrombotic Reactivity Indicator using Platelet GPVI, CD36 Expression, and age) score integrates three distinct parameters: platelet GPVI and CD36 surface expression together with patient age. By effectively identifying prothrombotic platelet phenotypes, this novel method may serve as a useful platelet-

specific tool for the identification and stratification of patients with enhanced thrombotic risk also in the context of different CVDs [402]. Recently Krott *et al.* identified a novel mechanism for the interaction of platelets and RBC interaction via the CD36–TSP-1-signalling axis as a prompt diver for aneurysm growth in both experimental mouse models and AAA patients. Thereby, CD36 was found to be markedly upregulated on the surface of platelets derived from an AAA patient cohort in comparison with healthy age-matched controls. This was paralleled by elevated levels of circulating CD36 in the plasma of AAA patients, which were found to highly correlate with the aneurysm growth [403]. Collectively with the GPVI upregulation in a small AAA patient cohort reported by Benson *et al.* the newly developed TRIPLE score may be a suitable diagnostic tool for the early identification of AAA development, especially considering that age remains the main risk factor for aneurysm formation. Thus, a successful implementation of the TRIPLE score into the clinical practice represents a promising approach for an effective risk stratification in the context of the AAA pathology [385, 402, 403].

4.3 Revacept (GPVI-FC) treatment attenuates experimental induced AAA formation in mice

Since the AAA pathology is mainly driven by the asymptomatic progressive dilation of the abdominal aortic diameter, the risk of a fatal aortic rupture increases over time [404, 405]. When the aortic diameter progression exceeds predefined threshold values, surgical intervention —either by OAR or EVAR— represents the only available treatment option [152, 406, 407]. To date no drug-based therapy targeting aneurysm growth and thereby AAA progression is available. Although several promising candidates for potential drug-based approaches have been evaluated over the last years, their clinical translation is still lacking and remains challenging. Different clinical trials of drug-based therapies have failed, as the primary endpoint of effectively targeting AAA growth and progression was not reached. For instance, it was reported that the antibiotic agent doxycycline, also acting as an unspecific MMP inhibitor, is capable of effectively protecting mice against experimental induced AAA formation in different *in vivo* models [308, 408-410]. However, the clinical translation of these promising experimental data remains challenging, as randomised trials have reported inconsistent results regarding its capacity to restrict aneurysm growth in patients with AAA [335-338]. In addition to that, administration of the antidiabetic agent metformin revealed beneficial effects on the aortic diameter progression in mice. Nevertheless, a randomised, placebo-controlled clinical trial (trial registration: NCT03507413) was not capable of corroborating these experimental findings, failing to demonstrate a therapeutic benefit of metformin in AAA patients [411]. Antiplatelet

therapies, including low-dose ASA, are broadly prescribed across CVDs to reduce the risk of secondary thrombotic events. Nevertheless, clinical evaluation of ASA in the setting of AAA has yielded conflicting results [244, 272]. Several trials have indicated that low-dose ASA can substantially restrict aneurysm growth in patients with small-size, respectively mid-size aneurysms [245, 246]. Conversely, a randomised controlled trial assessing low-dose ASA reported no therapeutic benefit for patients with small size aneurysms, emphasising the substantial difficulties in study comparability, as well as translation of clinical data with regard to the AAA pathology [245]. Notably, accumulating clinical evidence suggests, that the therapeutic efficacy of antiplatelet agents strongly correlates with the aneurysm size. Multiple studies have demonstrated that especially patients with mid- or large-size aneurysms may gain the greatest benefit from antiplatelet therapies [245, 393, 394]. These findings indicate that the outcomes of clinical trials evaluating, whether potential pharmacological treatment options are capable of effectively targeting aneurysm growth, are highly dependent on cohort size and composition. Therefore, a critical evaluation of the reported results from existing clinical studies with respect to these aspects is required. Taken these challenges into account, testing of potential candidates in *in vivo* animal models of experimental induced AAA formation is still of great importance. This is crucial in order to identify novel targets for the development of pharmacological therapies targeting AAA progression, which could potentially be more effectively translated into clinical practice.

As previously described (**Section 4.2.4**), a first translational approach by targeting GPVI signalling in platelets via GPVI-blocking antibodies *in vivo* revealed a beneficial effect on experimental induced AAA formation in mice [248, 385]. Based on these findings, this work focused on another promising candidate targeting GPVI signalling by investigating whether Revacept effectively addresses aneurysm growth in a preclinical setting *in vivo*. Revacept is a dimeric fusion protein consisting of a Fc fragment fused to endogenous platelet GPVI (dimeric GPVI-Fc). Unlike conventional antiplatelet therapies, which directly inhibit platelet function and therefore increase the risk of bleeding complications, Revacept selectively binds to the subendothelial collagen at the side of vascular injury [412]. Thereby, Revacept prevents collagen-mediated platelet activation and aggregation via GPVI, without affecting thrombin- or ADP-induced platelet responses. Compared to different GPVI-blocking antibodies, Revacept was shown to not affect platelet GPVI surface expression or platelet counts, indicating its highly selective and low-risk mechanism of action [413-416]. These findings were confirmed, as an initial clinical phase I study (trial registration: NCT01042964) revealed no notable off-target effects due to Revacept application in healthy volunteers. However, platelet aggregation was sufficiently targeted, while haemostasis, platelet counts as well as bleeding times were unaltered [253]. Beyond this, in a

randomised multi-centre phase II clinical trials Revacept showed a beneficial effect in symptomatic carotid stenosis patients (trial registration: NCT01645306) [116, 120], while an additional randomised, double-blind, placebo-controlled phase II trial (ISAR-PLASTER [Intracoronary Stenting and Antithrombotic Regimen: Lesion Platelet Adhesion as Selective Target of Endovenous Revacept] trial registration: NCT 03315285) reported no improvement in stable coronary heart disease patients upon Revacept application [254, 255]. Nevertheless, these initial clinical findings in patients with symptomatic carotid stenosis underscore the therapeutic potential of Revacept as a novel antiplatelet therapy in the context of different CVDs.

Therefore, this work evaluated as a next step whether Revacept is capable of effectively restricting aneurysm growth *in vivo* using the ePPE mouse model for experimental induced AAA formation. In this translational approach, prophylactic administration of Revacept markedly attenuated aortic diameter progression (**Section 3.3, Figure 13**), which was paralleled by a substantially reduced aneurysm growth rate (**Section 3.3, Figure 14B**). Therefore, these first findings provide compelling evidence that a prophylactic administration of Revacept sufficiently limits AAA progression in a preclinical setting. Notably, platelet counts (**Section 3.3, Figure 15A**), platelet activation (**Section 3.3, Figure 16A** and **B**), as well as surface expression of key platelet receptors (**Section 3.3, Figure 15A**–**D**) were unaffected, suggesting a preserved platelet function in the presence of Revacept. Consistently, neither bleeding complications nor an increased incidence of aortic rupture were observed in Revacept treated mice, culminating in an unaffected overall survival rate and thus initially proving the preclinical safety of Revacept as a novel antiplatelet therapy in the context of the AAA pathology (**Section 3.3, Figure 13B**). These findings align with data from the previously mentioned initial clinical phase I trial (trial registration: NCT01042964), which revealed no notable off-target effects upon Revacept application in healthy volunteers, which was paralleled by an unaffected haemostasis, as platelet counts and bleeding times were unaltered. Thus, these initial experimental data emphasise the potential of Revacept as a compelling candidate for further preclinical evaluation, with the potential to culminate into clinical translation as a pharmacological intervention targeting AAA progression. As highlighted above, Revacept has previously been reported to not affect platelet GPVI surface expression [253]. In contrast, this present study observed a reduction in GPVI surface abundance upon Revacept administration at day 28 following experimental indued AAA formation (**Section 3.3, Figure 17A** and **E**), which potentially indicates enhanced receptor shedding in these mice. Both ligand engagement and pathological shear stress, as present within the aneurysmal segment, are known to induce proteolytic cleavage of GPVI from the platelet surface by the metalloproteinase ADAM10, resulting in the release of

sGPVI into the circulation [99, 100, 417]. As discussed previously (**Section 4.2.4**), plasma level of circulating sGPVI were found to be markedly enhanced in the AAA pathology in both mice (**Section 3.2, Figure 8B**), and humans (**Section 3.2, Figure 10A**). Recent studies further propose that sGPVI may serve as a reliable biomarker for risk stratification, as sGPVI plasma levels were shown to positively correlate with aneurysm growth rates in experimental and clinical data [248, 385]. Thus, analysing circulating sGPVI levels following experimental AAA induction would represent a promising strategy in order to verify whether the observed reduction in platelet GPVI surface abundance after Revacept treatment reflects a reinforced receptor shedding. Importantly, the decrease in GPVI surface expression did not translate into an impaired platelet reactivity. Neither α-granule secretion nor integrin $\alpha_{IIb}\beta_3$ activation were altered upon GPVI stimulation via CRP, indicating a preserved platelet function upon Revacept administration in the setting of experimentally induced AAA.

Recently, Wagenhäuser *et al*. demonstrated that increased PS exposure on the platelet surface —an indicator of procoagulant activity— represents a platelet-specific hallmark within the AAA pathology (**Section 3.1, Figure 7B**). This reinforced procoagulant state may derive from a persistent hyperreactivity of platelets, in both experimental mouse models and AAA patients [256]. In this context, prophylactic Revacept administration following experimental AAA induction in mice, markedly suppressed procoagulant activity of platelets *in vivo*. These findings provide compelling evidence that GPVI-dependent platelet activation is a major driver of the aberrant PS exposure of platelets in the AAA pathology. This conclusion is further supported by additional experimental data from the present study, as prophylactic GPVI-blocking resulted in a significantly reduced pro-coagulant activity of platelets during ePPE-induced AAA formation and progression [248]. Mechanistically, PS exposure on platelets represents a crucial step in thrombus formation, providing a procoagulant surface that amplifies local thrombin generation, thereby promoting the continued recruitment of circulating platelets into the growing thrombus [23, 58, 418]. Thus, by reinforcing a prothrombotic environment GPVI-mediated PS exposure may not only contribute to the enhanced thrombin plasma level, indicated by elevated TAT complex concentrations, observed in AAA patients, but also promotes recruitment of platelets to the aneurysmal site, thereby facilitating ILT formation and growth [268-270]. Therefore, therapeutic targeting of GPVI, either by using receptor-blocking antibodies or via Revacept, may offer a promising approach to restrict the reinforced procoagulant activity of platelets in the AAA pathology. In this regard, Revacept may has the potential to not only effectively limit aneurysm progression, but also to restrict ILT growth by reducing PS-promoted local thrombin generation in patients with AAA [272]. However, this pharmacological interference of GPVI-mediated PS exposure requires further evaluation as procoagulant activity of platelets is known

to be crucial for thrombus stability [419, 420]. Considering the potential biomechanical protective role of the ILT, reported by different studies, by reducing both peak wall stress and mean wall stress, targeting of GPVI via Revacept *in vivo* may cause a destabilisation of the persistent ILT. This in turn potentially increases the risk for fatal aortic rupture in AAA patients [231, 232, 421].

In conclusion, this present study demonstrated first evidence, that Revacept effectively restricted aneurysm growth *in vivo* in a preclinical setting. This underscores the potential of Revacept as a candidate for novel pharmacological antiplatelet therapy to attenuate AAA formation and progression. Nevertheless, further preclinical evaluation regarding safety and efficacy of Revacept in the context of the AAA pathology are needed to foster the translation of these experimental findings into potential clinical studies. Thus, testing of Revacept in established large animal models (sheep or pig) of experimental induced AAA formation would represent a next step towards a successful clinical implementation [422, 423]. Despite these promising initial preclinical data, it remains an open question whether Revacept will demonstrate comparable efficacy in a clinical setting. Due to the presence of the ILT, persistent in approximately 80% of all diagnosed cases, most of the compromised aortic vessel wall within the aneurysm segment is covered, which consequently may limit the amount of collagen which is exposed towards the circulation [125, 126, 424]. This in turn may substantially compromise the therapeutic impact of Revacept on aneurysm growth in patients with AAA.

4.4 Conclusion and outlook

Over recent years, several preclinical studies have demonstrated beneficial effects of different widely prescribed antiplatelet therapies on AAA formation and progression, by effectively attenuating aneurysm growth and rupture risk across different experimental animal models [241]. However, the underlying mechanisms by which platelets promote aneurysm formation are still poorly understood. The findings presented in this work provide first mechanistic insights into the underlying effects of dysregulated platelet function —as evident in the AAA pathology— for the pathophysiological manifestation of aneurysm formation and progression. Within this framework, platelets were identified as critical mediators of the AAA pathology by driving both the vascular inflammatory response and the adverse remodelling within the aneurysmal tissue. Accordingly, considering the here demonstrated persistent platelet hyperreactivity in AAA patients, antiplatelet therapies emerge as a promising therapeutic strategy to effectively restrict aneurysm growth, thus reducing the risk of fatal aortic rupture. However, the inconsistent efficacy of antiplatelet therapies, especially regarding the administration of low-dose ASA,

observed in clinical trials raises the essential question, which AAA patient subcohorts are most likely to derive a therapeutic benefit [244-246, 272, 393]. This highlights both the crucial importance of cohort composition for clinical studies and the urgent need for further clinical investigations of antiplatelet therapies in the context of the AAA pathology. In this context, an experimental study revealed promising results of ASA (COX1 inhibitor) application in combination with ticagrelor ($P2Y_{12}$ inhibitor) in a preclinical setting using an *in vivo* model for experimental induced AAA formation [241]. Therefore, the use of dual antiplatelet therapies as clinical intervention may offer a promising strategy in order to optimise the treatment efficiency across broader patient cohorts. However, the heterogeneous outcomes of antiplatelet therapies in clinical trials also underline the need for in-depth preclinical investigations, to identify novel platelet-specific therapeutic targets.

Given its central role in collagen-mediated platelet activation, therapeutical targeting of GPVI already emerged as potential antithrombotic therapy, as GPVI-signalling has been linked to the pathophysiology of various CVDs [79, 117, 425-427]. Accordingly, the experimental evidence presented in this work demonstrated a major contribution of GPVI-signalling to platelet-driven pathological mechanisms that reinforce aneurysm initiation and growth. Consequently, therapeutic targeting of GPVI-mediated platelet activation may represent an effective strategy to restrict the AAA pathogenesis, with potential translational relevance as clinical intervention. In regard to the promising experimental evidence of *in vivo* GPVI-blocking using the Fab Y020347 blocking antibody presented in this work, preclinical evaluation of Glenzocimab (GPVI Fab fragment inhibitor) in an experimental AAA model would represent a coherent follow-up approach. Thereby, a successful preclinical validation would provide an important basis for advancing a novel platelet-specific pharmacological intervention, particularly as Glenzocimab has already demonstrated safety and efficiency in clinical trials [386]. Therefore, Glenzocimab emerges as a leading candidate among GPVI inhibitors for potential clinical implementation [115]. Beyond this, the here presented work provided first preclinical evidence that the collagen-blocking agent Revacept effectively restricts aneurysm growth *in vivo*, emphasising its potential as a novel antiplatelet therapy in the context of the AAA pathology. However, considering these preliminary data further experimental evaluation is needed to ensure a successful translation into a clinical routine. Accordingly, evaluation of Revacept in established large-animal models of AAA formation, such as sheep or pigs, would constitute an important follow-up to validate the here presented findings observed in mice and facilitate their translation towards a clinical application.

5 References

1. Broos, K., et al., *Platelets at work in primary hemostasis.* Blood Rev, 2011. **25**(4): p. 155–67.
2. Golebiewska, E.M. and A.W. Poole, *Platelet secretion: From haemostasis to wound healing and beyond.* Blood Rev, 2015. **29**(3): p. 153–62.
3. Tian, Y., et al., *Platelets and diseases: signal transduction and advances in targeted therapy.* Signal Transduct Target Ther, 2025. **10**(1): p. 159.
4. Tyagi, T., et al., *A guide to molecular and functional investigations of platelets to bridge basic and clinical sciences.* Nat Cardiovasc Res, 2022. **1**(3): p. 223–237.
5. Gowert, N.S., et al., *Blood platelets in the progression of Alzheimer's disease.* PLoS One, 2014. **9**(2): p. e90523.
6. Lebas, H., et al., *Platelets Are at the Nexus of Vascular Diseases.* Front Cardiovasc Med, 2019. **6**: p. 132.
7. Sun, W., J. Zheng, and Y. Gao, *Targeting Platelet Activation in Abdominal Aortic Aneurysm: Current Knowledge and Perspectives.* Biomolecules, 2022. **12**(2).
8. Kehrel, B.E., *[Blood platelets: biochemistry and physiology].* Hamostaseologie, 2003. **23**(4): p. 149–58.
9. Ghoshal, K. and M. Bhattacharyya, *Overview of platelet physiology: its hemostatic and nonhemostatic role in disease pathogenesis.* ScientificWorldJournal, 2014. **2014**: p. 781857.
10. Schmitt, A., et al., *Of mice and men: comparison of the ultrastructure of megakaryocytes and platelets.* Exp Hematol, 2001. **29**(11): p. 1295–302.
11. Linden, M.D., *Platelet physiology.* Methods Mol Biol, 2013. **992**: p. 13–30.
12. George, J.N., *Platelets.* Lancet, 2000. **355**(9214): p. 1531–9.
13. Jurk, K. and B.E. Kehrel, *[Pathophysiology and biochemistry of platelets].* Internist (Berl), 2010. **51**(9): p. 1086, 1088–92, 1094.
14. Pogorzelska, K., et al., *Characteristics of platelet indices and their prognostic significance in selected medical condition - a systematic review.* Adv Med Sci, 2020. **65**(2): p. 310–315.
15. Warny, M., et al., *Arterial and venous thrombosis by high platelet count and high hematocrit: 108 521 individuals from the Copenhagen General Population Study.* J Thromb Haemost, 2019. **17**(11): p. 1898–1911.
16. Malte, A.L., J.A. Hojbjerg, and J.B. Larsen, *Platelet Parameters as Biomarkers for Thrombosis Risk in Cancer: A Systematic Review and Meta-analysis.* Semin Thromb Hemost, 2024. **50**(3): p. 360–383.
17. Ruggeri, Z.M., *Platelets in atherothrombosis.* Nat Med, 2002. **8**(11): p. 1227–34.
18. Jurk, K. and B.E. Kehrel, *Platelets: physiology and biochemistry.* Semin Thromb Hemost, 2005. **31**(4): p. 381–92.
19. Freedman, J.E. and J. Loscalzo, *Nitric oxide and its relationship to thrombotic disorders.* J Thromb Haemost, 2003. **1**(6): p. 1183–8.
20. Ruggeri, Z.M. and G.L. Mendolicchio, *Adhesion mechanisms in platelet function.* Circ Res, 2007. **100**(12): p. 1673–85.
21. Koupenova, M., et al., *Thrombosis and platelets: an update.* Eur Heart J, 2017. **38**(11): p. 785–791.
22. Varga-Szabo, D., I. Pleines, and B. Nieswandt, *Cell adhesion mechanisms in platelets.* Arterioscler Thromb Vasc Biol, 2008. **28**(3): p. 403–12.
23. de Witt, S.M., et al., *Insights into platelet-based control of coagulation.* Thromb Res, 2014. **133 Suppl 2**: p. S139–48.
24. Clemetson, K.J. and J.M. Clemetson, *Platelet GPIb-V-IX complex. Structure, function, physiology, and pathology.* Semin Thromb Hemost, 1995. **21**(2): p. 130–6.

25. Berndt, M.C., et al., *The vascular biology of the glycoprotein Ib-IX-V complex.* Thromb Haemost, 2001. **86**(1): p. 178–88.
26. Kauskot, A. and M.F. Hoylaerts, *Platelet receptors.* Handb Exp Pharmacol, 2012(210): p. 23–57.
27. Clemetson, J.M., et al., *The platelet collagen receptor glycoprotein VI is a member of the immunoglobulin superfamily closely related to FcalphaR and the natural killer receptors.* J Biol Chem, 1999. **274**(41): p. 29019–24.
28. Nieswandt, B. and S.P. Watson, *Platelet-collagen interaction: is GPVI the central receptor?* Blood, 2003. **102**(2): p. 449–61.
29. Nieswandt, B., et al., *Glycoprotein VI but not alpha2beta1 integrin is essential for platelet interaction with collagen.* EMBO J, 2001. **20**(9): p. 2120–30.
30. Sosnoski, D.M., et al., *Chromosomal localization of the genes for the vitronectin and fibronectin receptors alpha subunits and for platelet glycoproteins IIb and IIIa.* J Clin Invest, 1988. **81**(6): p. 1993–8.
31. Wagner, C.L., et al., *Analysis of GPIIb/IIIa receptor number by quantification of 7E3 binding to human platelets.* Blood, 1996. **88**(3): p. 907–14.
32. Hynes, R.O., *Integrins: a family of cell surface receptors.* Cell, 1987. **48**(4): p. 549–54.
33. Estevez, B., B. Shen, and X. Du, *Targeting integrin and integrin signaling in treating thrombosis.* Arterioscler Thromb Vasc Biol, 2015. **35**(1): p. 24–9.
34. Gremmel, T., A.L. Frelinger, 3rd, and A.D. Michelson, *Platelet Physiology.* Semin Thromb Hemost, 2016. **42**(3): p. 191–204.
35. Pfaff, M., et al., *Selective recognition of cyclic RGD peptides of NMR defined conformation by alpha IIb beta 3, alpha V beta 3, and alpha 5 beta 1 integrins.* J Biol Chem, 1994. **269**(32): p. 20233–8.
36. Sanchez-Cortes, J. and M. Mrksich, *The platelet integrin alphaIIbbeta3 binds to the RGD and AGD motifs in fibrinogen.* Chem Biol, 2009. **16**(9): p. 990–1000.
37. Nieswandt, B., D. Varga-Szabo, and M. Elvers, *Integrins in platelet activation.* J Thromb Haemost, 2009. **7 Suppl 1**: p. 206–9.
38. Kashiwagi, H., et al., *Affinity modulation of platelet integrin alphaIIbbeta3 by beta3-endonexin, a selective binding partner of the beta3 integrin cytoplasmic tail.* J Cell Biol, 1997. **137**(6): p. 1433–43.
39. Arita, H., T. Nakano, and K. Hanasaki, *Thromboxane A2: its generation and role in platelet activation.* Prog Lipid Res, 1989. **28**(4): p. 273–301.
40. Offermanns, S., *Activation of platelet function through G protein-coupled receptors.* Circ Res, 2006. **99**(12): p. 1293–304.
41. Huang, J.S., et al., *Cell signalling through thromboxane A2 receptors.* Cell Signal, 2004. **16**(5): p. 521–33.
42. Narumiya, S., Y. Sugimoto, and F. Ushikubi, *Prostanoid receptors: structures, properties, and functions.* Physiol Rev, 1999. **79**(4): p. 1193–226.
43. Ting, H.J., et al., *Thromboxane A2 receptor: biology and function of a peculiar receptor that remains resistant for therapeutic targeting.* J Cardiovasc Pharmacol Ther, 2012. **17**(3): p. 248–59.
44. Nakahata, N., *Thromboxane A2: physiology/pathophysiology, cellular signal transduction and pharmacology.* Pharmacol Ther, 2008. **118**(1): p. 18–35.
45. Mills, D.C., *ADP receptors on platelets.* Thromb Haemost, 1996. **76**(6): p. 835–56.
46. Fabre, J.E., et al., *Decreased platelet aggregation, increased bleeding time and resistance to thromboembolism in P2Y1-deficient mice.* Nat Med, 1999. **5**(10): p. 1199–202.
47. Mangin, P., et al., *The P2Y1 receptor plays an essential role in the platelet shape change induced by collagen when TxA2 formation is prevented.* J Thromb Haemost, 2004. **2**(6): p. 969–77.
48. Cattaneo, M., *P2Y12 receptors: structure and function.* J Thromb Haemost, 2015. **13 Suppl 1**: p. S10–6.

49. Kauffenstein, G., et al., *The P2Y(12) receptor induces platelet aggregation through weak activation of the alpha(IIb)beta(3) integrin--a phosphoinositide 3-kinase-dependent mechanism.* FEBS Lett, 2001. **505**(2): p. 281–90.
50. Bye, A.P., A.J. Unsworth, and J.M. Gibbins, *Platelet signaling: a complex interplay between inhibitory and activatory networks.* J Thromb Haemost, 2016. **14**(5): p. 918–30.
51. Riddel, J.P., Jr., et al., *Theories of blood coagulation.* J Pediatr Oncol Nurs, 2007. **24**(3): p. 123–31.
52. Wood, J.P., et al., *Prothrombin activation on the activated platelet surface optimizes expression of procoagulant activity.* Blood, 2011. **117**(5): p. 1710–8.
53. Kahn, M.L., et al., *A dual thrombin receptor system for platelet activation.* Nature, 1998. **394**(6694): p. 690–4.
54. Shapiro, M.J., et al., *Protease-activated receptors 1 and 4 are shut off with distinct kinetics after activation by thrombin.* J Biol Chem, 2000. **275**(33): p. 25216–21.
55. Gale, A.J., *Continuing education course #2: current understanding of hemostasis.* Toxicol Pathol, 2011. **39**(1): p. 273–80.
56. Dachary-Prigent, J., et al., *Annexin V as a probe of aminophospholipid exposure and platelet membrane vesiculation: a flow cytometry study showing a role for free sulfhydryl groups.* Blood, 1993. **81**(10): p. 2554–65.
57. Schreuder, M., P.H. Reitsma, and M.H.A. Bos, *Blood coagulation factor Va's key interactive residues and regions for prothrombinase assembly and prothrombin binding.* J Thromb Haemost, 2019. **17**(8): p. 1229–1239.
58. Klatt, C., et al., *Platelet-RBC interaction mediated by FasL/FasR induces procoagulant activity important for thrombosis.* J Clin Invest, 2018. **128**(9): p. 3906–3925.
59. Rayes, J., S.P. Watson, and B. Nieswandt, *Functional significance of the platelet immune receptors GPVI and CLEC-2.* J Clin Invest, 2019. **129**(1): p. 12–23.
60. Ezumi, Y., T. Uchiyama, and H. Takayama, *Molecular cloning, genomic structure, chromosomal localization, and alternative splice forms of the platelet collagen receptor glycoprotein VI.* Biochem Biophys Res Commun, 2000. **277**(1): p. 27–36.
61. Stegner, D., E.J. Haining, and B. Nieswandt, *Targeting glycoprotein VI and the immunoreceptor tyrosine-based activation motif signaling pathway.* Arterioscler Thromb Vasc Biol, 2014. **34**(8): p. 1615–20.
62. Janus-Bell, E., et al., *Differential Role of Glycoprotein VI in Mouse and Human Thrombus Progression and Stability.* Thromb Haemost, 2021. **121**(4): p. 543–546.
63. Dutting, S., M. Bender, and B. Nieswandt, *Platelet GPVI: a target for antithrombotic therapy?!* Trends Pharmacol Sci, 2012. **33**(11): p. 583–90.
64. Clark, J.C., et al., *Evidence that GPVI is Expressed as a Mixture of Monomers and Dimers, and that the D2 Domain is not Essential for GPVI Activation.* Thromb Haemost, 2021. **121**(11): p. 1435–1447.
65. Jandrot-Perrus, M., et al., *Cloning, characterization, and functional studies of human and mouse glycoprotein VI: a platelet-specific collagen receptor from the immunoglobulin superfamily.* Blood, 2000. **96**(5): p. 1798–807.
66. Andrews, R.K., et al., *Interaction of calmodulin with the cytoplasmic domain of platelet glycoprotein VI.* Blood, 2002. **99**(11): p. 4219–21.
67. Suzuki-Inoue, K., et al., *Association of Fyn and Lyn with the proline-rich domain of glycoprotein VI regulates intracellular signaling.* J Biol Chem, 2002. **277**(24): p. 21561–6.
68. Locke, D., et al., *Fc Rgamma -independent signaling by the platelet collagen receptor glycoprotein VI.* J Biol Chem, 2003. **278**(17): p. 15441–8.
69. Tsuji, M., et al., *A novel association of Fc receptor gamma-chain with glycoprotein VI and their co-expression as a collagen receptor in human platelets.* J Biol Chem, 1997. **272**(38): p. 23528–31.
70. Watson, S.P., et al., *GPVI and integrin alphaIIb beta3 signaling in platelets.* J Thromb Haemost, 2005. **3**(8): p. 1752–62.

71. Quek, L.S., et al., *Fyn and Lyn phosphorylate the Fc receptor gamma chain downstream of glycoprotein VI in murine platelets, and Lyn regulates a novel feedback pathway.* Blood, 2000. **96**(13): p. 4246–53.
72. Perrella, G., et al., *Platelet GPVI (Glycoprotein VI) and Thrombotic Complications in the Venous System.* Arterioscler Thromb Vasc Biol, 2021. **41**(11): p. 2681–2692.
73. Induruwa, I., S.M. Jung, and E.A. Warburton, *Beyond antiplatelets: The role of glycoprotein VI in ischemic stroke.* Int J Stroke, 2016. **11**(6): p. 618–25.
74. Kehrel, B., et al., *Glycoprotein VI is a major collagen receptor for platelet activation: it recognizes the platelet-activating quaternary structure of collagen, whereas CD36, glycoprotein IIb/IIIa, and von Willebrand factor do not.* Blood, 1998. **91**(2): p. 491–9.
75. Miura, Y., et al., *Analysis of the interaction of platelet collagen receptor glycoprotein VI (GPVI) with collagen. A dimeric form of GPVI, but not the monomeric form, shows affinity to fibrous collagen.* J Biol Chem, 2002. **277**(48): p. 46197–204.
76. Herr, A.B. and R.W. Farndale, *Structural insights into the interactions between platelet receptors and fibrillar collagen.* J Biol Chem, 2009. **284**(30): p. 19781–5.
77. Horii, K., M.L. Kahn, and A.B. Herr, *Structural basis for platelet collagen responses by the immune-type receptor glycoprotein VI.* Blood, 2006. **108**(3): p. 936–42.
78. Bultmann, A., et al., *Impact of glycoprotein VI and platelet adhesion on atherosclerosis--a possible role of fibronectin.* J Mol Cell Cardiol, 2010. **49**(3): p. 532–42.
79. Schonberger, T., et al., *The dimeric platelet collagen receptor GPVI-Fc reduces platelet adhesion to activated endothelium and preserves myocardial function after transient ischemia in mice.* Am J Physiol Cell Physiol, 2012. **303**(7): p. C757–66.
80. Inoue, O., et al., *Laminin stimulates spreading of platelets through integrin alpha6beta1-dependent activation of GPVI.* Blood, 2006. **107**(4): p. 1405–12.
81. Donner, L., et al., *The collagen receptor glycoprotein VI promotes platelet-mediated aggregation of beta-amyloid.* Sci Signal, 2020. **13**(643).
82. Riba, R., et al., *Globular adiponectin induces platelet activation through the collagen receptor GPVI-Fc receptor gamma chain complex.* J Thromb Haemost, 2008. **6**(6): p. 1012–20.
83. Mammadova-Bach, E., et al., *Platelet glycoprotein VI binds to polymerized fibrin and promotes thrombin generation.* Blood, 2015. **126**(5): p. 683–91.
84. Niedergang, F., et al., *Convulxin binding to platelet receptor GPVI: competition with collagen related peptides.* Biochem Biophys Res Commun, 2000. **273**(1): p. 246–50.
85. Kato-Takagaki, K., et al., *Structural and interaction analysis of glycoprotein VI-binding peptide selected from a phage display library.* J Biol Chem, 2009. **284**(16): p. 10720–7.
86. Lecut, C., et al., *Identification of residues within human glycoprotein VI involved in the binding to collagen: evidence for the existence of distinct binding sites.* J Biol Chem, 2004. **279**(50): p. 52293–9.
87. Gibbins, J., et al., *Tyrosine phosphorylation of the Fc receptor gamma-chain in collagen-stimulated platelets.* J Biol Chem, 1996. **271**(30): p. 18095–9.
88. Reth, M., *Antigen receptor tail clue.* Nature, 1989. **338**(6214): p. 383–4.
89. Pasquet, J.M., et al., *LAT is required for tyrosine phosphorylation of phospholipase cgamma2 and platelet activation by the collagen receptor GPVI.* Mol Cell Biol, 1999. **19**(12): p. 8326–34.
90. Watson, S.P., et al., *The role of ITAM- and ITIM-coupled receptors in platelet activation by collagen.* Thromb Haemost, 2001. **86**(1): p. 276–88.
91. Judd, B.A., et al., *Differential requirement for LAT and SLP-76 in GPVI versus T cell receptor signaling.* J Exp Med, 2002. **195**(6): p. 705–17.
92. Gibbins, J.M., et al., *The p85 subunit of phosphatidylinositol 3-kinase associates with the Fc receptor gamma-chain and linker for activitor of T cells (LAT) in platelets stimulated by collagen and convulxin.* J Biol Chem, 1998. **273**(51): p. 34437–43.

93. Watanabe, N., et al., *Functional phenotype of phosphoinositide 3-kinase p85alpha-null platelets characterized by an impaired response to GP VI stimulation.* Blood, 2003. **102**(2): p. 541–8.
94. Quek, L.S., J. Bolen, and S.P. Watson, *A role for Bruton's tyrosine kinase (Btk) in platelet activation by collagen.* Curr Biol, 1998. **8**(20): p. 1137–40.
95. Oda, A., et al., *Rapid tyrosine phosphorylation and activation of Bruton's tyrosine/Tec kinases in platelets induced by collagen binding or CD32 cross-linking.* Blood, 2000. **95**(5): p. 1663–70.
96. El-Daher, S.S., et al., *Distinct localization and function of (1,4,5)IP(3) receptor subtypes and the (1,3,4,5)IP(4) receptor GAP1(IP4BP) in highly purified human platelet membranes.* Blood, 2000. **95**(11): p. 3412–22.
97. Quotti Tubi, L., et al., *CK2beta Regulates Hematopoietic Stem Cell Biology and Erythropoiesis.* Hemasphere, 2023. **7**(12): p. e978.
98. Borst, O. and M. Gawaz, *Glycoprotein VI - novel target in antiplatelet medication.* Pharmacol Ther, 2021. **217**: p. 107630.
99. Al-Tamimi, M., et al., *Pathologic shear triggers shedding of vascular receptors: a novel mechanism for down-regulation of platelet glycoprotein VI in stenosed coronary vessels.* Blood, 2012. **119**(18): p. 4311–20.
100. Montague, S.J., et al., *Soluble GPVI is elevated in injured patients: shedding is mediated by fibrin activation of GPVI.* Blood Adv, 2018. **2**(3): p. 240–251.
101. Baaten, C., et al., *Platelet heterogeneity in activation-induced glycoprotein shedding: functional effects.* Blood Adv, 2018. **2**(18): p. 2320–2331.
102. Neagoe, R.A.I., et al., *Rac Inhibition Causes Impaired GPVI Signalling in Human Platelets through GPVI Shedding and Reduction in PLCgamma2 Phosphorylation.* Int J Mol Sci, 2022. **23**(7).
103. Gardiner, E.E., et al., *Regulation of platelet membrane levels of glycoprotein VI by a platelet-derived metalloproteinase.* Blood, 2004. **104**(12): p. 3611–7.
104. Gardiner, E.E., et al., *Controlled shedding of platelet glycoprotein (GP)VI and GPIb-IX-V by ADAM family metalloproteinases.* J Thromb Haemost, 2007. **5**(7): p. 1530–7.
105. Bender, M., et al., *Differentially regulated GPVI ectodomain shedding by multiple platelet-expressed proteinases.* Blood, 2010. **116**(17): p. 3347–55.
106. Bigalke, B., et al., *Regulation of platelet glycoprotein VI (GPVI) surface expression and of soluble GPVI in patients with atrial fibrillation (AF) and acute coronary syndrome (ACS).* Basic Res Cardiol, 2009. **104**(3): p. 352–7.
107. Reusswig, F., et al., *Only Acute but Not Chronic Thrombocytopenia Protects Mice against Left Ventricular Dysfunction after Acute Myocardial Infarction.* Cells, 2022. **11**(21).
108. Al-Tamimi, M., et al., *Soluble glycoprotein VI is raised in the plasma of patients with acute ischemic stroke.* Stroke, 2011. **42**(2): p. 498–500.
109. Stack, J.R., et al., *Soluble glycoprotein VI, a specific marker of platelet activation is increased in the plasma of subjects with seropositive rheumatoid arthritis.* PLoS One, 2017. **12**(11): p. e0188027.
110. Laske, C., et al., *Association of platelet-derived soluble glycoprotein VI in plasma with Alzheimer's disease.* J Psychiatr Res, 2008. **42**(9): p. 746–51.
111. Bigalke, B., et al., *Diagnostic and therapeutic potentials of platelet glycoprotein VI.* Semin Thromb Hemost, 2010. **36**(2): p. 203–11.
112. Bigalke, B., et al., *Glycoprotein VI as a prognostic biomarker for cardiovascular death in patients with symptomatic coronary artery disease.* Clin Res Cardiol, 2010. **99**(4): p. 227–33.
113. Bigalke, B., et al., *Platelet glycoprotein VI (GPVI) for early identification of acute coronary syndrome in patients with chest pain.* Thromb Res, 2010. **125**(5): p. e184–9.
114. Mazighi, M., et al., *Safety and efficacy of platelet glycoprotein VI inhibition in acute ischaemic stroke (ACTIMIS): a randomised, double-blind, placebo-controlled, phase 1b/2a trial.* Lancet Neurol, 2024. **23**(2): p. 157–167.

115. Wichaiyo, S., W. Parichatikanond, and W. Rattanavipanon, *Glenzocimab: A GPVI (Glycoprotein VI)-Targeted Potential Antiplatelet Agent for the Treatment of Acute Ischemic Stroke.* Stroke, 2022. **53**(11): p. 3506–3513.
116. Uphaus, T., et al., *Revacept, an Inhibitor of Platelet Adhesion in Symptomatic Carotid Stenosis: A Multicenter Randomized Phase II Trial.* Stroke, 2022. **53**(9): p. 2718–2729.
117. Navarro, S., et al., *The humanized platelet glycoprotein VI Fab inhibitor EMA601 protects from arterial thrombosis and ischaemic stroke in mice.* Eur Heart J, 2024. **45**(43): p. 4582–4597.
118. Burkard, P., et al., *A key role for platelet GPVI in neutrophil recruitment, migration, and NETosis in the early stages of acute lung injury.* Blood, 2023. **142**(17): p. 1463–1477.
119. Bieber, M., et al., *Targeting platelet glycoprotein VI attenuates progressive ischemic brain damage before recanalization during middle cerebral artery occlusion in mice.* Exp Neurol, 2021. **344**: p. 113804.
120. Groschel, K., et al., *Revacept, an Inhibitor of Platelet Adhesion in Symptomatic Carotid Artery Stenosis: Design and Rationale of a Randomized Phase II Clinical Trial.* TH Open, 2020. **4**(4): p. e393–e399.
121. Lederle, F.A., et al., *Rupture rate of large abdominal aortic aneurysms in patients refusing or unfit for elective repair.* JAMA, 2002. **287**(22): p. 2968–72.
122. Johansson, G., et al., *Survival in patients with abdominal aortic aneurysms. Comparison between operative and nonoperative management.* Eur J Vasc Surg, 1990. **4**(5): p. 497–502.
123. Cornuz, J., et al., *Risk factors for asymptomatic abdominal aortic aneurysm: systematic review and meta-analysis of population-based screening studies.* Eur J Public Health, 2004. **14**(4): p. 343–9.
124. Sakalihasan, N., et al., *Abdominal aortic aneurysms.* Nat Rev Dis Primers, 2018. **4**(1): p. 34.
125. Jana, S., et al., *Extracellular matrix, regional heterogeneity of the aorta, and aortic aneurysm.* Exp Mol Med, 2019. **51**(12): p. 1–15.
126. Johnston, K.W., et al., *Suggested standards for reporting on arterial aneurysms. Subcommittee on Reporting Standards for Arterial Aneurysms, Ad Hoc Committee on Reporting Standards, Society for Vascular Surgery and North American Chapter, International Society for Cardiovascular Surgery.* J Vasc Surg, 1991. **13**(3): p. 452–8.
127. Alcorn, H.G., et al., *Risk factors for abdominal aortic aneurysms in older adults enrolled in The Cardiovascular Health Study.* Arterioscler Thromb Vasc Biol, 1996. **16**(8): p. 963–70.
128. Jongkind, V., et al., *Juxtarenal aortic aneurysm repair.* J Vasc Surg, 2010. **52**(3): p. 760–7.
129. Studzinska, D., et al., *Infrarenal versus Suprarenal Abdominal Aortic Aneurysms: Comparison of Associated Aneurysms and Renal Artery Stenosis.* Ann Vasc Surg, 2019. **58**: p. 248–254 e1.
130. Hirsch, A.T., et al., *ACC/AHA 2005 Practice Guidelines for the management of patients with peripheral arterial disease (lower extremity, renal, mesenteric, and abdominal aortic): a collaborative report from the American Association for Vascular Surgery/Society for Vascular Surgery, Society for Cardiovascular Angiography and Interventions, Society for Vascular Medicine and Biology, Society of Interventional Radiology, and the ACC/AHA Task Force on Practice Guidelines (Writing Committee to Develop Guidelines for the Management of Patients With Peripheral Arterial Disease): endorsed by the American Association of Cardiovascular and Pulmonary Rehabilitation; National Heart, Lung, and Blood Institute; Society for Vascular Nursing; TransAtlantic Inter-Society Consensus; and Vascular Disease Foundation.* Circulation, 2006. **113**(11): p. e463–654.
131. McGregor, J.C., J.G. Pollock, and H.C. Anton, *The value of ultrasonography in the diagnosis of abdominal aortic aneurysm.* Scott Med J, 1975. **20**(3): p. 133–7.

132. Moll, F.L., et al., *Management of abdominal aortic aneurysms clinical practice guidelines of the European society for vascular surgery.* Eur J Vasc Endovasc Surg, 2011. **41 Suppl 1**: p. S1–S58.
133. Lederle, F.A., et al., *Prevalence and associations of abdominal aortic aneurysm detected through screening. Aneurysm Detection and Management (ADAM) Veterans Affairs Cooperative Study Group.* Ann Intern Med, 1997. **126**(6): p. 441–9.
134. Ozawa, H., et al., *Saccular and Fusiform Abdominal Aortic Aneurysms Treated With Endovascular Repair Differ in Presentation and Treatment Threshold: Analyses Using a National Clinical Database in Japan.* J Am Heart Assoc, 2024. **13**(11): p. e032715.
135. Rastogi, V., et al., *Clinical presentation, outcomes, and threshold for repair by sex in degenerative saccular vs fusiform aneurysms in the descending thoracic aorta.* J Vasc Surg, 2023. **78**(6): p. 1392–1401 e1.
136. Bengtsson, H. and D. Bergqvist, *Ruptured abdominal aortic aneurysm: a population-based study.* J Vasc Surg, 1993. **18**(1): p. 74–80.
137. Johansson, G. and J. Swedenborg, *Ruptured abdominal aortic aneurysms: a study of incidence and mortality.* Br J Surg, 1986. **73**(2): p. 101–3.
138. Hoornweg, L.L., et al., *Meta analysis on mortality of ruptured abdominal aortic aneurysms.* Eur J Vasc Endovasc Surg, 2008. **35**(5): p. 558–70.
139. Golledge, J., et al., *Pathogenesis and management of abdominal aortic aneurysm.* Eur Heart J, 2023. **44**(29): p. 2682–2697.
140. Zhang, P., et al., *Risk factors for abdominal aortic aneurysm in general populations: A systematic review and meta-analysis.* PLoS One, 2025. **20**(9): p. e0329500.
141. Sakalihasan, N., et al., *Family members of patients with abdominal aortic aneurysms are at increased risk for aneurysms: analysis of 618 probands and their families from the Liege AAA Family Study.* Ann Vasc Surg, 2014. **28**(4): p. 787–97.
142. Forsdahl, S.H., et al., *Risk factors for abdominal aortic aneurysms: a 7-year prospective study: the Tromso Study, 1994-2001.* Circulation, 2009. **119**(16): p. 2202–8.
143. Wong, D.R., W.C. Willett, and E.B. Rimm, *Smoking, hypertension, alcohol consumption, and risk of abdominal aortic aneurysm in men.* Am J Epidemiol, 2007. **165**(7): p. 838–45.
144. Tang, W., et al., *Lifetime Risk and Risk Factors for Abdominal Aortic Aneurysm in a 24-Year Prospective Study: The ARIC Study (Atherosclerosis Risk in Communities).* Arterioscler Thromb Vasc Biol, 2016. **36**(12): p. 2468–2477.
145. Yuan, Z., et al., *Abdominal Aortic Aneurysm: Roles of Inflammatory Cells.* Front Immunol, 2020. **11**: p. 609161.
146. Lopez-Candales, A., et al., *Decreased vascular smooth muscle cell density in medial degeneration of human abdominal aortic aneurysms.* Am J Pathol, 1997. **150**(3): p. 993–1007.
147. Didangelos, A., et al., *Extracellular matrix composition and remodeling in human abdominal aortic aneurysms: a proteomics approach.* Mol Cell Proteomics, 2011. **10**(8): p. M111 008128.
148. O'Leary, S.A., et al., *The biaxial mechanical behaviour of abdominal aortic aneurysm intraluminal thrombus: classification of morphology and the determination of layer and region specific properties.* J Biomech, 2014. **47**(6): p. 1430–7.
149. Vorp, D.A., et al., *Potential influence of intraluminal thrombus on abdominal aortic aneurysm as assessed by a new non-invasive method.* Cardiovasc Surg, 1996. **4**(6): p. 732–9.
150. Jubouri, M., et al., *Endovascular solutions for abdominal aortic aneurysms: A comparative review of clinical outcomes with custom-made endografts.* Asian Cardiovasc Thorac Ann, 2023. **31**(7): p. 565–576.
151. Silaghi, H., et al., *Management of small asymptomatic abdominal aortic aneurysms - a review.* Int J Angiol, 2007. **16**(4): p. 121–7.
152. Chaikof, E.L., et al., *The Society for Vascular Surgery practice guidelines on the care of patients with an abdominal aortic aneurysm.* J Vasc Surg, 2018. **67**(1): p. 2–77 e2.

153. Swerdlow, N.J., W.W. Wu, and M.L. Schermerhorn, *Open and Endovascular Management of Aortic Aneurysms.* Circ Res, 2019. **124**(4): p. 647–661.
154. van der Meij, E., et al., *A clinical evaluation of statin pleiotropy: statins selectively and dose-dependently reduce vascular inflammation.* PLoS One, 2013. **8**(1): p. e53882.
155. Propanolol Aneurysm Trial, I., *Propranolol for small abdominal aortic aneurysms: results of a randomized trial.* J Vasc Surg, 2002. **35**(1): p. 72–9.
156. Wemmelund, H., et al., *Low-dose aspirin and rupture of abdominal aortic aneurysm.* J Vasc Surg, 2017. **65**(3): p. 616–625 e4.
157. Vaduganathan, M., et al., *The Global Burden of Cardiovascular Diseases and Risk: A Compass for Future Health.* J Am Coll Cardiol, 2022. **80**(25): p. 2361–2371.
158. Song, P., et al., *The Global and Regional Prevalence of Abdominal Aortic Aneurysms: A Systematic Review and Modeling Analysis.* Ann Surg, 2023. **277**(6): p. 912–919.
159. Tian, C., et al., *Disease burden of aortic aneurysm from 1990 to 2021 with a forecast to 2045: insights from the global burden of disease 2021.* BMC Public Health, 2025. **25**(1): p. 1829.
160. Woo, E.Y., et al., *Open abdominal aortic aneurysm repair is feasible and can be done with excellent results in octogenarians.* J Vasc Surg, 2011. **53**(2): p. 278–84.
161. Guirguis-Blake, J.M., et al., *Primary Care Screening for Abdominal Aortic Aneurysm: Updated Evidence Report and Systematic Review for the US Preventive Services Task Force.* JAMA, 2019. **322**(22): p. 2219–2238.
162. Vardulaki, K.A., et al., *Quantifying the risks of hypertension, age, sex and smoking in patients with abdominal aortic aneurysm.* Br J Surg, 2000. **87**(2): p. 195–200.
163. Brady, A.R., et al., *Abdominal aortic aneurysm expansion: risk factors and time intervals for surveillance.* Circulation, 2004. **110**(1): p. 16–21.
164. Norman, P.E. and J.A. Curci, *Understanding the effects of tobacco smoke on the pathogenesis of aortic aneurysm.* Arterioscler Thromb Vasc Biol, 2013. **33**(7): p. 1473–7.
165. Schupper, A.J., et al., *Sex and Racial Disparity in Outcome of Aneurysmal Subarachnoid Hemorrhage in the United States: A 20-Year Analysis.* Stroke, 2023. **54**(5): p. 1347–1356.
166. Yang, Y., E.B. Lehman, and F. Aziz, *African Americans are less likely to have elective endovascular repair of abdominal aortic aneurysms.* J Vasc Surg, 2019. **70**(2): p. 462–470.
167. Ribieras, A.J., et al., *Racial disparities in presentation and outcomes for endovascular abdominal aortic aneurysm repair.* J Vasc Surg, 2023. **77**(1): p. 69–77.
168. Komutrattananont, P., P. Mahakkanukrauh, and S. Das, *Morphology of the human aorta and age-related changes: anatomical facts.* Anat Cell Biol, 2019. **52**(2): p. 109–114.
169. Wang, X., et al., *A review on the biomechanical behaviour of the aorta.* J Mech Behav Biomed Mater, 2023. **144**: p. 105922.
170. Safar, M.E., B.I. Levy, and H. Struijker-Boudier, *Current perspectives on arterial stiffness and pulse pressure in hypertension and cardiovascular diseases.* Circulation, 2003. **107**(22): p. 2864–9.
171. Franklin, S.S., et al., *Hemodynamic patterns of age-related changes in blood pressure. The Framingham Heart Study.* Circulation, 1997. **96**(1): p. 308–15.
172. Authors/Task Force, M., et al., *EACTS/STS Guidelines for Diagnosing and Treating Acute and Chronic Syndromes of the Aortic Organ.* Ann Thorac Surg, 2024. **118**(1): p. 5–115.
173. Gutterman, D.D., *Adventitia-dependent influences on vascular function.* Am J Physiol, 1999. **277**(4): p. H1265–72.
174. Coen, M., G. Gabbiani, and M.L. Bochaton-Piallat, *Myofibroblast-mediated adventitial remodeling: an underestimated player in arterial pathology.* Arterioscler Thromb Vasc Biol, 2011. **31**(11): p. 2391–6.
175. White, H.J., S.J. Bordes, and J. Borger, *Anatomy, Abdomen and Pelvis: Aorta*, in *StatPearls*. 2025: Treasure Island (FL).
176. Holzapfel, G.A. and H.W. Weizsacker, *Biomechanical behavior of the arterial wall and its numerical characterization.* Comput Biol Med, 1998. **28**(4): p. 377–92.

177. Suchy, T., et al., *Age-related changes in the biochemical composition of the human aorta and their correlation with the delamination strength.* Acta Biomater, 2024. **190**: p. 344–361.
178. Shahbad, R., et al., *Effects of age, elastin density, and glycosaminoglycan accumulation on the delamination strength of human thoracic and abdominal aortas.* Acta Biomater, 2024. **189**: p. 413–426.
179. Lyle, A.N. and U. Raaz, *Killing Me Unsoftly: Causes and Mechanisms of Arterial Stiffness.* Arterioscler Thromb Vasc Biol, 2017. **37**(2): p. e1–e11.
180. Moulakakis, K.G., et al., *Arterial Stiffness and Aortic Aneurysmal Disease - A Narrative Review.* Vasc Health Risk Manag, 2024. **20**: p. 47–57.
181. Touat, Z., et al., *Renewal of mural thrombus releases plasma markers and is involved in aortic abdominal aneurysm evolution.* Am J Pathol, 2006. **168**(3): p. 1022–30.
182. Harter, L.P., et al., *Ultrasonic evaluation of abdominal aortic thrombus.* J Ultrasound Med, 1982. **1**(8): p. 315–8.
183. Kontopodis, N., et al., *The - Not So - Solid 5.5 cm Threshold for Abdominal Aortic Aneurysm Repair: Facts, Misinterpretations, and Future Directions.* Front Surg, 2016. **3**: p. 1.
184. Seeburun, S., et al., *Insights into elastic fiber fragmentation: Mechanisms and treatment of aortic aneurysm in Marfan syndrome.* Vascul Pharmacol, 2023. **153**: p. 107215.
185. Tamarina, N.A., et al., *Expression of matrix metalloproteinases and their inhibitors in aneurysms and normal aorta.* Surgery, 1997. **122**(2): p. 264–71; discussion 271–2.
186. Tsarouhas, K., et al., *Transcriptional regulation of TIMPs in ascending aorta aneurysms.* Thromb Res, 2010. **126**(5): p. 399–405.
187. Annabi, B., et al., *Differential regulation of matrix metalloproteinase activities in abdominal aortic aneurysms.* J Vasc Surg, 2002. **35**(3): p. 539–46.
188. Wilson, W.R., et al., *Elevated plasma MMP1 and MMP9 are associated with abdominal aortic aneurysm rupture.* Eur J Vasc Endovasc Surg, 2008. **35**(5): p. 580–4.
189. Davis, V., et al., *Matrix metalloproteinase-2 production and its binding to the matrix are increased in abdominal aortic aneurysms.* Arterioscler Thromb Vasc Biol, 1998. **18**(10): p. 1625–33.
190. Curci, J.A., et al., *Expression and localization of macrophage elastase (matrix metalloproteinase-12) in abdominal aortic aneurysms.* J Clin Invest, 1998. **102**(11): p. 1900–10.
191. Raffetto, J.D. and R.A. Khalil, *Matrix metalloproteinases and their inhibitors in vascular remodeling and vascular disease.* Biochem Pharmacol, 2008. **75**(2): p. 346–59.
192. Rabkin, S.W., *The Role Matrix Metalloproteinases in the Production of Aortic Aneurysm.* Prog Mol Biol Transl Sci, 2017. **147**: p. 239–265.
193. Ailawadi, G., et al., *Smooth muscle phenotypic modulation is an early event in aortic aneurysms.* J Thorac Cardiovasc Surg, 2009. **138**(6): p. 1392–9.
194. Riches, K., et al., *Progressive Development of Aberrant Smooth Muscle Cell Phenotype in Abdominal Aortic Aneurysm Disease.* J Vasc Res, 2018. **55**(1): p. 35–46.
195. Rombouts, K.B., et al., *The role of vascular smooth muscle cells in the development of aortic aneurysms and dissections.* Eur J Clin Invest, 2022. **52**(4): p. e13697.
196. Cao, G., et al., *How vascular smooth muscle cell phenotype switching contributes to vascular disease.* Cell Commun Signal, 2022. **20**(1): p. 180.
197. Quintana, R.A. and W.R. Taylor, *Cellular Mechanisms of Aortic Aneurysm Formation.* Circ Res, 2019. **124**(4): p. 607–618.
198. Cheng, J., et al., *Pharmacological inhibitor of notch signaling stabilizes the progression of small abdominal aortic aneurysm in a mouse model.* J Am Heart Assoc, 2014. **3**(6): p. e001064.
199. Miller, F.J., Jr., et al., *Oxidative stress in human abdominal aortic aneurysms: a potential mediator of aneurysmal remodeling.* Arterioscler Thromb Vasc Biol, 2002. **22**(4): p. 560–5.

200. Shimizu, K., R.N. Mitchell, and P. Libby, *Inflammation and cellular immune responses in abdominal aortic aneurysms.* Arterioscler Thromb Vasc Biol, 2006. **26**(5): p. 987–94.
201. Puchenkova, O.A., et al., *Cytokines in Abdominal Aortic Aneurysm: Master Regulators With Clinical Application.* Biomark Insights, 2022. **17**: p. 11772719221095676.
202. Marquez-Sanchez, A.C. and E.K. Koltsova, *Immune and inflammatory mechanisms of abdominal aortic aneurysm.* Front Immunol, 2022. **13**: p. 989933.
203. Li, H., et al., *Modulation of Immune-Inflammatory Responses in Abdominal Aortic Aneurysm: Emerging Molecular Targets.* J Immunol Res, 2018. **2018**: p. 7213760.
204. Turner, G.H., et al., *Assessment of macrophage infiltration in a murine model of abdominal aortic aneurysm.* J Magn Reson Imaging, 2009. **30**(2): p. 455–60.
205. Raffort, J., et al., *Monocytes and macrophages in abdominal aortic aneurysm.* Nat Rev Cardiol, 2017. **14**(8): p. 457–471.
206. Eliason, J.L., et al., *Neutrophil depletion inhibits experimental abdominal aortic aneurysm formation.* Circulation, 2005. **112**(2): p. 232–40.
207. Plana, E., et al., *Novel contributions of neutrophils in the pathogenesis of abdominal aortic aneurysm, the role of neutrophil extracellular traps: A systematic review.* Thromb Res, 2020. **194**: p. 200–208.
208. Tsuruda, T., et al., *Adventitial mast cells contribute to pathogenesis in the progression of abdominal aortic aneurysm.* Circ Res, 2008. **102**(11): p. 1368–77.
209. Bobryshev, Y.V. and R.S. Lord, *Vascular-associated lymphoid tissue (VALT) involvement in aortic aneurysm.* Atherosclerosis, 2001. **154**(1): p. 15–21.
210. Forester, N.D., et al., *Increased natural killer cell activity in patients with an abdominal aortic aneurysm.* Br J Surg, 2006. **93**(1): p. 46–54.
211. Krishna, S.M., et al., *Depletion of CD11c+ dendritic cells in apolipoprotein E-deficient mice limits angiotensin II-induced abdominal aortic aneurysm formation and growth.* Clin Sci (Lond), 2019. **133**(21): p. 2203–2215.
212. Kazaleh, M., et al., *Oxidative Stress and the Pathogenesis of Aortic Aneurysms.* Biomedicines, 2023. **12**(1).
213. Way, C.F., W.J. Dougherty, and J.A. Cook, *Effects of essential fatty acid deficiency and indomethacin on histologic, ultrastructural, and phagocytic responses of hepatic macrophages to glucan.* J Leukoc Biol, 1985. **37**(2): p. 137–50.
214. Saaki, A., et al., *[Combination chemotherapy with cyclophosphamide, adriamycin, vincristine and prednisolone (VEPA) for non-Hodgkin's lymphoma].* Gan To Kagaku Ryoho, 1986. **13**(1): p. 65–9.
215. Deanfield, J.E., J.P. Halcox, and T.J. Rabelink, *Endothelial function and dysfunction: testing and clinical relevance.* Circulation, 2007. **115**(10): p. 1285–95.
216. Marumo, T., et al., *Platelet-derived growth factor-stimulated superoxide anion production modulates activation of transcription factor NF-kappaB and expression of monocyte chemoattractant protein 1 in human aortic smooth muscle cells.* Circulation, 1997. **96**(7): p. 2361–7.
217. Walpola, P.L., et al., *Expression of ICAM-1 and VCAM-1 and monocyte adherence in arteries exposed to altered shear stress.* Arterioscler Thromb Vasc Biol, 1995. **15**(1): p. 2–10.
218. Lakshminarayanan, V., et al., *Differential regulation of interleukin-8 and intercellular adhesion molecule-1 by H2O2 and tumor necrosis factor-alpha in endothelial and epithelial cells.* J Biol Chem, 1997. **272**(52): p. 32910–8.
219. Piechota-Polanczyk, A., et al., *The Abdominal Aortic Aneurysm and Intraluminal Thrombus: Current Concepts of Development and Treatment.* Front Cardiovasc Med, 2015. **2**: p. 19.
220. Michel, J.B., et al., *Novel aspects of the pathogenesis of aneurysms of the abdominal aorta in humans.* Cardiovasc Res, 2011. **90**(1): p. 18–27.
221. Lewis, H.D., et al., *Inhibition of PAD4 activity is sufficient to disrupt mouse and human NET formation.* Nat Chem Biol, 2015. **11**(3): p. 189–91.

222. Wang, Y., et al., *Composition and Function of Neutrophil Extracellular Traps.* Biomolecules, 2024. **14**(4).
223. Lee, K.H., et al., *Neutrophil extracellular traps (NETs) in autoimmune diseases: A comprehensive review.* Autoimmun Rev, 2017. **16**(11): p. 1160–1173.
224. Eilenberg, W., et al., *Histone citrullination as a novel biomarker and target to inhibit progression of abdominal aortic aneurysms.* Transl Res, 2021. **233**: p. 32–46.
225. Martinez-Pinna, R., et al., *From tissue iron retention to low systemic haemoglobin levels, new pathophysiological biomarkers of human abdominal aortic aneurysm.* Thromb Haemost, 2014. **112**(1): p. 87–95.
226. Wang, D.H., et al., *Mechanical properties and microstructure of intraluminal thrombus from abdominal aortic aneurysm.* J Biomech Eng, 2001. **123**(6): p. 536–9.
227. Adolph, R., et al., *Cellular content and permeability of intraluminal thrombus in abdominal aortic aneurysm.* J Vasc Surg, 1997. **25**(5): p. 916–26.
228. Kazi, M., et al., *Influence of intraluminal thrombus on structural and cellular composition of abdominal aortic aneurysm wall.* J Vasc Surg, 2003. **38**(6): p. 1283–92.
229. Khan, J.A., et al., *Intraluminal thrombus has a selective influence on matrix metalloproteinases and their inhibitors (tissue inhibitors of matrix metalloproteinases) in the wall of abdominal aortic aneurysms.* Ann Vasc Surg, 2012. **26**(3): p. 322–9.
230. Wilson, J.S., et al., *Biochemomechanics of intraluminal thrombus in abdominal aortic aneurysms.* J Biomech Eng, 2013. **135**(2): p. 021011.
231. Haller, S.J., et al., *Intraluminal thrombus is associated with early rupture of abdominal aortic aneurysm.* J Vasc Surg, 2018. **67**(4): p. 1051–1058 e1.
232. Thubrikar, M.J., et al., *Effect of thrombus on abdominal aortic aneurysm wall dilation and stress.* J Cardiovasc Surg (Torino), 2003. **44**(1): p. 67–77.
233. Shaik, N.F., R.F. Regan, and U.P. Naik, *Platelets as drivers of ischemia/reperfusion injury after stroke.* Blood Adv, 2021. **5**(5): p. 1576–1584.
234. Klose, A.M., et al., *Enhanced Integrin Activation of PLD2-Deficient Platelets Accelerates Inflammation after Myocardial Infarction.* Int J Mol Sci, 2020. **21**(9).
235. Reusswig, F., et al., *Platelets modulate cardiac remodeling via the collagen receptor GPVI after acute myocardial infarction.* Front Immunol, 2023. **14**: p. 1275788.
236. Milne, A.A., et al., *Effects of asymptomatic abdominal aortic aneurysm on the soluble coagulation system, platelet count and platelet activation.* Eur J Vasc Endovasc Surg, 1999. **17**(5): p. 434–7.
237. Flondell-Site, D., et al., *Cytokines and systemic biomarkers are related to the size of abdominal aortic aneurysms.* Cytokine, 2009. **46**(2): p. 211–5.
238. Bieger, R., et al., *Arterial aneurysm as a cause of consumption coagulopathy.* N Engl J Med, 1971. **285**(3): p. 152–4.
239. Fransson, M., H. Rydningen, and A.E. Henriksson, *Early coagulopathy in patients with ruptured abdominal aortic aneurysm.* Clin Appl Thromb Hemost, 2012. **18**(1): p. 96–9.
240. Ma, X., et al., *The Detrimental Role of Intraluminal Thrombus Outweighs Protective Advantage in Abdominal Aortic Aneurysm Pathogenesis: The Implications for the Anti-Platelet Therapy.* Biomolecules, 2022. **12**(7).
241. Bontekoe, J., J. Matsumura, and B. Liu, *Thrombosis in the pathogenesis of abdominal aortic aneurysm.* JVS Vasc Sci, 2023. **4**: p. 100106.
242. Liu, O., et al., *Clopidogrel, a platelet P2Y12 receptor inhibitor, reduces vascular inflammation and angiotensin II induced-abdominal aortic aneurysm progression.* PLoS One, 2012. **7**(12): p. e51707.
243. Owens, A.P., 3rd, et al., *Platelet Inhibitors Reduce Rupture in a Mouse Model of Established Abdominal Aortic Aneurysm.* Arterioscler Thromb Vasc Biol, 2015. **35**(9): p. 2032–2041.
244. Kim, S.P., et al., *Low-dose aspirin in the primary prevention of cardiovascular diseases: A retrospective, propensity score matched study.* Atherosclerosis, 2023. **371**: p. 54–60.

245. Lindholt, J.S., et al., *Low-dose aspirin may prevent growth and later surgical repair of medium-sized abdominal aortic aneurysms.* Vasc Endovascular Surg, 2008. **42**(4): p. 329–34.
246. Lindholt, J.S., M. Bjorck, and J.B. Michel, *Anti-platelet treatment of middle-sized abdominal aortic aneurysms.* Curr Vasc Pharmacol, 2013. **11**(3): p. 305–13.
247. Lu, G., et al., *A novel chronic advanced stage abdominal aortic aneurysm murine model.* J Vasc Surg, 2017. **66**(1): p. 232–242 e4.
248. Feige, T., et al., *GP VI-Mediated Platelet Activation and Procoagulant Activity Aggravate Inflammation and Aortic Wall Remodeling in Abdominal Aortic Aneurysm.* Arterioscler Thromb Vasc Biol, 2024. **44**(11): p. 2294–2317.
249. de Witt, S.M., et al., *Identification of platelet function defects by multi-parameter assessment of thrombus formation.* Nat Commun, 2014. **5**: p. 4257.
250. Jamasbi, J., et al., *Differential Inhibition of Human Atherosclerotic Plaque-Induced Platelet Activation by Dimeric GPVI-Fc and Anti-GPVI Antibodies: Functional and Imaging Studies.* J Am Coll Cardiol, 2015. **65**(22): p. 2404–15.
251. Jamasbi, J., et al., *Cross-Linking GPVI-Fc by Anti-Fc Antibodies Potentiates Its Inhibition of Atherosclerotic Plaque- and Collagen-Induced Platelet Activation.* JACC Basic Transl Sci, 2016. **1**(3): p. 131–142.
252. Jung, S.M., K. Tsuji, and M. Moroi, *Glycoprotein (GP) VI dimer as a major collagen-binding site of native platelets: direct evidence obtained with dimeric GPVI-specific Fabs.* J Thromb Haemost, 2009. **7**(8): p. 1347–55.
253. Ungerer, M., et al., *Novel antiplatelet drug revacept (Dimeric Glycoprotein VI-Fc) specifically and efficiently inhibited collagen-induced platelet aggregation without affecting general hemostasis in humans.* Circulation, 2011. **123**(17): p. 1891–9.
254. Schupke, S., et al., *Revacept, a Novel Inhibitor of Platelet Adhesion, in Patients Undergoing Elective PCI-Design and Rationale of the Randomized ISAR-PLASTER Trial.* Thromb Haemost, 2019. **119**(9): p. 1539–1545.
255. Mayer, K., et al., *Efficacy and Safety of Revacept, a Novel Lesion-Directed Competitive Antagonist to Platelet Glycoprotein VI, in Patients Undergoing Elective Percutaneous Coronary Intervention for Stable Ischemic Heart Disease: The Randomized, Double-blind, Placebo-Controlled ISAR-PLASTER Phase 2 Trial.* JAMA Cardiol, 2021. **6**(7): p. 753–761.
256. Wagenhauser, M.U., et al., *Crosstalk of platelets with macrophages and fibroblasts aggravates inflammation, aortic wall stiffening, and osteopontin release in abdominal aortic aneurysm.* Cardiovasc Res, 2024. **120**(4): p. 417–432.
257. Gerdes, N., et al., *Platelet CD40 Exacerbates Atherosclerosis by Transcellular Activation of Endothelial Cells and Leukocytes.* Arterioscler Thromb Vasc Biol, 2016. **36**(3): p. 482–90.
258. Rahman, M., et al., *Platelet-derived CD40L (CD154) mediates neutrophil upregulation of Mac-1 and recruitment in septic lung injury.* Ann Surg, 2009. **250**(5): p. 783–90.
259. Vanichakarn, P., et al., *Neutrophil CD40 enhances platelet-mediated inflammation.* Thromb Res, 2008. **122**(3): p. 346–58.
260. Morrell, C.N., et al., *Platelet olfactory receptor activation limits platelet reactivity and growth of aortic aneurysms.* J Clin Invest, 2022. **132**(9).
261. Robless, P.A., et al., *Increased platelet aggregation and activation in peripheral arterial disease.* Eur J Vasc Endovasc Surg, 2003. **25**(1): p. 16–22.
262. Kasjanovova, D. and V. Balaz, *Age-related changes in human platelet function in vitro.* Mech Ageing Dev, 1986. **37**(2): p. 175–82.
263. Bastyr, E.J., 3rd, M.M. Kadrofske, and A.I. Vinik, *Platelet activity and phosphoinositide turnover increase with advancing age.* Am J Med, 1990. **88**(6): p. 601–6.
264. Gleerup, G. and K. Winther, *The effect of ageing on platelet function and fibrinolytic activity.* Angiology, 1995. **46**(8): p. 715–8.
265. Jones, C.I., *Platelet function and ageing.* Mamm Genome, 2016. **27**(7-8): p. 358–66.

266. Reusswig, F., O. An, and C. Deppermann, *Platelet life cycle during aging: function, production and clearance.* Platelets, 2024. **35**(1): p. 2433750.
267. Gnanenthiran, S.R., et al., *Identification of a Distinct Platelet Phenotype in the Elderly: ADP Hypersensitivity Coexists With Platelet PAR (Protease-Activated Receptor)-1 and PAR-4-Mediated Thrombin Resistance.* Arterioscler Thromb Vasc Biol, 2022. **42**(8): p. 960–972.
268. Davies, R.S., et al., *Coagulation, fibrinolysis, and platelet activation in patients undergoing open and endovascular repair of abdominal aortic aneurysm.* J Vasc Surg, 2011. **54**(3): p. 865–78.
269. Sundermann, A.C., et al., *Prognostic value of D-dimer and markers of coagulation for stratification of abdominal aortic aneurysm growth.* Blood Adv, 2018. **2**(22): p. 3088–3096.
270. Wallinder, J., D. Bergqvist, and A.E. Henriksson, *Haemostatic markers in patients with abdominal aortic aneurysm and the impact of aneurysm size.* Thromb Res, 2009. **124**(4): p. 423–6.
271. Abdelhamid, M.F., et al., *Changes in thrombin generation, fibrinolysis, platelet and endothelial cell activity, and inflammation following endovascular abdominal aortic aneurysm repair.* J Vasc Surg, 2012. **55**(1): p. 41–6.
272. Cameron, S.J., H.M. Russell, and A.P. Owens, 3rd, *Antithrombotic therapy in abdominal aortic aneurysm: beneficial or detrimental?* Blood, 2018. **132**(25): p. 2619–2628.
273. Wang, K.X. and D.T. Denhardt, *Osteopontin: role in immune regulation and stress responses.* Cytokine Growth Factor Rev, 2008. **19**(5-6): p. 333–45.
274. Singh, M., S. Dalal, and K. Singh, *Osteopontin: At the cross-roads of myocyte survival and myocardial function.* Life Sci, 2014. **118**(1): p. 1–6.
275. Singh, M., et al., *Osteopontin: a novel inflammatory mediator of cardiovascular disease.* Front Biosci, 2007. **12**: p. 214–21.
276. Trueblood, N.A., et al., *Exaggerated left ventricular dilation and reduced collagen deposition after myocardial infarction in mice lacking osteopontin.* Circ Res, 2001. **88**(10): p. 1080–7.
277. Stawowy, P., et al., *Increased myocardial expression of osteopontin in patients with advanced heart failure.* Eur J Heart Fail, 2002. **4**(2): p. 139–46.
278. Scatena, M., L. Liaw, and C.M. Giachelli, *Osteopontin: a multifunctional molecule regulating chronic inflammation and vascular disease.* Arterioscler Thromb Vasc Biol, 2007. **27**(11): p. 2302–9.
279. Lin, E.Y., et al., *Osteopontin (OPN)/SPP1: from its biochemistry to biological functions in the innate immune system and the central nervous system (CNS).* Int Immunol, 2023. **35**(4): p. 171–180.
280. Bruemmer, D., et al., *Angiotensin II-accelerated atherosclerosis and aneurysm formation is attenuated in osteopontin-deficient mice.* J Clin Invest, 2003. **112**(9): p. 1318–31.
281. Wang, S.K., et al., *Osteopontin may be a driver of abdominal aortic aneurysm formation.* J Vasc Surg, 2018. **68**(6S): p. 22S–29S.
282. Golledge, J., et al., *Association between osteopontin and human abdominal aortic aneurysm.* Arterioscler Thromb Vasc Biol, 2007. **27**(3): p. 655–60.
283. Rittling, S.R., *Osteopontin in macrophage function.* Expert Rev Mol Med, 2011. **13**: p. e15.
284. Lund, S.A., et al., *Osteopontin mediates macrophage chemotaxis via alpha4 and alpha9 integrins and survival via the alpha4 integrin.* J Cell Biochem, 2013. **114**(5): p. 1194–202.
285. Mukherjee, B.B., et al., *Interaction of osteopontin with fibronectin and other extracellular matrix molecules.* Ann N Y Acad Sci, 1995. **760**: p. 201–12.
286. Kaartinen, M.T., et al., *Transglutaminase-catalyzed cross-linking of osteopontin is inhibited by osteocalcin.* J Biol Chem, 1997. **272**(36): p. 22736–41.
287. Martin, S.M., et al., *Enhancing the biological activity of immobilized osteopontin using a type-1 collagen affinity coating.* J Biomed Mater Res A, 2004. **70**(1): p. 10–9.

288. Zhu, J., et al., *Inflammation in Abdominal Aortic Aneurysm: Cause or Comorbidity?* Can J Cardiol, 2024. **40**(12): p. 2378–2391.
289. Chang, T.W., et al., *Exploring autoimmunity in the pathogenesis of abdominal aortic aneurysms.* Am J Physiol Heart Circ Physiol, 2015. **309**(5): p. H719–27.
290. Kim, H.W., et al., *Role of myeloperoxidase in abdominal aortic aneurysm formation: mitigation by taurine.* Am J Physiol Heart Circ Physiol, 2017. **313**(6): p. H1168–H1179.
291. Klopf, J., et al., *Neutrophils as Regulators and Biomarkers of Cardiovascular Inflammation in the Context of Abdominal Aortic Aneurysms.* Biomedicines, 2021. **9**(9).
292. Fontaine, V., et al., *Role of leukocyte elastase in preventing cellular re-colonization of the mural thrombus.* Am J Pathol, 2004. **164**(6): p. 2077–87.
293. Vandestienne, M., et al., *TREM-1 orchestrates angiotensin II-induced monocyte trafficking and promotes experimental abdominal aortic aneurysm.* J Clin Invest, 2021. **131**(2).
294. Peshkova, I.O., et al., *IL-27 receptor-regulated stress myelopoiesis drives abdominal aortic aneurysm development.* Nat Commun, 2019. **10**(1): p. 5046.
295. Meher, A.K., et al., *Novel Role of IL (Interleukin)-1beta in Neutrophil Extracellular Trap Formation and Abdominal Aortic Aneurysms.* Arterioscler Thromb Vasc Biol, 2018. **38**(4): p. 843–853.
296. Boilard, E., et al., *Platelets amplify inflammation in arthritis via collagen-dependent microparticle production.* Science, 2010. **327**(5965): p. 580–3.
297. Devi, S., et al., *Platelet recruitment to the inflamed glomerulus occurs via an alphaIIbbeta3/GPVI-dependent pathway.* Am J Pathol, 2010. **177**(3): p. 1131–42.
298. Claushuis, T.A.M., et al., *Platelet glycoprotein VI aids in local immunity during pneumonia-derived sepsis caused by gram-negative bacteria.* Blood, 2018. **131**(8): p. 864–876.
299. Pachel, C., et al., *Inhibition of Platelet GPVI Protects Against Myocardial Ischemia-Reperfusion Injury.* Arterioscler Thromb Vasc Biol, 2016. **36**(4): p. 629–35.
300. Kleinschnitz, C., et al., *Targeting platelets in acute experimental stroke: impact of glycoprotein Ib, VI, and IIb/IIIa blockade on infarct size, functional outcome, and intracranial bleeding.* Circulation, 2007. **115**(17): p. 2323–30.
301. Thalin, C., et al., *Quantification of citrullinated histones: Development of an improved assay to reliably quantify nucleosomal H3Cit in human plasma.* J Thromb Haemost, 2020. **18**(10): p. 2732–2743.
302. Ibrahim, N., et al., *Reducing Abdominal Aortic Aneurysm Progression by Blocking Neutrophil Extracellular Traps Depends on Thrombus Formation.* JACC Basic Transl Sci, 2024. **9**(3): p. 342–360.
303. Isenburg, J.C., et al., *Elastin stabilization for treatment of abdominal aortic aneurysms.* Circulation, 2007. **115**(13): p. 1729–37.
304. Bank, A.J., et al., *Contribution of collagen, elastin, and smooth muscle to in vivo human brachial artery wall stress and elastic modulus.* Circulation, 1996. **94**(12): p. 3263–70.
305. Campa, J.S., R.M. Greenhalgh, and J.T. Powell, *Elastin degradation in abdominal aortic aneurysms.* Atherosclerosis, 1987. **65**(1-2): p. 13–21.
306. Tromp, G., et al., *Elevated expression of matrix metalloproteinase-13 in abdominal aortic aneurysms.* Ann Vasc Surg, 2004. **18**(4): p. 414–20.
307. Wilson, W.R., et al., *Matrix metalloproteinase 8 (neutrophil collagenase) in the pathogenesis of abdominal aortic aneurysm.* Br J Surg, 2005. **92**(7): p. 828–33.
308. Pyo, R., et al., *Targeted gene disruption of matrix metalloproteinase-9 (gelatinase B) suppresses development of experimental abdominal aortic aneurysms.* J Clin Invest, 2000. **105**(11): p. 1641–9.
309. Longo, G.M., et al., *Matrix metalloproteinases 2 and 9 work in concert to produce aortic aneurysms.* J Clin Invest, 2002. **110**(5): p. 625–32.
310. Leite, T.F.O., et al., *Expression of plasma levels of MMP-2, MMP-9, TIMP-1, and TIMP-2 in patients with abdominal aortic aneurysms.* J Vasc Bras, 2025. **24**: p. e20240163.

311. Crowther, M., et al., *Localization of matrix metalloproteinase 2 within the aneurysmal and normal aortic wall.* Br J Surg, 2000. **87**(10): p. 1391–400.
312. McMillan, W.D. and W.H. Pearce, *Increased plasma levels of metalloproteinase-9 are associated with abdominal aortic aneurysms.* J Vasc Surg, 1999. **29**(1): p. 122–7; discussion 127–9.
313. Watanabe, T., et al., *The elevated level of circulating matrix metalloproteinase-9 in patients with abdominal aortic aneurysms decreased to levels equal to those of healthy controls after an aortic repair.* Ann Vasc Surg, 2006. **20**(3): p. 317–21.
314. Hovsepian, D.M., et al., *Elevated plasma levels of matrix metalloproteinase-9 in patients with abdominal aortic aneurysms: a circulating marker of degenerative aneurysm disease.* J Vasc Interv Radiol, 2000. **11**(10): p. 1345–52.
315. Grodin, J.L., et al., *Circulating levels of matrix metalloproteinase-9 and abdominal aortic pathology: from the Dallas Heart Study.* Vasc Med, 2011. **16**(5): p. 339–45.
316. Chesney, C.M., E. Harper, and R.W. Colman, *Human platelet collagenase.* J Clin Invest, 1974. **53**(6): p. 1647–54.
317. Gresele, P., et al., *Platelets and Matrix Metalloproteinases: A Bidirectional Interaction with Multiple Pathophysiologic Implications.* Hamostaseologie, 2021. **41**(2): p. 136–145.
318. Galt, S.W., et al., *Outside-in signals delivered by matrix metalloproteinase-1 regulate platelet function.* Circ Res, 2002. **90**(10): p. 1093–9.
319. Sawicki, G., et al., *Localization and translocation of MMP-2 during aggregation of human platelets.* Thromb Haemost, 1998. **80**(5): p. 836–9.
320. Wang, J., et al., *Matrix metalloproteinase12 facilitated platelet activation by shedding carcinoembryonic antigen related cell adhesion molecule1.* Biochem Biophys Res Commun, 2017. **486**(4): p. 1103–1109.
321. Howes, J.M., et al., *MMP-13 binds to platelet receptors alphaIIbbeta3 and GPVI and impairs aggregation and thrombus formation.* Res Pract Thromb Haemost, 2018. **2**(2): p. 370–379.
322. Kazes, I., et al., *Platelet release of trimolecular complex components MT1-MMP/TIMP2/MMP2: involvement in MMP2 activation and platelet aggregation.* Blood, 2000. **96**(9): p. 3064–9.
323. Cecchetti, L., et al., *Megakaryocytes differentially sort mRNAs for matrix metalloproteinases and their inhibitors into platelets: a mechanism for regulating synthetic events.* Blood, 2011. **118**(7): p. 1903–11.
324. Radomski, A., et al., *Identification, regulation and role of tissue inhibitor of metalloproteinases-4 (TIMP-4) in human platelets.* Br J Pharmacol, 2002. **137**(8): p. 1330–8.
325. Murate, T., et al., *The production of tissue inhibitors of metalloproteinases (TIMPs) in megakaryopoiesis: possible role of platelet- and megakaryocyte-derived TIMPs in bone marrow fibrosis.* Br J Haematol, 1997. **99**(1): p. 181–9.
326. Falcinelli, E., et al., *Intraplatelet signaling mechanisms of the priming effect of matrix metalloproteinase-2 on platelet aggregation.* J Thromb Haemost, 2005. **3**(11): p. 2526–35.
327. Mastenbroek, T.G., et al., *Platelet-Associated Matrix Metalloproteinases Regulate Thrombus Formation and Exert Local Collagenolytic Activity.* Arterioscler Thromb Vasc Biol, 2015. **35**(12): p. 2554–61.
328. Fernandez-Patron, C., et al., *Differential regulation of platelet aggregation by matrix metalloproteinases-9 and -2.* Thromb Haemost, 1999. **82**(6): p. 1730–5.
329. Seizer, P. and A.E. May, *Platelets and matrix metalloproteinases.* Thromb Haemost, 2013. **110**(5): p. 903–9.
330. Choi, W.S., et al., *MMP-2 regulates human platelet activation by interacting with integrin alphaIIbbeta3.* J Thromb Haemost, 2008. **6**(3): p. 517–23.
331. Sawicki, G., et al., *Release of gelatinase A during platelet activation mediates aggregation.* Nature, 1997. **386**(6625): p. 616–9.

332. Gresele, P., et al., *Platelets release matrix metalloproteinase-2 in the coronary circulation of patients with acute coronary syndromes: possible role in sustained platelet activation.* Eur Heart J, 2011. **32**(3): p. 316–25.
333. Santos-Martinez, M.J., et al., *Role of metalloproteinases in platelet function.* Thromb Res, 2008. **121**(4): p. 535–42.
334. Atkinson, G., et al., *The contribution of matrix metalloproteinases and their inhibitors to the development, progression, and rupture of abdominal aortic aneurysms.* Front Cardiovasc Med, 2023. **10**: p. 1248561.
335. Mosorin, M., et al., *Use of doxycycline to decrease the growth rate of abdominal aortic aneurysms: a randomized, double-blind, placebo-controlled pilot study.* J Vasc Surg, 2001. **34**(4): p. 606–10.
336. Baxter, B.T., et al., *Prolonged administration of doxycycline in patients with small asymptomatic abdominal aortic aneurysms: report of a prospective (Phase II) multicenter study.* J Vasc Surg, 2002. **36**(1): p. 1–12.
337. Ding, R., et al., *Matrix metalloproteinases in the aneurysm wall of patients treated with low-dose doxycycline.* Vascular, 2005. **13**(5): p. 290–7.
338. Baxter, B.T., et al., *Effect of Doxycycline on Aneurysm Growth Among Patients With Small Infrarenal Abdominal Aortic Aneurysms: A Randomized Clinical Trial.* JAMA, 2020. **323**(20): p. 2029–2038.
339. Fingleton, B., *MMPs as therapeutic targets--still a viable option?* Semin Cell Dev Biol, 2008. **19**(1): p. 61–8.
340. Pozzi, A., et al., *Integrin alpha1beta1 mediates a unique collagen-dependent proliferation pathway in vivo.* J Cell Biol, 1998. **142**(2): p. 587–94.
341. Hellenthal, F.A., et al., *Biomarkers of AAA progression. Part 1: extracellular matrix degeneration.* Nat Rev Cardiol, 2009. **6**(7): p. 464–74.
342. Howard, P.S. and E.J. Macarak, *Localization of collagen types in regional segments of the fetal bovine aorta.* Lab Invest, 1989. **61**(5): p. 548–55.
343. Xu, J. and G.P. Shi, *Vascular wall extracellular matrix proteins and vascular diseases.* Biochim Biophys Acta, 2014. **1842**(11): p. 2106–2119.
344. Stepien, K.L., et al., *Role of Extracellular Matrix and Inflammation in Abdominal Aortic Aneurysm.* Int J Mol Sci, 2022. **23**(19).
345. Dobrin, P.B., W.H. Baker, and W.C. Gley, *Elastolytic and collagenolytic studies of arteries. Implications for the mechanical properties of aneurysms.* Arch Surg, 1984. **119**(4): p. 405–9.
346. Dobrin, P.B. and R. Mrkvicka, *Failure of elastin or collagen as possible critical connective tissue alterations underlying aneurysmal dilatation.* Cardiovasc Surg, 1994. **2**(4): p. 484–8.
347. Carmo, M., et al., *Alteration of elastin, collagen and their cross-links in abdominal aortic aneurysms.* Eur J Vasc Endovasc Surg, 2002. **23**(6): p. 543–9.
348. Bode, M.K., et al., *Increased amount of type III pN-collagen in human abdominal aortic aneurysms: evidence for impaired type III collagen fibrillogenesis.* J Vasc Surg, 2000. **32**(6): p. 1201–7.
349. Amar, S., L. Smith, and G.B. Fields, *Matrix metalloproteinase collagenolysis in health and disease.* Biochim Biophys Acta Mol Cell Res, 2017. **1864**(11 Pt A): p. 1940–1951.
350. Silver, F.H., I. Horvath, and D.J. Foran, *Viscoelasticity of the vessel wall: the role of collagen and elastic fibers.* Crit Rev Biomed Eng, 2001. **29**(3): p. 279–301.
351. Sinha, S., D. Iyer, and A. Granata, *Embryonic origins of human vascular smooth muscle cells: implications for in vitro modeling and clinical application.* Cell Mol Life Sci, 2014. **71**(12): p. 2271–88.
352. Qian, G., et al., *Abdominal Aortic Aneurysm Formation with a Focus on Vascular Smooth Muscle Cells.* Life (Basel), 2022. **12**(2).
353. Gomez, D. and G.K. Owens, *Smooth muscle cell phenotypic switching in atherosclerosis.* Cardiovasc Res, 2012. **95**(2): p. 156–64.

354. Chen, R., et al., *Phenotypic Switching of Vascular Smooth Muscle Cells in Atherosclerosis.* J Am Heart Assoc, 2023. **12**(20): p. e031121.
355. Humphrey, J.D., E.R. Dufresne, and M.A. Schwartz, *Mechanotransduction and extracellular matrix homeostasis.* Nat Rev Mol Cell Biol, 2014. **15**(12): p. 802–12.
356. Faris, B., et al., *The synthesis of connective tissue protein in smooth muscle cells.* Biochim Biophys Acta, 1976. **418**(1): p. 93–103.
357. Johnson, J.L., *Matrix metalloproteinases: influence on smooth muscle cells and atherosclerotic plaque stability.* Expert Rev Cardiovasc Ther, 2007. **5**(2): p. 265–82.
358. Airhart, N., et al., *Smooth muscle cells from abdominal aortic aneurysms are unique and can independently and synergistically degrade insoluble elastin.* J Vasc Surg, 2014. **60**(4): p. 1033–41; discussion 1041–2.
359. Shen, M., et al., *Divergent roles of matrix metalloproteinase 2 in pathogenesis of thoracic aortic aneurysm.* Arterioscler Thromb Vasc Biol, 2015. **35**(4): p. 888–98.
360. Moen, P.T., Jr., E. Fox, and J.W. Bodnar, *Adenovirus and minute virus of mice DNAs are localized at the nuclear periphery.* Nucleic Acids Res, 1990. **18**(3): p. 513–20.
361. Song, T., et al., *SLC44A2 regulates vascular smooth muscle cell phenotypic switching and aortic aneurysm.* J Clin Invest, 2024. **134**(16).
362. Manso, E., et al., *[Campylobacter pyloridis and gastritis: endoscopic, histological and microbiological correlations].* Boll Ist Sieroter Milan, 1987. **66**(5): p. 384–8.
363. Ramadan, A., et al., *Loss of vascular smooth muscle cell autophagy exacerbates angiotensin II-associated aortic remodeling.* J Vasc Surg, 2018. **68**(3): p. 859–871.
364. Henderson, E.L., et al., *Death of smooth muscle cells and expression of mediators of apoptosis by T lymphocytes in human abdominal aortic aneurysms.* Circulation, 1999. **99**(1): p. 96–104.
365. Lee, T. and L. Chau, *Fas/Fas ligand-mediated death pathway is involved in oxLDL-induced apoptosis in vascular smooth muscle cells.* Am J Physiol Cell Physiol, 2001. **280**(3): p. C709–18.
366. Chen, Y., et al., *Targeting regulated cell death in aortic aneurysm and dissection therapy.* Pharmacol Res, 2022. **176**: p. 106048.
367. Fulda, S. and K.M. Debatin, *Extrinsic versus intrinsic apoptosis pathways in anticancer chemotherapy.* Oncogene, 2006. **25**(34): p. 4798–811.
368. Strasser, A., P.J. Jost, and S. Nagata, *The many roles of FAS receptor signaling in the immune system.* Immunity, 2009. **30**(2): p. 180–92.
369. Griffith, T.S., et al., *Fas ligand-induced apoptosis as a mechanism of immune privilege.* Science, 1995. **270**(5239): p. 1189–92.
370. Dockrell, D.H., et al., *The expression of Fas Ligand by macrophages and its upregulation by human immunodeficiency virus infection.* J Clin Invest, 1998. **101**(11): p. 2394–405.
371. Sica, M., M. Roussel, and P. Legembre, *CD95/Fas stoichiometry in future precision medicine.* Cell Death Differ, 2025. **32**(9): p. 1570–1577.
372. Hahne, M., et al., *Activated B cells express functional Fas ligand.* Eur J Immunol, 1996. **26**(3): p. 721–4.
373. Suda, T., et al., *Expression of the Fas ligand in cells of T cell lineage.* J Immunol, 1995. **154**(8): p. 3806–13.
374. Tateyama, M., et al., *CD4 T lymphocytes are primed to express Fas ligand by CD4 cross-linking and to contribute to CD8 T-cell apoptosis via Fas/FasL death signaling pathway.* Blood, 2000. **96**(1): p. 195–202.
375. Oyaizu, N., et al., *Monocytes express Fas ligand upon CD4 cross-linking and induce CD4+ T cells apoptosis: a possible mechanism of bystander cell death in HIV infection.* J Immunol, 1997. **158**(5): p. 2456–63.
376. Medvedev, A.E., et al., *Regulation of Fas and Fas-ligand expression in NK cells by cytokines and the involvement of Fas-ligand in NK/LAK cell-mediated cytotoxicity.* Cytokine, 1997. **9**(6): p. 394–404.

377. Sata, M. and K. Walsh, *Oxidized LDL activates fas-mediated endothelial cell apoptosis.* J Clin Invest, 1998. **102**(9): p. 1682–9.
378. Geng, Y.J., et al., *Fas is expressed in human atherosclerotic intima and promotes apoptosis of cytokine-primed human vascular smooth muscle cells.* Arterioscler Thromb Vasc Biol, 1997. **17**(10): p. 2200–8.
379. Fukuo, K., et al., *Possible participation of Fas-mediated apoptosis in the mechanism of atherosclerosis.* Gerontology, 1997. **43 Suppl 1**: p. 35–42.
380. Nagata, S., *Fas-induced apoptosis, and diseases caused by its abnormality.* Genes Cells, 1996. **1**(10): p. 873–9.
381. Stoneman, V.E. and M.R. Bennett, *Role of Fas/Fas-L in vascular cell apoptosis.* J Cardiovasc Pharmacol, 2009. **53**(2): p. 100–8.
382. Clarke, M.C., et al., *Apoptosis of vascular smooth muscle cells induces features of plaque vulnerability in atherosclerosis.* Nat Med, 2006. **12**(9): p. 1075–80.
383. Boatright, K.M., et al., *Activation of caspases-8 and -10 by FLIP(L).* Biochem J, 2004. **382**(Pt 2): p. 651–7.
384. Schleicher, R.I., et al., *Platelets induce apoptosis via membrane-bound FasL.* Blood, 2015. **126**(12): p. 1483–93.
385. Benson, T.W., et al., *Soluble glycoprotein VI predicts abdominal aortic aneurysm growth rate and is a novel therapeutic target.* Blood, 2024. **144**(16): p. 1663–1678.
386. Voors-Pette, C., et al., *Safety and Tolerability, Pharmacokinetics, and Pharmacodynamics of ACT017, an Antiplatelet GPVI (Glycoprotein VI) Fab.* Arterioscler Thromb Vasc Biol, 2019. **39**(5): p. 956–964.
387. Dumont, B., et al., *Absence of collagen-induced platelet activation caused by compound heterozygous GPVI mutations.* Blood, 2009. **114**(9): p. 1900–3.
388. Arai, M., et al., *Platelets with 10% of the normal amount of glycoprotein VI have an impaired response to collagen that results in a mild bleeding tendency.* Br J Haematol, 1995. **89**(1): p. 124–30.
389. Nurden, A.T., *Clinical significance of altered collagen-receptor functioning in platelets with emphasis on glycoprotein VI.* Blood Rev, 2019. **38**: p. 100592.
390. Kato, K., et al., *The contribution of glycoprotein VI to stable platelet adhesion and thrombus formation illustrated by targeted gene deletion.* Blood, 2003. **102**(5): p. 1701–7.
391. Nieswandt, B., et al., *Long-term antithrombotic protection by in vivo depletion of platelet glycoprotein VI in mice.* J Exp Med, 2001. **193**(4): p. 459–69.
392. Hill, G.L., et al., *Changes in body weight and body protein with intravenous nutrition.* JPEN J Parenter Enteral Nutr, 1979. **3**(4): p. 215–8.
393. Wanhainen, A., et al., *The effect of ticagrelor on growth of small abdominal aortic aneurysms-a randomized controlled trial.* Cardiovasc Res, 2020. **116**(2): p. 450–456.
394. Balceniuk, M.D., et al., *Aspirin use is associated with decreased radiologically-determined thrombus sac volume in abdominal aortic aneurysms.* Vascular, 2018. **26**(4): p. 440–444.
395. Bigalke, B., et al., *Platelet and soluble glycoprotein VI - novel applications in diagnosis and therapy.* Curr Drug Targets, 2011. **12**(12): p. 1821–30.
396. Folsom, A.R., et al., *Circulating Biomarkers and Abdominal Aortic Aneurysm Incidence: The Atherosclerosis Risk in Communities (ARIC) Study.* Circulation, 2015. **132**(7): p. 578–85.
397. Golledge, J., et al., *Evaluation of the diagnostic and prognostic value of plasma D-dimer for abdominal aortic aneurysm.* Eur Heart J, 2011. **32**(3): p. 354–64.
398. Vele, E., et al., *Plasma D-dimer as a predictor of the progression of abdominal aortic aneurysm.* J Thromb Haemost, 2016. **14**(11): p. 2298–2303.
399. Takagi, H., et al., *Plasma fibrinogen and D-dimer concentrations are associated with the presence of abdominal aortic aneurysm: a systematic review and meta-analysis.* Eur J Vasc Endovasc Surg, 2009. **38**(3): p. 273–7.

400. Parry, D.J., et al., *Haemostatic and fibrinolytic factors in men with a small abdominal aortic aneurysm.* Br J Surg, 2009. **96**(8): p. 870–7.
401. Zagrapan, B., et al., *A Novel Diagnostic and Prognostic Score for Abdominal Aortic Aneurysms Based on D-Dimer and a Comprehensive Analysis of Myeloid Cell Parameters.* Thromb Haemost, 2019. **119**(5): p. 807–820.
402. Bye, A.P., et al., *TRIPLE Score: GPVI and CD36 Expression Predict a Prothrombotic Platelet Function Phenotype.* Circ Res, 2025. **136**(4): p. 439–441.
403. Krott, K.J., et al., *Interplay Between Thrombospondin-1 and CD36 Modulates Platelet-RBC Interaction in Thrombosis and Abdominal Aneurysm Formation.* Circ Res, 2025. **137**(12): p. 1459–1479.
404. Cosford, P.A. and G.C. Leng, *Screening for abdominal aortic aneurysm.* Cochrane Database Syst Rev, 2007(2): p. CD002945.
405. Aggarwal, S., et al., *Abdominal aortic aneurysm: A comprehensive review.* Exp Clin Cardiol, 2011. **16**(1): p. 11–5.
406. Hay, N., et al., *Endovascular stent-grafts for the treatment of abdominal aortic aneurysms: NICE technology appraisal guidance.* Heart, 2009. **95**(21): p. 1798–800.
407. Williamson, A.J. and T. Babrowski, *Current endovascular management of complex pararenal aneurysms.* J Cardiovasc Surg (Torino), 2018. **59**(3): p. 336–341.
408. Yu, M., et al., *Inhibitory effects of doxycycline on the onset and progression of abdominal aortic aneurysm and its related mechanisms.* Eur J Pharmacol, 2017. **811**: p. 101–109.
409. Prall, A.K., et al., *Doxycycline in patients with abdominal aortic aneurysms and in mice: comparison of serum levels and effect on aneurysm growth in mice.* J Vasc Surg, 2002. **35**(5): p. 923–9.
410. Turner, G.H., et al., *In vivo serial assessment of aortic aneurysm formation in apolipoprotein E-deficient mice via MRI.* Circ Cardiovasc Imaging, 2008. **1**(3): p. 220–6.
411. Eilenberg, W., et al., *Editor's Choice - Metformin to Inhibit Progression of Abdominal Aortic Aneurysm: A Randomised, Placebo Controlled Clinical Trial.* Eur J Vasc Endovasc Surg, 2025. **70**(4): p. 417–425.
412. Massberg, S., et al., *Soluble glycoprotein VI dimer inhibits platelet adhesion and aggregation to the injured vessel wall in vivo.* FASEB J, 2004. **18**(2): p. 397–9.
413. Schulz, C., et al., *Platelet GPVI binds to collagenous structures in the core region of human atheromatous plaque and is critical for atheroprogression in vivo.* Basic Res Cardiol, 2008. **103**(4): p. 356–67.
414. Gruner, S., et al., *Relative antithrombotic effect of soluble GPVI dimer compared with anti-GPVI antibodies in mice.* Blood, 2005. **105**(4): p. 1492–9.
415. Goebel, S., et al., *The GPVI-Fc fusion protein Revacept improves cerebral infarct volume and functional outcome in stroke.* PLoS One, 2013. **8**(7): p. e66960.
416. Ungerer, M., et al., *The GPVI-Fc fusion protein Revacept reduces thrombus formation and improves vascular dysfunction in atherosclerosis without any impact on bleeding times.* PLoS One, 2013. **8**(8): p. e71193.
417. Montague, S.J., R.K. Andrews, and E.E. Gardiner, *Mechanisms of receptor shedding in platelets.* Blood, 2018. **132**(24): p. 2535–2545.
418. Swieringa, F., et al., *Integrating platelet and coagulation activation in fibrin clot formation.* Res Pract Thromb Haemost, 2018. **2**(3): p. 450–460.
419. Nechipurenko, D.Y., et al., *Clot Contraction Drives the Translocation of Procoagulant Platelets to Thrombus Surface.* Arterioscler Thromb Vasc Biol, 2019. **39**(1): p. 37–47.
420. Monroe, D.M., M. Hoffman, and H.R. Roberts, *Platelets and thrombin generation.* Arterioscler Thromb Vasc Biol, 2002. **22**(9): p. 1381–9.
421. Gasser, T.C., et al., *Failure properties of intraluminal thrombus in abdominal aortic aneurysm under static and pulsating mechanical loads.* J Vasc Surg, 2008. **48**(1): p. 179–88.
422. Kalder, J., et al., *New Large Animal Model for Aortic Aneurysms in the Viscerorenal Segment.* J Surg Res, 2019. **240**: p. 156–164.

423. Shannon, A.H., et al., *Porcine Model of Infrarenal Abdominal Aortic Aneurysm.* J Vis Exp, 2019(153).
424. Labruto, F., L. Blomqvist, and J. Swedenborg, *Imaging the intraluminal thrombus of abdominal aortic aneurysms: techniques, findings, and clinical implications.* J Vasc Interv Radiol, 2011. **22**(8): p. 1069–75; quiz 1075.
425. Al-Tamimi, M., et al., *Coagulation-induced shedding of platelet glycoprotein VI mediated by factor Xa.* Blood, 2011. **117**(14): p. 3912–20.
426. Li, R., et al., *Blocking platelet glycoprotein VI (GPVI) as a promising antithrombotic treatment.* Drug Discov Today, 2025. **30**(10): p. 104473.
427. Slater, A., S. Khattak, and M.R. Thomas, *GPVI inhibition: Advancing antithrombotic therapy in cardiovascular disease.* Eur Heart J Cardiovasc Pharmacother, 2024. **10**(5): p. 465–473.

6 Appendix

6.1 Supplemental figures

6.1.1 GPVI-mediated platelet activation and procoagulant activity aggravate inflammation and aortic wall remodelling in abdominal aortic aneurysm

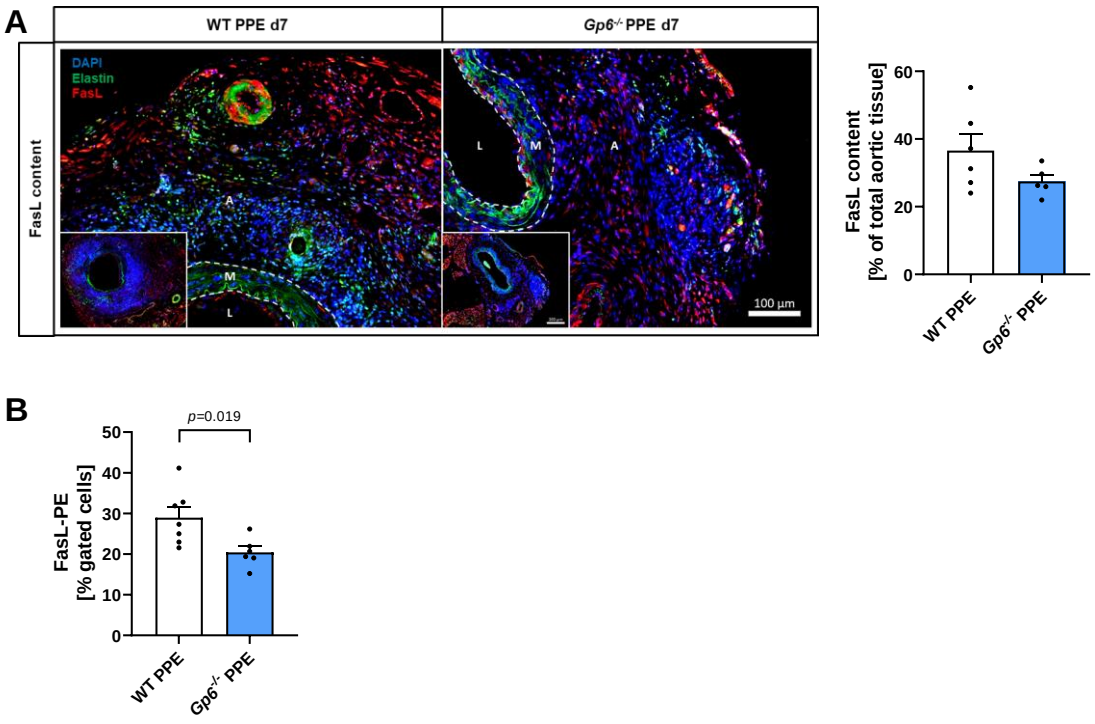


Figure S1. Reduced number of FasL positive platelets in GPVI-deficient mice during early PPE-induced AAA formation. (**A** and **B**) Representative immunofluorescence images and quantification of FasL within the aneurysm segment of PPE operated WT (*n* = 6) and *Gp6*$^{-/-}$ (*n* = 5) mice at day 7. Aortic tissue was specifically stained for FasL (anti-FasL/Cy3; red). Nuclei were stained with DAPI (blue). Scale bars: 100 µm and 200 µm (zoom in). (**B**) Frequency of FasL positive platelets in washed murine whole blood from WT (*n* = 7) and *Gp6*$^{-/-}$ (*n* = 6) PPE mice at day 7 post surgery analysed via flow cytometry. Data are represented as mean values ± SEM. Statistical analysis was performed using (**A** and **B**) an unpaired student's t-test. FasL = Fas ligand; PPE = Porcine pancreatic elastase (infusion).

6.1.2 Revacept (GPVI-FC) treatment attenuates experimental induced abdominal aortic aneurysm formation in mice

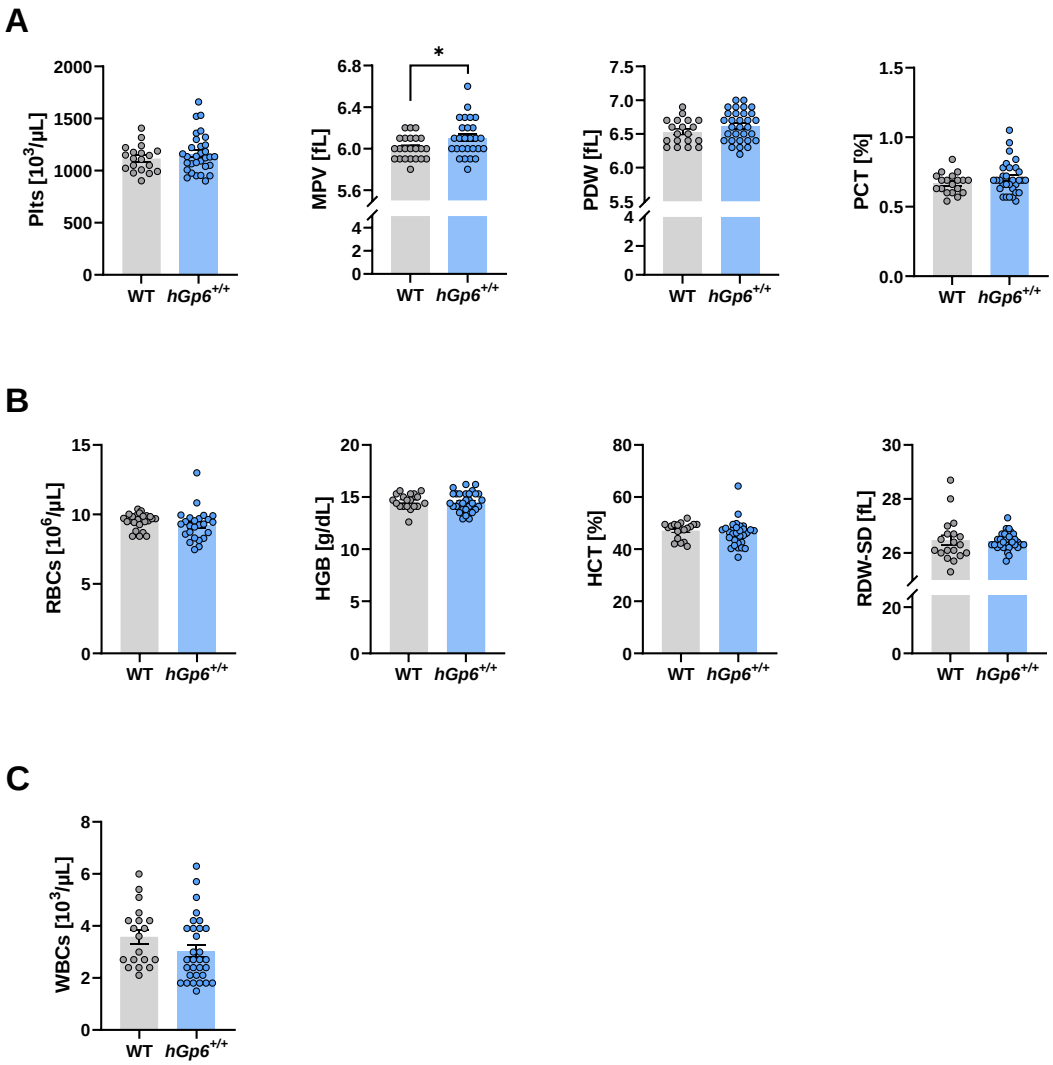


Figure S2. Platelet, RBC and WBC counts of naive humanised *(h)Gp6*$^{+/+}$ mice. (**A**) Platelet counts and platelet specific blood parameters of whole blood samples from naive C57BL/6N (WT) mice (*n* = 19-23), exhibiting the murine GPVI receptor on the platelet surface and humanised (h)*Gp6*$^{+/+}$ mice (*n* = 31), exhibiting the human GPVI receptor on the platelet surface. (**B**) RBC counts and RBC specific blood parameters of WT (*n* = 19) and *hGp6*$^{+/+}$ (*n* = 31) mice (**C**) WBC counts of WT (*n* = 19) and *hGp6*$^{+/+}$ (*n* = 31) mice. Data are represented as mean values ± SEM. Statistical analysis was performed using (**A**–**C**) an unpaired student's t-test; *$p < 0.05$. HCT = Haematocrit; HGB = Haemoglobin; MPV = Mean platelet volume; PCT = Plateletcrit; PDW = Platelet distribution width; Plts = Platelets; RBCs = Red blood cells; WBCs = White blood cells; RDW = Red blood cell distribution width; WT = Wild-type.

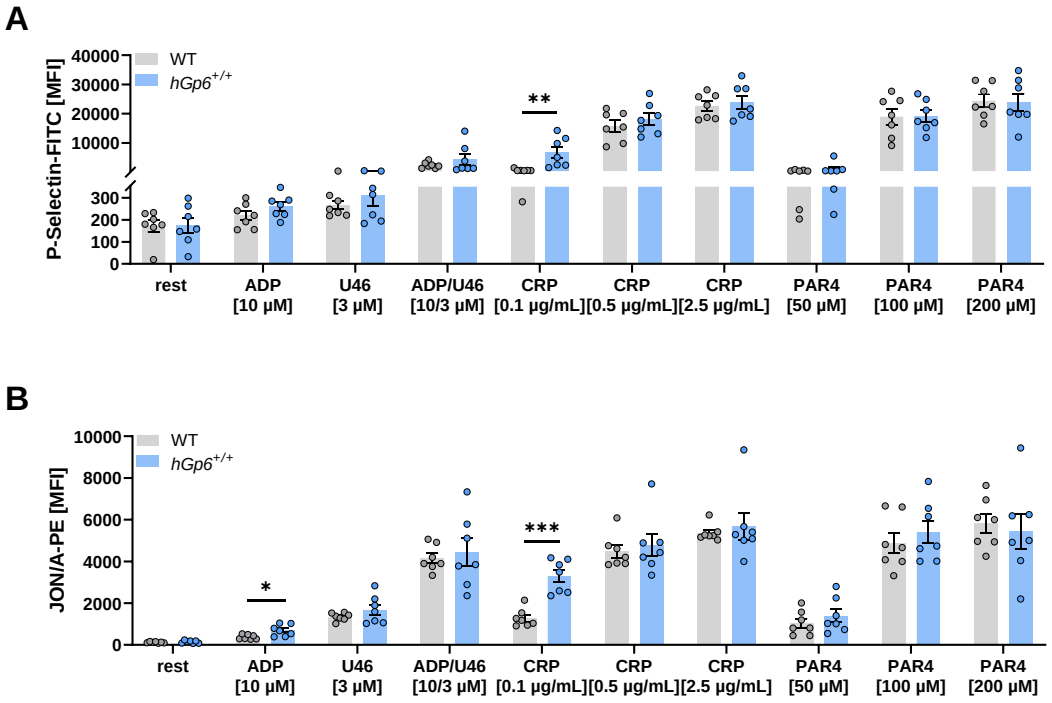


Figure S3. Platelet activation profile of naive *hGp6*$^{+/+}$ mice. (**A** and **B**) Washed murine whole blood from WT and *hGp6*$^{+/+}$ mice was analysed via flow cytometry. (**A**) Platelet degranulation (P-selectin-FITC) and (**B**) active integrin $\alpha_{IIb}\beta_3$ (JON/A-PE) of WT (n = 7) and *hGp6*$^{+/+}$ (n = 7) mice. Platelets were stimulated with indicated agonists. Data are represented as mean values ± SEM. Statistical analysis was performed using (**A** and **B**) an unpaired multiple t-test; *p < 0.05, **p < 0.01, ***p < 0.001 ADP = Adenosine diphosphate; CRP = Collagen-related peptide; MFI = Mean fluorescence intensity; PAR4 = Protease-activated receptor 4 activating peptide; U46619 (U46) = Thromboxane A_2 analogue; rest = Resting; WT = Wild-type.

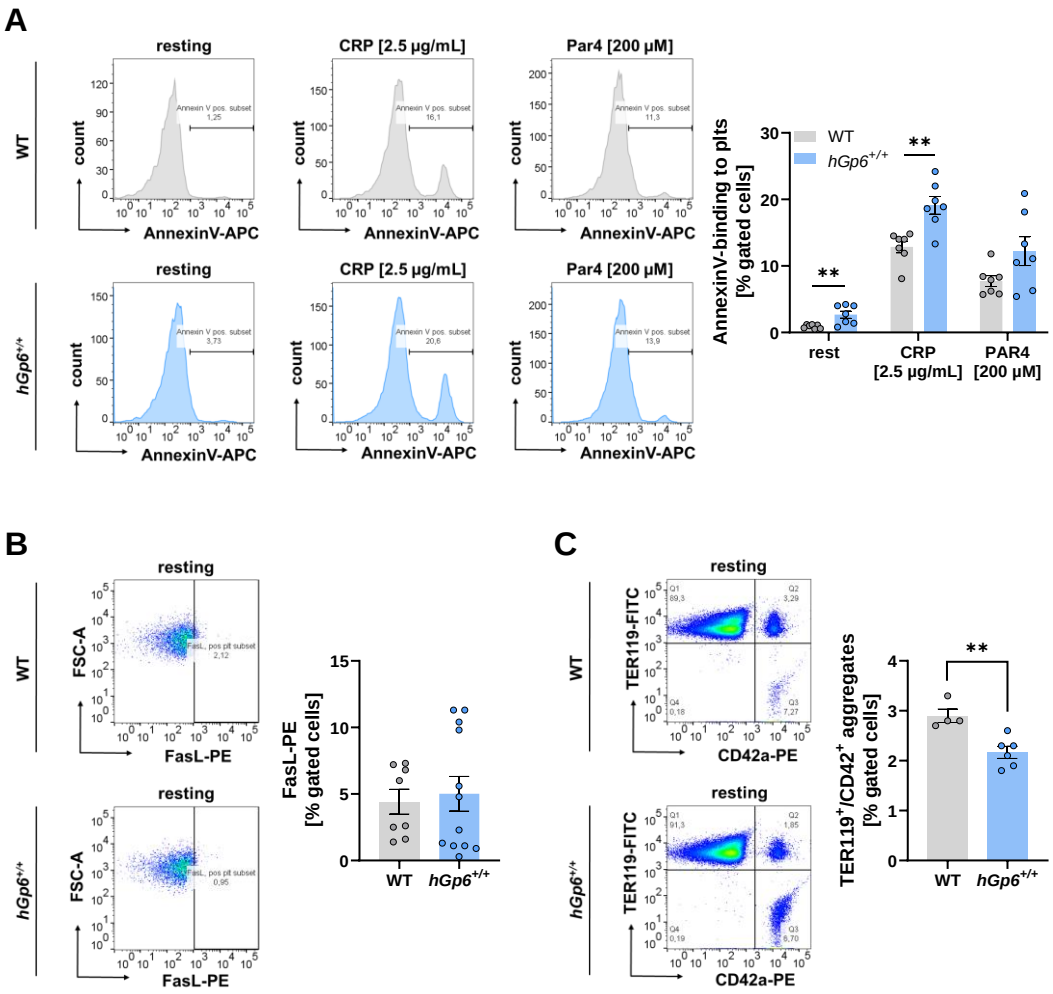


Figure S4. Platelets from naive *hGp6*$^{+/+}$ mice revealed an enhanced procoagulant activity. (**A**-**C**) Washed murine whole blood from naive WT and *hGp6*$^{+/+}$ mice was analysed via flow cytometry. (**A**) AnnexinV-binding to platelets from naive WT (n = 7) and *hGp6*$^{+/+}$ (n = 7) mice. Platelets were stimulated with indicated agonists. Representative histograms are shown. (**B**) Frequency of FasL positive platelets from WT (n = 8) and *hGp6*$^{+/+}$ (n = 12) mice. Representative histograms are shown. (**C**) Platelet-RBC aggregate formation from WT (n = 4) and *hGp6*$^{+/+}$ (n = 6) mice was determined as double-positive events for CD42b (platelet maker, GPIbα) and TER119 (RBC marker). Data are represented as mean values ± SEM. Statistical analysis was performed using (**A**) an unpaired multiple t-test and (**B** and **C**) an unpaired student's t-test; **p < 0.01. CRP = Collagen-related peptide; FasL = Fas ligand; PAR4 = Protease-activated receptor 4 activating peptide; rest = Resting; WT = Wild-type.

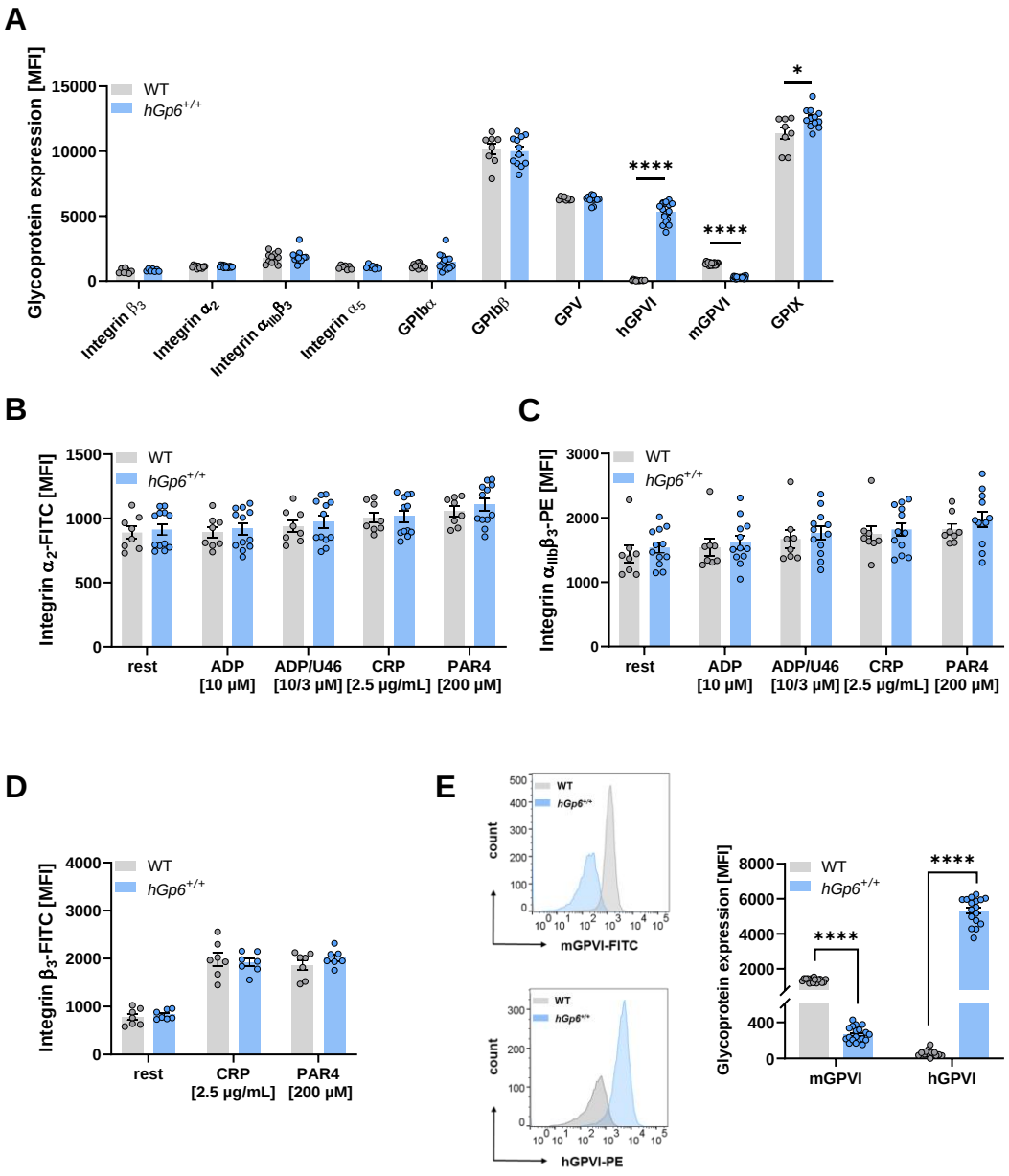


Figure S5. Platelet glycoprotein exposition of naive *hGp6*$^{+/+}$ mice. (**A**–**E**) Washed murine whole blood from WT and *hGp6*$^{+/+}$ mice was analysed via flow cytometry. (**A**) Platelet surface exposure of integrin β_3, integrin α_2, integrin α_5, integrin $\alpha_{IIb}\beta_3$, GPIbα, GPIbβ, GPV, GPVI and GPIX of WT (n = 7-14) and *hGp6*$^{+/+}$ (n = 7-17) mice. (**B**–**D**) Externalisation of (**B**) Integrin α_2 (CD49b), (**C**) integrin $\alpha_{IIb}\beta_3$ (CD41/61) and (**D**) integrin β_3 (CD61) on the platelet surface of WT (n = 8) and *hGp6*$^{+/+}$ (n = 12) mice. Platelets were stimulated with indicated agonists. (**E**) Exposition of murine (m) and human (h) GPVI on the platelet surface of WT (n = 14-15) and *hGp6*$^{+/+}$ (n = 17-19) mice. Representative histograms are shown. Data are represented as mean values ± SEM. Statistical analysis was performed using (**A**–**D**) an unpaired multiple t-test or (**E**) a two-way ANOVA with a Tukey's multiple comparison post-hoc test; *$p < 0.05$, ****$p < 0.0001$. ADP = Adenosine diphosphate; CRP = Collagen-related peptide; MFI = Mean fluorescence intensity; PAR4 = Protease-activated receptor 4 activating peptide; U46619 (U46) = Thromboxane A_2 analogue; rest = Resting; WT = Wild-type.

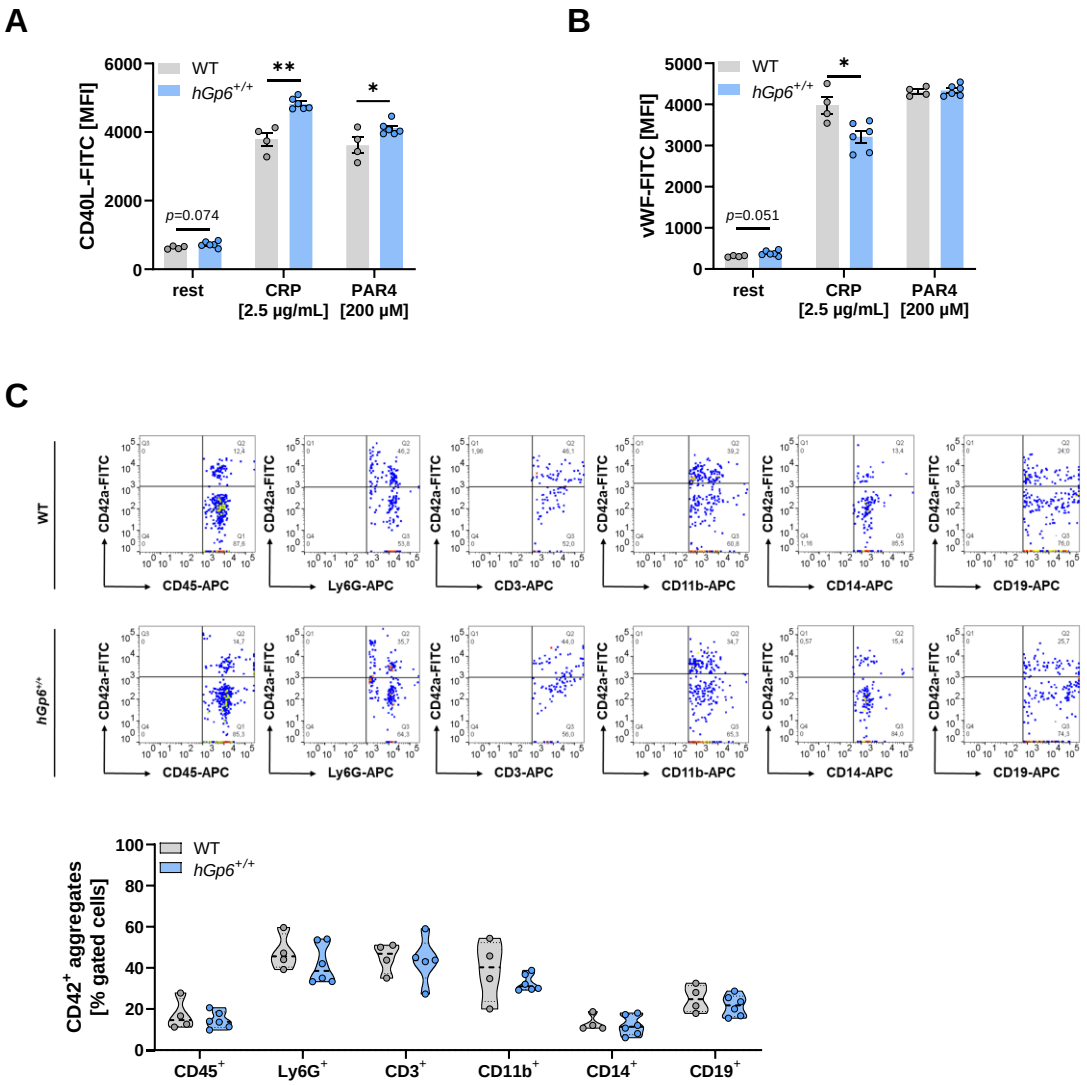


Figure S6. CD40L exposition, VWF binding and platelet-leukocyte aggregate formation in naive *hGp6*$^{+/+}$ mice. (**A**–**C**) Washed murine whole blood from naive WT and *hGp6*$^{+/+}$ mice was analysed via flow cytometry. (**A**) CD40L surface exposition of platelets from naive WT (n = 4) and *hGp6*$^{+/+}$ (n = 6) mice. Platelets were stimulated with indicated agonists. (**B**) VWF-binding to platelets naive WT (n = 4) and *hGp6*$^{+/+}$ (n = 6) mice. Platelets were stimulated with indicated agonists. (**C**) Platelet-leukocyte aggregate formation in naive WT (n = 4) and *hGp6*$^{+/+}$ (n = 6) mice. Aggregate formation of platelets with different leukocyte subtypes was determined as double-positive events for CD42b (platelet maker, GPIbα) and the respective leukocyte marker. Representative histograms are shown. Data are represented as mean values ± SEM. Statistical analysis was performed using (**A**–**C**) an unpaired multiple t-test; *p < 0.05, **p < 0.01. CRP = Collagen-related peptide; PAR4 = Protease-activated receptor 4 activating peptide; rest = Resting; WT = Wild-type.

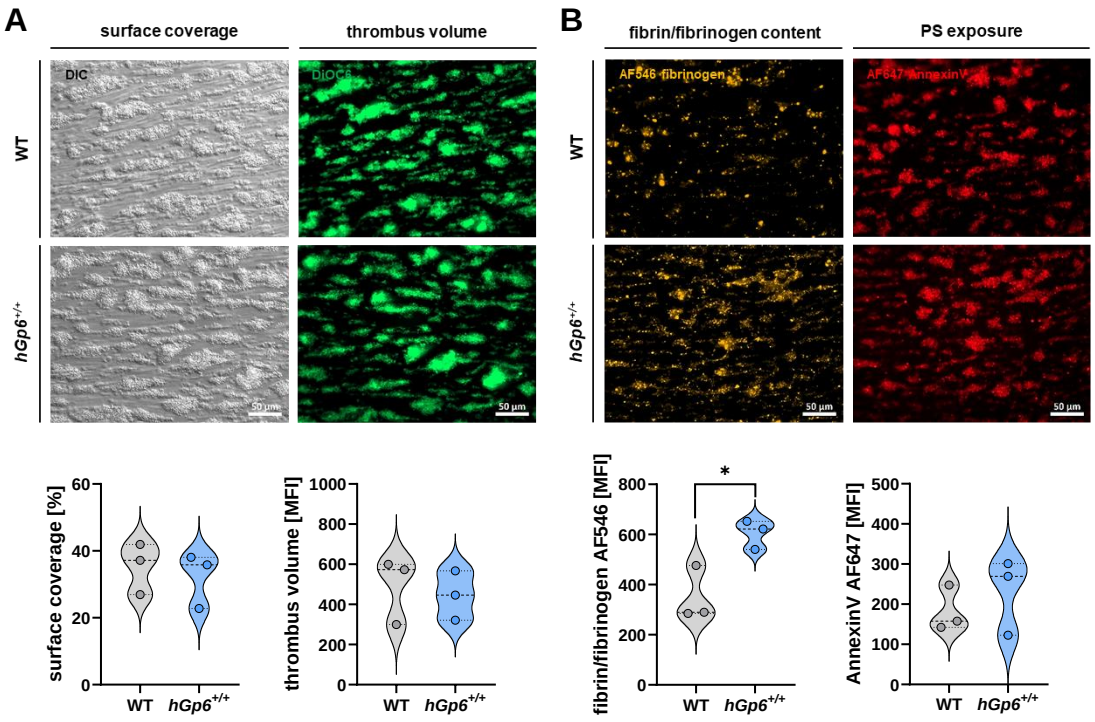


Figure S7. Naive *hGp6*$^{+/+}$ mice revealed an unaltered *ex vivo* thrombus formation under high arterial shear rates. (**A** and **B**) Representative fluorescence images and quantification of *ex vivo* flow chamber experiments. Murine whole blood samples from naive WT and *hGp6*$^{+/+}$ mice were perfused over a collagen matrix (200 µg/mL) under an arterial shear rate of 1,700 s^{-1}. (**A**) Analysis of surface coverage and thrombus volume of murine thrombi. Platelets were pre-labelled with DiOC6 (green). Scale bar: 50 µm (**B**) Fibrin/fibrinogen content and PS exposure of murine thrombi after flow. Whole blood samples were pre-incubated with 8.5 µg/mL AF546 fibrinogen (orange). For PS exposure analysis murine thrombi were stained with AF647 AnnexinV after flow (red). Scale bar: 50 µm. Data are represented as mean values ± SEM. Statistical analysis was performed using (**A** and **B**) an unpaired student's t-test *$p < 0.05$. MFI = Mean fluorescence intensity; PS = Phosphatidylserine; WT = Wild-type.

6.2 List of publications

2021: Donner L, **Feige T**, Freiburg C, Toska LM, Reichert AS, Chatterjee M, Elvers M. Impact of Amyloid-β on Platelet Mitochondrial Function and Platelet-Mediated Amyloid Aggregation in Alzheimer's Disease. *Int J Mol Sci*. 2021 Sep 6;22(17):9633. doi: 10.3390/ijms22179633. PMID: 34502546; PMCID: PMC8431787.

2023: Metz LM*, **Feige T***, de Biasi L, Ehrenberg A, Mulorz J, Toska LM, Reusswig F, Quast C, Gerdes N, Kelm M, Schelzig H, Elvers M. Platelet pannexin-1 channels modulate neutrophil activation and migration but not the progression of abdominal aortic aneurysm. *Front Mol Biosci*. 2023 Mar 6;10:1111108. doi: 10.3389/fmolb.2023.1111108. PMID: 36950521; PMCID: PMC10025481.

2023: Krott KJ, **Feige T**, Elvers M. Flow Chamber Analyses in Cardiovascular Research: Impact of Platelets and the Intercellular Crosstalk with Endothelial Cells, Leukocytes, and Red Blood Cells. *Hamostaseologie*. 2023 Oct;43(5):338-347. doi: 10.1055/a-2113-1134. Epub 2023 Oct 19. PMID: 37857296.

2024: Wagenhäuser MU*, Mulorz J*, Krott KJ*, Bosbach A*, **Feige T**, Rhee YH, Chatterjee M, Petzold N, Böddeker C, Ibing W, Krüger I, Popovic AM, Roseman A, Spin JM, Tsao PS, Schelzig H, Elvers M. Crosstalk of platelets with macrophages and fibroblasts aggravates inflammation, aortic wall stiffening, and osteopontin release in abdominal aortic aneurysm. *Cardiovasc Res.* 2024 Mar 30;120(4):417-432. doi: 10.1093/cvr/cvad168. PMID: 37976180.

2024: Reusswig F, Dille M, Krüger E, Ortscheid J, **Feige T**, Gorressen S, Fischer JW, Elvers M. Platelets modulate cardiac remodeling via the collagen receptor GPVI after acute myocardial infarction. *Front Immunol*. 2024 Jan 11;14:1275788. doi: 10.3389/fimmu.2023.1275788. PMID: 38274818; PMCID: PMC10808189.

2024: **Feige T***, Bosbach A*, Krott KJ*, Mulorz J, Chatterjee M, Ortscheid J, Krüger E, Krüger I, Salehzadeh N, Goebel S, Ibing W, Grandoch I, Münch G, Wagenhäuser MU, Schelzig H, Elvers M. GP VI–Mediated Platelet Activation and Procoagulant Activity Aggravate Inflammation and Aortic Wall Remodeling in Abdominal Aortic Aneurysm. *Arterioscler Thromb Vasc Biol.* 2024; 44:2294-2317. doi: 10.1161/ATVBAHA.123.320615.

2025: Krott KJ, **Feige T**, Elvers M. Platelet-Red Blood Cell Interactions. In: Gresele P, López JA, Angiolillo DJ, Page CP. (eds) Platelet Physiology II and Laboratory Testing. Platelets in Thrombotic and Non-Thrombotic Disorders. Springer, Cham. 2025. doi: 10.1007/978-3-031-96344-5_12

2025: Niemann V*, Brack F*, Rolauer, Kaczur J, Petzsch P, Köhrer K, Quast C, Gerdes N, Bouvain P, Voigt K, Krüger M, Brückner A, Fleischmann BK, Wenzel D, Barnowski P, Zimmermann LM, Simsekyilmaz S, Filler T, Ibing W, **Feige T**, Krott KJ, Wagenhäuser MU, Fischer JW, Elvers M, Sengle G, Flögel U, Hundhausen C, Suvorava T, Grandoch M. Hyaluronan synthase 3 deficiency lowers the incidence of ruptures of abdominal aortic aneurysms by reducing monocyte infiltration. *Front Immunol.* 2025; 16:1680246. doi: 10.3389/fimmu.2025.168024

2025: Krott KJ*, **Feige T***, Bosbach A*, Beele AN, Krüger I, Reusswig F, Schickentanz-Dey E, Pfeiler S, Chadt A, Kelm M, Gerdes N, Jurk K, Kiouptsi K, Reinhardt C, Al-Hasani H, Kehrel BE, Karray S, Chatterjee M, Schelzig H, Wagenhäuser MU, Elvers M. Interplay Between Thrombospondin-1 and CD36 Modulates Platelet–RBC Interaction in Thrombosis and Abdominal Aneurysm Formation. *Circ Res*. 2025. doi:10.1161/CIRCRESAHA.125.326701

2026: **Feige T**, Bosbach A, Krott KJ, Elvers M. Role of Platelets in Abdominal Aortic Aneurysm Formation and Progression: New Aspects from Experimental and Clinical Approaches. *Hamostaseologie*. 2026; 46(01): 053 - 064. doi: 1010.1055/a-2749-2763.

* The authors contributed equally to this work

The publications “Crosstalk of platelets with macrophages and fibroblasts aggravates inflammation, aortic wall stiffening, and osteopontin release in abdominal aortic aneurysm” (*CVR*, 2024) and “GP VI–Mediated Platelet Activation and Pro-coagulant Activity Aggravate Inflammation and Aortic Wall Remodeling in Abdominal Aortic Aneurysm” (*ATVB*, 2024) are reprinted in this dissertation.

6.3 International conferences

2021: 65th Annual Meeting of the Society of Thrombosis and Hemostasis Research (GTH), virtual congress
Poster presentation: *The role of platelet mitochondrial function on platelet-mediated Aβ40 aggregation*

2022: 66th Annual Meeting of the Society of Thrombosis and Hemostasis Research (GTH), virtual congress
Poster presentation: *The impact of platelets on inflammation and extracellular matrix remodelling in abdominal aortic aneurysm formation*

2023: International Society on Thrombosis and Haemostasis (ISTH), Montreal, Canada
Oral presentation: *The impact of the platelet collagen receptor GPVI on inflammation and extracellular matrix remodelling in abdominal aortic aneurysm formation*

2025: 7th EUPLAN International Conference, Wuerzburg, Germany
Poster presentation: *GPVI-signalling promotes inflammation and progressive aortic wall remodelling in abdominal aortic aneurysm formation*

2026: 70th Annual Meeting of the Society of Thrombosis and Hemostasis Research (GTH), Bonn, Germany
Oral presentation: *Histological characterisation of intraluminal thrombi from patients with abdominal aortic aneurysm*
Poster presentation: *Effects of the antidiabetic drug metformin on platelet activation and ex vivo thrombus formation*

6.4 Reuse of own publications

Wagenhäuser MU*, Mulorz J*, Krott KJ*, Bosbach A*, **Feige T**, Rhee YH, Chatterjee M, Petzold N, Böddeker C, Ibing W, Krüger I, Popovic AM, Roseman A, Spin JM, Tsao PS, Schelzig H, Elvers M. Crosstalk of platelets with macrophages and fibroblasts aggravates inflammation, aortic wall stiffening, and osteopontin release in abdominal aortic aneurysm. *Cardiovasc Res.* 2024 Mar 30; 120(4):417-432. doi: 10.1093/cvr/cvad168. PMID: 37976180.

Published in: *Cardiovascular Research (CVR)* in 2024

Impact Factor: 13.3 (2024)

License number for republishing: 6192491110157. Licensed content publisher: Oxford University Press. Publisher's terms and conditions: https://s100.copyright.com/CustomerAdmin/PLF.jsp?ref=7323ac9f-fd8c-47ba-8013-b171898bf774

Feige T*, Bosbach A*, Krott KJ*, Mulorz J, Chatterjee M, Ortscheid J, Krüger E, Krüger I, Salehzadeh N, Goebel S, Ibing W, Grandoch I, Münch G, Wagenhäuser MU, Schelzig H, Elvers M. GP VI–Mediated Platelet Activation and Procoagulant Activity Aggravate Inflammation and Aortic Wall Remodeling in Abdominal Aortic Aneurysm. *Arterioscler Thromb Vasc Biol.* 2024; 44:2294-2317. doi: 10.1161/ATVBAHA.123.320615.

Published in: *Arteriosclerosis, Thrombosis, and Vascular Biology (ATVB)* in 2024

Impact Factor: 7.4 (2024)

License number for republishing: According to the Copyright © 2024, Wolters Kluwer Health policy, no special permission license for the reuse of this publication –published in ATVB– within this thesis is needed. Author Guidelines: https://cdn-tp2.mozu.com/16833-m1/cms/files/Author-Document.pdf?_mzts=636410951730000000.

6.5 Publishing licences of self-created figures

Figure title: Figure1. Platelet-related physiological and pathophysiological processes

Agreement number: UF299C6UUI

Citation to use: Created in BioRender (2026) https://BioRender.com/xzrlyuf

Figure title: Figure2. The role of platelets in primary haemostasis.

Agreement number: RL299C75FN

Citation to use: Created in BioRender (2026) https://BioRender.com/1hxqugy

Figure title: Figure4. Structure of the main collagen receptor GPVI.

Agreement number: SP299C7BJ2

Citation to use: Created in BioRender (2026) https://BioRender.com/8i5riui

Figure title: Figure 5. GPVI-mediated intracellular signalling pathways.

Agreement number: JO299C7IME

Citation to use: Created in BioRender (2026) https://BioRender.com/6mj6cav

Figure title: Figure 9. In vivo Revacept application in ePPE operated mice

Agreement number: LD299C8ESX

Citation to use: Created in BioRender (2026) https://BioRender.com/ldxq5mu

Figure title: Figure13A Revacept treatment attenuates aortic diameter progression in ePPE induced AAA progression

Agreement number: LD299C8ESX

Citation to use: Created in BioRender (2026) https://BioRender.com/ldxq5mu

Figure title: Figure 11. Revacept: Mechanism of action.

Agreement number: AP299C7ZYE

Citation to use: Created in BioRender (2026) https://BioRender.com/cz56k3q

6.6 Curriculum vitae

Personal information

Name:	Tobias Feige
Degree:	Master of Science (M.Sc.)
Date of birth:	08.10.1995
Nationality:	German
Place of residence:	[redacted]

Current position

Since 2020:	**Research associate (PhD student)** Clinic of Vascular and Endovascular Surgery, Research Group for Experimental Vascular Medicine, University Hospital of the Heinrich-Heine-University, Duesseldorf, Germany Project title: *The impact of GPVI signalling on abdominal aortic aneurysm formation and progression*

Scientific education

2014-2018:	**Bachelor's degree in biology (B.Sc.)** Heinrich-Heine-University Duesseldorf, Germany Title bachelor thesis: *Influence of type 2 diabetes mellitus on the development of myocardial infarction* Institute for Metabolic Physiology, Heinrich-Heine-University, Duesseldorf, Germany
2018-2020:	**Master's degree in biology (M.Sc.)** Heinrich-Heine-University Duesseldorf, Germany Title master thesis: *The role of amyloid-beta 40 on mitochondrial function in platelets* Research Group for Experimental Vascular Medicine, University Hospital of the Heinrich-Heine-University, Duesseldorf, Germany

6.7 Affidavit

I herewith declare in lieu of an oath that this dissertation was written by me independently and without unauthorised outside help, in compliance with the "Principles for Ensuring Good Scientific Practice at the Heinrich-Heine-University of Duesseldorf".

Furthermore, I confirm that this thesis has not yet been submitted as part of another examination process neither in identical nor in similar form.

Düsseldorf, March 2026

6.8 Eidesstattliche Erklärung

Ich versichere hiermit an Eides Statt, dass diese Dissertation von mir selbstständig und ohne unzulässige fremde Hilfe unter Beachtung der „Grundsätze zur Sicherung guter wissenschaftlicher Praxis an der Heinrich-Heine-Universität Düsseldorf“ erstellt worden ist.

Ich erkläre außerdem, dass die Dissertation weder in gleicher noch in ähnlicher Form bereits in einem anderen Prüfungsverfahren vorgelegen hat.

Düsseldorf, März 2026

7 Danksagung

Im Folgenden möchte ich mich bei all denjenigen herzlich bedanken, die mich während der Anfertigung dieser Dissertation begleitet und unterstützt haben.

Mein besonderer Dank gilt Frau Prof. Dr. Elvers für die Vergabe dieses äußerst interessanten und wissenschaftlich spannenden Themas. Ich danke ihr zudem für die hervorragende Betreuung, die fachlichen Diskussionen sowie die sorgfältige Durchsicht und Korrektur dieser Arbeit. Besonders dankbar bin ich auch für die Möglichkeit, meine Forschung auf nationalen und internationalen Konferenzen präsentieren zu dürfen. Des Weiteren möchte ich mich bei Prof. Dr. Schelzig und Prof. Dr. Wagenhäuser für die umfassende Unterstützung des im Rahmen des TRR259 durchgeführten Projektes herzlich bedanken. Ebenso danke ich Frau Prof. Dr. Hidalgo für die freundliche Übernahme des Zweitgutachtens.

Von Herzen danken möchte ich schließlich meiner Familie. Besonders meinen Eltern, Birgit und Detlev, sowie meiner Schwester Jenna gilt mein tiefster Dank: Sie haben mich nicht nur während der Promotion, sondern während meines gesamten Studiums jederzeit unterstützt, ermutigt und an mich geglaubt. Ohne eure Unterstützung und euren Rückhalt wäre dies alles nicht möglich gewesen. Außerdem möchte ich meinen Großeltern —Oma Waltraud und Opa Fedor, sowie Oma Uschi und Opa Manfred—, die mich stets unterstützt haben von ganzen Herzen danken, ihr fehlt mir.

Mein weiterer Dank gilt allen Mitgliedern der Arbeitsgruppe für die gemeinsame Zeit und die stets angenehme und lockere Arbeitsatmosphäre. Vielen Dank an Laura, Lisa, Friedrich, Lili, Meike, Irena, Sevgi, Niloo, Michaela, Dennis, Elena, Christopher, Leo, Jelveh und Marten für die gegenseitige Unterstützung und Hilfsbereitschaft. Ein besonderer Dank gilt Agnes und Kim mit denen ich in den letzten Jahren an diesem Projekt gearbeitet habe. Ich denke wir sind wirklich ein super Team geworden, ohne euch als Leidensgenossen hätte die Arbeit an diesem Projekt nicht so erfolgreich geworden und hätte nicht so viel Spaß gemacht. Ebenfalls möchte ich Martina danken. Du hast dir immer Zeit für meine Fragen genommen (seien sie auch noch so dumm gewesen). Danke dir auch, dass du stets da warst um meine Rechnungen zu überprüfen, wärst du nicht gewesen hätte ich wahrscheinlich öfters die falschen Konzentrationen in meinen Versuchen verwendet.

Zum Schluss möchte ich meiner Freundin Leonie danken, die mich gerade während der letzten Phase meiner Promotion oft zum Lachen gebracht und unterstützt hat (und auch manchmal auf eine liebenswerte Art genervt hat). Ohne dich wäre das letzte Jahr nicht so schön gewesen, liebe dich.